

**COMPUTATIONAL MODELLING
OF LOWER-LIMB
MUSCLE FUNCTION
IN HUMAN RUNNING**

Tim W. Dorn

*Submitted in total fulfilment of the requirements
of the degree of Doctor of Philosophy*

November, 2011

Department of Mechanical Engineering
Melbourne School of Engineering
The University of Melbourne



I dedicate this work to my parents, Eric and Elizabeth and to my brother Andrew. I also dedicate this work to the memory of special family members who are not here with us today:

Troy DeSouza (1983 - 2008)

Olympia De Freitas (1922 - 2011)

Freda Dorn (1917 - 2011)



Abstract

The purpose of this dissertation was to investigate the biomechanics of human running. Running is one of the world's most popular sporting and leisure activities and is widely regarded as the most convenient and least costly form of exercise. For the elite population in particular, running is more than just a hobby; it is a profession in a highly competitive world where athletes strive to improve performance and develop technique. It is therefore not surprising that running is associated with the highest proportion of musculoskeletal injury in the sporting world, occurring in both the elite and non-elite population. Despite the vast wealth of knowledge on joint function during running, it is still not understood how the actions of the individual lower-limb muscles coordinate the motion of the body to reach the fastest speeds possible.

Running, like all human movements, are achieved through the contraction of skeletal muscle, providing the forces and energy required to support the body against gravity, propel the body forward, and maintain balance and stability in each stride. Because it is not possible to non-invasively measure the forces developed by individual muscle forces in vivo, musculoskeletal models of the body are the only means available to explore the large-scale synergies of muscle coordination and ascertain the roles of individual muscles.

In this dissertation, detailed computer models of the musculoskeletal system were used in conjunction with novel experimental data of the motion and ground forces produced by nine habitual runners to simulate

the task of overground running at four different speeds (3.5 m/s, 5.2 m/s, 7.0 m/s and 9.0 m/s). Using the simulation results, the key muscle groups responsible for: (i) accelerating the lower limbs and whole-body center-of-mass; and (ii) transferring mechanical energy throughout the segments of the body were determined. These data provide a deeper understanding of locomotive control, beyond the current knowledge of joint function, by describing the individual muscular strategies used to increase running speed.

A particular emphasis of this dissertation was placed in evaluating existing models of ground contact, which form the interface between the skeleton and its external surroundings. Ground contact models are considered one of the most difficult problems in computational mechanics and have the potential to influence interpretations of muscle function predicted by musculoskeletal models. In the process, a novel, multiple-point ground contact model with smoothly transitioning constraints was adapted to provide robust interpretations of muscle function across all running speeds and under all contact conditions, catering for both rear-foot-strikers and toe-strikers.

Taken together, accurate models of both the musculoskeletal system and ground interaction facilitate the quantitative predictions of individual muscle forces and work during the stride cycle, and, ultimately, how these individual muscle forces synergise to achieve a common goal and produce coordinated running movement patterns.

Finally, the computational models and experimental data from this dissertation can be freely downloaded (see the websites in the Preface) and results reproduced in OpenSim, an open source biomechanical research platform to accelerate collaborative research with the ultimate goal of improving running technique and reducing musculoskeletal injury.

Declaration

This is to certify that:

- (i) the thesis comprises only my original work towards the PhD except where indicated in the Preface,
- (ii) due acknowledgement has been made in the text to all other material used,
- (iii) the thesis is less than 80,000 words in length, exclusive of table, maps, bibliographies, appendices and footnotes.

Tim W. Dorn

4th November 2011



Preface

A number of published works have resulted from this dissertation. They are listed collectively below for reference and noted individually at the beginning of the chapters where relevant.

Peer-reviewed journal articles

- **Dorn, T.W., Lin, Y.C., Pandy, M.G. (2011).** Estimates of leg-muscle function in human gait depend on how foot-ground contact is modeled, *Computer Methods in Biomechanics and Biomedical Engineering*, In press.
- **Dorn, T.W., Schache, A.G., Pandy, M.G. (2011).** Mechanical strategy shift in human running: dependence of running speed on hip and ankle muscle performance, *The Journal of Experimental Biology*, In press.
- **Lin, Y.C., Dorn, T.W., Schache, A.G., Pandy, M.G. (2011).** Comparison of different methods for estimating muscle forces in human movement, *Journal of Engineering in Medicine*, In press.

-
- **Schache, A.G., Blanch, P.D., Dorn, T.W., Brown, N.A., Rosemond, D., Pandy, M.G. (2011).** Effect of Running Speed on Lower-Limb Joint Kinetics, *Medicine & Science in Sports & Exercise*, 43(7):1260-1271.
 - **Schache, A.G., Dorn, T.W., Blanch, P.D., Brown, N.A., Pandy, M.G. (2011).** Mechanics of the human hamstring muscles during sprinting, *Medicine & Science in Sports & Exercise*, In press.

In the studies mentioned above, all authors contributed to the conception, experimental design and interpretation of the data contained in these studies. Tim Dorn and Anthony Schache conducted all human gait experiments with the help of Peter Blanch, Nick Brown, and Doug Rosemond from the Australian Institute of Sport, Canberra, Australia. Tim Dorn, Anthony Schache, and Yi-Chung Lin processed the experimental data using computer models. Marcus Pandy provided invaluable insight in the interpretation of results. All authors were involved in drafting and revising the journal manuscripts, and approved the final version of the manuscripts submitted for publication.

Conference proceedings

- **Dorn, T.W., Lin, Y.C., Pandy, M.G. (2011).** Estimates of leg-muscle function in human gait depend on how foot-ground contact is modeled, *International Society of Biomechanics: Technical group on Computer Simulation in Biomechanics - 13th Biennial International Symposium, June 30 - July 2, 2011, Leuven, Belgium.*
- **Dorn, T.W., Schache, A.G., Pandy, M.G. (2011).** Biomechanical strategies for increasing running speed, *23rd International Society of Biomechanics Congress, July 3 - July 7, 2011, Brussels, Belgium.*
- **Dorn, T.W., Schache, A.G., Pandy, M.G. (2011).** Muscle coordination of human sprinting, *23rd International Society of Biomechanics Congress, July 3 - July 7, 2011, Brussels, Belgium.*
- **Dorn, T.W., Lin, Y.C., Schache, A.G., Pandy, M.G. (2012).** Which muscles power the human running stride?, *American Society of Mechanical Engineers 2012 Summer Bioengineering Conference, June 20 - June 23, 2012, Fajardo, Puerto Rico.*

A number of travel grants and scholarships were awarded to provide financial assistance for international conference attendance and they are graciously are acknowledged below:

- Australian Postgraduate Award (APA) Scholarship
- International Society of Biomechanics (ISB) Congress Travel Grant
- Melbourne Abroad Travelling Scholarship (MATS)
- Research Training Conference Assistance Scheme (RT-CAS)

Software releases

- **Dorn, T.W. (2008)** Gait-Extract toolbox for MATLAB
<https://simtk.org/home/c3dtoolbox>
- **Dorn, T.W. (2011)** Pseudo-inverse muscle induced acceleration plugin for OpenSim
https://simtk.org/home/tims_plugins
- **Dorn, T.W. (2011)** Repository for overground running data and musculoskeletal models
<https://simtk.org/home/runningspeeds>

Signed (November 2011)

Tim W. Dorn

Anthony G. Schache

Yi-Chung Lin

Marcus G. Pandy

Acknowledgements

I am deeply thankful to my advisor, Professor Marcus Pandy, for his support and leadership throughout my research endeavours. During the time under his supervision, I have grown to recognise the true value of his honest, straightforward and thoughtful advice. Without his insightful comments, thoughtful suggestions and attention to detail, the completion of this dissertation would not have been possible.

The vital contributions from dozens of others, however, also deserve equal acknowledgement because good research is never tackled alone. Even the smallest discussions can open up new lines of thought and make one appreciate the value of collaboration. I have had the good fortune to work with some amazingly talented academic mentors to whom this dissertation should also belong. Anthony Schache taught me how to do research, and do it well. His background in sports medicine made me realise the true clinical nature of the results from my computer simulations, seeing them not just as numbers and graphs, but as biomechanical mechanisms and strategies that have the potential to improve our understanding of human locomotion. Yi-Chung Lin helped to develop my engineering skills in applying computational methods to biomechanics problems. He has always been available to guide my technical prowess and offer invaluable advice. For this I owe him my sincere thanks. I would also like to especially thank my PhD neighbour and good friend, Tom Correa for the numerous fascinating discussions about life, love and biomechanics. In particular, his attention to detail in reading over

early drafts of work has no doubt improved the quality of this dissertation. I am also appreciative for the encouragement and good cheer he provided during the stressful times.

This work could have not been performed without the efforts of our collaborators at the Australian Institute of Sport, particularly Doug Rosemond, Nick Brown and Peter Blanch. I wish to express my gratitude for helping with the data collection required for my research, and making every effort to ensure that the data was of the highest quality possible. I am a firm believer that the integrity of findings obtained from any experimental project directly reflects the quality of the data, so I thank you for investing your time in this project.

On a more personal level, I am profoundly indebted to my parents, Eric and Elizabeth Dorn and my brother, Andrew, for their endless encouragement and unwavering support during my academic pursuits. My determination and motivation to perform at the best of my ability has risen from your love and support over the many years. And thanks Mum, for the many meals you prepared during the long nights spent in the office!

During the course of my research, I have found a passion for science and developed new life skills, technical skills, communication skills, patience (desperately needed, but not quite refined) — but above all I have found great friendships which has made coming into work fun each and every day. So I would like to conclude by thanking my fellow researchers, past and present: Massoud Akbarshahi, David Ackland, Jay Yu, Farzad Keynejad, Dale Robinson, Kay Crossley, Josien van den Noort, Mariana Kersh and Katie Ewing whose good humour and companionship helped get me through to completion, and I sincerely hope that our paths will cross once again in life.

Contents

1	Introduction	1
1.1	Motivation for the study of running	1
1.2	Rationale for simulating human movement using computer-based musculoskeletal models	3
1.3	OpenSim: software for simulating human movement	6
1.4	Contributions of the dissertation	7
1.5	Outline of the dissertation	8
2	Background	11
2.1	Fundamental biomechanical variables in running	11
2.1.1	The running stride cycle	11
2.1.2	Acceleration and steady-state stages of running	13
2.1.3	Stretch-shortening cycle	14
2.1.4	Stride length and stride frequency	15
2.1.5	Relationship between effective vertical impulse and stride length in running	17
2.2	Limits to running speed	19
2.3	Challenges in modelling and simulating human running	20
2.4	Computer-based joint models to study running	21
2.5	Dynamic coupling in the skeleton	24
2.6	Contact between the foot and ground	25
2.7	Muscle function in running	26
2.7.1	Electromyographic studies of running	26
2.7.2	Computer-based musculoskeletal models to study running	28
2.8	Specific questions addressed in this dissertation	31
3	Methods	33

CONTENTS

3.1	Experimental data collection	35
3.1.1	Recruitment Process	35
3.1.2	Subject Preparation	35
3.1.3	Data collection protocol	41
3.1.4	Data preprocessing	42
3.2	Computational model analyses	42
3.2.1	Model scaling	44
3.2.2	Inverse kinematics	46
3.2.3	Inverse dynamics	47
3.2.4	Static optimisation	48
3.2.5	Musculotendon force evaluation	52
3.2.6	Power and work calculations	52
3.2.7	Pseudo-inverse induced acceleration analysis	54
3.2.8	Instantaneous segment power decomposition	65
4	Comparison of ground contact models	67
4.1	Introduction	69
4.2	Methods	70
4.3	Results	75
4.4	Discussion	82
4.4.1	Influence of kinematic constraints	82
4.4.2	Influence of the number of foot-contact points	86
4.4.3	Superposition errors across foot-contact models	88
4.4.4	Limitations and future work	89
5	Mechanical strategy shift in running	91
5.1	Introduction	93
5.2	Methods	95
5.2.1	Ethical approval	95
5.2.2	Experimental protocol	95
5.2.3	Musculoskeletal model	97
5.2.4	Ground contact model	98
5.2.5	Data analysis	98
5.2.6	Data presentation and statistical analysis	101
5.3	Results	102
5.3.1	Dependence of stride length and stride frequency on running speed	102
5.3.2	Lower-limb muscle forces in running	104
5.3.3	Muscle function during stance	105
5.3.4	Muscle function during swing	108
5.4	Discussion	110

5.4.1	Hypothesis 1: The ankle plantarflexors are mainly responsible for increasing stride length during stance.	115
5.4.2	Hypothesis 2: The hip muscles are mainly responsible for increasing stride frequency during swing.	116
5.4.3	Biological limit to running speed	117
5.4.4	Limitations of the study	119
5.4.5	Summary	122
6	How leg muscles power human running	123
6.1	Introduction	125
6.2	Methods	127
6.2.1	Experimental data collection	127
6.2.2	Musculoskeletal model	128
6.2.3	Model analyses	130
6.3	Results	132
6.4	Discussion	135
6.4.1	Muscle contributions to external power during the stance phase	140
6.4.2	Muscle contributions to internal segment power during the swing phase	141
6.4.3	Power transfer between limb segments	142
6.4.4	Limitations of the study	143
6.4.5	Summary	143
7	Summary and future work	145
A	Musculoskeletal model	151
A.1	Musculoskeletal model equations	151
A.1.1	Rigid body equations of motion	152
A.1.2	Musculoskeletal geometry	154
A.1.3	Muscle contraction dynamics	155
A.1.4	Foot-ground contact model	156
A.2	Musculoskeletal models in this thesis	159
A.3	Reserve actuators and specific tension of muscle	165
A.4	Pelvic coordinate system	169
A.5	Hamstring EMG and joint moment paradox	169
A.5.1	Hip and knee joint moments	170
A.5.2	Ground reaction force filter frequency	172
B	Gait-Extract toolbox	175
B.1	Coordinate systems	176

CONTENTS

B.2	Foot detection algorithm	176
B.3	Center-of-pressure calculation	179
B.4	EMG processing	182
C	Modelling results: Quick reference	185
D	Supplementary publications	219
	References	263

List of Tables

3.1	Marker set description used for motion data capture	37
3.2	EMG electrode layout used for EMG data capture	39
3.3	Individual subject running speeds	40
3.4	Constraint weightings w for each foot contact point	60
4.1	Summary of the six ground-contact models evaluated in this study	73
4.2	Peak force contributions to the ground reaction force in walking	78
4.3	Peak force contributions to the ground reaction force in running	79
5.1	Mean stride characteristics	104
A.1	Description of the two musculoskeletal models used in this thesis. DOF represents degrees of freedom.	160
A.2	OpenSim model joint conventions	161
A.3	Individual muscles contained in the musculoskeletal model . .	162

LIST OF TABLES

List of Figures

1.1	100m sprint world record trends	4
1.2	Thesis chapter outline	10
2.1	Running stride cycle	12
2.2	Running performance variables	16
2.3	Point-mass model of running	18
2.4	Muscle contributions to the ground reaction force during running	30
3.1	Experimental and computational pipeline	34
3.2	Experimental marker set	38
3.3	Experimental data capture photos	43
3.4	Musculoskeletal model scaling	46
3.5	Bottom-up inverse dynamics approach	49
3.6	Definition of mechanical power	53
3.7	Multi-scale power calculations in the body	54
3.8	Foot contact locations	56
3.9	Kinematic constraints during stance phase of locomotion . . .	61
4.1	Multiple-point foot contact models	74
4.2	Musculotendon forces and EMG for walking and running . . .	76
4.3	Muscle contributions to the ground reaction force for each contact model in walking	80
4.4	Muscle contributions to the ground reaction force for each contact model in running	81
4.5	Action force contributions to the ground reaction force for each contact model in walking	83
4.6	Action force contributions to the ground reaction force for each contact model in running	84
4.7	Superposition errors generated by each foot contact model . .	85

LIST OF FIGURES

4.8	Foot-ground contact model sensitivity	87
5.1	Three-dimensional full body musculoskeletal model	99
5.2	Stride measurements at each running speed	103
5.3	Musculotendon forces calculated for each running speed	106
5.4	Muscle contributions to the sagittal-plane joint moment for each running speed	107
5.5	Vertical ground reaction force muscle contributions at each running speed	108
5.6	Soleus and gastrocnemius length-velocity profile during running	109
5.7	Hip muscle work trends during the swing phase of running . . .	110
5.8	Muscle contributions to hip and knee joint accelerations at each running speed	111
5.9	Inverse dynamics moments and muscle computed moments for each running speed	113
5.10	Experimental and model predicted ground forces and joint accelerations	114
5.11	Sensitivity of muscle force predictions to the objective function exponent in running at 5.2 m/s and 9.7 m/s	121
6.1	Three-dimensional full body musculoskeletal model	129
6.2	Computational pipeline for computing internal and external power	131
6.3	Musculotendon forces calculated for each running speed	133
6.4	Experimental and model trajectories of hip, knee and ankle joint accelerations for each running speed	134
6.5	Individual muscle contributions to the ground reaction force and external power at all speeds of running	136
6.6	Individual muscle contributions to the trunk and pelvis segment power	137
6.7	Individual muscle contributions to the thigh and shank-foot complex segment power	138
6.8	Ipsilateral muscle contributions to segmental power over a full stride cycle	139
A.1	Musculoskeletal model properties	153
A.2	Musculotendon properties	157
A.3	Foot-ground contact points	158
A.4	Soleus contribution to ground force	159
A.5	Joint and muscle geometry	165

A.6 Comparison between joint torques and muscular torques in sprinting	168
A.7 OpenSim VS anatomical pelvic coordinate systems	170
A.8 Ground reaction forces, hip and knee joint moments, and hamstring forces at different filtering frequencies	173
B.1 Gait-Extract toolbox website	177
B.2 Experimental and model coordinate systems	178
B.3 Calculation of the center-of-pressure	180
B.4 Center-of-pressure enhancement	182
B.5 Comparison of EMG filters	183
C.1 OpenSim musculoskeletal model	186
C.2 Stride measurements at each speed	187
C.3 Pictorial locomotion at each speed	188
C.4 Joint angles at each speed	189
C.5 Musculotendon force at each speed	190
C.6 Calf, quad and hip muscle length-velocity profiles during running	191
C.7 Musculotendon power at each speed	192
C.8 Muscle contributions to sagittal joint moments	193
C.9 Muscle contributions to non-sagittal joint moments	194
C.10 Muscle contributions to the ground reaction force	195
C.11 Action force contributions to the ground reaction force	196
C.12 Ipsilateral muscle contributions to ipsilateral sagittal joint accelerations	197
C.13 Contralateral muscle contributions to contralateral sagittal joint accelerations	198
C.14 Action force contributions to the net sagittal joint accelerations	199
C.15 Ipsilateral muscle contributions to ipsilateral non-sagittal joint accelerations	200
C.16 Contralateral muscle contributions to contralateral non-sagittal joint accelerations	201
C.17 Action force contributions to the net non-sagittal joint accelerations	202
C.18 Muscle contributions to the sagittal joint accelerations during walking 1.5 m/s	203
C.19 Muscle contributions to the sagittal joint accelerations during running 3.5 m/s	204
C.20 Muscle contributions to the sagittal joint accelerations during running 5.2 m/s	205

LIST OF FIGURES

C.21 Muscle contributions to the sagittal joint accelerations during running 7.0 m/s	206
C.22 Muscle contributions to the sagittal joint accelerations during sprinting 9.0 m/s	207
C.23 Muscle contributions to TRUNK and PELVIS segment power	208
C.24 Muscle contributions to THIGH and SHANK-FOOT segment power	209
C.25 Distribution of power from ILPSO, GMAX and GMED to the body segments	210
C.26 Distribution of power from HAMS, RF and VAS to the body segments	211
C.27 Distribution of power from GAS, SOL and TIBANT to the body segments	212
C.28 Contribution of muscle powers to the total model power	213
C.29 Muscle contributions to components of total model power	214
C.30 Musculotendon work done by individual muscles at each speed	215
C.31 Musculotendon work transfer to limb segments by individual muscles at each speed	216
C.32 Angular momentum of legs and arms at each speed	217
C.33 Residual loads between the pelvis and environment	218

Chapter 1

Introduction

1.1 Motivation for the study of running

This dissertation is concerned with the biomechanics of human running. Running is one of the world's most popular sporting and leisure activities and participation rates continue to grow each year. Originally, this popularity was driven by the running boom of the 1970s and '80s, but today is mainly driven by both the low costs and large health benefits associated with running: improved cardiovascular function, reduced risk of heart disease, improved blood pressure, improved bone density, weight management and mental alertness, to name a few. Indeed, in 2011, over 13 million US citizens finished in one of 22,800 road running events held throughout the year. This rate represents an increase of 300% from 1989 and is showing no signs of slowing down in the future (<http://runningusa.org>).

Despite the increased popularity in running, the rate of injury, even to this day remains exceptionally high and is not showing signs of decline. A recent systematic review reported the incidence rates of lower extremity running injuries ranged from 19.4% to 79.3% with the most common injury sites being the lower leg (shin, Achilles tendon, calf, and heel) and upper leg (hamstring, thigh, and quadriceps), with incidence rates ranging from 9.0% to 32.2%, and 3.4% to 38.1%, respectively (van Gent et al., 2007).

The majority of these injuries require specialised medical attention (Byrnes et al., 1993) and are likely to re-occur in the future (van Mechelen, 1992). Several studies have attributed the indirect cause of running related injuries to training related factors, health factors and lifestyle factors (Macera et al., 1989; Walter et al., 1989; Macera et al., 1991; Wen et al., 1998; Satterthwaite et al., 1999); however, a fundamental understanding of the musculoskeletal mechanics of running is required to begin to identify the direct causes of injury if there is to be any chance of reducing its frequency.

Running, like any human movement, is achieved through the contraction of skeletal muscle. Forces developed in muscles are transmitted to the bones of the skeleton, generating rotational moments at each of the joints, thus accelerating the joints in a coordinated manner. Musculoskeletal injuries may occur when the forces or strains exhibited by muscles exceed critical limits (acute injury), or when a number of muscles act together to produce a combined fatigued effect above and beyond some critical limit (chronic overuse injury) (Nigg, 1985).

Musculoskeletal injuries in running have been widely studied from a biomechanical perspective with the objectives of identifying causal and preventative factors (Winter and Bishop, 1992; Byrnes et al., 1993; Novacheck, 1995; Hreljac et al., 2000; Hreljac, 2004, 2005); however, because the vast majority of research is not based on quantitative estimates of loads and strains developed by individual muscles, only limited references can be made about the mechanisms that cause injury to occur. Unfortunately, the majority of research in the field of injury prevention has not translated to a reduction in overall injury rates (Nigg, 2001), suggesting that the biomechanical basis of injury is not yet well understood. Studies investigating musculoskeletal injuries in running should therefore be based on the mechanical loads and strains being exerted by the *individual muscles* of the lower-limb joints.

There is also a more fundamental motivation for studying the mechanics of running. A simple but elusive goal shared by athletes, coaches and sport scientists alike is to maximise running performance and improve overall technique. In the last century, world 100 m sprinting times have

1.2. RATIONALE FOR SIMULATING HUMAN MOVEMENT USING COMPUTER-BASED MUSCULOSKELETAL MODELS

continued to improve (Fig. 1.1), perhaps reflecting the progressive development of sprint technique and application of plyometric strength training. With the help of ever improving training equipment and computer aided analysis it is possible to identify and develop athletes' strengths better than ever before. However, most research studies completed to date with regards to improving running technique and performance have been based on measurements of joint motion and ground reaction forces (Davies, 1980; Mero et al., 1992; Delecluse et al., 1995; Keller et al., 1996; Delecluse, 1997; Thordarson, 1997; Weyand et al., 2000; Kivi et al., 2002; Myer et al., 2007; Weyand et al., 2009, 2010; Salo et al., 2011). For example, although it is well known that achieving greater stride lengths and/or stride frequencies will increase running speed, the specific muscular strategies that generate these changes are yet to be determined. Again, understanding how running speed is increased requires a set of analyses that are capable of quantifying the forces and strains being developed by *individual muscles* throughout the stride cycle.

1.2 Rationale for simulating human movement using computer-based musculoskeletal models

Direct non-invasive experimental measurement of muscle force *in vivo* is not possible. Although invasive techniques such as strain-gauge transducers have been used to measure muscle forces in living humans (Komi et al., 1987; Fukashiro et al., 1995; Komi et al., 1996; Komi, 2000), ethical considerations discourage their regular use. Moreover, such methods are limited to measuring the force of a single muscle and therefore cannot be used to investigate the coordination of multiple muscles working in synergy to achieve a common goal. Computer-based musculoskeletal models, consisting of a multibody representation of the lower limbs and driven by physiological musculotendon actuators, are attractive alternatives for investigating muscle coordination in locomotion because they provide the

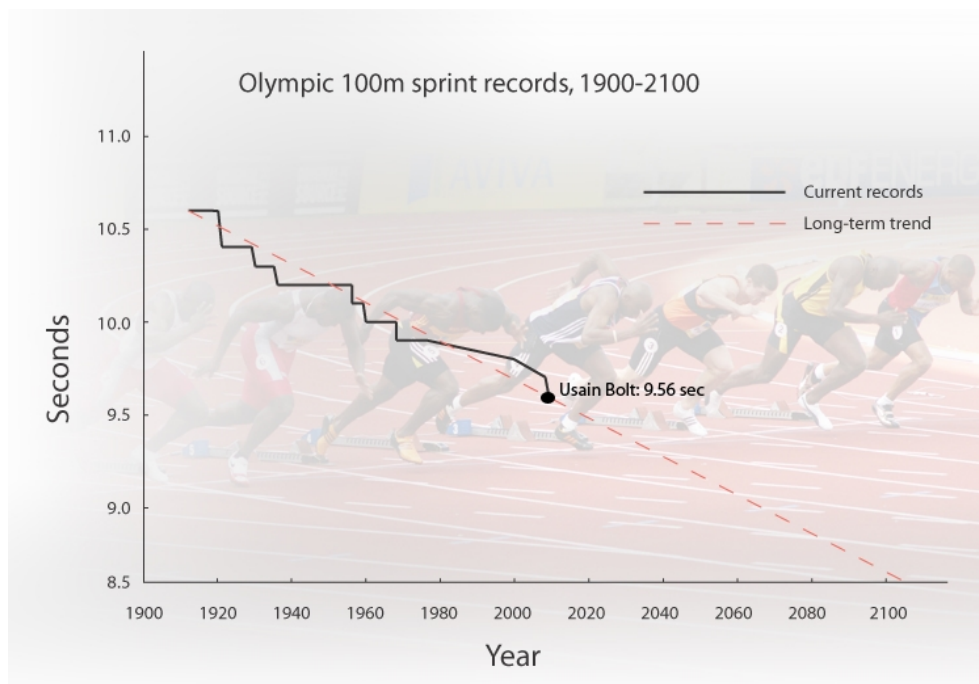


Figure 1.1: 100m sprint world record trends from 1900 to 2010 and linear extrapolation to 2100. Adapted from <http://www.futuretimeline.net/21stcentury/2060-2069.htm>

capability to quantitatively predict the loads and strains developed by individual muscles.

One of the main challenges in predicting muscle forces in computer-based musculoskeletal models, however, is the *muscle force distribution problem* (Crowninshield, 1978). Because there are many more muscles than joints in the lower limbs, the musculoskeletal system is redundantly actuated; i.e., there exists an infinite set of different muscle force combinations, each potentially generating the same movement. The selection of one particular combination from a vast pool is a decision making process influenced largely by the performance criterion (alternatively known as the objective or cost function). Optimisations that are subject to a performance criterion provide a unique solution to the muscle force distribution problem and therefore result in quantitative predictions of muscle forces required to generate a given movement. The a

1.2. RATIONALE FOR SIMULATING HUMAN MOVEMENT USING COMPUTER-BASED MUSCULOSKELETAL MODELS

priori knowledge of model-predicted muscle force then opens the door to analyses that are impossible to conduct experimentally — such as the capability to estimate how individual muscle forces contribute to the angular acceleration of lower-limb joints and the acceleration of the whole-body center-of-mass (herein referred to as *muscle function*). Such biomechanical quantities ultimately define the functional role of a muscle, providing new insights into the coordination strategies that underlie human movement (Pandy, 2001; Delp et al., 2007; Erdemir et al., 2007; Heintz and Gutierrez-Farewik, 2007; Pandy and Andriacchi, 2010).

Computer-based musculoskeletal models can also be particularly advantageous for investigating the mechanics of a specific muscle group, such as the hamstrings in sprinting (Thelen et al., 2006; Schache et al., 2010; Chumanov et al., 2011). This is because computer models have the capacity to estimate a number of additional and potentially significant parameters within the muscle that are relevant to its function. For example, computer models allow a time history of musculotendon length to be calculated during dynamic movements. This parameter is likely to be of particular relevance in the context of muscle strain-type injuries, as animal-based studies have provided experimental evidence demonstrating that the amount of change in musculotendon length that occurs during repeated eccentric contractions is highly related to the severity of the subsequent muscle damage (Lieber and Friden, 1993; Talbot and Morgan, 1998). The accuracy with which computer models reflect the anatomy and anthropometry of the individual has been extensively evaluated during walking, running and jumping (Delp and Loan, 1995; Anderson and Pandy, 1999; Arnold et al., 2000; Anderson and Pandy, 2001a; Raikova and Prilutsky, 2001; Liu et al., 2006; Chumanov et al., 2011; Hamner et al., 2010). Hence, they form an invaluable tool for conducting non-invasive musculoskeletal analyses for understanding motor control in human movement.

1.3 OpenSim: software for simulating human movement

OpenSim (<https://simtk.org/home/opensim>) is an open-source biomechanical research platform intended for simulating, visualizing and analysing biological movement using detailed computer models of the musculoskeletal system (Delp et al., 2007). Beginning with a generic musculoskeletal model (Delp et al., 1990; Anderson and Pandy, 1999), analyses can be performed to investigate the coordination of movement. Musculoskeletal models can be made publicly available and are often reused for multiple investigations because they provide a rich set of behaviours that enable different lines of inquiry. OpenSim was the primary software package used throughout this dissertation and was chosen for three reasons:

MULTI-SCALE DYNAMICS: Multiple scales of inquiry can be represented to generate a simulation of movement in the OpenSim framework (see Appendix A.1). On a biological scale, time delays representing the binding of myosin and actin to form cross-bridges are approximated as first order differential equations, resulting in muscle activation. Activations that cause contractions of the muscle fibres are represented by Hill-type musculotendon models, which take into account the physiological force-length-velocity properties of muscle (Hill, 1938; Katz, 1939). On a macro-mechanical scale, the bones and joints of the skeleton through which musculotendon forces are transmitted are represented using rigid body mechanics (i.e., the Newtonian equations of motion). These systems are coupled together, resulting in detailed multi-scale models of the musculoskeletal system.

MODEL VISUALISATION: Animating the solution of an analysis helps to identify the relative success or failure of its implementation. OpenSim provides the capability for visualising the model's kinematics, muscle forces and internal parameters (e.g., model-based marker locations, segment center-of-mass locations, joint axes, joint centers, muscle

attachment points and muscle paths). This helps to debug analyses when they fail, and provides increased confidence in the results when they succeed.

OPEN SOURCE SOFTWARE: OpenSim is open-source software that is freely available at <https://simtk.org/home/opensim>. It has a growing user base, and allows a range of musculoskeletal models, custom made actuators and custom made analyses to be easily shared and distributed. Most importantly, OpenSim provides a common platform where the research of others can be easily reproduced and extended. Overall, this facilitates external collaboration, extensible code, faster learning and the sharing of knowledge. In this dissertation, a custom plug-in analysis and toolbox was developed for the OpenSim platform in the hope of providing additional research tools to investigators for the future (see Preface).

1.4 Contributions of the dissertation

The objective of this dissertation was to extend the current understanding of human running by: (i) recording the overground movement patterns of habitual runners across a wide range of running speeds; and (ii) simulating these running experiments using computer-based musculoskeletal models in OpenSim. Three specific areas of research outlined below were chosen as a focus for the dissertation, based on broad questions related to muscle coordination that would most benefit the academic and clinical communities across multiple disciplines (e.g., physiology, sports science, biomechanical engineering and computer modelling):

1. Evaluate the effectiveness and suitability of a range of commonly used foot-ground contact models to determine the most suitable contact model for estimating muscle function in both walking and running.
2. Identify key muscle groups responsible for accelerating the lower limbs and center-of-mass as running speed increases from slow running to maximal sprinting.

3. Determine how the mechanical energy derived from muscles is transferred to the skeleton as running speed increases from slow running to maximal sprinting.

1.5 Outline of the dissertation

The outline of the dissertation is presented in Fig. 1.2 and describes the specific research questions stated in Section 1.4.

- Chapter 2 presents a thorough review of the literature with an emphasis on experimental and computational studies of human running.
- Chapter 3 describes the methods used to collect experimental data and describes the computational analyses performed to determine muscle function.
- Chapter 4 evaluates the sensitivity of the calculations of muscle function to the model used to simulate foot-ground interaction.
- Chapter 5 investigates how muscles work together to increase stride length and stride frequency, which together, constitute overall running speed.
- Chapter 6 investigates how muscles transmit energy to the body segments to power the running stride cycle, from slow running to maximal sprinting.
- Chapter 7 summarises the major findings of each chapter and highlights key areas where future work would provide greater confidence in musculoskeletal simulations of running.
- Appendix A describes the OpenSim musculoskeletal model in detail with an emphasis on model equations and parameters.
- Appendix B describes the raw data processing techniques using the Gait-Extract toolbox.
- Appendix C provides a comprehensive set of modelling results during self-selected walking and all speeds of running. Together, these results constitute a complete dataset — they are not all used within the studies of this thesis, but rather, may be used as reference material for future

1.5. OUTLINE OF THE DISSERTATION

work.

- Appendix D contains a set of co-authored supplementary publications related to but not directly part of this dissertation:

What are the roles of individual muscles in human running?

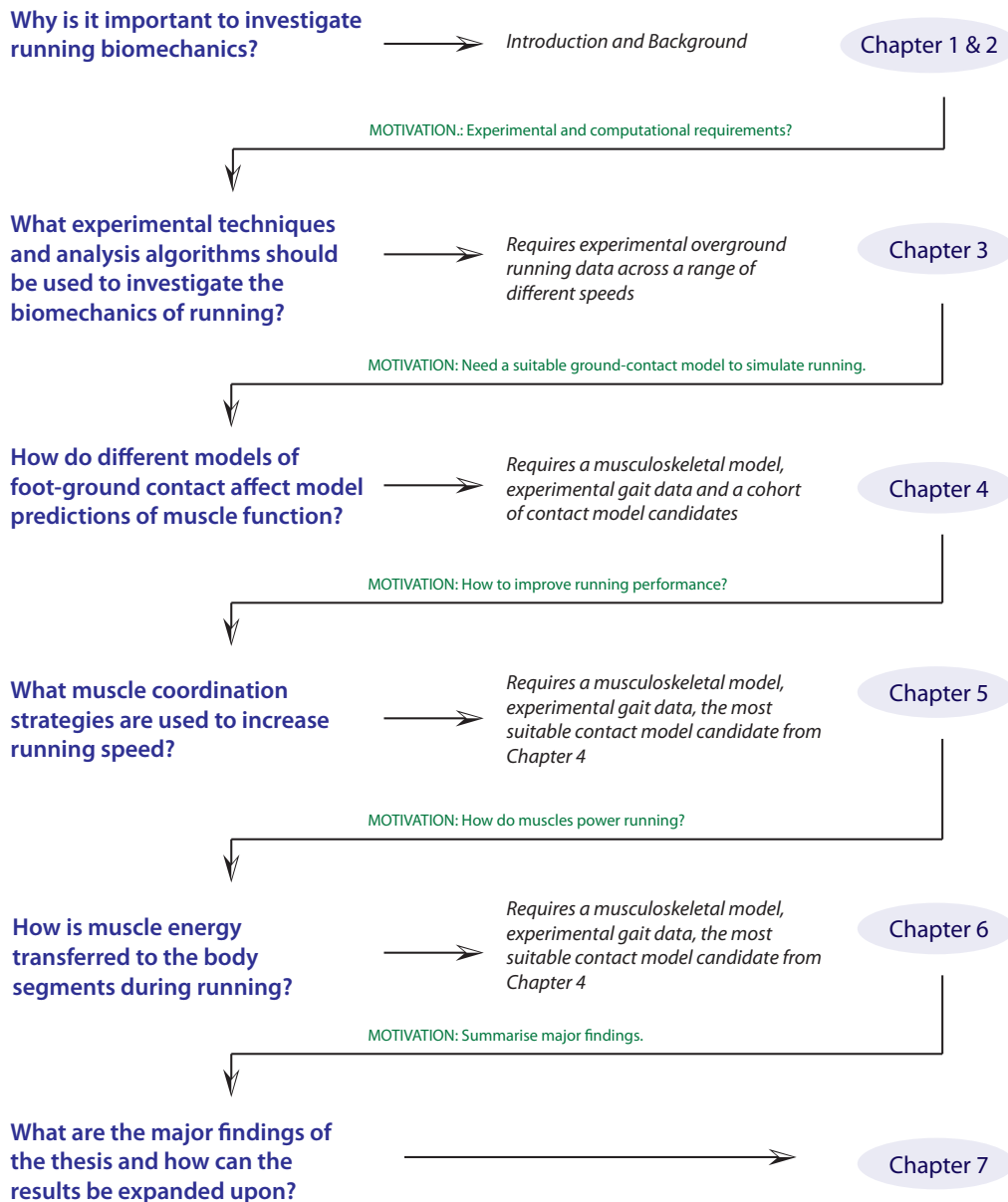


Figure 1.2: Thesis chapter outline presented as a flow chart.

Chapter 2

Background

This chapter provides a comprehensive review of the running biomechanics literature. It begins by reviewing the fundamental biomechanical variables associated with running with a focus on experimental *in vivo* studies, after which a computational perspective is taken, discussing the insights provided by modelling and simulation studies with their associated limitations. The chapter concludes with the specific questions addressed by this dissertation.

2.1 Fundamental biomechanical variables in running

2.1.1 The running stride cycle

A typical stride cycle of steady-state running is illustrated in Fig. 2.1. The stride cycle begins and ends at initial ground contact on the ipsilateral leg. Like walking, running contains a stance phase where the foot is in contact with the ground, and a swing phase where the foot is not in contact with the ground. The demarcation between walking and running occurs when periods of double-support during the stance phase of the stride cycle (both feet are simultaneously in contact with the ground) give way to two periods of double-float at the beginning and the end of the swing phase of gait (both feet are off the ground).

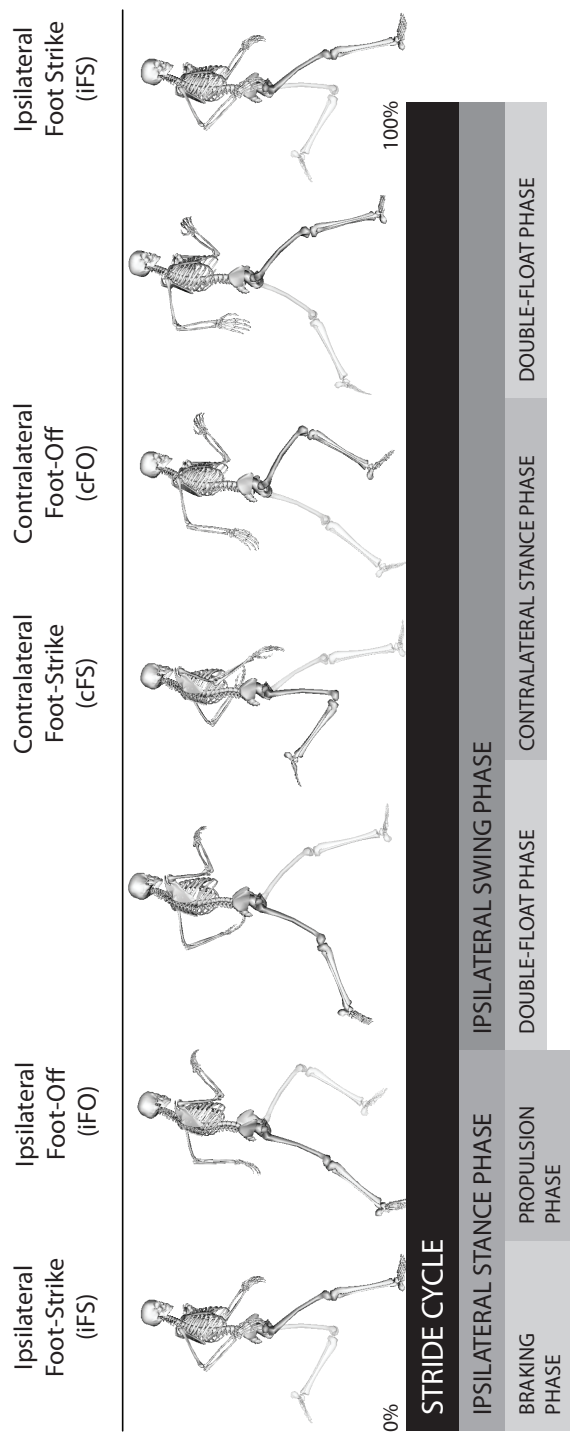


Figure 2.1: The running stride cycle for a subject running at 5.0 m/s. The stride cycle consists of a stance (ground contact) and swing phase. The swing phase can be further divided into the contralateral stance phase and aerial times where both feet are off the ground.

2.1. FUNDAMENTAL BIOMECHANICAL VARIABLES IN RUNNING

During double-float, assuming negligible air resistance, gravity is the only external force acting on the body and therefore completely governs the motion of the center-of-mass (Willems et al., 1995). Although muscles may still act to accelerate the joints of the body during aerial time, motion of the center-of-mass can only be influenced by muscles when external contact is made between the foot and the ground. During the stance phase, muscles transmit their loads through adjacent segments, terminating at the ground (Section 2.5). From Newton's Third Law of Motion, the actions of the muscles at the ground produce an equal and opposite ground reaction force, which then, together with gravity, act to accelerate the center-of-mass vertically (i.e., up and down), horizontally (i.e., forwards and backwards) and mediolaterally (i.e., left and right).

2.1.2 Acceleration and steady-state stages of running

Running can be decomposed into two distinct stages, both of which are equally important in developing running technique: the acceleration stage and the steady-state stage. The acceleration stage is concerned with reaching maximum speed in the least amount of time, beginning from rest. For this to happen, the application of ground forces in a predominantly horizontal direction is required to project the center-of-mass of the body forwards (Corn and Knudson, 2003). The forward propulsion ground reaction force during the acceleration stage was found to be 46% greater than during the steady-state stage (Mero, 1988), emphasising the importance of muscle power generation and transfer during acceleration. The extent to which muscles directly contribute to the rapid augmentation of horizontal ground force during the acceleration phase of running, however, remains unknown. Using computer-based musculoskeletal models to simulate the acceleration phase of running would allow individual muscles to be targeted for plyometric training and may provide a competitive edge to those involved in competitive athletic sports.

The steady-state stage of running is concerned with maintaining a maximal running velocity for as long as possible without fatigue or subsequent deceleration. Although the body undergoes periods of

deceleration and acceleration, respectively, within the stance phase of the stride (Fig. 2.1), the steady-state stage of running occurs when the *average* stride acceleration is zero. Here, the primary emphasis is on mechanical efficiency and endurance, requiring the management of vertical ground forces to support the body against gravity (Weyand et al., 2000, 2010). At steady-state speeds of maximal sprinting, vertical forces as high as 4.6 times body weight and ground contact times as low as 94 ms have been recorded (Mero et al., 1992), suggesting that the muscles which make up the vertical ground force must be capable of developing large forces and do so in small amounts of time. Furthermore, the ground reaction forces developed by muscles should be generated as effectively as possible, thus utilising the stretch-shortening cycle to minimise energy loss (Komi, 1984, 2000; Kubo et al., 2000; Hennessy and Kilty, 2001; Ishikawa and Komi, 2007; Lichtwark et al., 2007).

2.1.3 Stretch-shortening cycle

The stretch-shortening cycle can be simply defined as a stretch of muscle or tendon followed by an immediate shortening (Roberts et al., 1997; Komi, 2000). Although stretch-shortening cycles are exhibited by all leg muscles to some extent during locomotion, they are of particular importance in the calf muscles (i.e., soleus and gastrocnemius) (Kubo et al., 2000; Ishikawa and Komi, 2007; Ishikawa et al., 2007; Lichtwark et al., 2007). In walking, gastrocnemius fibres were discovered to isometrically contract during the stance phase allowing the muscle to operate at its plateau region on the force-length curve, and develop force with great efficiency. At the same time, the passive elastic tendon and aponeurosis performed cycles of stretch-shortening, storing elastic strain energy in the first half of stance and then releasing the same energy in the second half of stance to propel the body forwards.

In running, the gastrocnemius fibres were observed to shorten throughout the *entire* stance phase. According to the force-velocity relation of muscle, this means that muscle forces cannot be developed as effectively in running as they can in walking. In addition, the contractile velocity of

2.1. FUNDAMENTAL BIOMECHANICAL VARIABLES IN RUNNING

the gastrocnemius has also been shown to increase with increasing running speed, further diminishing the capacity of the muscle to generate force. Electromyography studies have also shown the gastrocnemius to be increasingly activated as running speeds increase (Kyrolainen et al., 2005; Gazendam and Hof, 2007), so that the increased ankle plantarflexion moments can be satisfied under adverse contractile velocity conditions. If greater forces are required from the gastrocnemius as running speeds increase, there will likely be a time where the gastrocnemius is maximally activated and unable to generate further ankle plantarflexion moments.

Stretch-shortening is not observed in the muscle itself during the stance phase of running, but the Achilles tendon has been shown to maintain effective utilisation of elastic strain energy by stretching and shortening during stance (Ishikawa and Komi, 2007; Ishikawa et al., 2007), illustrating the complex interactions between muscle and tendon in human movement. Ultimately, the forces produced by muscles and tendons in the lower limbs are transferred to the bones to produce coordinated motion. With regard to running, an important question is: how do the actions of individual muscles help to increase running speed?

2.1.4 Stride length and stride frequency

Stride length is the horizontal distance travelled in a single stride (e.g., ipsilateral foot-strike to ipsilateral foot-strike). Stride frequency is the measure of how many strides can be completed in one second. Together, the relationship between stride length (λ), stride frequency (f) and running speed (v) can be represented by a simple equation: $v = \lambda \times f$. Therefore, the key to increasing running speed lies in the body's ability to (i) push on the ground harder and increase stride length; or (ii) push on the ground more frequently and increase stride frequency (Luhtanen and Komi, 1978; Mann and Herman, 1985; Hunter et al., 2004; Salo et al., 2011).

Pushing on the ground harder means that larger forces are transmitted to the ground, which increases the distance covered by each stride, i.e., stride length (see Section 2.1.5). Pushing on the ground more frequently means that the lower limbs must swing through more rapidly in preparation for

foot-strike, thereby increasing the number of strides performed per second, i.e., stride frequency. Although faster running speeds can be theoretically achieved by increasing one or both of these variables, manipulating these changes in practice is difficult because stride length and stride frequency are not independent. Indeed, these two variables are approximately inversely related (Cavagna et al., 1988; Kaneko, 1990; Cavagna et al., 1991; Weyand et al., 2000; Hunter et al., 2004), so that an improvement in running speed will be achieved only when an increase in one variable is not countered by an equal or larger decrease in the other. The precise relationship between stride length and stride frequency is a complex one, consisting of the outcome of many mechanical and neuromuscular processes (Fig. 2.2), making the investigation of coordination strategies for increasing running speed challenging.

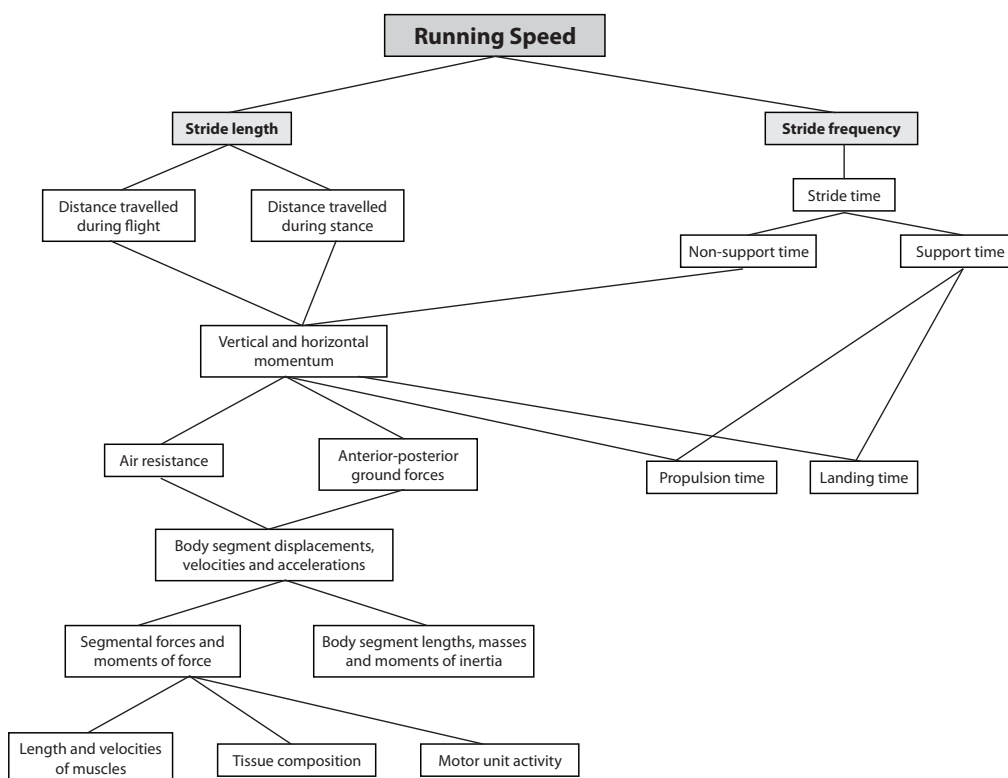


Figure 2.2: Schema of biomechanical factors in running. Adapted from Wood (1987).

2.1.5 Relationship between effective vertical impulse and stride length in running

Despite the complex relationship between stride length and stride frequency, simplified models of running can nevertheless be used to understand their causes. For a specific example, we show that using a simple point-mass model of running, a relationship can be derived between the effective vertical impulse generated by the leg muscles during stance (I_v^{eff}) and stride length (L) achieved by the body during running (see Fig. 2.3). Assume that the body is represented by a point mass m and consider the stride cycle divided into a stance phase ($t = 0$ to $t = i$) and a swing phase ($t = i$ to $t = f$). Furthermore, assume that the vertical velocity of the body at foot-strike ($t = 0$ and $t = f$) is equal and opposite to the vertical velocity of the body at foot-off ($t = i$), thus:

$$v_f = v_0 = -v_i \quad (2.1)$$

Applying the impulse-momentum theorem in the vertical direction, a relation can be found between the effective vertical ground impulse (I_v^{eff}) and the vertical velocity at foot-off:

$$\int_{t=0}^{t=i} F_v dt = I_v^{eff} = m(v_i - v_0) = 2mv_i \quad (2.2)$$

$$v_i = \frac{I_v^{eff}}{2m} \quad (2.3)$$

Furthermore, assuming that: i) the vertical position of the body is the same at foot-strike and foot-off; and ii) the vertical acceleration of the body is only due to the force of gravity ($a_y = 9.8 \text{ ms}^{-2}$), the kinematic equations governing motion of the body in the vertical direction can be used to solve for the time spent in the air (t_{aerial}) as follows:

$$4.9t_{aerial}^2 - \left(\frac{I_v^{eff}}{2m}\right)t_{aerial} = 0 \quad (2.4)$$

$$t_{aerial} = \frac{I_v^{eff}}{9.8m} \quad (2.5)$$

Given that running speed (v_{run}) is constant and applying the kinematic equations of motion in the horizontal direction, stride length (L) can be found as a function of the effective vertical ground impulse (I_v^{eff}):

$$L = v_{run} \cdot t_{aerial} = \frac{v_{run} I_v^{eff}}{9.8m} \quad (2.6)$$

Equations 2.5 and 2.6 show that increases in the effective vertical ground impulse will increase aerial time and produce larger stride lengths during running.

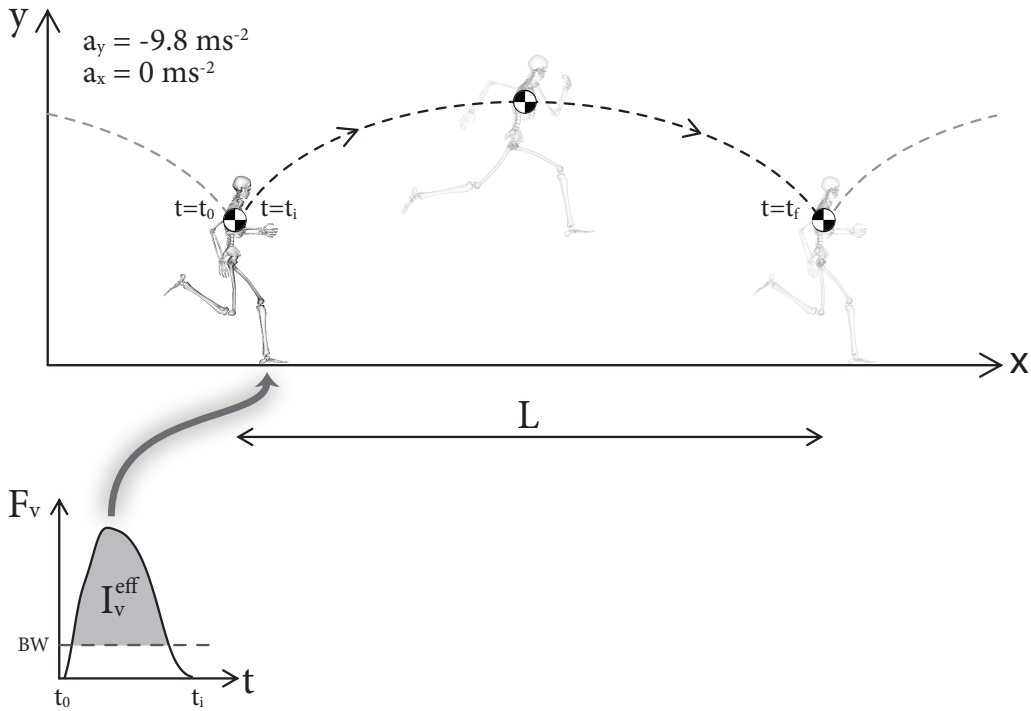


Figure 2.3: Point-mass model used to derive the relationship between effective vertical ground impulse (I_v^{eff}) and stride length (L). Symbols appearing in the diagram are defined in the text.

2.2 Limits to running speed

Previous research has shown that to achieve speeds greater than ~ 7.0 m/s, runners appear to become increasingly reliant upon more frequent ground contacts of similar force magnitudes rather than more forceful ground contacts (Weyand et al., 2000). This study has also suggested that the force applied to the ground determines not only the stride length but also the stride frequency. Because stride frequency is comprised of both stance phase time (i.e., ground contact time) and swing phase time, a reduced duration of either component will increase stride frequency. Weyand et al. (2000) showed that faster runners at their maximum speed had identical swing phase times to slower runners at their maximum speed, and concluded that stride frequency is increased solely by a reduction in ground contact time. Kinetic studies on elite athletes have similarly shown that faster sprinters tend to spend less time on the ground than slower sprinters (Kunz and Kaufmann, 1981; Mann, 1981; Mann and Herman, 1985).

A decrease in ground contact time requires the lower-limb muscles to generate larger forces in smaller periods of time to support the body against gravity and accelerate the center-of-mass upwards. The potential for skeletal muscle to generate and transmit such forces to the ground may be compromised as running speed limits are approached. For example, the muscles that accelerate the body vertically must contract at progressively larger velocities as the speed of running increases, potentially reducing their power output according to the force-velocity relation of muscle (Cavagna et al., 1971). Of particular interest are the calf muscles (i.e., soleus and gastrocnemius), which undergo significant periods of stretch-shortening during ground contact (Section 2.1.3) (Komi, 1984, 2000; Kubo et al., 2000; Hennessy and Kilty, 2001; Ishikawa and Komi, 2007; Lichtwark et al., 2007). Indeed, it has been suggested that the stance phase limits to running speed are imposed not by the magnitude of force that the lower-limb muscles must apply to the ground, but by the time available for these forces to be generated (Weyand et al., 2010).

To substantiate this assertion, the individual muscles which contribute

to the vertical ground reaction force need to be quantified — this is currently only possible through the use of computer-based musculoskeletal models (Section 1.2). The remainder of this chapter will be devoted to joint and muscle function during running, but from the perspective of computer model analyses.

2.3 Challenges in modelling and simulating human running

In contrast to walking, very little work has been done using computer-based musculoskeletal models to understand the mechanics of running, despite the surge in the popularity of running and the high incidence of injury. Three possible reasons for this are described below.

First, walking represents the dominant mode of locomotion in humans, so a scientific understanding of walking will have far greater impact on the general population than in running. Moreover, many walking disabilities exist in both the young (e.g., cerebral palsy) and the old (e.g., osteoarthritis and balance control), severely impacting the mobility and quality of life of these people. A thorough understanding of able-bodied gait in a control population is required to help diagnose the cause of such disabilities and work towards a clinically viable remedy. Musculoskeletal simulations of able-bodied walking in this regard define the set of controls in which simulations of pathological gait can be compared to (Besier et al., 2009; Correa et al., 2011; Correa and Pandy, 2011).

Second, obtaining motion and ground force data in *overground* running is much more difficult than obtaining the same dataset in walking. A laboratory to collect running data would require a significantly larger capture volume than that for walking. Within the larger capture volume, there would need to be a greater number of optical cameras and force platforms. Due to the high costs of laboratory equipment, such laboratories are rare — indeed most experimental studies of running are conducted on force-instrumented treadmills (Thelen et al., 2005; Chumanov et al., 2007; Gazendam and Hof, 2007; Hamner et al., 2010). However, there is evidence to suggest that the

kinematics and ground reaction forces of treadmill and overground running are not always directly equivalent, particularly at higher speeds (Nelson et al., 1972; Elliott and Blanksby, 1976; Frishberg, 1983; Nigg et al., 1995; Riley et al., 2008), implying that fast running and sprinting trials should ideally be recorded overground so that the natural style of gait is unimpeded.

Third, the muscle properties contained in current computer-based musculoskeletal models may not be optimised to simulate running movements (Anderson and Pandy, 2001a; Delp et al., 2007). For example: (i) muscle strengths may not be capable of generating the large joint moments required for sprinting (Thelen et al., 2005; Chumanov et al., 2007); or (ii) muscle moment arms may only be defined over the limited ranges of joint motion suitable for walking and not the extreme ranges of motion observed in sprinting. In addition to these potential modelling limitations, the parameters that define the physiological characteristics of muscle are numerous (see Appendix A.1.3), difficult to measure and difficult to validate from experiments (Thelen, 2003; Klein Horsman et al., 2007; Ward et al., 2009).

2.4 Computer-based joint models to study running

In contrast to muscle properties, the dynamic joint properties of the lower limbs have been well established in the literature. These joint properties include segment masses and inertias, segment lengths and center-of-mass locations, axes of rotation and joint degrees-of-freedom, all of which have been used in inverse dynamics analyses (see Section 3.2.3 and 3.2.6) to compute joint torques, powers and work during running (Chapman and Caldwell, 1983a; Winter, 1983; Ae et al., 1987; Buczek and Cavanagh, 1990; Devita and Skelly, 1990; Simpson and Bates, 1990; Glitsch and Baumann, 1997; Arampatzis et al., 1999; McClay and Manal, 1999; Swanson and Caldwell, 2000; Belli et al., 2002; Kuitunen et al., 2002; Biewener et al., 2004; Yokozawa et al., 2007), and sprinting (Mann and Hagy, 1980; Mann, 1981; Simonsen et al., 1985; Vardaxis and Hoshizaki, 1989; Johnson and

Buckley, 2001; Belli et al., 2002; Kuitunen et al., 2002; Bezodis et al., 2008). Although these studies have provided much insight into the biomechanical function of major lower-limb muscle groups across a range of running speeds, their models do not include muscles. Hence their potential for investigating specific muscle-related mechanisms for increasing running speed and reducing injury is limited.

In addition, most studies have evaluated only certain phases of the stride cycle; specifically, either the stance (Mann and Hagy, 1980; Buczek and Cavanagh, 1990; Devita and Skelly, 1990; Simpson and Bates, 1990; Glitsch and Baumann, 1997; Arampatzis et al., 1999; McClay and Manal, 1999; Belli et al., 2002; Biewener et al., 2004; Bezodis et al., 2008) or swing phase (Chapman and Caldwell, 1983a; Vardaxis and Hoshizaki, 1989; Swanson and Caldwell, 2000). Inverse dynamics studies of running have also obtained data for a single speed (Mann and Hagy, 1980; Mann, 1981; Winter, 1983; Simonsen et al., 1985; Vardaxis and Hoshizaki, 1989; Buczek and Cavanagh, 1990; Devita and Skelly, 1990; Glitsch and Baumann, 1997; Johnson and Buckley, 2001; Bezodis et al., 2008) or have obtained data across a range of speeds but have not included maximal sprinting (Simpson and Bates, 1990; Arampatzis et al., 1999; Swanson and Caldwell, 2000; Biewener et al., 2004; Yokozawa et al., 2007). More importantly, however, almost all studies have utilised a two-dimensional approach focusing exclusively on sagittal-plane dynamics (Mann and Hagy, 1980; Mann, 1981; Chapman and Caldwell, 1983a; Winter, 1983; Simonsen et al., 1985; Vardaxis and Hoshizaki, 1989; Buczek and Cavanagh, 1990; Devita and Skelly, 1990; Simpson and Bates, 1990; Arampatzis et al., 1999; Swanson and Caldwell, 2000; Johnson and Buckley, 2001; Belli et al., 2002; Kuitunen et al., 2002; Biewener et al., 2004; Yokozawa et al., 2007; Bezodis et al., 2008). Both Glitsch and Baumann (1997) and McClay and Manal (1999) demonstrated that during an almost planar movement such as running the lower-limb joints are associated with significant three-dimensional torques, especially in the frontal plane. Furthermore, Stefanyshyn et al. (2006) found a relationship between frontal-plane knee-joint dynamics during running and risk of injury. Even though these studies highlight the potential importance of non-sagittal-plane dynamics during running, data

2.4. COMPUTER-BASED JOINT MODELS TO STUDY RUNNING

from both Glitsch and Baumann (1997) and McClay and Manal (1999) were limited to the stance phase of the stride cycle and a single speed of running only.

Schache et al. (2011a) were the first to evaluate the effects of running speed on the three-dimensional joint kinetics of the lower-limb across the entire stride cycle. In this study, the sagittal-plane torques, net powers and work done at the hip and knee during terminal swing demonstrated the largest increases in absolute magnitude with faster running. In contrast, the work done at the knee joint during stance was unaffected by increasing running speed, whereas the work done at the ankle joint during stance increased when running speed changed from 3.5 m/s to 7.0 m/s, but appeared to plateau thereafter. This result suggests, like Weyand et al. (2000), that a possible change in strategy is used to increase speed beyond 7.0 m/s.

During initial swing, the hip-flexor muscles were found to generate energy at the same time as the knee-extensor muscles absorbed energy, whereas during terminal swing the hip-extensor muscles were found to generate energy at the same time as the knee-flexor muscles absorbed energy. However, calculations of joint work cannot account for the contributions of individual muscles, particularly those that cross more than one joint. For example, despite the hip joint acting as an energy generator and the knee joint acting as an energy absorber, it is not possible to determine whether a biarticular muscle spanning both of these joints (i.e., hamstrings or rectus femoris), is absorbing energy from, or generating energy to the skeleton.

Furthermore, inverse dynamic analyses cannot determine the direction of energy flow into and out of the skeletal segments. As a muscle develops force, mechanical energy is generated to and absorbed from the body segments, providing the power required for limb coordination. Therefore, a fundamental component of muscle function is the extent to which muscles can generate power and transfer it around the skeleton. Indeed, the joints of the skeleton have been previously described to act as “energy straps” by harnessing muscle energy from a moving body segment and transferring that energy to the next

adjacent segment (Novacheck, 1998). In this way, the energy from any muscle can flow through an arbitrary number of adjacent joints and be delivered to any segment of the skeleton. This phenomena is known as dynamic coupling (Zajac and Gordon, 1989), and it plays a vital role in the understanding of human movement coordination.

2.5 Dynamic coupling in the skeleton

A muscle can exert a torque about a joint only if it spans that joint. However, a muscle can simultaneously deliver energy to all segments in the skeleton and thus accelerate all the joints in the skeleton, including those not spanned by the muscle. This effect is a consequence of dynamic coupling, whereby the force applied by a muscle is transmitted through the bones to all the joints in the body (Zajac and Gordon, 1989). If a muscle force contributes to the accelerations of the joints, then it also must contribute to the acceleration of the body's center-of-mass and hence, by Newton's Second Law of Motion (i.e., $F = ma$), to the force exerted on the ground. Thus, the functional role of a muscle may be determined by quantifying its contribution to the ground reaction force, typically measured on force plates embedded into the ground. Specifically: (i) muscles that contribute to the vertical ground reaction force help to accelerate the center-of-mass upwards in the presence of gravity; (ii) muscles that contribute to the anterior-posterior ground reaction force help to accelerate the center-of-mass forwards and backwards; and (iii) muscles that contribute to the mediolateral ground reaction force help to accelerate the center-of-mass medially and laterally to preserve balance and maintain stability.

Dynamic coupling is not limited to muscle forces. Any "action" force acting on the skeleton such as gravity and centrifugal (velocity related) forces also have the ability to influence the accelerations of joints and make contributions to the ground reaction force. For example, at self-selected speeds of walking: (i) gravity was shown to contribute significantly to the mediolateral acceleration of the center-of-mass in stance (Pandy et al., 2010); and (ii) centrifugal forces making important contributions to knee

joint flexion and extension accelerations in terminal-swing (Arnold et al., 2007).

2.6 Contact between the foot and ground

Calculations of leg muscle function as a result of dynamic coupling (i.e., individual muscle contributions to the ground reaction forces and joint accelerations) require contact between the foot and the ground to be modelled. In reality, foot-ground contact during gait represents a complex interaction of physical phenomena (e.g., impact, friction and slipping) that vary throughout the period of ground contact. Moreover, contact takes place over a finite surface area, during which motion of the foot is constrained until horizontal friction can be overcome by muscle action (Wojtyra, 2003; Cheung and Zhang, 2005). Studies that describe leg muscle function in locomotion using computer-based musculoskeletal models often use simplified ways to describe ground contact, herein referred to as *ground contact models*. These simplified ground contact models assume that contact takes place at discrete points on the foot, which vary in number from a single moving point located at the center-of-pressure (Kepple et al., 1997b; Liu et al., 2008; Goldberg and Kepple, 2009; Hamner et al., 2010) to multiple fixed points distributed over the sole of the foot (Neptune et al., 2000; Anderson and Pandy, 2003; Pandy et al., 2010). At each contact point, kinematic constraints are applied, either explicitly as hard constraints (Kepple et al., 1997b; Anderson and Pandy, 2003; Hamner et al., 2010; Pandy et al., 2010) or implicitly, using springs and dampers to simulate foot-ground interaction (Sasaki and Neptune, 2006; Liu et al., 2008). Kinematic constraints alter the motion of the foot and therefore potentially influence the model calculations of muscle function.

Models of ground contact should include the effects of impact, friction and distributed contact, all of which are manifested as kinematic constraints. Unfortunately, the effects of these kinematic constraints cannot be directly measured, and so model predictions of muscle function cannot be rigorously validated. However, a theoretical principle called

“superposition” may be used to gain confidence in the model predictions (Anderson and Pandy, 2003; Hamner et al., 2010; Lin et al., 2011a; Pandy et al., 2010). This principle states that the sum of the contributions of all action forces (e.g., muscles, gravity and centrifugal forces) to the ground reaction force must be equal to the total ground reaction force measured experimentally. Although superposition is a necessary condition for evaluating the accuracy of the model calculations of muscle function, it is not sufficient for determining the validity of the individual contributions of the various action forces to the total ground reaction force. Results obtained from a given model of ground contact may therefore satisfy superposition and still yield erroneous estimates of muscle function.

A thorough evaluation of foot-ground contact models is required to determine how best to proceed in investigating muscle coordination in running. One of the challenges in modelling foot contact patterns in running is that they can vary depending on the running speed and footwear worn by the runner. For example, as running speed increases, initial impact takes place at more anterior positions on the foot, and is located wholly on the toes during maximal sprinting (Nett, 1964; Novacheck, 1998). Furthermore, barefoot runners have been shown to land more often on the fore-foot whereas runners wearing shoes mostly impact on the heel (Lieberman et al., 2010). If the functional roles of individual muscles are to be correctly elucidated for running, ground contact models need to be able to adapt to the contact patterns exhibited by both rearfoot- and forefoot-striking runners. No evaluation of model predictions of muscle function currently exists using a cohort of different contact modelling assumptions.

2.7 Muscle function in running

2.7.1 Electromyographic studies of running

Electromyographic (EMG) activity reveals the complex sequencing of muscle activation in the body and has been used to investigate the roles of lower-limb

muscles at different speeds of running (Mero and Komi, 1987; Jacobs et al., 1993; Kyrolainen et al., 2005; Gazendam and Hof, 2007). In general, more pronounced EMG activity has been observed with an increase in running speed, particularly in the biarticular muscles of the lower-limb.

As running speed increases, greater levels of EMG activity become evident in the gluteus maximus, hamstrings, vasti and gastrocnemius muscles just before initial ground contact (Dietz et al., 1979; Mero and Komi, 1987). In maximal sprinting, the magnitudes of preactivation can range from 50 to 70% of the maximum EMG recorded in stance. Preactivity of the major leg-muscles is important so that the leg becomes sufficiently stiff prior to and at the moment of foot-ground contact, where large impact forces are known to occur. Throughout ground contact, the high activations present in the quadriceps and calf muscles continue to resist impact forces from the ground.

For the biarticular rectus femoris muscle, two distinct phases of EMG activity are present in the stride cycle: one in stance, presumably to generate moments of knee extension; and one in initial swing, presumably to generate moments of hip flexion. As running speed increases, swing phase activity becomes more pronounced than stance phase activity (Mero and Komi, 1987; Kyrolainen et al., 2005), suggesting that the role of rectus femoris as a hip flexor in running is more important than that of a knee extensor, particularly at higher speeds of running (Dillman, 1975).

For the biarticular hamstring muscles, EMG activity was observed to increase during terminal swing and early stance (Jacobs et al., 1993; Kyrolainen et al., 2005; Gazendam and Hof, 2007). Simonsen et al. (1985) have interpreted this phenomenon as the hamstrings storing energy in terminal swing when they are eccentrically contracting, and releasing them during concentric contractions in early stance.

There are however, several limitations associated with EMG studies of muscle function. First, to evaluate an assertion on the role of a muscle based on EMG data alone can be problematic. For example, inferences on muscle function assume that the muscle is generating force. EMG activity alone is not a direct indicator of muscle force. Muscles that contract at

great velocities or contract in adverse fibre-length ranges have severely compromised force generating capacities, regardless of activation (Zajac, 1989). Second, additional muscle quantities may be required to determine the true potential of its function. For example, a muscle's contraction velocity is required in addition to EMG data to determine whether the muscle is contracting eccentrically or concentrically and therefore providing negative or positive work to a joint (Simonsen et al., 1985). Finally, non-invasive measurements of EMG activity are limited to superficial muscles, and quantitative estimates of muscle excitation are difficult to obtain experimentally (Lloyd and Besier, 2003; Buchanan et al., 2004; Kyrolainen et al., 2005).

2.7.2 Computer-based musculoskeletal models to study running

To evaluate muscle coordination strategies in running, quantitative estimates of the individual muscle forces are first required. Several studies have used musculoskeletal models to estimate muscle forces from experimental running data (Glitsch and Baumann, 1997; Sasaki and Neptune, 2006; Chumanov et al., 2007; Yokozawa et al., 2007; Hamner et al., 2010; Pandy and Andriacchi, 2010; Schache et al., 2010; Chumanov et al., 2011), but most experiments were conducted on instrumented treadmills (Glitsch and Baumann, 1997; Sasaki and Neptune, 2006; Chumanov et al., 2007; Yokozawa et al., 2007; Chumanov et al., 2011; Hamner et al., 2010), which may not ideally simulate the conditions of overground running (Nelson et al., 1972; Elliott and Blanksby, 1976; Frishberg, 1983; Nigg et al., 1995; Riley et al., 2008). Some of the aforementioned studies analysed only a few muscles (Chumanov et al., 2007, 2011; Schache et al., 2010), some analysed only selected parts of the gait cycle (Glitsch and Baumann, 1997; Chumanov et al., 2007; Hamner et al., 2010; Schache et al., 2010), and some analysed only individual speeds (Glitsch and Baumann, 1997; Sasaki and Neptune, 2006; Schache et al., 2010). No study to date has calculated the forces developed by all lower-limb muscles: (i) during overground running; (ii) over the entire

stride cycle; and (iii) across the full spectrum of human running speeds.

Only when all lower-limb muscle forces are known, can function be established. Indeed, only four modelling studies to date have investigated muscle function in running using musculoskeletal models (Sasaki and Neptune, 2006; Hamner et al., 2010; Lin et al., 2011a; Pandy and Andriacchi, 2010). These studies are all limited to speeds of up to 4.0 m/s and do not consider how muscles accelerate individual joints.

Sasaki and Neptune (2006) simulated a full cycle of running at 2.0 m/s using a forward driven dynamic optimisation algorithm. Dominant contributions to the vertical and anterior-posterior ground force were made by the soleus, vasti and gluteus maximus muscles (Fig. 2.4, TOP). Notably, the gastrocnemius did not contribute substantially to any ground reaction force. The musculoskeletal model in this study was two-dimensional, so the actions of muscles outside the sagittal plane were not considered. The importance of using three-dimensional models has been emphasised when simulating human locomotion, suggesting that two-dimensional models may underestimate muscle forces by up to 60% (Glitsch and Baumann, 1997; Xiao and Higginson, 2008).

Many lower-limb muscles that play an important role during running have specific actions that are not limited to a single anatomical plane. For example, in addition to being a strong hip extensor, the gluteus maximus also has a large capacity for producing hip external rotation (Delp et al., 1999; Pandy et al., 2010). Similarly, the rectus femoris and biceps femoris have been shown to be capable of inducing both sagittal and frontal plane hip motion (Hunter et al., 2009). Consequently, running is likely to be fundamentally governed by coordinated synchronous muscle activity in all three anatomical planes, which would suggest that any investigation into the biomechanics of running ideally should be approached from a three-dimensional perspective.

Lin et al. (2011a) and Pandy and Andriacchi (2010) simulated running at 3.5 m/s using a three-dimensional musculoskeletal model. Vertical support and horizontal progression were mostly provided by the actions of five muscles: soleus, gastrocnemius, vasti, gluteus medius and gluteus maximus (Fig 2.4, BOTTOM) Specifically, (i) soleus, gastrocnemius, vasti

and gluteus maximus were largely responsible for accelerating the body upwards in the presence of gravity; (ii) soleus and vasti provided a retarding backwards acceleration of the center-of-mass in the first half of stance; and (iii) soleus, gastrocnemius and gluteus medius propelled the center-of-mass forwards in the second half of stance.

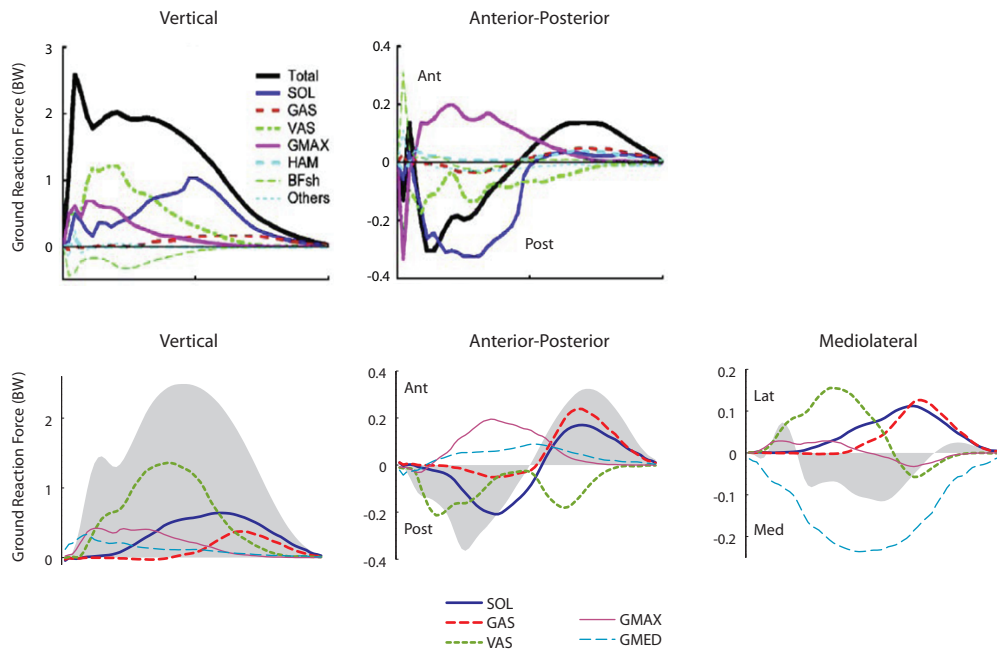


Figure 2.4: Muscle contributions to the ground reaction force during running. *TOP:* 2.0 m/s running (adapted from Sasaki and Neptune (2006)). *BOTTOM:* 3.5 m/s running (adapted from Lin et al. (2011a)). Shaded region represents the total measured ground reaction force. Muscle symbols appearing in the graphs are: SOL (soleus), GAS (medial and lateral compartments of gastrocnemius combined), VAS (vastus medialis, vastus intermedius and vastus lateralis combined), GMAX (superior, middle and inferior gluteus maximus) and GMED (anterior, middle and posterior compartments of gluteus medius).

Although differences between the results of Sasaki and Neptune (2006) and Lin et al. (2011a) are most likely due to the difference in running speed, many other factors can influence the muscle contributions to the ground reaction force. For example, Hamner et al. (2010) obtained similar results to Lin et al. (2011a) except that the predicted magnitudes of the soleus and vasti contributions in the vertical direction were opposite (i.e.,

the force of soleus contributed twice as much as the force of vasti to the vertical ground reaction force). This contradictory result could be due to: (i) differences in musculoskeletal model architecture; (ii) different models of foot-ground contact (Section 2.6) and/or (iii) different algorithms for calculating muscle forces. Although Hamner et al. (2010) used Computed Muscle Control and Lin et al. (2011a) used Static Optimisation to compute muscle forces, they also used slightly different musculoskeletal models. Detailed analysis suggests that the difference was likely due to a discrepancy in the models used rather than the algorithm for calculating muscle forces (see the paper entitled: *Comparison of different methods for estimating muscle forces in human movement* in Appendix D). Nevertheless, the inconsistent results obtained from these two studies highlight the need for further work aimed at validating model predictions of leg-muscle function across the spectrum of running speeds.

2.8 Specific questions addressed in this dissertation

In light of the limitations of previous computational running studies, the three specific aims of Section 1.4 are now elaborated upon to highlight the context of this dissertation.

1. **Evaluate the effectiveness and suitability of a range of commonly used foot-ground contact models to determine the most suitable contact model for estimating muscle function in both walking and running.** *This is an important step preceding the investigation of coordination strategies in running because: (i) different assumptions of foot-ground interaction are likely to influence the functional interpretation of the role of a particular muscle; and (ii) unlike walking, there are a variety of foot-striking patterns in running (Section 2.6).*

2. **Identify the key muscle groups responsible for accelerating the lower limbs and center-of-mass as running speed increases from slow running to maximal sprinting.** *Because running speed is a product of stride length and stride frequency (Section 2.1.4), understanding how the individual leg muscles contribute to concurrent increases in stride length and stride frequency will reveal the strategies that muscles use to increase running speed. Calculations of individual muscle force and their contributions to the ground reaction force and lower-limb joint accelerations will help determine how muscles: (i) push on the ground harder to increase stride length; and (ii) push on the ground more frequently to increase stride frequency.*

3. **Determine how the mechanical energy derived from muscles is transferred to the skeleton as running speed increases from slow running to maximal sprinting.** *As running speed increases, the power delivered to the lower-limb joints increases, signifying greater energy requirements from the muscles. (Section 2.1.4). Understanding how energy is distributed between individual muscles and the skeleton will highlight the strategies used to supply the power needed to run at the fastest speeds possible.*

Chapter 3

Experimental and computational methods

All computational analyses described in this chapter were performed on experimentally recorded running data. Therefore, one of the primary goals of this dissertation was to acquire the highest quality running data possible and analyse the data using the most detailed and accurate rigid body musculoskeletal models available. The reasons for this goal is clear: any outputs and interpretations obtained from computer-based musculoskeletal models are only as reliable as the experimental data being used as input (Thelen and Anderson, 2006; Seth and Pandy, 2007). Three aspects in particular were identified as having the greatest influence on the quality of model predictions: (i) the experimental protocol; (ii) parameters of the musculoskeletal model; and (iii) the analyses being used to generate model predictions. This chapter describes in detail the experimental and computational pipeline used to collect and process the experimental running data, from initial subject recruitment to the calculation of muscle forces and their functional roles in coordinating the lower limbs (Fig. 3.1). The studies of Chapters 4, 5 and 6 use the methodology described in this chapter; they will also be briefly repeated in the methods section of each chapter for clarity.

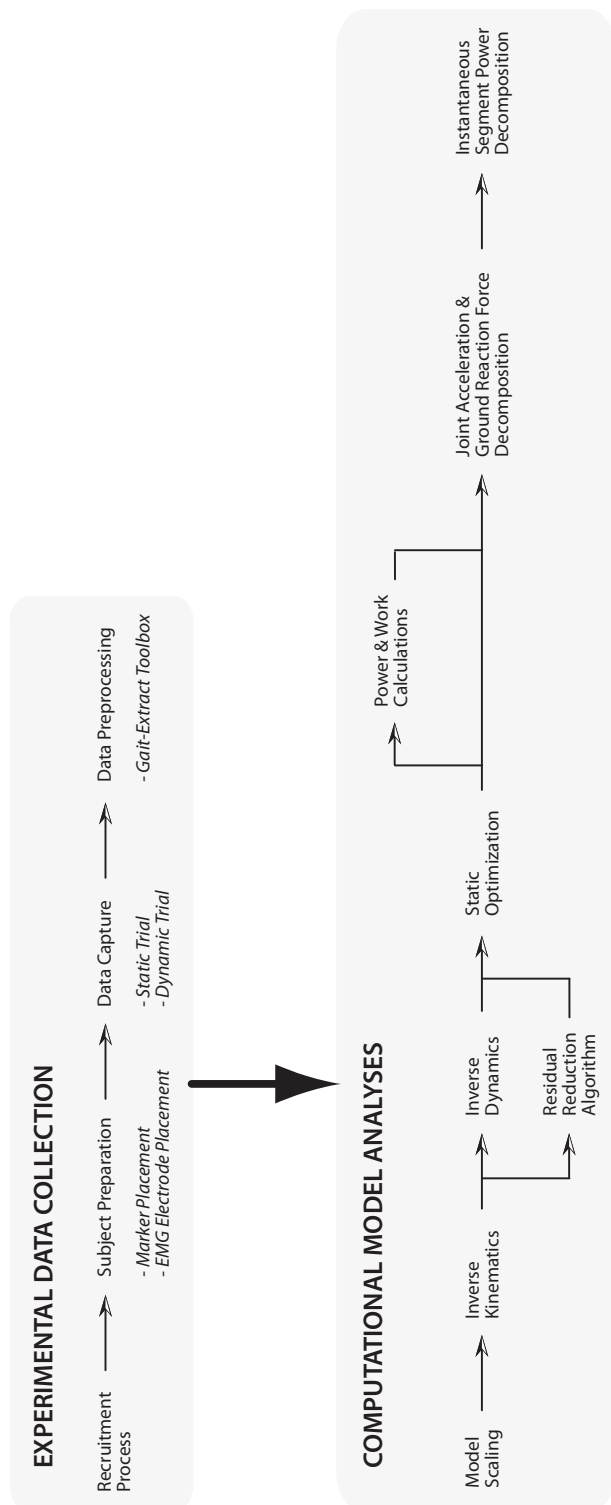


Figure 3.1: *Experimental and computational pipeline used throughout the thesis.*

3.1 Experimental data collection

Marker derived kinematics, ground reaction force and electromyographic (EMG) data were collected for nine participants during self selected walking (1.5 m/s), and at four target speeds of running (3.5 m/s, 5.0 m/s, 7.0 m/s and 9.0 m/s). Data were collected at the Australian Institute of Sport, Canberra, Australia. All participants were actively fit, regular runners and were free from any musculoskeletal injuries deemed likely to affect their running performance. Written consent was obtained from each participant after approval was obtained from the ethics committees of the Australian Institute of Sport and the University of Melbourne.

3.1.1 Recruitment Process

A cohort of past and present athletes was recruited from within the Australian Institute of Sport and the ACT Athletic Association. Recruitment processes were made by way of “word of mouth”, poster advertisements and information in electronic newsletters, which were emailed to registered athletes. Potential participants were then filtered according to a specific inclusion criterion. Subjects had to be:

- aged between 18 and 40 years
- free from any musculoskeletal injury at the time of testing
- well accustomed to sprinting (i.e., actively training and/or participating in a sprint-based event at least once per week)
- able to understand written and spoken English

3.1.2 Subject Preparation

Anthropometric data were recorded for each subject (e.g., height, pelvic width, segment lengths) and a test leg was determined randomly by a coin toss, which was designated as the ipsilateral leg for the purposes of the experiment.

Kinematic data were acquired using a three-dimensional motion

analysis system (VICON, Oxford Metrics, Oxford, UK). Small reflective markers (14 mm) were cleaned with an alcoholic solution before being mounted over specific locations on the trunk, lower limbs and arms using double sided adhesive tape (Table 3.1, Fig. 3.2). Running sandals (NIKE Straprunner IV) were worn by the subject rather than traditional runners or spikes to maintain exposure of the foot for marker placement and ensure consistent footwear across all participants. Moreover, the high stiffness of the running sandals compared to typical running shoes allowed foot markers to be tracked with greater rigidity. A set of twenty-two optical infra-red cameras (VICON, Oxford Metrics, Oxford, UK) were positioned around the laboratory to capture the marker trajectories over a distance of 11.5 m. Ground reaction force data were captured using a series of eight force plates (Kistler Instrument Corp., Amherst, NY, USA) placed within the capture volume.

Electromyographic (EMG) data were recorded using a telemetered system (Noraxon Telemetry 2400T G2, Noraxon, USA). Pairs of Ag/AgCl surface electrodes (inter-electrode distance of 20 mm) were mounted on the skin directly over the bellies of 12 lower-limb muscles on the test leg (gluteus maximus, gluteus medius, tensor fascia latae, rectus femoris, vastus medialis, vastus lateralis, medial hamstrings, lateral hamstrings, tibialis anterior, medial gastrocnemius, lateral gastrocnemius and soleus) (Table 3.2). To ensure suitable skin conductivity under the surface electrodes, the skin was prepared at these locations by shaving existing hair, cleaning the skin surface with an alcohol wipe and gently abrading the skin surface. Elastic polyester netting (Surgifix, Smith & Nephew) was placed over the leg to prevent lead swing and reduce noise in the EMG signal. Electrode placements were based on the guidelines provided by Hermens et al. (2000) and all signals were checked for clarity and strength of signal during isolated limb movements. Analog force plate and muscle EMG data were sampled at 1500 Hz and marker kinematics were sampled at 250 Hz. A fully prepared leg for a representative subject just prior to the capture of a running trial is shown in Fig. 3.3A. Individual subject characteristics are shown in Table 3.3.

3.1. EXPERIMENTAL DATA COLLECTION

Table 3.1: *Marker set description used for motion data capture*

Trunk	
LSH	14mm marker over tip of left shoulder (AC joint)
RSH	14mm marker over tip of right shoulder (AC joint)
C7	14mm marker over spinous process of 7th cervical vertebra
T7	14mm marker over spinous process of 7th thoracic vertebra
MAN	14mm marker over manubrium of thoracic cage
Pelvis	
RASI	14mm marker placed over right anterior superior iliac spine (ASIS)
LASI	14mm marker placed over left anterior superior iliac spine (ASIS)
SACR	14mm marker placed over midpoint between left and right posterior superior iliac spines (PSIS)
Right Thigh	
RTHAP	14mm marker located at the proximal anterior aspect of the right thigh
RTHAD	14mm marker located at the distal anterior aspect of the right thigh
RTHLP	14mm marker located at the proximal lateral aspect of the right thigh
RTHLD	14mm marker located at the distal lateral aspect of the right thigh
RLEPI	14mm marker over lateral epicondyle of right femur
RMEPI*	14mm marker over medial epicondyle of right femur
Left Thigh	
LTHAP	14mm marker located at the proximal anterior aspect of the left thigh
LTHAD	14mm marker located at the distal anterior aspect of the left thigh
LTHLP	14mm marker located at the proximal lateral aspect of the left thigh
LTHLD	14mm marker located at the distal lateral aspect of the left thigh
LLEPI	14mm marker over lateral epicondyle of left femur
LMEPI*	14mm marker over medial epicondyle of left femur
Right Shank	
RTIAP	14mm marker located on the proximal 1/3 of the anterior shaft of the right tibia
RTIAD	14mm marker located on the distal 1/3 of the anterior shaft of the right tibia
RTLAT	14mm marker located on the mid lateral aspect of the right tibia
RLMAL	14mm marker located over the right lateral malleolus
RMMAL*	14mm marker located over the right medial malleolus
Left Shank	
LTIAP	14mm marker located on the proximal 1/3 of the anterior shaft of the left tibia
LTIAD	14mm marker located on the distal 1/3 of the anterior shaft of the left tibia
LTILAT	14mm marker located on the mid lateral aspect of the left tibia
LLMAL	14mm marker located over the left lateral malleolus
LMMAL*	14mm marker located over the left medial malleolus
Right Foot	
RHEEL	14mm marker on distal aspect of bisection of right posterior calcaneum
RMD	14mm marker on medial right midfoot
RLATMID	14mm marker on lateral right midfoot
RP1MT	14mm marker on medial aspect of right 1 st MTP joint
RP5MT	14mm marker on lateral aspect of right 5th MTP joint
RTOE	14mm marker on distal end of 1 st toe of right foot
Left Foot	
LHEEL	14mm marker on distal aspect of bisection of left posterior calcaneum
LMID	14mm marker on medial left midfoot
LLATMID	14mm marker on lateral left midfoot
LP1MT	14mm marker on medial aspect of left 1 st MTP joint
LP5MT	14mm marker on lateral aspect of left 5th MTP joint
LTOE	14mm marker on distal end of 1 st toe of left foot
Right Arm	
RARM	14mm marker located at the half way point laterally on the right humerus
RELB	14mm marker over lateral epicondyle of right humerus
RFOREARM	14mm marker located at the half way point laterally on the right forearm
RWR	14mm marker over dorsal aspect of right wrist
Left Arm	
LARM	14mm marker located at the half way down laterally on the left humerus
LELB	14mm marker over lateral epicondyle of left humerus
LFOREARM	14mm marker located at the half way point laterally on the left forearm
LWR	14mm marker over dorsal aspect of left wrist

* Markers required for static calibration trial only.

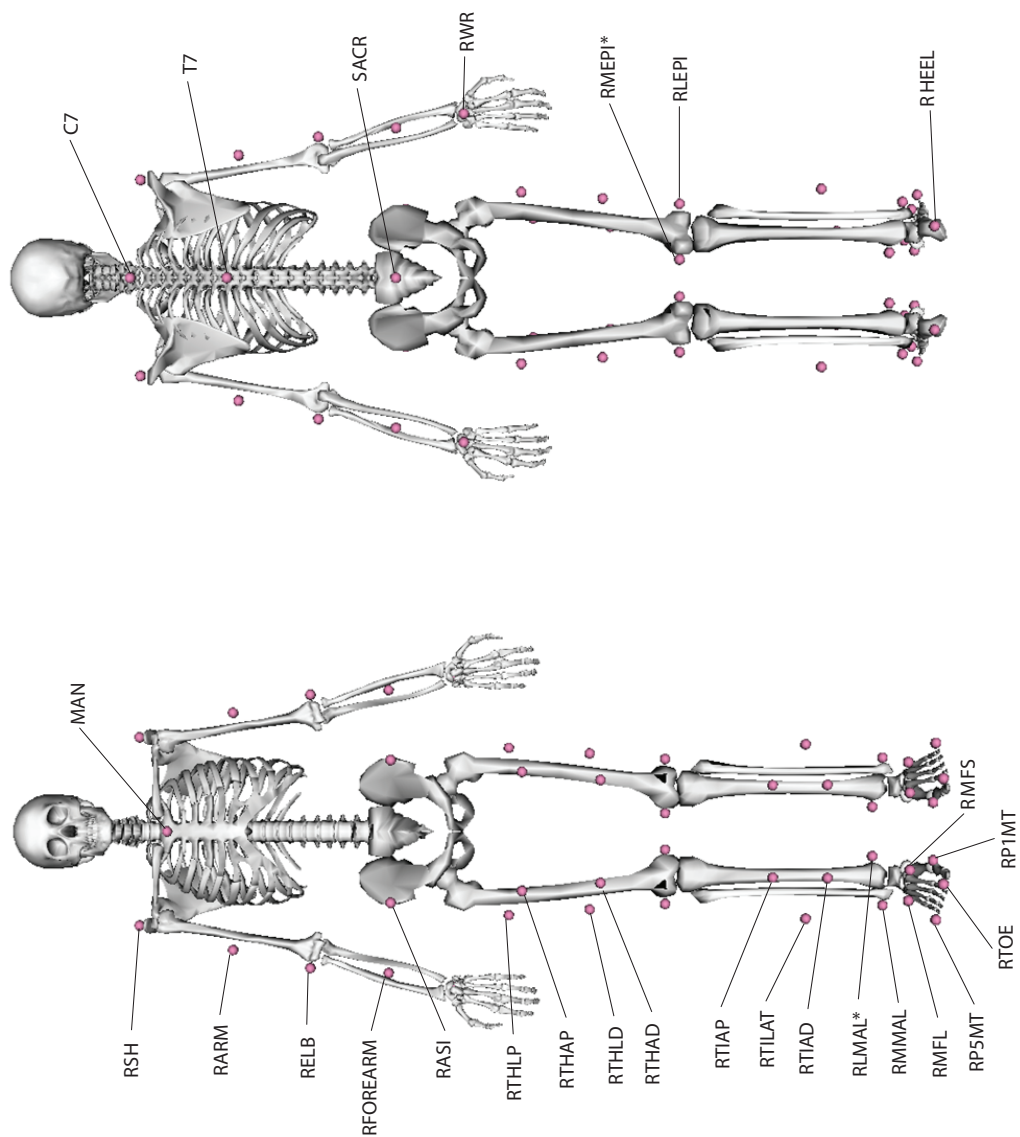


Figure 3.2: Experimental marker set used for subject preparation. Only the right leg and trunk markers are labelled for clarity. * denotes a marker used only in the static pose.

3.1. EXPERIMENTAL DATA COLLECTION

Table 3.2: *EMG electrode layout used for EMG data capture*

Muscle	Location	Subject pose
Tibialis anterior	Electrodes positioned approx 33% down from head of fibula along a line connecting head of fibula and medial malleolus (or 3cm lateral and 3cm inferior to tibial tubercle). Line connecting electrodes is parallel to line of head of fibula to medial malleolus	Supine
Vastus medialis	Over area of greatest muscle bulk. Electrodes placed approx 20% up from MFC along a line connecting ASIS and MFC. Line connecting electrodes is perpendicular to the ASIS-MFC line	Supine, quads over fulcrum
Vastus lateralis	Over area of greatest muscle bulk. Electrodes placed approx 33% up from patella along a line connecting ASIS to lateral margin of patella. Line connecting electrodes is parallel to muscle fibres	Supine, quads over fulcrum
Rectus femoris	Electrodes placed 50% along a line connecting AIIS and superior patella. Line connecting electrodes is parallel to AIIS-patella line	Supine, quads over fulcrum
Tensor fasciae latae	Over area of greatest muscle bulk. Electrodes positioned at proximal end of line connecting ASIS and LFC. Line connecting electrodes is parallel to ASIS-LFC line	Sidelying
Gluteus medius	Electrodes positioned 50% along a line connecting iliac crest and GT (or 3cm inferior to ASIS-PSIS, on a line with GT). Line connecting electrodes is parallel to iliac crest-GT line	Sidelying
Gluteus maximus	Over greatest prominence of the middle of the buttocks. Electrodes positioned 50% along a line connecting middle of sacrum and GT. Line connecting electrodes is parallel to line connecting PSIS and mid posterior thigh	Prone
Medial hamstrings	Electrodes positioned 50% along a line connecting ischial tuberosity and medial tibial condyle. Line connecting electrodes is parallel to line connecting ischial tuberosity and medial tibial condyle	Prone with knee slightly flexed
Lateral hamstrings	Electrodes positioned 50% along a line connecting ischial tuberosity and lateral tibial condyle. Line connecting electrodes is parallel to line connecting ischial tuberosity and lateral tibial condyle	Prone with knee slightly flexed
Medial gastrocnemius	Over area of greatest muscle bulk, along a line from medial tibial condyle to heel. Line connecting electrodes is parallel to line of leg	Prone, fulcrum under ankle, foot plantar flexed
Lateral gastrocnemius	Over area of greatest muscle bulk. Electrodes positioned approx 33% down from head of fibula along a line from head of fibula to heel. Line connecting electrodes is parallel to line of head of fibula to heel	Prone, fulcrum under ankle, foot plantar flexed
Medial soleus	Electrodes positioned approx 66% down from MFC along a line connecting MFC and medial malleolus. Line connecting electrodes is parallel to line of MFC to medial malleolus	Supine with knee flexed to 90 degrees
GROUND	Electrodes positioned over the medial flat region of the tibia (approx middle of the tibia)	Supine

Table 3.3: Subject characteristics, measured running speeds, and foot-strike patterns measured for each target running speed.

Subject	Mass <i>kg</i>	Gender	Height <i>m</i>	Age <i>yrs</i>	Leg length <i>m</i>	Test leg	Target speed	Target speed	Target speed	Target speed	Target speed		
							slow running 3.5 m/s <i>m/s [strike]*</i>	running 5.0 m/s <i>m/s [strike]*</i>	fast running 7.0 m/s <i>m/s [strike]*</i>	sprinting 9.0 m/s <i>m/s [strike]*</i>			
1	79.2	M	1.82	32	0.95	right	[R]	5.20	[F]	7.07	[F]	9.38	[F]
2	74.9	M	1.72	42	0.91	left	[R]	4.92	[R]	6.93	[F]	8.37	[F]
3	88.1	M	1.86	24	1.01	left	[R]	5.21	[F]	6.73	[F]	9.43	[F]
4	64.4	F	1.77	25	0.93	right	[R]	5.16	[F]	6.86	[F]	8.01	[F]
5	65.2	F	1.64	29	0.88	left	[F]	5.09	[F]	6.89	[F]		
6	64.1	F	1.72	37	0.91	left	[R]	5.07	[R]				
7	66.1	F	1.70	20	0.89	right	[F]	5.41	[F]	7.13	[F]	8.53	[F]
8	80.3	M	1.77	21	0.92	left	[F]	5.24	[F]	7.07	[F]	9.73	[F]
9	75.9	M	1.82	19	1.00	right	[F]	5.20	[F]	7.00	[F]	9.49	[F]

* [R] denotes a rearfoot-strike and [F] denotes a forefoot-strike

3.1.3 Data collection protocol

A static trial was recorded to define the marker locations in a standing pose. Subjects were instructed to stand still on a force plate with their arms abducted to approx 30°(Fig. 3.3B). Data collected from the static trial were used to determine a precise measure of the subject’s weight and segment lengths (distances between marker pairs), which were subsequently used to scale the generic musculoskeletal model (see Section 3.2.1). Prior to commencing the dynamic running trials, subjects completed a standardised warm up routine to become accustomed to running with the markers and surface electrodes *in situ*.

Marker trajectories, ground reaction forces and EMG data were simultaneously collected in VICON Nexus (Version V1.4.116, VICON, Oxford Metrics, Oxford, UK) for incremental speeds of locomotion, beginning with a self-selected walk, progressing up to and including maximal sprinting (Fig. 3.3C).¹ Timing gates (Speedlight TT, SwiftSports, NSW, Australia) were installed at each end of the capture volume to monitor the average speed of each subject and verbal feedback was provided in order to obtain the desired target speeds.

One walking speed and four running speeds were targeted by each subject:

- **1.5 m/s** (*WALK*)
- **3.5 m/s** (*SLOW RUN*)
- **5.0 m/s** (*MEDIUM-PACED RUN*)
- **7.0 m/s** (*FAST RUN*)
- **9.0 m/s** (*SPRINT*)

Although the speed of 9.0 m/s was targeted as a sprint, where runners could not attain this speed, a sprint was defined as any speed above 8.0 m/s. The laboratory provided approximately 40 m of track prior to the first timing gates for the subject to accelerate to the target speed and approximately 50 m

¹Although the aim of this dissertation was to investigate running, we nevertheless recorded normal walking trials to evaluate our analyses with previously published results of walking biomechanics (some of the walking results are shown in Appendix C).

of track after the final timing gates for the subject to decelerate safely, thereby allowing unimpeded steady state locomotion inside the capture volume (Fig. 3.3C). Adequate recovery time was provided between each trial to avoid the effects of fatigue. Total testing time was approximately three hours per subject.

An experimental trial was deemed successful if:

- the speed for the trial was within $\pm 5\%$ of the target speed (with the exception of a sprint trial)
- two or more force platforms were consecutively struck cleanly
- EMG activity was visible for at least 10 of the 12 muscles

3.1.4 Data preprocessing

Markers were labeled in VICON Nexus (Version V1.4.116, VICON, Oxford Metrics, Oxford, UK) and any gaps existing between subsequent time frames were filled using spline interpolation. The large number of motion capture cameras ensured that markers were generally always visible to at least three cameras during a trial, therefore gap filling was rarely needed. A Gait-Extract toolbox developed in MATLAB (The MathWorks, Inc., Natick, MA, USA) was used to extract and transform the marker positions, ground reaction force and EMG data into a suitable format for input into the OpenSim musculoskeletal model (B). The Gait-Extract toolbox is open-source software and is freely available from <https://simtk.org/home/c3dtoolbox>.

3.2 Computational model analyses

After collection and preprocessing, all experimental data were exported to OpenSim for analysis. First, a generic musculoskeletal model (Appendix A.2) was scaled to reflect the mass and anthropometry of the subject. Using this model, an inverse kinematics analysis was executed to determine the optimal set of model joint angles from the experimental marker trajectory. Joint moments were calculated using inverse dynamics, and static optimisation



Figure 3.3: *Experimental data capture photos. (A) a prepared leg containing markers and EMG electrodes. (B) capture of a static trial. (C) capture of a running trial at 7.0 m/s.*

then used to decompose the joint moments into individual musculotendon forces acting along their respective lines of action. The musculotendon forces were then successively applied in isolation to the musculoskeletal model to calculate their relative contributions to joint accelerations, ground reaction forces and instantaneous segment powers.

3.2.1 Model scaling

Generic musculoskeletal models are typically based on cadaveric data from multiple specimens, and therefore represent the *average* human musculoskeletal system (Brand et al., 1982; Delp et al., 1990; Friederich and Brand, 1990; Anderson and Pandy, 1999). Such models, need to be scaled to the specific anatomy and mass distribution of the individual to provide joint moments and muscle forces indicative of reality (Reinbolt et al., 2007). Acquiring non-invasive parameters of each muscle fibre of each leg muscle (i.e., optimal fibre length, tendon slack length, maximum isometric force and maximum shortening velocity) *in vivo* is currently impossible, hence investigative analyses are performed on generic models that are scaled to the subject's anthropometry and mass during a static pose (Thelen and Anderson, 2006; Liu et al., 2008)(Fig. 3.4).

Prior to scaling, the original generic OpenSim musculoskeletal model (Delp et al., 1990; Anderson and Pandy, 1999; Delp et al., 2007) was updated with muscle parameters from a recent large scale cadaver dissection (Ward et al., 2009). The optimal fibre length and pennation angle of each muscle in the model were compared to the experimental mean values obtained from Ward et al. (2009), and were modified to the mean values if the model values fell outside the reported experimental standard deviation. Furthermore, the value of passive muscle strain at the maximum isometric force was modified from the nominal value of 3.3% (Zajac, 1989; Anderson and Pandy, 2001a) where experimental data were available. For example, the muscles attached to the Achilles tendon (medial gastrocnemius, lateral gastrocnemius and soleus) were modified to 7.0%, in line with experimental ultrasound measurements (Muramatsu et al., 2001; Lichtwark and Wilson, 2005; Muraoka et al., 2005; Hoang et al., 2007).

Tendon slack lengths were left unchanged from the values assumed in the original OpenSim model because no new experimental data were available. We note here, that the tendon slack length parameter may be one of the most sensitive parameters affecting the operating fibre length of the muscle, which in turn can significantly affect the force generating capacity of muscle (Xiao and Higginson, 2010; De Groot et al., 2010). Therefore, care was taken that the modified optimal fibre lengths and pennation angles in conjunction with the unmodified tendon slack lengths did not significantly compromise the operating fibre length at each recorded running speed.

The maximum isometric force of each muscle was uniformly increased to three times that of the original OpenSim model (see Appendix A.3). This represented the minimum model strength required to successfully produce a static optimisation solution of muscle forces during maximal sprinting (Section 3.2.4). Because maximal sprinting represents an approximate level of maximum muscular performance in the human body, the maximum isometric forces used to simulate sprinting were assumed to represent the upper limits of the model's isometric performance. A new emerging alternative to muscle strength scaling is to directly scale the maximum isometric force according to body weight, height, or height/weight ratios to make the models more subject specific (Folland et al., 2008; Bazett-Jones et al., 2011; Correa and Pandy, 2011), however these scaling laws were not applied in this dissertation.

The updated generic musculoskeletal model was used to generate scaled subject-specific models. First, a scale factor was computed for each segment of the model. The scale factor was based on the relative distances between experimentally placed marker pairs and marker pairs attached to the model. The dimensions of each segment were scaled by the segment's scale factor, which also implicitly scaled the musculotendon length and moment arms of each muscle attached to the segment.

The optimal muscle fibre length and tendon slack length of each muscle were also scaled, but using a different scale factor. The scale factor used here was determined such that the force generating capacities (i.e., force-length-velocity properties) were preserved from the generic model to

the scaled model (Delp et al., 2007). Finally, the mass of the model were scaled to match the subject's recorded mass, with inertia tensors modified accordingly (Forwood et al., 1985). Finally, marker locations on the model were relocated to the experimental marker locations recorded during a stationary static standing pose. In this pose, no dynamic based soft tissue artifact was assumed, hence relocating the markers would theoretically minimise soft tissue artifact during a dynamic trial. The final result of the scaling process was a subject-specific musculoskeletal model that better reflected the anatomy and anthropometry of the individual. The same generic model was used in the scaling process for all subjects.



Figure 3.4: *Musculoskeletal model scaling was performed based on a standing static trial to better match the musculoskeletal model to the anthropometry of the subject.*

3.2.2 Inverse kinematics

Inverse kinematics is the process of determining the generalised coordinates of a kinematic multibody chain to achieve a desired pose. Each time frame of inverse kinematics was formulated as a weighted least squares optimisation problem (Equation 3.1), based on the search for an optimal kinematic pose

by minimising the sum of the squared differences between experimental and model markers (Lu and O'Connor, 1999).

$$\min \left(J = \sum_{\text{markers}}^{i=1} w_i \left(\mathbf{x}_i^{\text{subject}} - \mathbf{x}_i^{\text{model}} \right) \right) \quad (3.1)$$

where $\mathbf{x}_i^{\text{subject}}$ and $\mathbf{x}_i^{\text{model}}$ are position vectors of the i th marker on the subject and model, respectively; and w_i are the respective weighting factors. Kinematic joint constraints were enforced during the search for the optimal pose, reducing the potential for joint dislocations that are common in inverse kinematic methods that match segment poses using marker positions alone (Kadaba et al., 1990; Challis, 1995).

3.2.3 Inverse dynamics

Inverse dynamics is an iterative method for computing the generalised forces (linear forces and angular moments of force) of a multibody linkage system based on the joint kinematics and inertial properties of each link. Because the human skeleton is modelled as a multibody linkage, its mechanical behaviour is governed by equations of motion derived using the laws of classical mechanics (e.g., Newtonian, Lagrangian or Kane mechanics).

Although the classical definition of the equations of motion of the skeleton dictate that only joint position, velocity and acceleration data are required to compute all joint moments of the skeleton, additional ground reaction force data improves the accuracy of the inverse dynamics solution because it relies less on potentially noisy angular accelerations (from double differentiating joint position), and more on the ground reaction force data, which can be measured very accurately on force platforms (Kuo, 1998). Known as the “bottom-up” approach to inverse dynamics, joint moments are derived from the equations of motion of a single segment, working recursively by initially applying ground reaction loads to the foot, solving for joint reactions at the ankle, then using the joint reactions at the ankle to solve for joint reactions at the knee, and so forth, iterating upwards

throughout the skeleton (Fig. 3.5).

Although the “bottom-up” approach produces more accurate joint moments than the classical approach, incorporating the additional ground force measurements produces an over-determined system (Kuo, 1998). When the measured ground reaction force and joint kinematics are not dynamically consistent with the skeleton model, residual forces and moments can arise between the most proximal segment and the surrounding environment (Fig. 3.5). These forces and moments do not exist in reality, but simply represent the lumped errors in both the experimental data and the skeleton model. In the skeleton model used in this thesis, residual loads are applied between the pelvis and the surrounding environment (where a six degree-of-freedom free joint permits the whole model to translate and rotate in space — see Appendix A.2). Despite the limitation of having residual loads present in inverse dynamics, it nevertheless represents a simple and reliable analysis that is commonly implemented and widely accepted in the movement biomechanics community (Nagano et al., 2000; Belli et al., 2002; Yokozawa et al., 2007; Devita et al., 2008; Schache et al., 2011a).

3.2.4 Static optimisation

The joint moments calculated from inverse dynamics represent the summation of individual moments generated by the muscle actuators that span each joint. Because there are many more muscles than joints in the lower limbs, the musculoskeletal system is redundantly actuated, and hence there exists an infinitely large set of different musculotendon force combinations that could all potentially generate the net joint moments needed to reproduce experimental motion.

Static optimisation decomposes the net joint moments into individual muscle forces by minimising the sum of the squares of all muscle activations. This objective is equivalent to minimising the simultaneous mechanical stress across all muscles (Crowninshield and Brand, 1981). The muscle forces predicted by static optimisation are further constrained to physiological bounds on each muscle according to its force-length-velocity

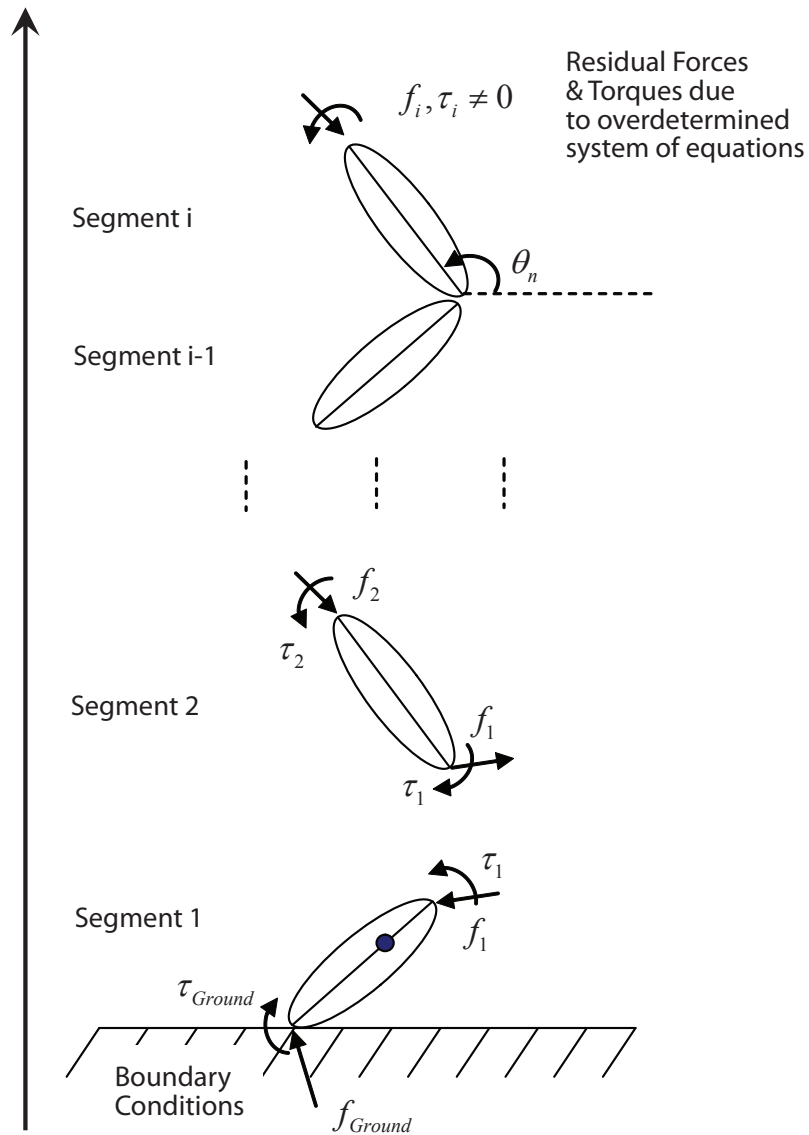


Figure 3.5: Bottom-up inverse dynamics approach. Joint moments are derived from the equations of motion of a single segment, working recursively from distal to proximal.

properties (Hill, 1938; Katz, 1939) with activations bounded between zero (corresponding to zero force) and one (corresponding to maximum isometric force).

Apart from muscle actuators, several other actuators are included in the musculoskeletal model and therefore included in the static optimisation problem formulation. Ideal force and torque “residual” actuators applied between the pelvis and the surrounding environment supply any non-zero residual loads required throughout the analysis (see Section 3.2.3).²

Ideal reserve torque actuators exist at each lower-limb joint to provide an additional moment generating capacity when no combination of muscle forces are able to satisfy the required net joint moments (e.g., muscle strength deficiencies in the lower-limb³). Lower-limb reserve actuators should theoretically contribute zero moment to the skeleton during the static optimisation analysis, but nevertheless need to be included in musculoskeletal models to permit the optimisation to numerically converge to arbitrarily tight tolerances. Ideal torque actuators also exist at each upper extremity joint (upper-limb reserve actuators) so that the dynamics of arm swing can be simulated.

The static optimisation problem is formally stated as follows:

²Some argue that residual loads should be constrained to zero because they reflect non physiological loadings that do not exist in reality (Riemer and Hsiao-Wecksler, 2008; Remy and Thelen, 2009), while others attribute the existence of residual loads to the combined effect of un-modelled or inaccurately modelled phenomena (Delp et al., 2007; Liu et al., 2008). Both points of view are equally valid — the former argument assumes that the skeleton model is perfectly dynamically consistent with the experimental gait data, reducing the overdetermined skeleton system to a determinate one. In this scenario, any inconsistencies in the experimental gait data are reflected by the model-predicted kinematics which form the output of the simulation. The latter argument recognises model imperfections (e.g., simplified ball-and-socket back joint) and provides the ability to better match experimental kinematics at the expense of introducing residual loads between the pelvis and the external environment. As multibody models of the skeleton become more complex and subject specific, residual loads calculated from an inverse dynamics analysis should therefore naturally decrease.

³For example, if all hip flexor muscles are fully activated and cannot satisfy the desired net hip flexion moment, the hip reserve actuator reserve moment will produce the difference, implying a hip flexor strength deficiency. The reader is referred to Appendix A.3 for additional examples of the use of reserve torques.

$$\text{calculate: } \mathbf{a} = \begin{bmatrix} \mathbf{a}^M \\ \mathbf{a}^R \\ \mathbf{a}^r \end{bmatrix}$$

$$\text{by minimising: } J(\mathbf{a}) = \underbrace{\sum_{i=1}^{nm} w_i (a_i^M)^2}_{\text{muscle}} + \underbrace{\sum_{j=1}^6 w_j (a_j^R)^2}_{\text{residual}} + \underbrace{\sum_{k=1}^{nq} w_k (a_k^r)^2}_{\text{reserve}}$$

subject to:

$$\underbrace{\sum_{i=1}^{nm} [a_i^M \cdot f_i(F_0^M, l^M, v^M)] \cdot s_{i,n}}_{\text{muscle}} + \underbrace{\sum_{j=1}^6 [a_j^R \cdot F_j^R]}_{\text{residual}} + \underbrace{\sum_{k=1}^{nq} [a_k^r \cdot F_k^r]}_{\text{reserve}} = \tau_n$$

$$\mathbf{0} < \mathbf{a}^M < \mathbf{1} \tag{3.2}$$

where \mathbf{a}^M , \mathbf{a}^R and \mathbf{a}^r represent the muscle, residual and reserve actuator activation values, respectively; nm is the number of muscle actuators in the model; nq is the number of kinematic degrees of freedom in the model; w_i , w_j and w_k are weightings to penalise the force generating capacities of the muscles, residual and reserve actuators, respectively; $f_i(F_0^M, l^M, v^M)$ represents the force-length-velocity surface of muscle i ; F_j^R is the peak strength of the residual actuator j , F_j^r is the peak strength of the reserve actuator j (for both lower and upper limbs); $s_{i,n}$ is the moment arm of muscle i about coordinate n ; and τ_n is the net joint moment of generalised coordinate n , as derived from inverse dynamics.

Static optimisation solves for all actuator forces at each time instant and therefore cannot incorporate time-dependent activation or contraction dynamics in the problem formulation. However, the force-length-velocity curves are included in the problem formulation by using static lookup tables (Anderson and Pandy, 2001b). The reader is referred to the paper: *Comparison of different methods for estimating muscle forces in human movement* in Appendix D for a study on the effects of time-dependent dynamics in model predictions of muscle force during walking and running.

3.2.5 Musculotendon force evaluation

Because *in vivo* muscle forces cannot be measured non-invasively, techniques of evaluating the accuracy of model predictions of muscle forces remain limited to this day. In the majority of cases, studies that predict muscle forces using computer-based musculoskeletal models are temporally evaluated using surface electromyography (EMG) data (Erdemir et al., 2007). EMG is a measure of the electrical activity that is spreading across the muscle, causing it to activate and produce force. Although the timing of an EMG signal has been shown to correlate well with the timing of model predictions of muscle force (Anderson and Pandy, 2001b; Liu et al., 2008; Hamner et al., 2010), the magnitude of the EMG signal is much more difficult to validate. This is because the relationship between muscle force magnitude and EMG magnitude is a non-linear one (Buchanan et al., 1993; Jonkers et al., 2002; Manal et al., 2002; Lloyd and Besier, 2003; Buchanan et al., 2004, 2005). For example, a muscle may be fully excited, but if it is operating outside its physiological fibre length range, or shortening beyond its maximum shortening velocity, it will generate very little force.

In this dissertation, EMG was used only to evaluate the timing of model predictions of musculotendon force (see Section B.4). Raw EMG data were processed using the Teager-Kaiser Energy (TKE) operator (Li et al., 2007; Solnik et al., 2008; Hortobagyi et al., 2009; Solnik et al., 2010). Unlike traditional methods of processing EMG using high- and low-pass Butterworth filters (Lloyd and Besier, 2003; Buchanan et al., 2004), the TKE operator has been shown to better highlight the onset and offset of motor unit activity. The discrete TKE operator at time n is defined as:

$$TKE[x(n)] = x^2(n) - x(n+1)x(n-1) \quad (3.3)$$

3.2.6 Power and work calculations

Mechanical power is the rate at which work is performed on a mechanical system (alternatively, it can be defined as the rate at which energy passes between the boundary of a mechanical system). The instantaneous power

delivered to a system is equal to the product of the instantaneous force acting on the system boundary and the system's instantaneous velocity. Hence, mechanical work is calculated as the integral of mechanical power between two temporal events e.g., one full stride cycle (Fig. 3.6).

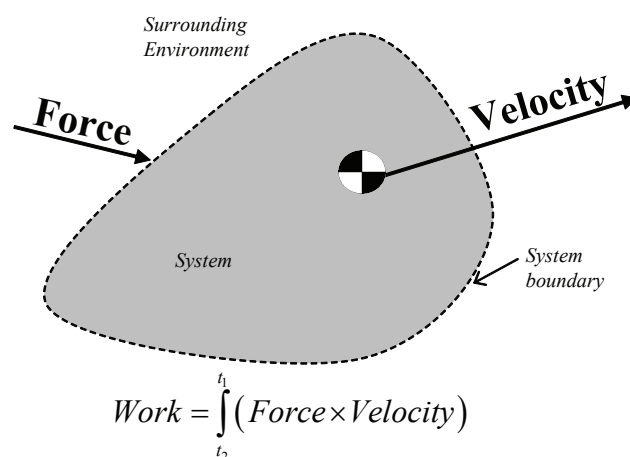


Figure 3.6: Mechanical power is equal to the vector product of force and velocity acting on a system boundary.

In human locomotion, there are many ways that mechanical power can be calculated (Arampatzis et al., 2000). The simplest method to calculate power is by computing the *external* power of the entire body, i.e., the dot-product of the ground reaction force and the velocity of the whole-body center-of-mass (Cavagna et al., 1971; Willems et al., 1995; Donelan et al., 2002). Although the external work calculated using this method provides an accurate value for the net energy generated and absorbed by muscles, the system boundary encompasses the entire body, so the energy generated by individual muscles, joints or segments cannot be elucidated. *Internal* methods for calculating power and work redefine the system boundaries to lie within the body. Consequently, internal work can be calculated at either the segment level (Elftman, 1940; Cavagna and Kaneko, 1977; Williams and Cavanagh, 1983; Willems et al., 1995), joint level (Novacheck, 1998; Swanson and Caldwell, 2000; Biewener et al., 2004; McIntosh et al., 2006; Devita et al., 2007; Schache et al., 2011a), or muscle level (Thelen et al., 2005) (Fig. 3.7).

Positive work denotes energy generation (i.e., energy flowing into the system) and negative work denotes energy absorption (i.e., energy flowing out of the system).

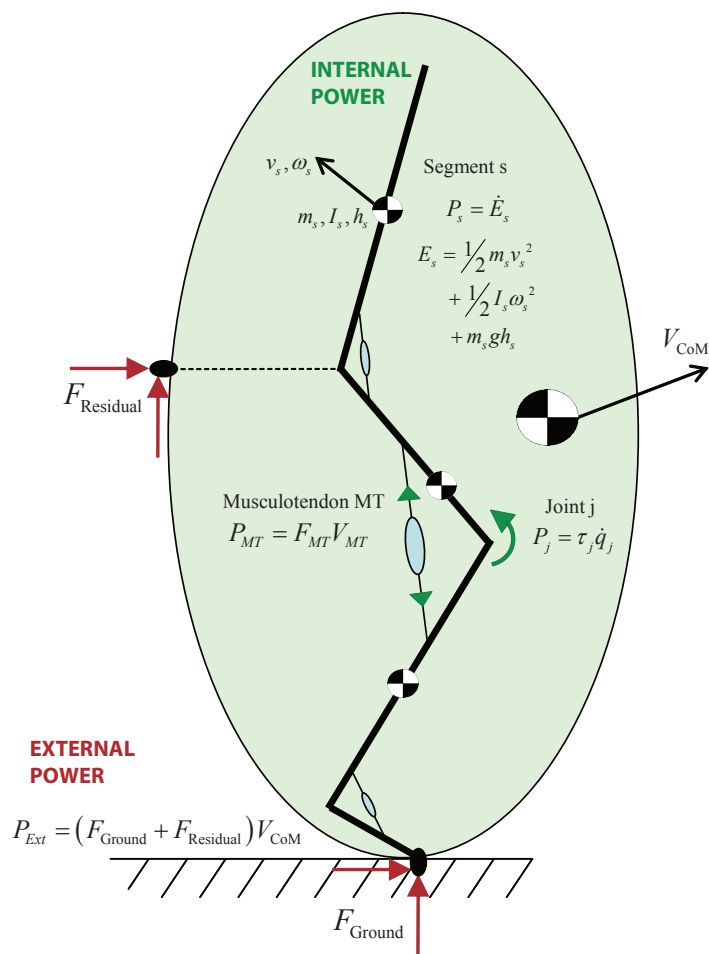


Figure 3.7: Multi-scale approaches to calculate mechanical power in human locomotion.

3.2.7 Pseudo-inverse induced acceleration analysis

The skeleton is a complex mechanical system. The large number of segments interconnected by a variety of different joint types (e.g., ball, universal and hinge joints) create significant coupling in the equations that define its dynamics (more specifically, the mass matrix of the equations of

motion are densely populated with non-zero elements — see Appendix A.1). Consequently, all forces acting on the skeleton will simultaneously induce accelerations in every joint and segment in the skeleton (Zajac and Gordon, 1989). Furthermore, non-explicit velocity forces (i.e., Coriolis/centripetal forces) that naturally arise from rotating bodies will also contribute to the accelerations of the joints and segments throughout the skeleton.

Induced acceleration analyses aim to quantify the contributions of each force acting on the system to: (i) the net ground reaction force; and (ii) the net acceleration of each joint. For the remainder of this chapter, the term “*actuator*” will represent the actuators present in the musculoskeletal models (i.e., musculotendon forces, arm torques, reserve lower-limb torques and residual loads) and the term “*action force*” will represent the forces present in the musculoskeletal model. Action forces include all “*actuators*” as well as gravity and Coriolis/centripetal forces. The result of an induced acceleration analysis should always satisfy the superposition principle. This principle states that the sum of all “*action forces*” to the ground reaction force (or joint acceleration) must equal the total ground reaction force (or total joint acceleration) measured during a gait experiment (Anderson and Pandy, 2003).

An induced acceleration analysis requires every joint in the skeleton to be well defined, including that between the skeleton and the external environment. Hence, a description of the mechanical constraints acting between the foot and ground (herein referred to as a *ground contact model*) is required to facilitate the generation of ground reaction forces in the computer-based musculoskeletal model.

The ground contact model described below was adapted from Lin et al. (2011a) and implemented as an OpenSim plug-in. It is used throughout Chapters 4 (as the MULTIPOINT contact model), 5 and 6.

Contact between the foot and the ground was assumed to occur at a set of five points geometrically located around the foot (Anderson and Pandy, 2003; Liu et al., 2006) (Fig. 3.8, see also Fig. A.3 in Appendix A). The five foot contact points were modelled in OpenSim as additional markers attached to the musculoskeletal model and consisted of two heel

markers (A&B) located on medial and lateral sides of the mid calcaneus, the line between them forming an approximate heel hinge axis, two metatarsal markers (C&D) located at the first and fifth metatarsal junctions, the line between them forming an approximate metatarsal axis, and a toe marker representing the anterior boundary of the foot.

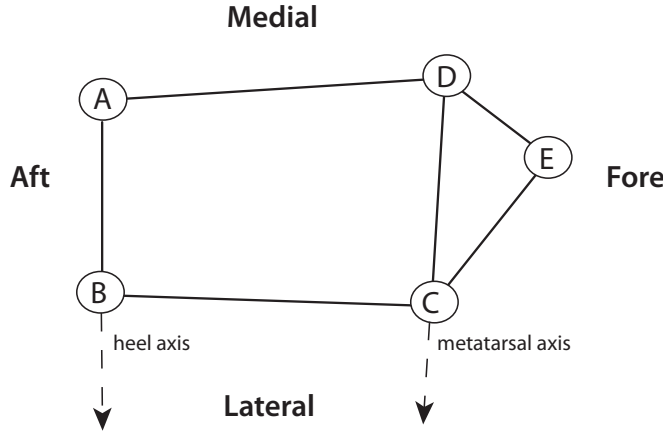


Figure 3.8: Five ground contact points on each foot are defined by marker locations.

Assuming that all contact between the foot and ground occurs at these prescribed foot points, the equations of motion for the n degree-of-freedom skeleton with k musculotendon units can be formulated:

$$\mathbf{M}(\mathbf{q}) \ddot{\mathbf{q}} = \mathbf{C}(\mathbf{q}, \dot{\mathbf{q}}) + \mathbf{G}(\mathbf{q}) + \begin{bmatrix} \mathbf{0}_{6 \times 1} \\ \mathbf{S}(\mathbf{q}) \mathbf{F}^M \end{bmatrix} + \begin{bmatrix} \mathbf{R}_{6 \times 1} \\ \mathbf{r}_{n\tau \times 1} \end{bmatrix} + \mathbf{E}(\mathbf{q}) \mathbf{F}_{ext} \quad (3.4)$$

where \mathbf{q} , $\dot{\mathbf{q}}$ and $\ddot{\mathbf{q}}$ are vectors of generalised displacements, velocities and accelerations, respectively; \mathbf{M} is an $n \times n$ system mass matrix used to specify the mass and inertial properties of the body segments; \mathbf{C} is an $n \times 1$ generalised force vector due to velocity related Coriolis/centripetal forces; \mathbf{G} is an $n \times 1$ generalised force vector due to a uniform gravity field; \mathbf{S} is an $n \times k$ matrix of muscular moment arms that maps a $k \times 1$ vector of muscle forces \mathbf{F}^M into an $n \times 1$ vector of generalised forces; \mathbf{F}_{ext} is a $3f \times 1$ vector of external reaction forces exerted between the foot and ground by the f

3.2. COMPUTATIONAL MODEL ANALYSES

contact points; and \mathbf{E} is an $n \times 3f$ linear *generalised Jacobian matrix* (also known as the matrix of partial velocities) that defines the relationship between the generalised velocity vector $\dot{\mathbf{q}}$ and the linear velocity vector of the foot-ground contact points $\dot{\mathbf{x}}$. In other words, the Jacobian matrix maps the external foot contact forces \mathbf{F}_{ext} into generalised forces:

$$\mathbf{E}(\mathbf{q}) = \frac{\partial \dot{\mathbf{x}}}{\partial \dot{\mathbf{q}}}(\mathbf{q}) = \frac{\partial \ddot{\mathbf{x}}}{\partial \ddot{\mathbf{q}}}(\mathbf{q}) =$$

$$\left[\begin{array}{ccc|ccc} \frac{\partial \dot{x}_{1X}}{\partial \dot{q}_1} & \frac{\partial \dot{x}_{1Y}}{\partial \dot{q}_1} & \frac{\partial \dot{x}_{1Z}}{\partial \dot{q}_1} & \frac{\partial \dot{x}_{2X}}{\partial \dot{q}_1} & \frac{\partial \dot{x}_{2Y}}{\partial \dot{q}_1} & \frac{\partial \dot{x}_{2Z}}{\partial \dot{q}_1} & \dots & \frac{\partial \dot{x}_{fX}}{\partial \dot{q}_1} & \frac{\partial \dot{x}_{fY}}{\partial \dot{q}_1} & \frac{\partial \dot{x}_{fZ}}{\partial \dot{q}_1} \\ \frac{\partial \dot{x}_{1X}}{\partial \dot{q}_2} & \frac{\partial \dot{x}_{1Y}}{\partial \dot{q}_2} & \frac{\partial \dot{x}_{1Z}}{\partial \dot{q}_2} & \frac{\partial \dot{x}_{2X}}{\partial \dot{q}_2} & \frac{\partial \dot{x}_{2Y}}{\partial \dot{q}_2} & \frac{\partial \dot{x}_{2Z}}{\partial \dot{q}_2} & \dots & \frac{\partial \dot{x}_{fX}}{\partial \dot{q}_2} & \frac{\partial \dot{x}_{fY}}{\partial \dot{q}_2} & \frac{\partial \dot{x}_{fZ}}{\partial \dot{q}_2} \\ \vdots & \vdots & \vdots & \vdots & \vdots & \vdots & \ddots & \vdots & \vdots & \vdots \\ \frac{\partial \dot{x}_{1X}}{\partial \dot{q}_n} & \frac{\partial \dot{x}_{1Y}}{\partial \dot{q}_n} & \frac{\partial \dot{x}_{1Z}}{\partial \dot{q}_n} & \frac{\partial \dot{x}_{2X}}{\partial \dot{q}_n} & \frac{\partial \dot{x}_{2Y}}{\partial \dot{q}_n} & \frac{\partial \dot{x}_{2Z}}{\partial \dot{q}_n} & \dots & \frac{\partial \dot{x}_{fX}}{\partial \dot{q}_n} & \frac{\partial \dot{x}_{fY}}{\partial \dot{q}_n} & \frac{\partial \dot{x}_{fZ}}{\partial \dot{q}_n} \end{array} \right] \quad (3.5)$$

where \mathbf{x} , $\dot{\mathbf{x}}$ and $\ddot{\mathbf{x}}$ represent the linear positions, velocities and accelerations of all f foot points in contact with the ground, respectively. Grouping all internal generalised force contributions together as \mathbf{F}_{int} (i.e., muscle forces, reserve forces/torques, residual forces/torques, gravity forces and Coriolis/centripetal forces), Equation 3.4 can be rewritten as:

$$\mathbf{M} \cdot \ddot{\mathbf{q}} = \mathbf{F}_{int} + \mathbf{E} \cdot \mathbf{F}_{ext} \quad (3.6)$$

The linear velocity of the i th foot point can also be calculated using the generalised Jacobian matrix:

$$\dot{\mathbf{x}}_i = \mathbf{E}_i^T \dot{\mathbf{q}} \quad i = 1, 2, \dots, f \quad (3.7)$$

Differentiating Equation 3.7 with respect to time yields an expression for the linear acceleration of the i th foot point:

$$\ddot{\mathbf{x}}_i = \mathbf{E}_i^T \ddot{\mathbf{q}} + \dot{\mathbf{E}}_i^T \dot{\mathbf{q}} \quad i = 1, 2, \dots, f \quad (3.8)$$

When foot point i is in contact with the ground, rigid contact principles are assumed, requiring the linear acceleration of point i in all directions to

equal zero. Letting $\mathbf{K}_i = \dot{\mathbf{E}}_i^T \dot{\mathbf{q}}$:

$$\mathbf{E}_i^T \ddot{\mathbf{q}} + \mathbf{K}_i = \mathbf{0} \quad i = 1, 2, \dots, f \quad (3.9)$$

Instantaneous switching between contact conditions for individual foot points as they make and break contact with the ground would introduce discontinuities in the set of constraint equations and induced acceleration results. To implement smooth transitions between contact phases and constrain the contact points to maintain consistency with the actual movement of the foot during stance, a diagonal weighting matrix \mathbf{W} was introduced:

$$\mathbf{W}_{f \times f} \{ \mathbf{K} + \mathbf{E}^T \ddot{\mathbf{q}} \}_{3f \times 1} = \mathbf{0}_{3f \times 1} \quad (3.10)$$

where each diagonal element of \mathbf{W} was itself a 3×3 diagonal matrix that weighted the X, Y and Z components of the linear acceleration constraint equally:

$$\mathbf{W}(i, i) = \begin{bmatrix} w & & \\ & w & \\ & & w \end{bmatrix} \quad i = 1 \dots f \quad (3.11)$$

where w is a non-negative weighting factor between zero and one, indicating the magnitude of the foot point constraint. Therefore $\mathbf{W}(i) = 0$ denotes a free i th foot contact point, $\mathbf{W}(i) = 1$ denotes a fully constrained i th foot contact point, and $0 < \mathbf{W}(i) < 1$ denotes a partially constrained i th foot contact point (Fig. 3.9).

Foot contact point weightings were determined by examining the experimental kinetics of the trial. If the Euclidean norm of the ground reaction force for a given foot was below a user defined threshold, then the foot was deemed to be off the ground and all foot contact points were set to *free*. In all other cases, at least one foot point had to be in rigid contact with the ground, so foot point constraint weightings needed to be specified. Four distinct phases of locomotion were defined, each having foot contact point weightings determined by the experimental center-of-pressure (CoP)

location (Fig. 3.9).

Phase 1 occurs when the CoP lies posterior to the heel axis AB, at which time, foot contact points A and B were fully constrained while C, D and E were free. This approximated the foot-ground interaction as a hinge constraint about the heel axis, from which the entire foot can rotate.

Phase 2 occurs between heel-strike and foot flat, when the CoP lies in the posterior half of the hind-foot boundary ABCD. The transition between phases 1 and 2 was implemented by introducing a weighting function ϕ , such that:

$$\phi(d_h, d_m) = \frac{d_h}{d_h + d_m} \quad (3.12)$$

where d_h and d_m are the shortest distances from the CoP to the heel axis AB and metatarsal axis CD, respectively. Foot points A and B remained fully constrained, while C and D had partially constrained weightings equal to 2ϕ . Therefore, as the CoP moves anteriorly from the heel axis, foot points C and D increased their weighting value from 0 to 1, transforming the foot-ground interaction from a hinge constraint about the heel axis to a weld constraint.

Phase 3 occurs when the CoP crosses into the anterior half of the hind-foot boundary ABCD ($\phi = 0.5$). Foot points C and D remained fully constrained, while the influence of foot points A and B decreased to zero according to $2(1 - \phi)$. Hence, the kinematic constraint of the foot-ground transformed from a weld constraint to a hinge constraint about the metatarsal axis. (Note that when the CoP lies exactly half way between the heel and metatarsal axis, foot points A, B, C and D were all fully constrained, representing a welded foot-flat pose).

Phase 4 occurs when the CoP lies inside the toe boundary CDE. The transition between phases 3 and 4 was implemented by introducing another weighting function γ such that:

$$\gamma(d_m, d_E) = \frac{d_m}{d_E} \quad (3.13)$$

where d_E is the shortest distance from point E to the metatarsal axis. When

phase 4 is reached: (i) foot points A and B are free; (ii) weightings of points C and D begin to decrease according to $1 - \gamma$; and (iii) the weighting of toe point E begins to increase according to γ . Hence, the kinematic constraint of the foot-ground transformed from a hinge constraint about the metatarsal axis to a ball constraint about toe point E. Kinematic constraint weightings are summarised in Table 3.4.

Table 3.4: *Constraint weightings w for each foot contact point. Weightings are calculated for each phase of locomotion as determined by the experimental center-of-pressure value. The same constraint weight is applied in all spatial directions.*

		FOOT PHASE				
		Off ground	Phase 1	Phase 2	Phase 3	Phase 4
FOOT CONTACT POINT	A	0	1	1	$2 \left(1 - \frac{d_h}{d_h + d_m} \right)$	0
	B	0	1	1	$2 \left(1 - \frac{d_h}{d_h + d_m} \right)$	0
	C	0	0	$2 \left(\frac{d_h}{d_h + d_m} \right)$	1	$1 - \frac{d_m}{d_E}$
	D	0	0	$2 \left(\frac{d_h}{d_h + d_m} \right)$	1	$1 - \frac{d_m}{d_E}$
	E	0	0	0	0	$\frac{d_m}{d_E}$

The ordered phase sequence (1-2-3-4) applies to typical heel striking gait (e.g., normal walking and slow running), however, as running speed increases, the position of initial foot strike is made more anteriorly toward the toe (Lieberman et al., 2010). This may result in a phase sequence like (4-3-4). The advantage of using the CoP to determine the phase sequence becomes evident when examining the various styles of running: because foot constraint weightings are based entirely on the experimental CoP, differences in foot-ground contact as a result of increased running speed are implicitly taken into account.

To calculate the contribution of each “*action force*” α (e.g., individual muscles, gravity and centrifugal/Coriolis forces) to the net ground reaction force and acceleration at each joint, the “*action force*” is applied in isolation to the model and Equation 3.14 is uniquely generated (from Equations 3.6

3.2. COMPUTATIONAL MODEL ANALYSES

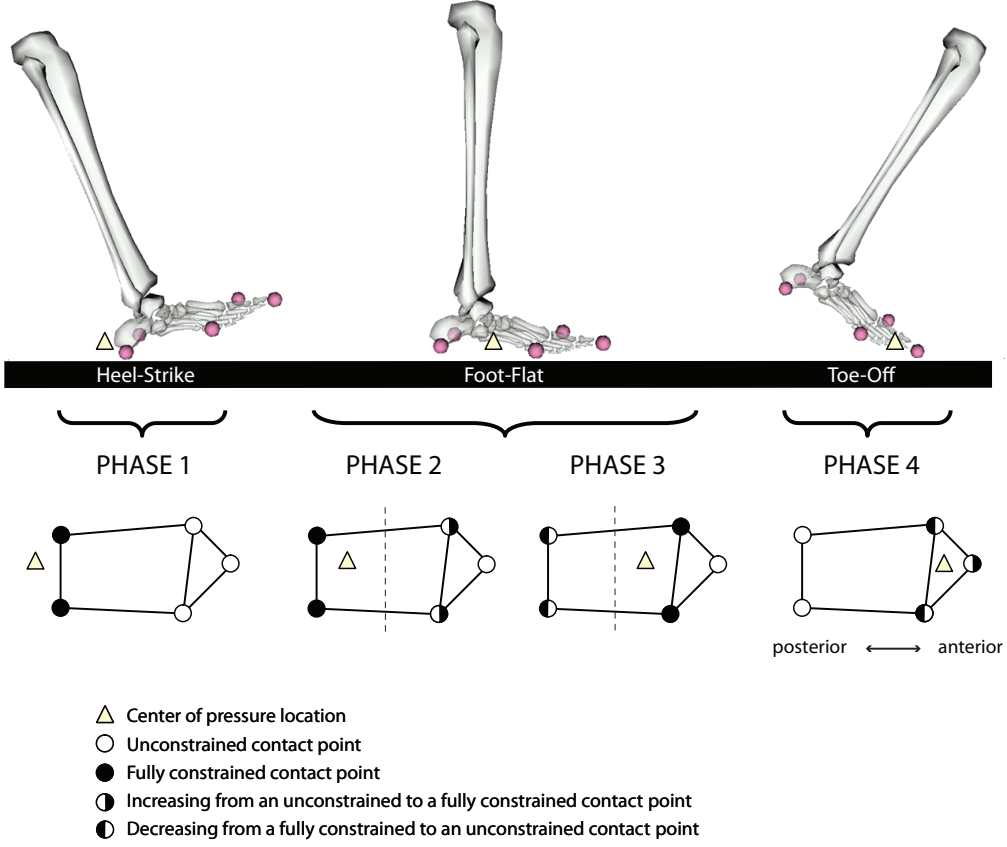


Figure 3.9: Kinematic constraints during stance phase of locomotion. Phase 1 is depicted during heel-strike; phases 2 and 3 are depicted during foot flat; and phase 4 is depicted during toe-off.

and 3.10):

$$\begin{cases} \mathbf{M} \cdot \ddot{\mathbf{q}}^\alpha = \mathbf{F}_{int}^\alpha + \mathbf{E} \cdot \mathbf{F}_{ext}^\alpha \\ \mathbf{W} \{ \mathbf{K}^\alpha + \mathbf{E}^T \ddot{\mathbf{q}}^\alpha \} = \mathbf{0} \end{cases} \quad (3.14)$$

At a given time instant, \mathbf{M} , \mathbf{E} and \mathbf{W} are constant for all “action forces”, allowing these values to be computed outside the “action force” loop. The \mathbf{F}_{int}^α and \mathbf{K}^α vectors, however, must be uniquely calculated for each “action force” α . The \mathbf{F}_{int}^α vector is the generalised force resulting from the isolated application of the “action force”. The \mathbf{K}^α vector forms part of the zero

acceleration foot point constraint. For all “*action forces*” except velocity, $\mathbf{K}^\alpha = \mathbf{0}$ because velocity is disabled in these cases (i.e., $\mathbf{K}^\alpha = \dot{\mathbf{E}}^T \dot{\mathbf{q}}$ and $\dot{\mathbf{q}} = \mathbf{0}$). For the velocity related centrifugal/Coriolis forces, Equation 3.8 is rearranged to calculate \mathbf{K}^{vel} :

$$\mathbf{K}^{vel} = \ddot{\mathbf{x}} - \mathbf{E}^T \ddot{\mathbf{q}} \quad (3.15)$$

The unknown quantities \mathbf{F}_{ext}^α and $\ddot{\mathbf{q}}^\alpha$ represent the contributions of α to the ground reaction force at each foot contact point and generalised acceleration *after* taking into account the foot contact point zero-acceleration constraint equations. These unknowns are calculated by solving an equality-constrained-least-squares optimisation problem: find the values of \mathbf{F}_{ext}^α and $\ddot{\mathbf{q}}^\alpha$ such that Equation 3.14 is satisfied, whilst minimising the objective function J consisting of the weighted squared sum of foot contact point forces:

$$J = \frac{1}{w} \cdot \sum_{i=1}^f \mathbf{F}_{ext_i}^\alpha \mathbf{F}_{ext_i}^\alpha \quad (3.16)$$

Because Equations 3.14 and 3.16) are linear in terms of the unknowns \mathbf{F}_{ext}^α and $\ddot{\mathbf{q}}^\alpha$, they can be represented in matrix form:

$$\tilde{\mathbf{W}} \begin{bmatrix} \mathbf{M} & -\mathbf{E} \\ \mathbf{W} \cdot \mathbf{E}^T & \mathbf{0}_{3f \times 3f} \\ \mathbf{0}_{3f \times n} & \mathbf{W}^{-1} \end{bmatrix} \begin{Bmatrix} \ddot{\mathbf{q}}^\alpha \\ \mathbf{F}_{ext}^\alpha \end{Bmatrix} = \tilde{\mathbf{W}} \begin{Bmatrix} \mathbf{F}^\alpha \\ -\mathbf{W} \cdot \mathbf{K}^\alpha \\ \mathbf{0}_{3f \times 1} \end{Bmatrix} \quad (3.17)$$

where $\tilde{\mathbf{W}}$ is a global diagonal matrix with weights placed on the diagonal elements to emphasise the relative importance of the solution satisfying the: (i) equation of motion equality constraint (Row 1); (ii) foot point acceleration equality constraint (Row 2); and (iii) cost function (Row 3). $\tilde{\mathbf{W}}$ is defined as:

$$\tilde{\mathbf{W}} = \begin{bmatrix} 10^4 \mathbf{I}_{n \times n} & & \\ & 10^2 \mathbf{I}_{3m \times 3m} & \\ & & \mathbf{I}_{3m \times 3m} \end{bmatrix} \quad (3.18)$$

Large penalties are applied to solutions that do not satisfy the equations of motion because they represent the dynamics of the model. In reality, the rigid contact assumption of foot points may not always hold (e.g., the foot may slide along the ground during initial and terminal stance), hence their constraint equations are penalised less. Note that during the flight phase of running when there is no contact between the foot and ground ($f = 0$), Equation 3.17 reduces to the rigid body equations of motion that can be solved determinately:

$$\begin{bmatrix} \mathbf{M} & -\mathbf{E} \end{bmatrix} \begin{Bmatrix} \ddot{\mathbf{q}}^\alpha \\ \mathbf{0} \end{Bmatrix} = \mathbf{F}^\alpha \quad (3.19)$$

Equation 3.17, can be expressed in a more compact form:

$$\mathbf{A} \begin{Bmatrix} \ddot{\mathbf{q}}^\alpha \\ \mathbf{F}_{ext}^\alpha \end{Bmatrix} = \mathbf{b} \quad (3.20)$$

where \mathbf{A} is an $(n + 6f) \times (n + 3f)$ matrix and \mathbf{b} is an $(n + 6f) \times 1$ vector. At a given time instant, the \mathbf{A} matrix is constant for all “*action forces*”, and the \mathbf{b} vector is unique for each individual “*action force*”. Thus, the principle of superposition will be satisfied:

$$\begin{aligned} \mathbf{A}\mathbf{x}_1 &= \mathbf{b}_1 \\ \mathbf{A}\mathbf{x}_2 &= \mathbf{b}_2 \\ &\vdots \\ \mathbf{A}\mathbf{x}_m &= \mathbf{b}_m \\ \mathbf{A}(\mathbf{x}_1 + \mathbf{x}_2 + \dots + \mathbf{x}_m) &= \mathbf{b}_1 + \mathbf{b}_2 + \dots + \mathbf{b}_m \end{aligned} \quad (3.21)$$

A least-squares pseudo-inverse operator provides an optimal analytical solution to the over-determined problem of Equation 3.20 without having to perform numerical iterations:

$$\begin{Bmatrix} \ddot{\mathbf{q}}^\alpha \\ \mathbf{F}_{ext}^\alpha \end{Bmatrix} = \mathbf{A}^+ \mathbf{b} \quad (3.22)$$

where \mathbf{A}^+ is the Moore-Penrose pseudo-inverse of the matrix \mathbf{A} . The least square error of the solution can also be computed, representing how well the solution matched the constraints:

$$\begin{Bmatrix} \mathbf{err_eom}_{n \times 1} \\ \mathbf{err_footconstraint}_{3f \times 1} \\ \mathbf{err_costfunction}_{3f \times 1} \end{Bmatrix} = \mathbf{A}^+ \begin{Bmatrix} \ddot{\mathbf{q}}^\alpha \\ \mathbf{F}_{ext}^\alpha \end{Bmatrix} - \mathbf{b} \quad (3.23)$$

At each time instant of the gait cycle, Equation 3.22 was solved repeatedly for each “*action force*” α in the model. Finally, the contribution of α to the net ground reaction force was obtained by summing the individual contributions of α on each foot point, on each foot and in each direction. After all “*action forces*” were summed, the superposition principle may still remain unsatisfied (i.e., the sum of all “*action forces*” to the ground reaction force may not sum exactly to the experimental ground reaction force). Such superposition errors arise due to the assumption of rigid foot-ground contact not being entirely accurate (Anderson and Pandy, 2003). To account for these inaccuracies, an additional fictitious force called an inertial force was defined as the *action force* required to equate the model and experimental totals together such that superposition will always be satisfied. The contribution of the inertial force to the joint acceleration and ground reaction force was solved using a slightly modified version of Equation 3.17:

$$\begin{bmatrix} \mathbf{M} & -\mathbf{E} \\ \mathbf{I}_{n \times n} & \mathbf{0}_{3f \times 3f} \end{bmatrix} \begin{Bmatrix} \ddot{\mathbf{q}}^I \\ \mathbf{F}_{ext}^I \end{Bmatrix} = \begin{Bmatrix} \mathbf{0}_{n \times 1} \\ (\ddot{\mathbf{q}}^{Exp} - \ddot{\mathbf{q}}^{Model}) \end{Bmatrix} \quad (3.24)$$

where $\ddot{\mathbf{q}}^{Exp}$ is the experimental generalised joint acceleration vector and $\ddot{\mathbf{q}}^{Model}$ is the sum of all induced accelerations from all “*action forces*”:

$$\ddot{\mathbf{q}}^{Model} = \sum_{\alpha=1}^{numActionForces} \ddot{\mathbf{q}}^\alpha \quad (3.25)$$

Equation 3.24 does not contain a third row (which was previously defined as the cost function in Equation 3.17), and hence reduces to a deterministic problem. Therefore, $\ddot{\mathbf{q}}^I$ and \mathbf{F}_{ext}^I were solved uniquely:

$$\ddot{\mathbf{q}}^I = \ddot{\mathbf{q}}^{Exp} - \ddot{\mathbf{q}}^{Model} \quad (3.26)$$

$$\mathbf{F}_{ext}^I = \mathbf{E}^+ (\mathbf{M} \cdot \ddot{\mathbf{q}}^I) \quad (3.27)$$

3.2.8 Instantaneous segment power decomposition

The instantaneous mechanical power P of a system can be written as:

$$P = [\mathbf{M}(\mathbf{q}) \ddot{\mathbf{q}} - \mathbf{C}(\mathbf{q}, \dot{\mathbf{q}}) - \mathbf{G}(\mathbf{q})] \dot{\mathbf{q}} \quad (3.28)$$

Following from the solution of the contribution of each “*action force*” α to the joint accelerations of the system $\ddot{\mathbf{q}}^\alpha$ at a given time frame (given by Equations 3.22 and 3.26), the mechanical power P_i of an individual segment i induced by an “*action force*” α can be found from Equation 3.29 by setting all masses and inertias to zero except the mass and inertia of segment i (Fregly and Zajac, 1996):

$$P_i = [\mathbf{M}_i(\mathbf{q}) \ddot{\mathbf{q}}^\alpha - \mathbf{C}_i(\mathbf{q}, \dot{\mathbf{q}}) - \mathbf{G}_i(\mathbf{q})] \dot{\mathbf{q}} \quad (3.29)$$

where the subscript i on the right hand side indicates that only the mass and inertia of segment i appear in these matrices. A positive value of P_i means that mechanical energy from “*action force*” α is flowing into the segment while a negative value of P_i means that mechanical energy from “*action force*” α is flowing out of the segment.

The *IndAccPI* plug-in implements the instantaneous segment power decomposition in a double nested loop: For each segment i , the $\mathbf{M}_i(\mathbf{q})$, $\mathbf{C}_i(\mathbf{q}, \dot{\mathbf{q}})$ and $\mathbf{G}_i(\mathbf{q})$ matrices are computed. This becomes the outer loop. The inner loop then cycles through each “*action force*” α , substituting $\ddot{\mathbf{q}}^\alpha$ as calculated from Equations 3.22 or 3.26, into one of Equations 3.30, 3.31

or 3.32.

If the “*action force*” is gravity:

$$P_i = [\mathbf{M}_i(\mathbf{q}) \ddot{\mathbf{q}}^\alpha - \mathbf{G}_i(\mathbf{q})] \dot{\mathbf{q}} \quad (3.30)$$

If the “*action force*” is velocity related (i.e., centrifugal and Coriolis forces):

$$P_i = [\mathbf{M}_i(\mathbf{q}) \ddot{\mathbf{q}}^\alpha - \mathbf{C}_i(\mathbf{q}, \dot{\mathbf{q}})] \dot{\mathbf{q}} \quad (3.31)$$

For all other action forces (e.g., muscles, reserve actuators or residual actuators):

$$P_i = [\mathbf{M}_i(\mathbf{q}) \ddot{\mathbf{q}}^\alpha] \dot{\mathbf{q}} \quad (3.32)$$

Because superposition holds for the “*action force*” contributions to joint acceleration, superposition will also hold for the “*action force*” contributions to the instantaneous segment power as the term $\ddot{\mathbf{q}}^\alpha$ appears linearly in Equations 3.30, 3.31 and 3.32.

At each time instant of the stride cycle, Equation 3.22 is solved repeatedly for each “*action force*” α applied to the model during a simulation. Then Equations 3.26 and 3.27 are solved to determine inertial “*action force*” contributions, after which Equations 3.30, 3.31 and 3.32 are generated for each “*action force*” to determine their contributions to the instantaneous segment power of the system. This process is repeated for all time frames of a stride cycle.

The joint acceleration, ground reaction force and instantaneous segment power decomposition methods (described here and in section 3.2.7) was developed as an OpenSim analysis plug-in and is freely available in the public domain (https://simtk.org/home/tims_plugins) to extend the functionality of OpenSim.

Chapter 4

Estimates of leg muscle function in human gait depend on how foot-ground contact is modelled

This chapter is based on the following published work:

- **Dorn, T.W., Lin, Y.C., Pandy, M.G. (2011).** Estimates of leg-muscle function in human gait depend on how foot-ground contact is modeled, *Computer Methods in Biomechanics and Biomedical Engineering*, In press.

ABSTRACT

Computational analyses of leg-muscle function in human locomotion commonly assume that contact between the foot and the ground occurs at discrete points on the sole of the foot. Kinematic constraints acting at these contact points restrict the motion of the foot and therefore alter model calculations of muscle function. The aim of this study was to evaluate how predictions of muscle function obtained from musculoskeletal models are influenced by the model used to simulate ground contact. Both single- and multiple-point contact models were evaluated. Muscle function during walking and running was determined by quantifying the contributions of individual muscles to the vertical, fore-aft and mediolateral components of the ground reaction force. The results showed that two factors - the number of foot-ground contact points assumed in the model and the type of kinematic constraint enforced at each point - affect the model predictions of muscle coordination. Whereas single- and multiple-point contact models produced similar predictions of muscle function in the sagittal plane, inconsistent results were obtained in the transverse plane. Kinematic constraints applied in the sagittal plane altered the model predictions of muscle contributions to the vertical and fore-aft ground reaction forces, while constraints applied in the frontal plane altered the calculations of muscle contributions to the mediolateral ground reaction force. The results illustrate the sensitivity of calculations of muscle coordination to the model used to simulate foot-ground contact.

4.1 Introduction

A muscle can exert a torque about a joint only if it spans that joint. However, a muscle can simultaneously accelerate all the joints in the body, even those not spanned by the muscle. This is a consequence of dynamic coupling, whereby the force applied by a muscle is transmitted through the bones to all the joints in the body (Zajac and Gordon, 1989). If a muscle force contributes to the accelerations of all the joints, then it also must contribute to the acceleration of the body's center-of-mass and hence, by Newton's Second Law of Motion (i.e., Force equals mass times acceleration), to the force exerted on the ground. Thus, the functional role of a muscle may be determined by quantifying its contribution to the ground reaction force.

A number of studies have described leg muscle function during gait by calculating the contributions of individual muscles to the accelerations of the lower-limb joints (Kepple et al., 1997a; Arnold et al., 2005; Goldberg and Kepple, 2009) and to the acceleration of the body's center-of-mass (Kepple et al., 1997b; Anderson and Pandey, 2003; Sasaki and Neptune, 2006; Liu et al., 2008; Xiao and Higginson, 2008; Hamner et al., 2010; Pandey et al., 2010). In each of these studies, a simplified model of ground contact was used to simulate the dynamic interaction between the foot and the ground. These simplified models often assume that foot-ground contact occurs at discrete points which vary in number from a single point located at the center-of-pressure (Kepple et al., 1997b; Liu et al., 2008; Goldberg and Kepple, 2009; Hamner et al., 2010) to multiple points distributed over the sole of the foot (Neptune et al., 2000; Anderson and Pandey, 2003; Pandey et al., 2010). At each contact point, kinematic constraints are applied, either explicitly as hard constraints (Kepple et al., 1997b; Anderson and Pandey, 2003; Hamner et al., 2010; Pandey et al., 2010) or implicitly by using springs and dampers to simulate the interaction between the foot and the ground (Sasaki and Neptune, 2006; Liu et al., 2008). Kinematic constraints alter the motion of the foot and therefore potentially influence the model calculations of muscle function.

Models of ground contact should include the effects of impact, friction

and distributed contact, all of which are manifested as kinematic constraints. Unfortunately, the effects of these kinematic constraints cannot be directly measured, and so model predictions of muscle function cannot be rigorously validated. However, a theoretical principle called 'superposition' may be used to gain confidence in the model predictions (Anderson and Pandy, 2003; Hamner et al., 2010; Lin et al., 2011a; Pandy et al., 2010). This principle states that the sum of the contributions of all action forces (e.g., muscles, gravity and centrifugal forces) to the ground reaction force must be equal to the total ground reaction force measured in a gait experiment. Although superposition is a necessary condition for evaluating the accuracy of the model calculations of muscle function, it is not sufficient for determining the validity of the individual contributions of the various action forces to the total ground reaction force. Results obtained from a given model of ground contact may therefore satisfy superposition and still yield erroneous estimates of muscle function.

The overall goal of this study was to evaluate how calculations of muscle function are influenced by the model used to simulate foot-ground contact. Our specific aim was to determine the effects of kinematic constraints and the number of foot-ground contact points on calculations of muscle contributions to the ground reaction force in walking and running.

4.2 Methods

Overground gait experiments were performed on 14 healthy adults (age, 28.5 ± 8.3 years; weight, 71.2 ± 8.0 kg; height, 176.2 ± 5.8 cm) as each subject walked and ran at their preferred speeds (walking: n=13, 1.46 ± 0.11 m/s; running: n=10, 3.42 ± 0.13 m/s). Experiments were conducted in the Human Motion Laboratory at the University of Melbourne and in the Biomechanics Laboratory at the Australian Institute of Sport. Subjects gave their informed consent after approval was obtained from the relevant institutional Human Research Ethics Committees.

Reflective markers were mounted over anatomical landmarks on the trunk and lower limbs of each subject. Kinematic data were acquired using

a three-dimensional video motion capture system (VICON, Oxford Metrics, UK). Ground reaction forces were measured simultaneously using a series of force plates embedded in the ground. In all trials, subjects made initial ground contact with their heels. Surface electromyographic (EMG) electrodes were placed over the bellies of six muscles in one leg: gluteus maximus, gluteus medius, medial hamstrings, vastus lateralis, medial gastrocnemius and soleus. The raw EMG signal was passed through a Teager-Kaiser energy filter to improve onset detection (Li et al., 2007). Marker trajectories were low-pass filtered using a fourth-order Butterworth filter with a cut-off frequency of 4 Hz. A Gait-Extract toolbox developed in MATLAB (freely available from <https://simtk.org/home/c3dtoolbox>) was used to extract and process the raw marker trajectories, ground reaction forces and EMG data for input into the musculoskeletal model.

The musculoskeletal model used in this study was identical to that described by Anderson and Pandy (1999). The skeleton was represented as a 10-segment, 23-degree-of-freedom mechanical linkage. The pelvis was free to translate and rotate in space. The head, arms and torso were lumped together as a single rigid body, which articulated with the pelvis via a ball-and-socket back joint. Each hip was modelled as a ball-and-socket joint, each knee as a hinge joint, each ankle-subtalar complex as a universal joint, and each metatarsal as a hinge joint. The skeleton was actuated by 54 muscle-tendon units, each unit represented as a Hill-type muscle in series with an elastic tendon.

Subject-specific models of the skeleton were generated by scaling the anthropometric properties of each segment according to each subject's height and weight (Section 3.1.1). Joint-center locations and joint axes of rotation were determined by minimising the differences between measured and model-computed marker positions during isolated joint motion trials (Reinbolt et al., 2005; Kim et al., 2009). Force generating properties, attachment sites and the paths of all muscles in the model were the same as those identified by Anderson and Pandy (1999).

Inverse kinematics, inverse dynamics and static optimisation were used to calculate leg muscle forces for walking and running (Section 3.2.2, 3.2.3

and 3.2.4). Joint kinematics and ground reaction forces were input into the model skeleton to calculate the net joint moments exerted about the back, hip, knee, ankle and metatarsal joints. At each time instant, the net joint moments were decomposed into individual muscle forces by solving an optimisation problem that minimised the sum of the squares of the muscle activations subject to physiological bounds imposed by each muscle's force-length-velocity property (Anderson and Pandy, 2001b).

Six different ground-contact models were evaluated in this study. These models were selected because they have been implemented in previous studies reported in the literature (see Table 4.1). Each contact model differed by either the number of contact points defined on the sole of the foot or the type of kinematic constraint enforced at each foot-contact point. Kinematic constraints were defined by specifying a set of weighting coefficients associated with the linear and/or rotational degrees of freedom permitted at each contact point. The value of each weighting coefficient ranged from 0 to 1, where 0 denoted no contact and 1 denoted rigid contact. Four of the models — BALL, UNIVERSAL, HINGE and WELD — assumed that ground contact occurred at a single point under the foot: the center-of-pressure. In each of these models the values of the weighting coefficients remained constant throughout the stance phase of gait, and so these models were categorised as time-independent. The remaining two models — SINGLEPOINT and MULTIPOINT — were categorised as time-dependent because the values of the weighting coefficients varied as a function of time to allow the foot to transition smoothly from heel-strike to foot-flat and from foot-flat to toe-off (see Fig. 4.1). The SINGLEPOINT model assumed that ground contact occurred at a single point under the foot, the center-of-pressure, whereas the MULTIPOINT model assumed that the foot contacted the ground at five discrete points. Because foot-ground contact actually occurs over a finite surface area with varying kinematic constraints (Wojtyra, 2003; Cheung and Zhang, 2005), the MULTIPOINT model represented the most realistic model of foot-ground contact evaluated in the present study.

A pseudo-inverse ground force decomposition method (Lin et al., 2011a) was used to determine the contributions of all action forces to the vertical,

Table 4.1: Summary of the six ground-contact models evaluated in this study. X , Y and Z define, respectively, the fore-aft, vertical and mediolateral axes of the foot segment in the model.

	Contact model	Contact location	Kinematic constraints		Degrees of freedom	Citation
			[X Y Z]			
			Linear	Rotational		
Time-independent	BALL	CoP	[1 1 1]	[0 0 0]	3	(Kepple et al., 1997b)
	UNIVERSAL	CoP	[1 1 1]	[0 1 0]	2	(Hamner et al., 2010)
	HINGE	CoP	[1 1 1]	[1 1 0]	1	*(Goldberg and Kepple, 2009)
	WELD	CoP	[1 1 1]	[1 1 1]	0	(Kepple et al., 1997a)
Time-dependent	SINGLEPOINT	CoP	[1 1 1]	$f(CoP)$	$f(CoP)$	** (Liu et al., 2008)
	MULTIPOINT	5 points	$f(CoP)$	N/A	$f(CoP)$	(Anderson and Pandy, 2003) (Arnold et al., 2005) (Pandy et al., 2010)

* Goldberg et al., 2009 prescribed a WELD constraint in the small amount of time between foot flat and heel off, and a HINGE constraint for the remainder of the gait cycle.

** Liu et al., 2008 determined the rotational kinematic constraints not as a function of center-of-pressure, but rather as an explicit function of time. From foot-flat to heel-off, rotational $[X, Y, Z] = [1 \ 1 \ 1]$, at all other times rotational $[X, Y, Z] = [0, 0, 0]$. Weightings were modulated using a smooth “falloff” function.

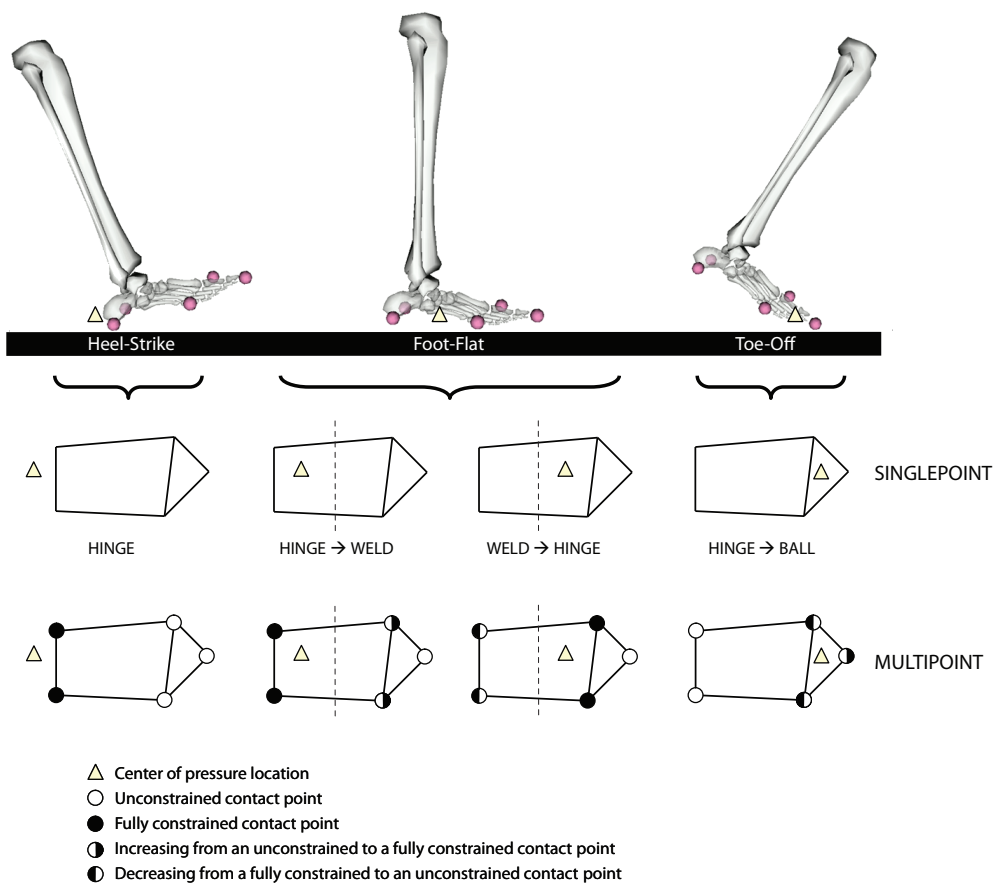


Figure 4.1: Diagram illustrating how the time-dependent kinematic constraints applied at the foot-contact points varied as a function of the location of the foot center-of-pressure in the SINGLEPOINT and MULTIPOINT models. In the SINGLEPOINT model, contact occurred at the center-of-pressure and the constraints transitioned from the HINGE at heel strike, to the WELD at mid-stance, and finally to the BALL at toe-off. In the MULTIPOINT model, contact occurred at five discrete points distributed over the foot. Weighting coefficients ranging from 0 and 1 were applied at each contact point to allow the foot to transition smoothly from heel-strike to foot-flat and from foot-flat to toe-off (see Table 4.1).

fore-aft and mediolateral components of the ground reaction force. At each instant of the stride cycle, each action force (e.g., a muscle force) obtained from the inverse dynamics analysis was applied in isolation to the model of the skeleton. A weighted least-squares optimisation problem was then solved to determine the contribution of each action force to the model-computed ground reaction forces.

Superposition error was defined as the difference between the measured and computed ground reaction forces. Superposition error was computed for each component of the ground reaction force using a normalised root-mean-square error (NRMSE) approach. The NRMSE was found by calculating the RMS error of the difference between the measured ground reaction force and the sum of all action force contributions to the model-computed ground reaction force. This difference represents the accuracy of the rigid contact assumption imposed at each foot-ground contact point in the model (Anderson and Pandy 2003). A non-zero superposition error indicates that an additional external (fictitious) force must be applied to the foot to satisfy the rigid contact assumption. The RMS superposition error was normalised by the peak value of the measured ground reaction force to obtain the NRMSE. The NRMSE was computed for each subject using all six ground contact models and then averaged across all subjects to obtain a mean NRMSE.

4.3 Results

The timing of muscle contractions predicted for walking and running was similar to those exhibited by EMG signals measured during the experiment (Fig. 4.2). The magnitudes of the muscle forces calculated for walking and running were also consistent with data reported previously by others (Anderson and Pandy, 2001a; Thelen and Anderson, 2006; Hamner et al., 2010).

In walking and running, five muscle groups — gluteus maximus, gluteus medius, vasti, soleus and gastrocnemius — contributed most significantly to the vertical and fore-aft components of the ground reaction force (Figs 4.3

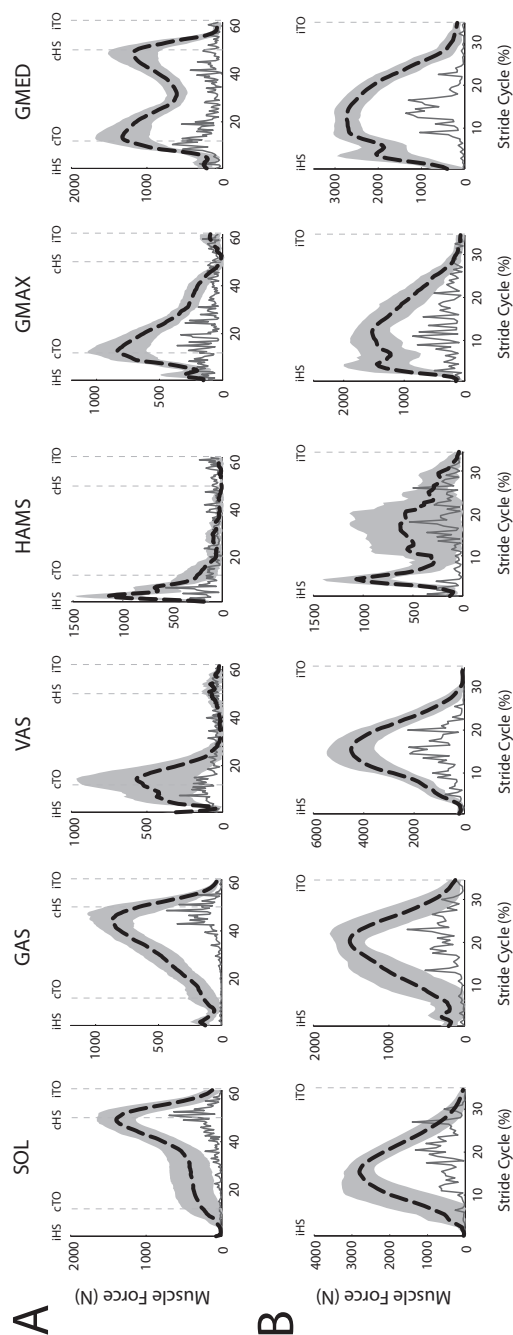


Figure 4.2: Musculotendon forces (dashed lines) calculated for walking (A) and running (B). The shaded regions represent 1 standard deviation from the mean. The wavy lines represent average muscle EMG data measured for the subjects. Muscle symbols: SOL (soleus), GAS (medial and lateral portions of gastrocnemius combined; medial gastrocnemius EMG shown), VAS (vastus medialis, vastus intermedialis and vastus lateralis combined; vastus lateralis EMG shown), HAMS (medial and lateral portions of hamstrings combined; medial hamstring EMG shown), GMAX (gluteus maximus), and GMED (anterior and posterior portions of gluteus medius). Major gait events: iHS, ipsilateral heel-strike; cHS, contralateral heel-strike; iTO, ipsilateral toe-off; cTO, contralateral toe-off.

and 4.4, TOTAL). The hamstrings and rectus femoris contributed relatively little (Tables 4.2 and 4.3).

Model estimates of muscle function were dependent on how foot-ground contact was modelled. For walking, the patterns of muscle function were similar in the vertical, fore-aft and mediolateral directions for the BALL and UNIVERSAL models. The HINGE model also predicted similar patterns of muscle function in the vertical and fore-aft directions; however, adding a kinematic constraint in the frontal plane (i.e., progressing from a UNIVERSAL joint to a HINGE joint) altered the actions of the gluteus maximus and the ankle plantarflexors in the mediolateral direction (Fig. 4.3, Table 4.2). Adding another constraint in the sagittal plane (i.e., progressing from a HINGE joint to a WELD joint) changed the actions of the soleus in all three directions.

Model predictions of muscle function were also influenced by the presence of time-dependent kinematic constraints in the ground-contact model. For walking, the contributions of the ankle plantarflexors to the vertical ground force were reduced in the first half of stance for the SINGLEPOINT and MULTIPOINT models (Fig. 4.3). These models also showed that the ankle plantarflexors accelerated the center-of-mass in late stance, contrary to the behavior predicted by the WELD model.

For running, the soleus generated the majority of support during stance when the BALL, UNIVERSAL and HINGE models were used to simulate ground contact, whereas the vasti contributed most significantly to support when the WELD, SINGLEPOINT and MULTIPOINT models were used (Fig. 4.4, Table 4.3). Whereas the SINGLEPOINT and MULTIPOINT models predicted similar patterns of muscle coordination for walking, differences were evident in the coordination predicted for running, particularly in the mediolateral direction (Figs 4.3 and 4.4, compare VAS and GAS). Calculations of muscle function in the mediolateral direction were most sensitive to the way in which foot-ground contact was modelled.

Superposition error was sensitive to both gait speed and the model used to simulate foot-ground contact (Figs 4.5 and 4.6). The errors for running were larger than those for walking. Superposition errors were

Table 4.2: Peak contributions of muscle forces and gravitational forces (Gravity) to the fore-aft (F-A), vertical (VERT) and mediolateral (M-L) ground reaction forces generated in walking.

	BALL			UNIVERSAL			HINGE			WELD			SINGLEPOINT			MULTIPOINT			
	F-A	VERT	M-L	F-A	VERT	M-L	F-A	VERT	M-L	F-A	VERT	M-L	F-A	VERT	M-L	F-A	VERT	M-L	
GMAX	Mean	-0.06	0.18	0.05	-0.06	0.21	0.06	-0.06	0.20	-0.03	-0.04	0.31	-0.03	-0.05	0.31	-0.03	-0.05	0.32	-0.02
	STD	0.02	0.06	0.03	0.03	0.06	0.05	0.03	0.06	0.02	0.05	0.13	0.02	0.04	0.14	0.02	0.04	0.14	0.03
GMED	Mean	-0.04	0.18	-0.08	-0.04	0.16	-0.13	-0.04	0.16	-0.14	0.17	0.36	-0.11	0.11	0.35	-0.12	0.04	0.32	-0.14
	STD	0.02	0.10	0.04	0.02	0.09	0.04	0.02	0.10	0.03	0.06	0.09	0.02	0.09	0.09	0.03	0.05	0.08	0.04
ILPSO	Mean	0.03	-0.05	0.02	0.03	-0.05	0.01	0.02	-0.06	0.04	0.25	0.38	0.07	0.17	0.27	0.05	0.07	0.05	0.03
	STD	0.04	0.09	0.02	0.04	0.09	0.03	0.05	0.10	0.03	0.12	0.26	0.04	0.11	0.25	0.04	0.07	0.25	0.04
HAMS	Mean	0.06	0.17	0.02	0.06	0.18	0.02	0.06	0.19	-0.01	0.12	0.02	-0.02	0.10	0.11	-0.02	0.08	0.13	-0.02
	STD	0.01	0.07	0.02	0.01	0.07	0.02	0.02	0.08	0.02	0.04	0.13	0.02	0.04	0.13	0.02	0.03	0.11	0.02
RF	Mean	-0.07	0.15	-0.01	-0.07	0.15	-0.01	-0.07	0.15	-0.02	0.05	0.29	-0.01	-0.07	0.18	-0.02	-0.08	0.17	-0.03
	STD	0.05	0.04	0.02	0.06	0.04	0.01	0.06	0.04	0.01	0.08	0.10	0.02	0.05	0.08	0.01	0.02	0.06	0.01
VAS	Mean	-0.12	0.24	-0.01	-0.12	0.25	-0.01	-0.12	0.24	0.02	-0.14	0.24	0.02	-0.13	0.22	0.02	-0.13	0.20	0.03
	STD	0.07	0.11	0.02	0.07	0.12	0.02	0.07	0.14	0.03	0.05	0.18	0.03	0.06	0.20	0.03	0.05	0.23	0.02
GAS	Mean	0.14	0.38	-0.05	0.14	0.38	-0.05	0.14	0.39	0.05	-0.04	0.05	0.00	0.11	0.11	0.02	0.12	0.27	0.05
	STD	0.03	0.26	0.04	0.03	0.26	0.05	0.03	0.26	0.01	0.01	0.04	0.01	0.05	0.31	0.03	0.04	0.21	0.01
SOL	Mean	0.18	0.73	-0.04	0.18	0.72	-0.04	0.17	0.73	0.06	-0.21	0.26	0.00	-0.02	0.54	0.03	0.14	0.65	0.08
	STD	0.04	0.10	0.07	0.04	0.10	0.07	0.04	0.10	0.03	0.03	0.07	0.03	0.19	0.24	0.03	0.12	0.13	0.02
Gravity	Mean	-0.04	0.25	0.02	-0.04	0.26	0.02	-0.05	0.27	0.02	0.05	0.32	0.03	0.02	0.30	0.02	-0.07	0.31	0.02
	STD	0.02	0.03	0.03	0.02	0.03	0.02	0.02	0.03	0.01	0.11	0.03	0.01	0.10	0.03	0.01	0.05	0.04	0.02

* [R] denotes a rearfoot-strike and [F] denotes a forefoot-strike

Table 4.3: Peak contributions of muscle forces and gravitational forces (Gravity) to the fore-aft (F-A), vertical (VERT) and mediolateral (M-L) ground reaction forces generated in running.

	BALL		UNIVERSAL		HINGE		WELD		SINGLEPOINT		MULTIPOINT								
	F-A	VERT	M-L	F-A	VERT	M-L	F-A	VERT	M-L	F-A	VERT	M-L							
GMAX	Mean	-0.07	0.41	0.07	-0.08	0.46	0.12	-0.07	0.44	-0.05	0.16	0.56	-0.04	0.16	0.56	-0.04	0.13	0.57	0.00
	STD	0.04	0.13	0.10	0.06	0.15	0.09	0.05	0.13	0.04	0.12	0.23	0.06	0.11	0.23	0.06	0.12	0.24	0.06
GMED	Mean	-0.04	0.29	-0.18	-0.02	0.25	-0.24	-0.03	0.28	-0.21	0.14	0.35	-0.21	0.12	0.35	-0.21	0.09	0.36	-0.21
	STD	0.06	0.10	0.06	0.05	0.09	0.08	0.05	0.10	0.06	0.07	0.12	0.05	0.07	0.12	0.05	0.05	0.12	0.05
ILPSO	Mean	0.05	-0.09	0.01	0.05	-0.09	0.01	0.05	-0.10	-0.01	0.01	-0.22	-0.03	-0.03	-0.21	-0.03	0.02	-0.19	0.01
	STD	0.06	0.16	0.03	0.06	0.17	0.03	0.06	0.18	0.03	0.18	0.23	0.04	0.15	0.22	0.04	0.10	0.20	0.04
HAMS	Mean	0.09	-0.01	0.01	0.10	-0.01	0.00	0.10	-0.02	-0.03	0.13	0.01	-0.03	0.13	0.04	-0.03	0.13	0.01	0.00
	STD	0.04	0.11	0.03	0.04	0.11	0.03	0.04	0.11	0.02	0.05	0.12	0.03	0.04	0.11	0.03	0.04	0.13	0.03
RF	Mean	-0.16	0.18	-0.04	-0.17	0.19	-0.01	-0.17	0.19	-0.04	-0.18	0.22	-0.04	-0.18	0.21	-0.04	-0.18	0.19	-0.03
	STD	0.05	0.04	0.02	0.05	0.03	0.03	0.05	0.03	0.02	0.06	0.04	0.02	0.06	0.04	0.02	0.06	0.04	0.01
VAS	Mean	-0.49	0.51	-0.05	-0.49	0.51	0.00	-0.49	0.52	0.11	-0.06	1.23	0.16	-0.19	1.19	0.15	-0.28	1.06	0.08
	STD	0.21	0.25	0.10	0.21	0.25	0.09	0.22	0.25	0.06	0.21	0.63	0.08	0.24	0.59	0.08	0.18	0.54	0.13
GAS	Mean	0.31	0.54	-0.02	0.31	0.54	-0.02	0.31	0.55	0.04	-0.09	-0.04	-0.01	0.13	0.27	0.01	0.17	0.18	0.10
	STD	0.09	0.32	0.08	0.09	0.32	0.09	0.09	0.34	0.05	0.14	0.20	0.04	0.20	0.32	0.05	0.11	0.34	0.05
SOL	Mean	0.29	1.20	-0.02	0.29	1.20	-0.02	0.29	1.20	0.11	-0.16	0.53	0.05	-0.13	0.67	0.06	-0.14	0.72	0.12
	STD	0.06	0.37	0.13	0.06	0.37	0.12	0.06	0.37	0.03	0.21	0.13	0.05	0.23	0.32	0.05	0.20	0.26	0.04
Gravity	Mean	0.00	0.25	0.02	0.00	0.25	0.01	0.00	0.27	-0.01	0.10	0.30	0.01	0.02	0.28	0.00	0.01	0.29	0.02
	STD	0.08	0.04	0.03	0.08	0.04	0.03	0.08	0.02	0.03	0.09	0.03	0.03	0.09	0.03	0.03	0.08	0.03	0.02

* [R] denotes a rearfoot-strike and [F] denotes a forefoot-strike

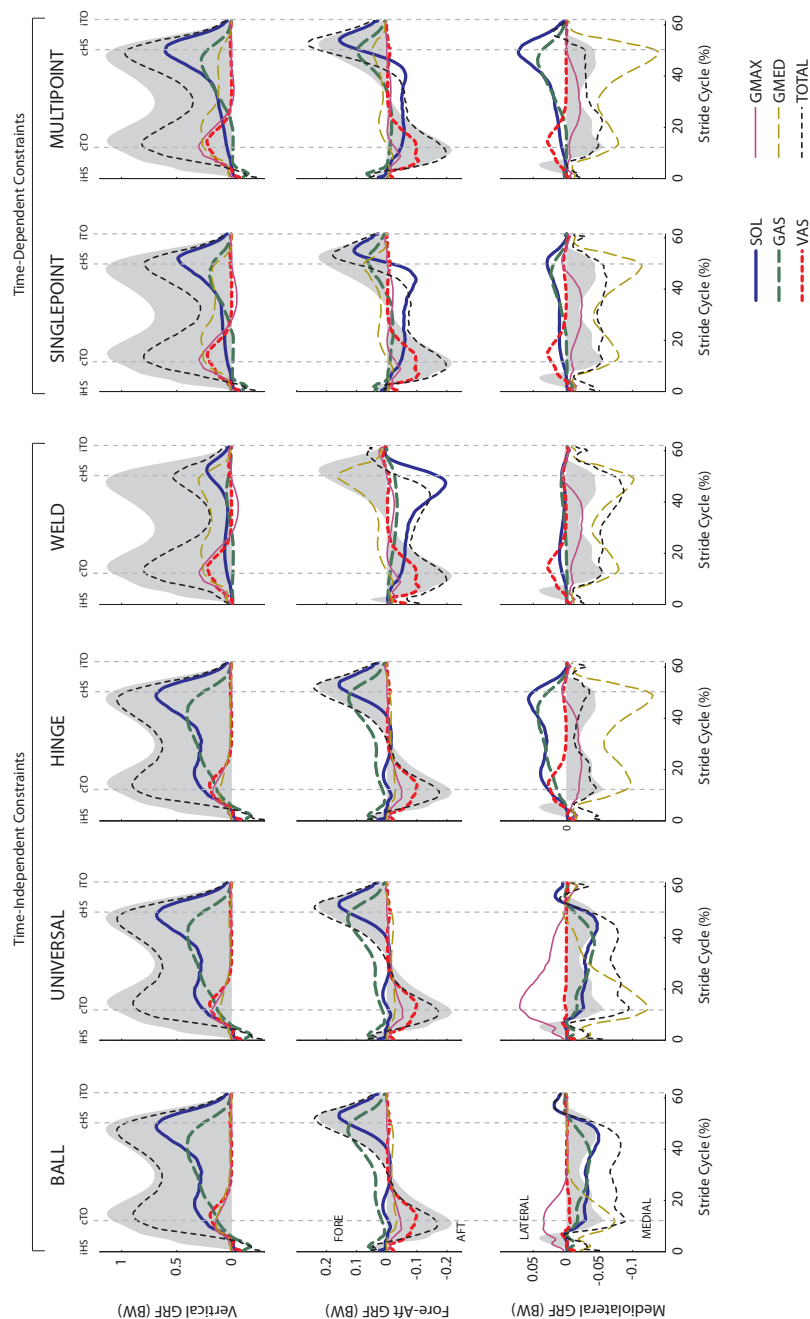


Figure 4.3: Muscle contributions to the vertical, fore-aft and mediolateral components of the ground reaction force (GRF) generated in walking. The shaded regions represent the forces recorded by the force plate. Results are shown for the six different ground contact models evaluated. The results for each contact model were averaged across all subjects. Muscle symbols as defined in Fig. 4.2. TOTAL represents the summed contributions of SOL, GAS, VAS, GMAX and GMED. Mediolateral ground forces are those represented for a right leg. Forces are expressed in units of body weight (BW); the average mass of the subjects was 71.2 kg.

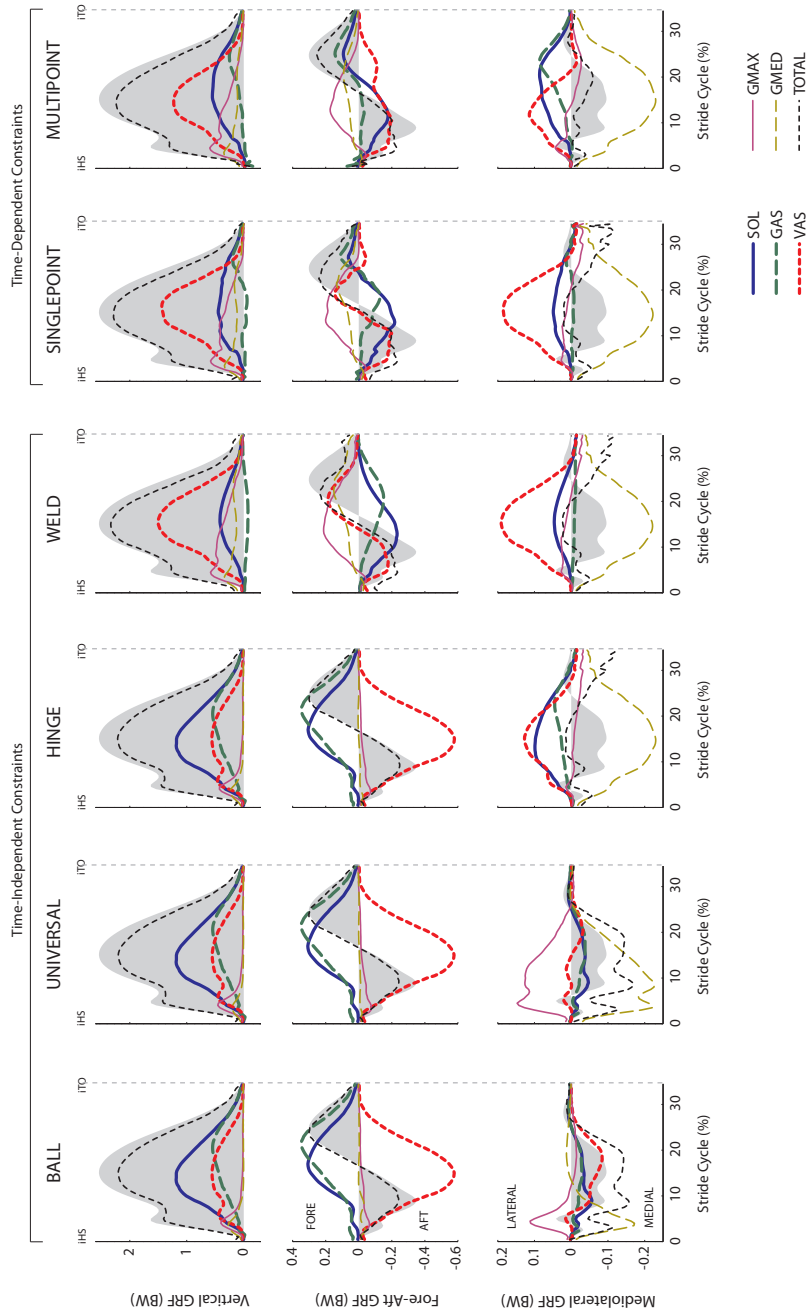


Figure 4.4: Muscle contributions to the vertical, fore-aft and mediolateral components of the ground reaction force (GRF) generated in running. The shaded regions represent the forces recorded by the force plate. Results are shown for the six different ground contact models evaluated. The results for each contact model were averaged across all subjects. Muscle symbols as defined in Fig. 4.2. TOTAL represents the summed contributions of SOL, GAS, VAS, GMAX and GMED. Mediolateral ground forces are those represented for a right leg. Forces are expressed in units of body weight (BW); the average mass of the subjects was 71.2 kg.

largest for the HINGE, WELD and SINGLEPOINT models, and they were also larger in the mediolateral direction than the vertical and fore-aft directions (Figs 4.7A and 4.7B). In running, for example, the HINGE, WELD and SINGLEPOINT models generated errors that were three times greater than the peak ground reaction force measured in the mediolateral direction. The total superposition errors for the BALL, UNIVERSAL, HINGE and WELD models increased as the number of degrees of freedom of the foot-ground contact model decreased (Fig. 4.7C).

4.4 Discussion

Calculations of muscle coordination in human gait are influenced by the model used to simulate foot-ground contact. Two factors — the number of foot-ground contact points assumed in the model and the type of kinematic constraint enforced at each contact point — can significantly alter the model predictions of muscle function for both walking and running.

4.4.1 Influence of kinematic constraints

Kinematic constraints act at each of the foot-contact points to restrict the motion of the foot and alter the calculated values of the muscle contributions to the ground reaction forces generated in walking and running (Figs 4.3 and 4.4). Our results indicate, firstly, that kinematic constraints applied in the sagittal plane affect the model calculations of muscle contributions to the vertical and fore-aft ground reaction forces; secondly, that kinematic constraints applied in the frontal plane affect the calculations of muscle contributions to the mediolateral ground reaction force; and thirdly, that kinematic constraints applied in the transverse plane have little effect on the model calculations of muscle function.

The extent to which changing a kinematic constraint affects muscle function is quantified in Fig. 4.8. Progressing from a BALL to UNIVERSAL kinematic constraint (by fully constraining foot axial rotation) yielded negligible difference in muscle contributions. This is

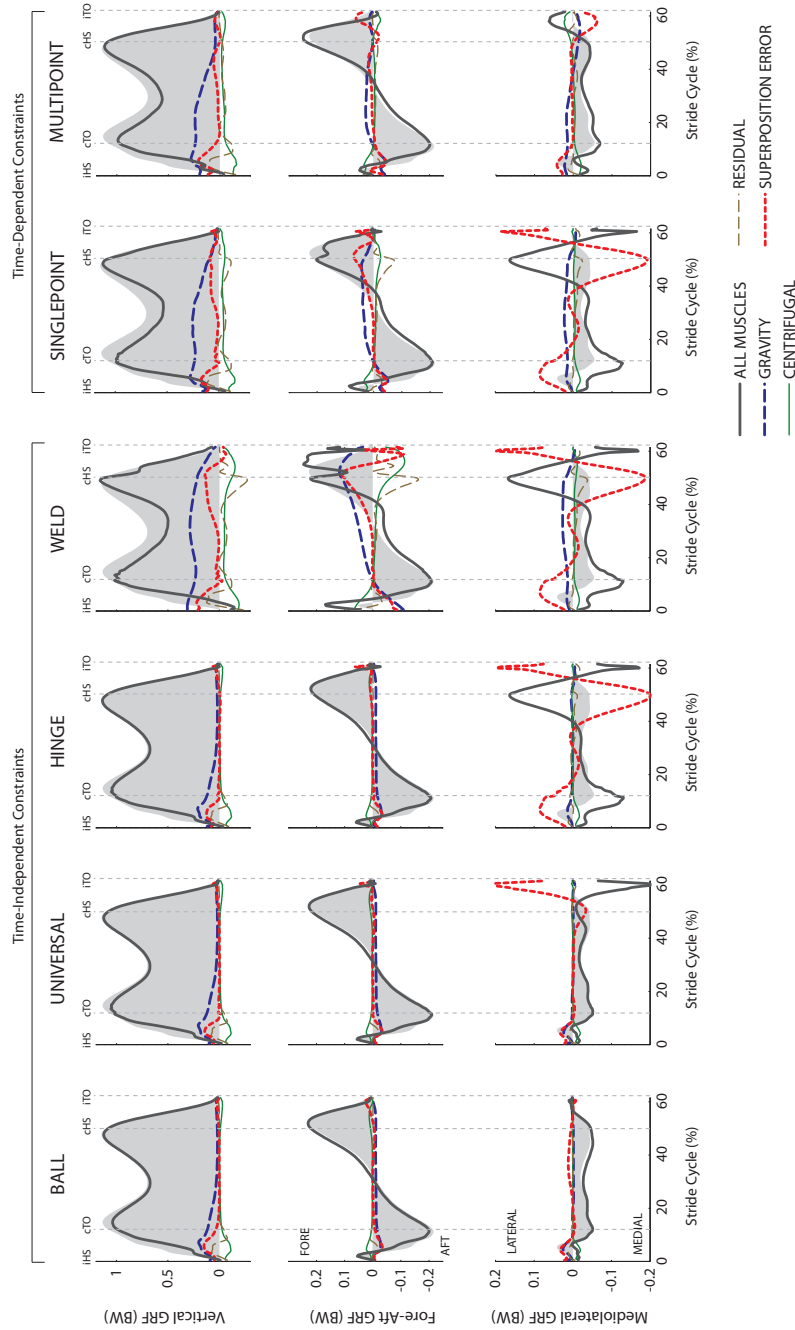


Figure 4.5: Contributions of all muscle forces (All Muscles), gravitational forces (Gravity), and centrifugal and Coriolis forces (Centrifugal) to the vertical, fore-aft and mediolateral components of the ground reaction forces generated in walking. The shaded regions represent the forces recorded by the force plate. Superposition error was found by subtracting the model-computed ground reaction force (i.e., All Muscles, Gravity and Centrifugal forces summed together) from the measured ground reaction force. Results are shown for the six different ground contact models evaluated. The results for each contact model were averaged across all subjects. Mediolateral ground forces are those represented for a right leg. Forces are expressed in units of body weight (BW); the average mass of the subjects was 71.2 kg.

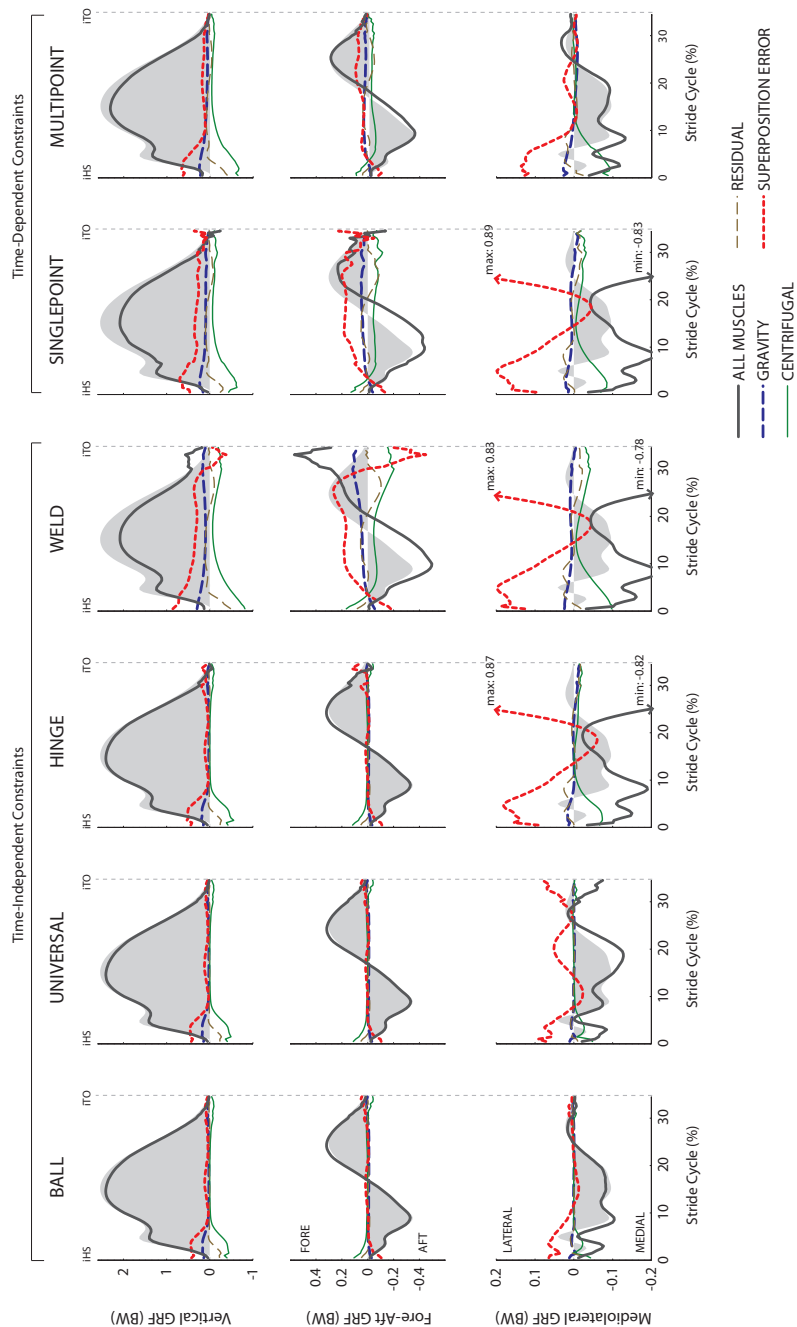


Figure 4.6: Contributions of all muscle forces (All Muscles), gravitational forces (Gravity), and centrifugal and Coriolis forces (Centrifugal) to the vertical, fore-aft and mediolateral components of the ground reaction forces generated in running. The shaded regions represent the forces recorded by the force plate. Superposition error was found by subtracting the model-computed ground reaction force (i.e., All Muscles, Gravity and Centrifugal forces summed together) from the measured ground reaction force. Results are shown for the six different ground contact models evaluated. The results for each contact model were averaged across all subjects. Mediolateral ground forces are those represented for a right leg. Forces are expressed in units of body weight (BW); the average mass of the subjects was 71.2 kg.

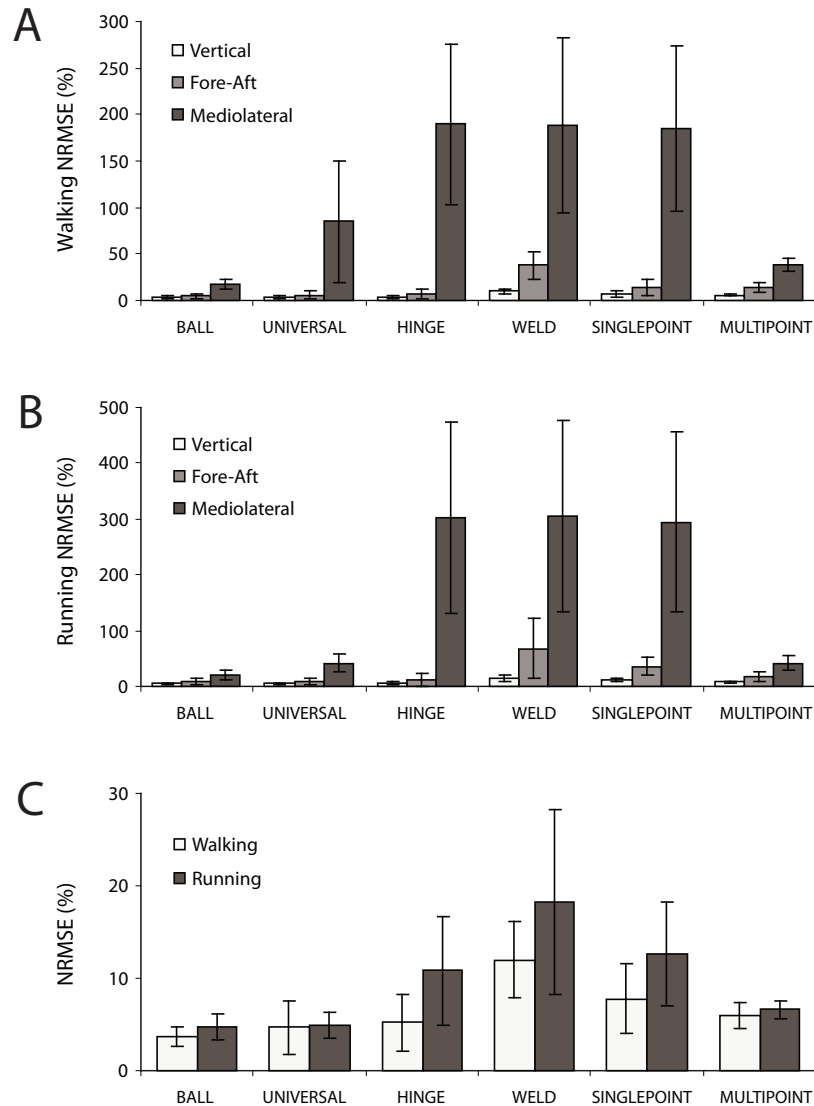


Figure 4.7: Normalise root mean square errors (NRMSE) calculated for the vertical, fore-aft and mediolateral components of the ground reaction force generated in walking (A) and running (B). NRMSE was found by subtracting the model-computed ground reaction force from the measured ground reaction force and then normalizing by the peak value of the measured ground reaction force (see text). The error bars indicate \pm one standard deviation from the mean. (C) Total NRMSE calculated for walking and running. Total NRMSE was found by performing a vector summation of the NRMSE values calculated for the vertical, fore-aft and mediolateral directions shown in (A) and (B) above.

because the ankle-joint complex was originally represented as a universal joint and did not permit axial rotation. However, the addition of further kinematic constraints to the contact model produced greater disparities in muscle function. For example, progressing from a UNIVERSAL to a HINGE kinematic constraint (by fully constraining foot coronal rotation) results in a 3% BW (walk) and 8% BW (run) change in mediolateral muscle function. Progressing from a HINGE to a WELD (by fully constraining sagittal foot rotation) results in a 3% BW (walk) and 7% BW (run) change in fore-aft muscle function and a 8% BW (walk) and 9% BW (run) change in vertical support muscle function. These additional kinematic constraints affected muscle function because they restricted frontal and sagittal plane rotations that were permitted in the ankle-complex joint.

4.4.2 Influence of the number of foot-contact points

Estimates of leg muscle function are also influenced by the number of foot-contact points included in the model. Muscle contributions to the vertical and fore-aft ground reaction forces were found to be similar for the SINGLEPOINT and MULTIPOINT models. The results obtained from these two models are consistent with the findings of Liu et al. (2008), who used a single contact point to simulate the interaction between the foot and the ground during walking, and with those of Sasaki and Neptune (2006), who used a more complex model comprised of 30 foot-springs distributed over the sole of the foot to simulate both walking and running. These findings suggest that predictions of muscle function in the sagittal plane are insensitive to the number of foot-contact points included in the model, provided that foot motion is adequately constrained. In contrast, muscle contributions to the mediolateral ground force were different for the SINGLEPOINT and MULTIPOINT models (Figs 4.3, 4.4, and 4.7), indicating that calculations of muscle function in the mediolateral direction are sensitive to the number and location of foot-contact points included in the model.

Different models of ground contact may also yield conflicting predictions of muscle function during gait. In walking the vasti and soleus

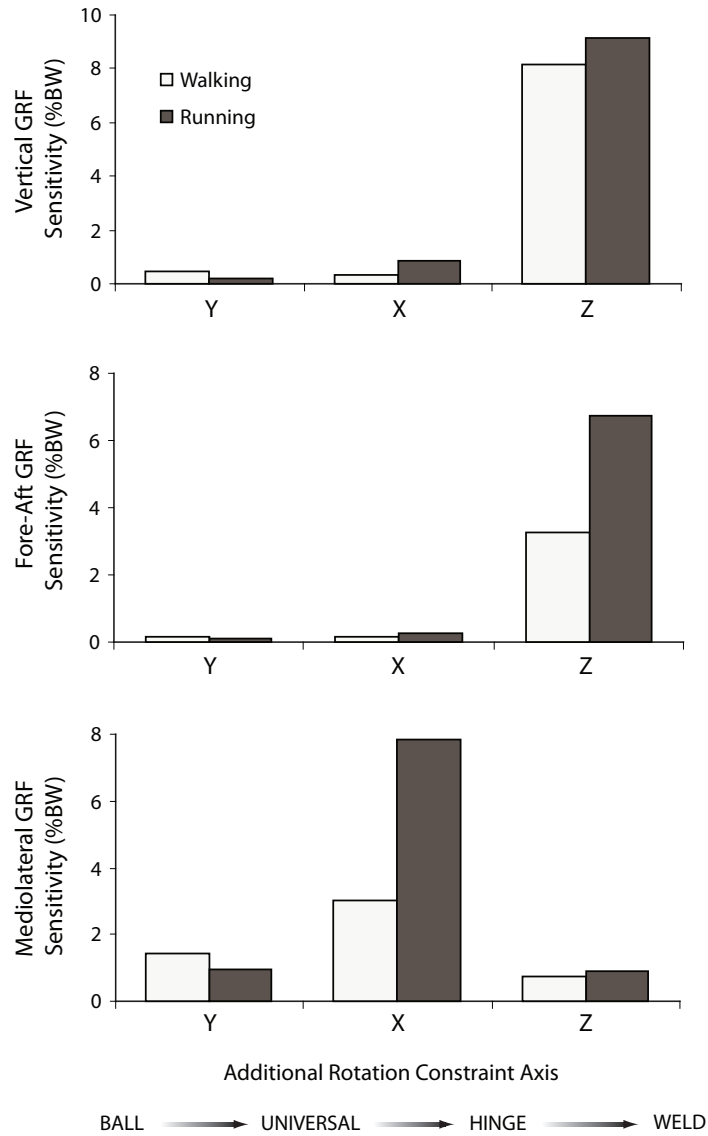


Figure 4.8: Sensitivity of the contribution of muscles to the ground reaction force as kinematic constraints are added to the contact model. Values represent the absolute difference of the contribution of all muscles between two time-invariant contact models, averaged across the stance phase for all subjects. From BALL to UNIVERSAL, a rotation constraint about the vertical axis is added; from UNIVERSAL to HINGE, a rotation constraint about the fore-aft axis is added; from HINGE to WELD, a rotation constraint about the mediolateral axis is added.

support the skeleton in early and late stance, respectively, whereas in running these muscles act in unison to provide a greater upward acceleration of the center-of-mass (Sasaki and Neptune, 2006; Pandy and Andriacchi, 2010). At running speeds similar to that adopted in the present study, Hamner et al. (2010) used the UNIVERSAL contact model and found the contribution of soleus to be twice that of vasti, whereas Pandy and Andriacchi (2010) used the MULTIPOINT model and obtained the opposite result (i.e., the force of vasti contributed twice as much as the force of soleus to the vertical ground reaction force). This contradictory result is likely due to (i) differences in musculoskeletal model architecture; and (ii) different models of foot-ground contact. With regard to the musculoskeletal model, many factors can influence the simulated activation of the vasti and soleus muscles (e.g., moment arm, maximum isometric force, optimal fibre length), and hence effect their relative contribution to the ground reaction force in gait. However, the present study illustrates nevertheless that vastly different functions may be predicted for vasti and soleus when using different ground contact models, despite employing the same musculoskeletal model and muscle forces across all trials (Fig 4.4, compare results for the UNIVERSAL and MULTIPOINT models in the vertical direction). Our results show that vasti generates the majority of the vertical ground reaction force when the sagittal plane rotational kinematic constraint is enforced, whereas soleus dominates when this constraint is removed (see Table 4.1). To our knowledge, the studies by Hamner et al. (2010) and Pandy and Andriacchi (2010) are the only ones to have evaluated muscle-induced accelerations at running speeds above 3.0 m/s. The inconsistent results obtained from these studies highlight the need for future work aimed at validating model predictions of leg muscle function in walking and running.

4.4.3 Superposition errors across foot-contact models

Lower superposition errors do not necessarily imply greater validity in the predictions of leg muscle function. The BALL contact model permitted foot movement about all three axes of rotation (Table 4.1) (i.e., kinematic

constraints were not enforced about any joint axis), which resulted in a superposition error lower than that obtained from any of the other models (Fig. 4.7). The MULTIPPOINT contact model produced a similar superposition error to that calculated in the BALL model, yet the predictions of individual muscle function obtained from these models were significantly different (Figs 4.3 and 4.4). These differences are attributed to the differences in the kinematic constraints acting at the points of contact between the foot and the ground, which change the equations of motion and influence the calculations of muscle function. Superposition error only quantifies the accuracy with which the various action forces sum to the total ground reaction force; it does not verify the calculations of the contributions of the individual action forces themselves.

Model predictions of muscle function have not been validated by experiment because muscle contributions to the ground reaction force are difficult to measure. However, Hunter et al. (2009) measured the induced hip— and knee-joint angular accelerations by electrically stimulating individual muscles in a range of postures during the swing phase of walking. In a similar fashion, one could electrically stimulate a single muscle and measure the resulting ground reaction force. Experiments such as these would be valuable in evaluating the suitability of different ground contact models in calculations of leg muscle function during gait.

4.4.4 Limitations and future work

The present study is limited in at least three respects. First, the same musculoskeletal model was used to simulate both walking and running in all subjects. Although body-segment parameters were scaled according to each subject's anthropometry, the same muscle-tendon properties were assumed for all subjects, which may have influenced the calculated values of muscle forces and hence the model predictions of muscle function. Second, the present analysis was limited to self-selected speeds of walking and running that were characterised by initial heel impact. As running speed increases, foot-ground contact occurs at more anterior positions on the foot, and is located wholly on the toes during maximal sprinting (Nett, 1964;

Novacheck, 1998). The MULTIPOINT model formulated in this study has the advantage that it may be used to simulate any form of running, including toe-running, because the kinematic constraints acting between the foot and the ground are governed by the location of the center-of-pressure, which can be measured accurately in a gait-analysis experiment. Last, relatively large superposition errors were observed close to heel-strike in all ground contact models, particularly in the mediolateral direction (Figs 4.5, 4.6 and 4.7). This may have been caused by small linear translations of the foot relative to the ground during impact. Though these translations may be small in life, they were not permitted in any of the contact models evaluated here. Future work should therefore be directed towards incorporating a more detailed representation of collision mechanics into existing models of foot-ground contact.

As ground-force decomposition analyses become more widespread (e.g., Delp et al., 2007), careful consideration should be given to the formulation of the model used to simulate ground contact. The results of the present study show that model calculations of muscle contributions to the ground reaction force, particularly the component in the mediolateral direction, are sensitive to the distribution of foot-contact points and the type of kinematic constraint used to model the interaction between the foot and the ground. These findings have important implications for analyses of leg muscle function in gait, particularly if the results of such analyses are to guide clinical decision making.

Chapter 5

Mechanical strategy shift in human running: Dependence of running speed on hip and ankle muscle performance

This chapter is based on the following published work:

- **Dorn, T.W., Schache, A.G., Pandy, M.G. (2012).** Mechanical strategy shift in human running: dependence of running speed on hip and ankle muscle performance, *The Journal of Experimental Biology*, In press.

ABSTRACT

Humans run faster by increasing a combination of stride length and stride frequency. In slow and medium-paced running, stride length is increased by exerting larger support forces during ground contact, whereas in fast running and sprinting, stride frequency is increased by swinging the legs more rapidly through the air. Many studies have investigated the mechanics of human running, yet little is known about how the individual leg muscles accelerate the joints and center-of-mass during this task. The aim of this study was to describe and explain the synergistic actions of the individual leg muscles over a wide range of running speeds, from slow running to maximal sprinting. Experimental gait data from nine subjects were combined with a detailed computer model of the musculoskeletal system to determine the forces developed by the leg muscles at different running speeds. For speeds up to 7 m/s, the ankle plantarflexors, soleus and gastrocnemius, contributed most significantly to vertical support forces and hence increases in stride length. At speeds greater than 7 m/s, these muscles shortened at relatively high velocities and had less time to generate the forces needed for support. Thus, above 7 m/s the strategy used to increase running speed shifted to the goal of increasing stride frequency. The hip muscles, primarily iliopsoas, gluteus maximus and hamstrings, achieved this goal by accelerating the hip and knee joints more vigorously during swing. These findings provide insight into the strategies used by the leg muscles to maximise running performance and have implications for the design of athletic training programs.

5.1 Introduction

Humans increase their running speed by taking longer strides and swinging their legs more quickly through the air. Running speed (v), stride length (λ) and stride frequency (f) are related by the simple equation: $v = \lambda \times f$. Although faster running speeds can be achieved by increasing either stride length or stride frequency, changing these parameters is difficult in practice because these two variables are not independent. Stride length is inversely proportional to stride frequency (Luhtanen and Komi, 1978; Cavagna et al., 1988; Kaneko, 1990; Cavagna et al., 1991; Weyand et al., 2000; Hunter et al., 2004; Salo et al., 2011), and so running speed can be increased only when an increase in stride length is not accompanied by a similar decrease in stride frequency and vice versa.

Runners appear to use two different strategies to increase their speed. Up to ~ 7 m/s running speed is increased by exerting larger support forces during ground contact, which has been shown to correlate with increases in stride length (Frederick, 1986; Derrick et al., 1998; Weyand et al., 2000; Mercer et al., 2002, 2005). Furthermore, using a simple point-mass model of running it is relatively straightforward to show that a larger support force produces a larger stride length because the body spends more time in the air (see Section 2.1.5). Larger ground forces can be generated at lower running speeds because the leg muscles have enough time to develop the forces needed to lift and accelerate the body during stance (Weyand et al., 2000). At speeds near 7 m/s, however, ground contact times become very small (Kunz and Kaufmann, 1981; Mann, 1981; Mann and Herman, 1985), limiting the ability of the leg muscles to generate the ground forces needed to increase running speed still further (Weyand et al., 2000). Of particular interest in this respect is the behaviour of the ankle plantarflexors, which undergo significant periods of stretch-shortening during stance (Komi, 1984, 2000; Kubo et al., 2000; Hennessy and Kilty, 2001; Ishikawa and Komi, 2007; Lichtwark et al., 2007). Greater rates of shortening of the plantarflexors due to reduced ground contact times decrease the power output of these muscles (Cavagna et al., 1971; Volkov and Lapin, 1979), and may limit their ability to generate the required thrust during terminal stance.

Above ~ 7 m/s, the primary strategy used to increase running speed shifts from the goal of increasing stride length to that of increasing stride frequency, which is achieved by accelerating the legs more rapidly through the air. Peak hip-flexor, hip-extensor and knee-flexor moments all increase significantly at speeds above 7 m/s (Belli et al., 2002; Schache et al., 2011a). Increases in the work done at the hip and knee during the swing phase also correlate with running speed above 7 m/s, as does the mechanical energy delivered by the leg muscles to the thigh and shank (Chapman and Caldwell, 1983b; Cavagna et al., 2008; Cavagna, 2009). Although many studies have calculated the net torques, power, and work done by the lower-limb joints during running (Novacheck, 1998; Biewener et al., 2004; McIntosh et al., 2006; Devita et al., 2007), little is known about how the actions of individual leg muscles coordinate motion of the lower-limb joints and the center-of-mass, particularly across a range of human running speeds.

Computational modelling is the only means available for studying the contributions of individual muscles to joint and body-segment accelerations, herein referred to as *muscle function* throughout this study (Pandy and Andriacchi, 2010). Detailed musculoskeletal models of the body have been used previously to quantify the function of individual muscles in various tasks, including walking, running and jumping (Pandy, 2001; Delp et al., 2007; Erdemir et al., 2007; Heintz and Gutierrez-Farewik, 2007; Pandy and Andriacchi, 2010; Pandy et al., 2010). In studies of walking, model simulations have shown that five muscle groups - gluteus maximus, gluteus medius, vasti, soleus, and gastrocnemius - contribute most significantly to the accelerations of the center-of-mass in the vertical, fore-aft and mediolateral directions (Anderson and Pandy, 2003; Liu et al., 2008; Pandy et al., 2010). Only two computer-based musculoskeletal modelling studies, however, have characterised the function of the individual leg muscles during running (Hamner et al., 2010; Sasaki and Neptune, 2006). Sasaki and Neptune (2006) generated muscle-actuated simulations of running at 1.96 m/s using a two-dimensional model of the body to calculate the individual contributions of leg muscles to the acceleration of the center-of-mass. Hamner et al. (2010) too calculated how individual muscles accelerate the center-of-mass by generating a three-dimensional running

simulation for a single subject at a more typical running speed, 3.96 m/s. However, no studies to our knowledge have evaluated lower-limb muscle function in running for speeds greater than 4 m/s within a consistent cohort of habitual runners.

The overall goal of the present study was to better understand how the leg muscles coordinate motion of the body segments during running. Our specific aim was to determine the contributions that individual leg muscles make to increases in stride length and stride frequency by evaluating muscle contributions to the ground reaction force and joint angular accelerations throughout the stride. Experimental gait data were combined with a detailed model of the musculoskeletal system to determine the forces developed by the leg muscles over a wide range of human running speeds, from slow running to maximal sprinting. The model calculations were used to evaluate two hypotheses: **(H1)** *The ankle plantarflexors are mainly responsible for increasing stride length during stance*; and **(H2)** *The hip flexors and extensors are mainly responsible for increasing stride frequency during swing*.

5.2 Methods

5.2.1 Ethical approval

The study was approved by the Human Research Ethics Committees of The University of Melbourne and The Australian Institute of Sport, and all participants gave their written informed consent prior to testing. All human testing procedures undertaken conformed to the standards of the *Declaration of Helsinki*.

5.2.2 Experimental protocol

Nine subjects (5 males, 4 females; age, 27.7 ± 8.0 years; mass, 73.1 ± 8.6 kg; height, 176 ± 7 cm; leg length 93 ± 5 cm) volunteered to participate in the study (Table 5.1). All subjects were experienced runners and at the

time of testing were not suffering from any musculoskeletal injury likely to adversely affect their sprinting ability. All experiments were conducted on an straight indoor synthetic running track in the Biomechanics Laboratory at the Australian Institute of Sport. Prior to data collection, a test leg, henceforth referred to as the ipsilateral leg (right = 4; left = 5), was randomly chosen by tossing a coin.

Each subject was asked to run at four steady-state target speeds: slow running at 3.5 m/s ($n=9$), medium-paced running at 5.0 m/s ($n=9$), fast running at 7.0 m/s ($n=8$) and sprinting at 8.0 m/s or greater ($n=7$). The total track was 110 m long, which provided subjects with 55 m to accelerate to a steady-state speed, 11.5 m to maintain the steady-state speed, and 43.5 m to safely decelerate to rest. All data were collected inside the volume where subjects were required to maintain steady-state speeds. Timing gates (Speedlight Telemetry Timing, Swift Performance Equipment, NSW, Australia) were positioned at the beginning and at the end of the data collection volume, 11.5 m apart, to monitor the average steady-state speed of each runner. Verbal feedback was provided after each trial to ensure the subject attained the desired target speed. Adequate recovery time was provided between trials to prevent fatigue.

Marker-derived kinematic data were acquired using a three-dimensional video motion capture system (VICON, Oxford Metrics, Oxford, UK). Small reflective markers (14 mm in diameter) were mounted over specific locations on the trunk, legs and arms (see Table 3.1 in Chapter 3). Marker trajectories were recorded using twenty-two optical infra-red cameras sampling at 250 Hz over a distance of 11.5 m. Ground reaction force and center-of-pressure data were measured using eight force plates (Kistler Instrument Corp., Amherst, NY, USA) sampling at 1500 Hz. Ground reaction forces were low-pass filtered at 60 Hz using a fourth-order Butterworth filter to remove high frequency noise. Muscle electromyographic (EMG) data were sampled at 1500 Hz using a telemetered system (Noraxon Telemetry 2400T G2, Noraxon USA Inc.). Pairs of Ag/AgCl surface electrodes were mounted on the skin to measure the activity of eleven lower-limb muscles: gluteus maximus, gluteus medius, medial hamstrings, lateral hamstrings, rectus femoris, vastus medialis,

vastus lateralis, medial gastrocnemius, lateral gastrocnemius, soleus and tibialis anterior (see Table 3.2 in Chapter 3). Electrode placements were based on the guidelines provided by Hermens et al. (2000) and all signals were checked for clarity and strength of signal during isolated limb movements. EMG onset and offset times were determined by applying a Teager-Kaiser Energy (TKE) filter to the raw EMG signal (Li et al., 2007; Solnik et al., 2010). Running sandals (NIKE Straprunner IV) rather than traditional shoes or spikes were worn by the subjects so that markers could be placed directly onto the foot.

Stride length, stride frequency, ground contact time, aerial time and effective vertical ground impulse were calculated for a single stride for each trial. Stride length was defined as the anterior distance travelled by consecutive ipsilateral foot-strikes, calculated from the heel marker at the time of initial foot-ground contact. Stride frequency was found by dividing running speed by stride length. Ground contact time was found by dividing the number of video frames for which the ipsilateral foot was in contact with the ground by the video sample frequency. Similarly, aerial time was determined by dividing the number of video frames for which both feet were off the ground by the sample frequency. Effective vertical ground impulse, which represents the net impulse responsible for accelerating the body upwards (Weyand et al., 2000; Hunter et al., 2005), was found by calculating the area between the vertical ground reaction force-time curve and the horizontal line representing the subject's body weight (BW).

A Gait-Extract toolbox (freely available from <https://simtk.org/home/c3dtoolbox>, see also Appendix B) was used to extract and process the raw kinematic marker, ground reaction force and muscle EMG data from each trial into a format suitable for input to the musculoskeletal model.

5.2.3 Musculoskeletal model

The generic musculoskeletal model described below was implemented in OpenSim (Delp et al., 2007) and is freely available with sample running data obtained from one subject at

<https://simtk.org/home/runningspeeds>.

The skeleton was represented as a three-dimensional, 12-segment, 31-degree-of-freedom articulated linkage (Fig. 5.1A). The head and torso were lumped together as a single rigid body that articulated with the pelvis via a ball-and-socket joint. Each hip was modelled as a ball-and-socket joint; each knee as a translating hinge joint (Seth et al., 2010); each ankle as a universal joint comprised of two non-intersecting hinge joints; each shoulder as a ball-and-socket joint; and each elbow as a universal joint. The lower-limb joints were actuated by 92 muscle-tendon units (Thelen, 2003), each unit represented as a Hill-type muscle in series with an elastic tendon (Figs 5.1B and C). Muscle lines of action were identical to that of Hamner et al. (2010); however, the optimal fibre lengths and pennation angles of some muscles were modified according to mean values reported in a recent cadaver study (Ward et al., 2009) (see Section 3.2.1 for further details). The shoulder and elbow joints were actuated by ten ideal torque motors.

5.2.4 Ground contact model

Five discrete points located on the sole of the model foot (Fig. 5.1D) were used to simulate the interaction between the foot and the ground (see Section 3.2.7). Two ground contact points were located at the heel, two at the metatarsal joint, and one at the end of the toes segment. During periods of ground contact, the measured center-of-pressure was used to control the stiffness of each contact point relative to the ground according to rules governing the heel-strike, foot-flat, and toe-off phases of stance (see Section 3.2.7 and in particular, Fig. 3.9). In this way, the ground contact model was naturally adapted to the contact patterns exhibited by both rearfoot- and forefoot-strike runners.

5.2.5 Data analysis

OpenSim was used to perform all model analyses (Delp et al., 2007). Subject-specific musculoskeletal models were developed by scaling the generic musculoskeletal model using the “scale” tool in OpenSim (see

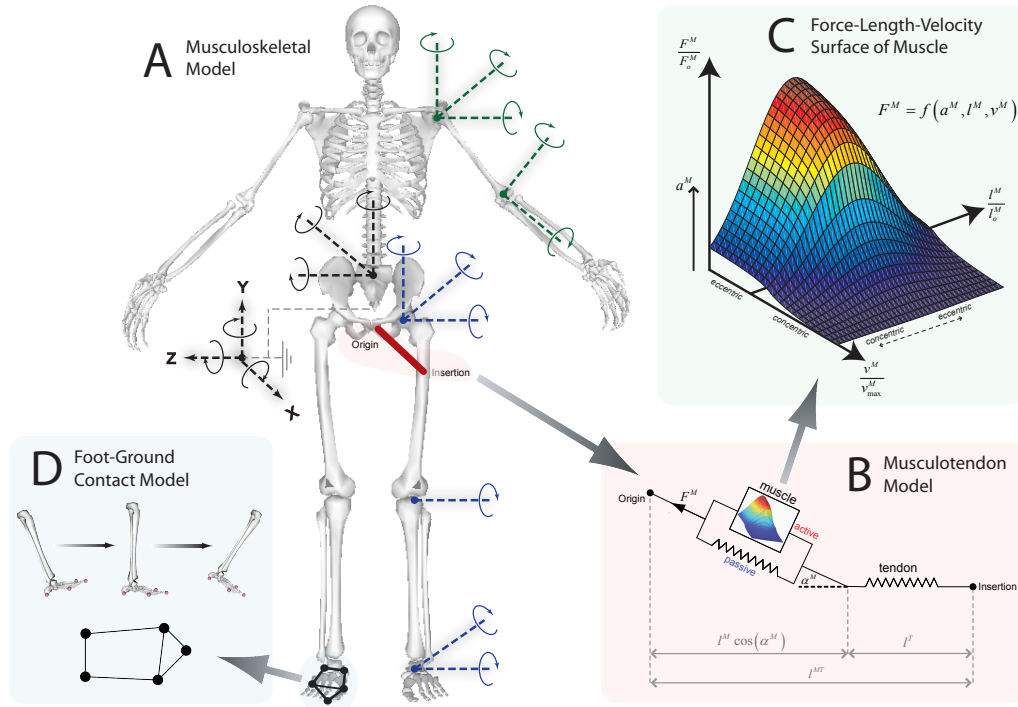


Figure 5.1: Three-dimensional full body musculoskeletal model used in the present study. (A) The skeleton was represented as a multibody linkage containing 31 degrees-of-freedom, driven by 92 musculotendon actuators (lower extremity and trunk) and 10 ideal torque actuators (upper extremity). (B) Each musculotendon actuator was represented as a Hill-type physiological muscle in series with tendon. Muscle fibre length l^M and tendon length l^T were governed by the distance between musculotendon origin and insertion l^{MT} , muscle pennation angle α^M and muscle force F^M . (C) The active force-length-velocity surface of physiological muscle was defined by the muscle's optimal fibre length l_0^M , maximum shortening velocity v_{max}^M and maximum isometric force F_0^M . Active muscle force generation was always constrained to this surface, scaled by the level of muscle activation a^M . (D) Foot-ground contact was assumed to take place at five discrete contact points distributed around the foot.

Section 3.2.1). Specifically, individual body-segment scaling factors were found using the ratio of the distances between two markers measured on the segment during a static standing trial and the distances between the same two markers located on the model. These scaling factors were then used to scale segment lengths, segment inertial properties, muscle attachment points, optimal fibre lengths and tendon slack lengths. The peak isometric force of each muscle was not scaled, and so the same values were assumed across all subjects and speeds.

Joint angles were computed at each time instant in the model using the “inverse kinematics” tool in OpenSim (see Section 3.2.2). The marker locations on the model were optimally matched to the trajectories of the corresponding marker locations measured on the subject, so that the sum of the squared error distances between the two marker sets was minimised, thereby yielding the optimal set of joint kinematics (Lu and O’Connor, 1999). Net joint moments were computed using the “inverse dynamics” tool in OpenSim (see Section 3.2.3). The measured ground reaction forces were applied directly to the feet of the model, and joint moments were iteratively calculated by solving the equations of motion for each segment of the model, starting from the foot segment and moving upwards (Winter, 2009). The net joint moments were then decomposed into individual musculotendon forces using the “static optimisation” tool in OpenSim (see Section 3.2.4). This procedure was used to solve an optimisation problem that minimised the sum of the squares of all muscle activations, which is analogous to minimizing total muscle stress (Crowninshield and Brand, 1981). The optimisation solution was constrained to the force-length-velocity surface of each muscle (Katz, 1939; Gordon et al., 1966; Zajac, 1989) (Fig. 5.1C).

Mechanical power developed by each muscle was found by taking the product of musculotendon force and musculotendon velocity. Mechanical work was determined by calculating the area under the power-time curve. Concentric contractions represented energy generated by the muscle (positive work), whereas eccentric contractions represented energy absorbed (negative work).

Lower-limb muscle function was quantified by calculating the contributions of each muscle to the ground reaction force and the lower-limb joint accelerations derived from experiment. This was performed using a 'pseudo-inverse induced acceleration analysis' (see Section 3.2.7), which was implemented in OpenSim as a custom-designed plug-in (the *IndAccPI* plug-in is freely available from https://simtk.org/home/tims_plugins). Each muscle force obtained from the static optimisation solution was successively applied to the model in isolation. As the isolated muscle force is transmitted to all the body segments, it simultaneously induces: i) a ground reaction force at the foot (via the foot-ground contact model shown in Fig. 5.1D); and ii) angular accelerations of all the body joints (Zajac and Gordon, 1989). This approach for calculating muscle contributions to ground reaction forces and lower-limb joint accelerations has been previously validated against gait data obtained for walking and running (Lin et al., 2011b).

Muscle contributions to the vertical ground reaction force were used to identify the muscle groups that contributed most significantly to increases in stride length. Similarly, muscle contributions to the sagittal-plane hip and knee-joint accelerations were used to identify the muscle groups that contributed most significantly to increases in stride frequency. Ankle-joint acceleration was neglected because its contribution to swinging the legs forward in running was presumed to be negligible.

5.2.6 Data presentation and statistical analysis

All trials were analysed over a single stride cycle beginning and ending at ipsilateral foot-strike. Results were time-normalised to a full stride cycle and then averaged across all subjects for each running speed. Ground reaction forces were normalised by the mean body weight of the subjects, and joint moments were normalised by the mean body mass. Muscle data (i.e., force, work and contributions to ground forces and joint accelerations) were combined into functional muscle groups by summing the contributions from each muscle line-of-action within the group: ILPSO (iliacus and psoas), GMAX (superior, middle and inferior gluteus maximus), GMED

(anterior, middle and posterior compartments of gluteus medius), HAMS (biceps femoris long head, semimembranosus and semitendinosus), RF (rectus femoris), VAS (vastus medialis, vastus intermedius and vastus lateralis), GAS (medial and lateral compartments of gastrocnemius), SOL (soleus) and TIBANT (tibialis anterior).

One-way repeated measures analysis of variance (ANOVA) tests were used to identify the muscles that i) developed significantly greater peak forces during the stride cycle with running speed; ii) contributed significantly greater peak forces to the vertical ground reaction force with running speed; and iii) performed a significantly greater amount of swing phase work with running speed. When significant F ratios were obtained, *post hoc* pairwise comparisons (paired t-tests) were used to determine differences between each of the running speeds. A conservative level of significance was set at $p < 0.01$ for all tests, which was determined by a Bonferroni correction to a significance level of $p < 0.06$ (i.e., a total of six *post hoc* pairwise comparisons was performed per dependent variable). The statistical association between running speed and work done by the major muscle groups was also calculated. Linear and second-order polynomial trend lines were fitted to the mechanical work generated and absorbed by the leg muscles and corresponding coefficients of determination (R^2) values were determined.

5.3 Results

5.3.1 Dependence of stride length and stride frequency on running speed

Mean running speeds recorded across subjects were 3.5 ± 0.1 m/s (slow running), 5.2 ± 0.1 m/s (medium-paced running), 7.0 ± 0.1 (fast running) and 9.0 ± 0.7 m/s (sprinting) (Table 3.3 in Chapter 3; see also Fig. C.3 in Appendix C). The percentage increase in stride length was greater than that in stride frequency as running speed increased from 3.5 m/s to 7.0 m/s, but the opposite effect was observed at speeds above 7.0 m/s (Fig. 5.2A

and Table 5.1). Ground contact time decreased monotonically as running speed increased ($p < 0.01$) (Fig. 5.2B and Table 5.1). Aerial time and effective vertical ground impulse both reached their maxima at 7.0 m/s before decreasing at higher speeds (Fig. 5.2B).

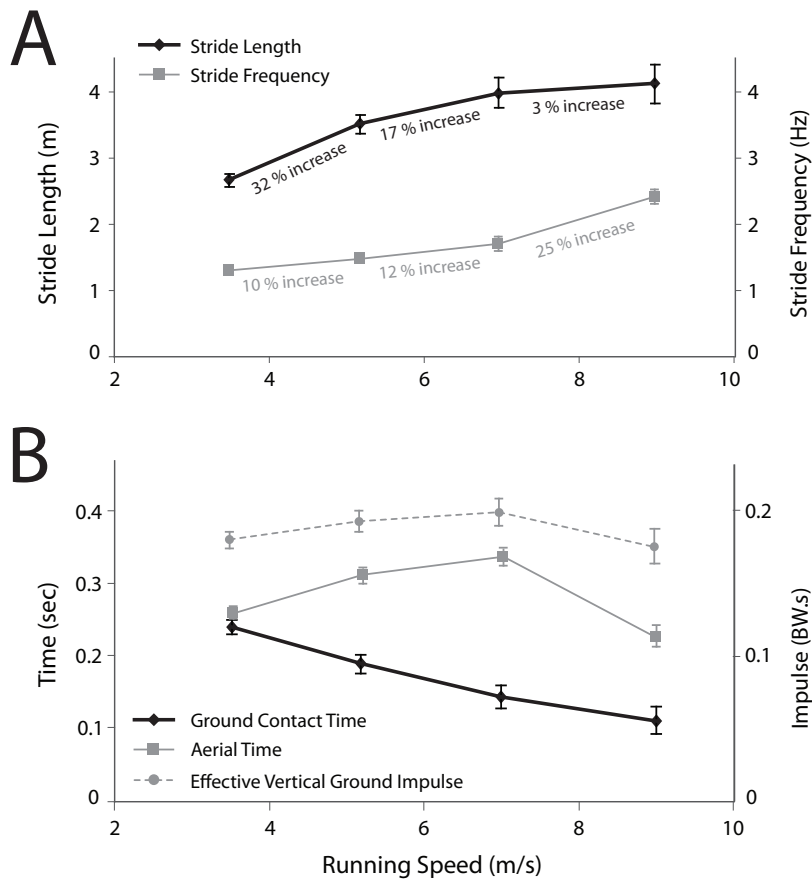


Figure 5.2: (A) Measured stride length and stride frequency plotted against running speed. (B) Ground contact time, aerial time and effective vertical ground impulse measured for each running speed. Effective vertical ground impulse was defined as the area bounded by the vertical ground reaction force and the horizontal line representing the subject's body weight. For each running speed, results were calculated for each subject and then averaged. Error bars represent 1SD of variance from the mean.

CHAPTER 5. MECHANICAL STRATEGY SHIFT IN RUNNING

Table 5.1: Mean (± 1 SD) magnitudes of stride length, stride frequency, ground contact time, peak muscle forces and peak muscle contributions to the vertical ground reaction force (GRF). Forces are normalised by body weight (BW) and mechanical work is normalised by body mass. Positive work represents energy generation; negative work represents energy absorption.

	Speed 1 (<i>n</i> =9) 3.49 (0.12) m/s	Speed 2 (<i>n</i> =9) 5.17 (0.13) m/s	Speed 3 (<i>n</i> =8) 6.96 (0.13) m/s	Speed 4 (<i>n</i> =7) 8.99 (0.67) m/s
Stride characteristics				
Stride length (<i>m</i>)	2.62 (0.10) ^{2,3,4}	3.42 (0.13) ^{1,3,4}	3.99 (0.22) ^{1,2}	4.10 (0.26) ^{1,2}
Stride frequency (<i>s</i> ⁻¹)	1.31 (0.03) ^{2,3,4}	1.47 (0.05) ^{1,3,4}	1.75 (0.10) ^{1,2,4}	2.18 (0.10) ^{1,2,3}
Ground contact (<i>ms</i>)	243 (22) ^{2,3,4}	188 (15) ^{1,3,4}	145 (9) ^{1,2,4}	118 (11) ^{1,2,3}
Peak forces developed by muscles (BW)				
ILPSO (swing)	1.97 (0.37) ^{2,3,4}	3.49 (0.51) ^{1,3,4}	5.91 (0.98) ^{1,2,4}	9.04 (1.71) ^{1,2,3}
GMAX (swing)	0.38 (0.12) ^{2,3,4}	0.64 (0.17) ^{1,3,4}	1.03 (0.29) ^{1,2,4}	2.22 (0.60) ^{1,2,3}
HAMS (swing)	2.10 (0.38) ^{2,3,4}	2.66 (0.31) ^{1,3,4}	4.61 (0.74) ^{1,2,4}	8.95 (1.66) ^{1,2,3}
RF (swing)	0.67 (0.06) ^{2,3,4}	1.19 (0.17) ^{1,3,4}	1.81 (0.28) ^{1,2,4}	4.89 (0.89) ^{1,2,3}
VAS (stance)	4.70 (0.57)	5.35 (1.21)	4.93 (0.94)	4.89 (0.89)
GAS (stance)	1.94 (0.25) ^{2,3,4}	2.65 (0.44) ^{1,3}	3.23 (0.49) ^{1,2}	2.97 (0.34) ¹
SOL (stance)	6.70 (0.66) ^{2,3,4}	7.92 (0.82) ^{1,3,4}	8.71 (0.83) ^{1,2,4}	7.34 (0.72) ^{1,2,3}
TA (swing)	0.17 (0.14) ⁴	0.22 (0.16) ⁴	0.31 (0.10) ⁴	0.50 (0.11) ^{1,2,3}
Peak muscle contributions to the vertical ground force (BW)				
VAS	1.12 (0.26)	1.02 (0.29)	0.92 (0.23)	0.74 (0.21)
GAS	0.53 (0.10) ^{2,3,4}	0.73 (0.16) ¹	0.81 (0.12) ¹	0.74 (0.08) ¹
SOL	1.61 (0.32) ^{2,3,4}	1.98 (0.53) ¹	2.40 (0.55) ¹	2.30 (0.59) ¹
Total vertical GRF	2.71 (0.46) ^{2,3,4}	3.14 (0.55) ^{1,3,4}	3.58 (0.67) ^{1,2}	3.59 (0.71) ^{1,2}
Mechanical work produced by hip muscles in swing phase (J/kg)				
ILPSO (1 st half of swing)	0.36 (0.07) ^{2,3,4}	0.64 (0.08) ^{1,3,4}	0.85 (0.09) ^{1,2,4}	1.12 (0.17) ^{1,2,3}
RF (1 st half of swing)	-0.11 (0.02) ^{2,3,4}	-0.21 (0.04) ^{1,3,4}	-0.31 (0.04) ^{1,2,4}	0.41 (0.05) ^{1,2,3}
GMAX (2 nd half of swing)	0.07 (0.02) ^{2,3,4}	0.19 (0.06) ^{1,3,4}	0.43 (0.08) ^{1,2,4}	0.77 (0.11) ^{1,2,3}
HAMS (2 nd half of swing)	-0.27 (0.04) ^{2,3,4}	-0.53 (0.12) ^{1,3,4}	-0.95 (0.15) ^{1,2,4}	-1.75 (0.31) ^{1,2,3}

Shaded rows indicate variables that displayed significant increases in absolute magnitude for *all* running speeds.

¹ Significantly different from running speed 1 ($p < 0.01$).

² Significantly different from running speed 2 ($p < 0.01$).

³ Significantly different from running speed 3 ($p < 0.01$).

⁴ Significantly different from running speed 4 ($p < 0.01$).

5.3.2 Lower-limb muscle forces in running

Model predictions of muscle forces were in temporal agreement with the patterns of measured EMG activity across all running speeds (Fig. 5.3). The one exception was the hamstrings, which was only lightly activated in the model during stance. As speed increased, ILPSO, GMAX, GMED, HAMS and RF all developed significantly larger peak forces throughout the stride cycle ($p < 0.01$) (Table 5.1). In particular, the peak forces of GMAX and HAMS doubled during terminal swing, increasing from 1.0 BW and 4.6 BW, respectively, at 7.0 m/s to 2.2 BW and 9.0 BW at 9.0 m/s. The peak force

developed by GAS increased as speed increased from 3.5 m/s to 7.0 m/s ($p < 0.01$), but showed no significant speed effects thereafter. The peak force developed by SOL also increased from 3.5 m/s to 7.0 m/s, but then decreased as running speed increased from 7.0 m/s and 9.0 m/s ($p < 0.01$). VAS showed no significant speed effects during stance.

The bi-articular muscles played a large role in generating the net joint moments needed to drive the motion of the lower limbs at all running speeds (Fig. 5.4). HAMS force increased with speed to satisfy the increase in hip-extensor and knee-flexor moments present during terminal swing. RF exhibited a biphasic force pattern; in the first half of swing RF force increased with running speed ($p < 0.01$) in response to larger moments required in hip flexion and knee extension, whereas during stance RF produced a knee-extensor moment to complement the action of VAS. GAS and RF were simultaneously activated during stance because GAS was required to produce a plantarflexor moment about the ankle at this time.

5.3.3 Muscle function during stance

The peak vertical ground force increased from 2.7 BW at 3.5 m/s to 3.6 BW at 7.0 m/s and did not change thereafter ($p < 0.01$) (Fig. 5.5 and Table 5.1). Across all running speeds, SOL, GAS and VAS provided roughly 75% of the total vertical support impulse needed to accelerate the body upward, with SOL contributing as much as 50%. For speeds up to 7.0 m/s, increases in the vertical ground reaction force were due almost entirely to the action of SOL. The contribution of VAS to the vertical ground force did not increase as running speed increased.

The ankle plantarflexors shortened at increasingly higher rates as running speed increased (Fig. 5.6A). At the times that SOL and GAS developed their peak forces during sprinting, the muscle fibres were contracting at 37% and 23% of their maximum shortening velocities, respectively. As a result, the peak forces that could potentially be developed by SOL and GAS during sprinting were only 30% and 40% of their peak isometric forces, respectively (Fig. 5.6B). Both SOL and GAS operated higher on their force-length curves as running speed increased, but

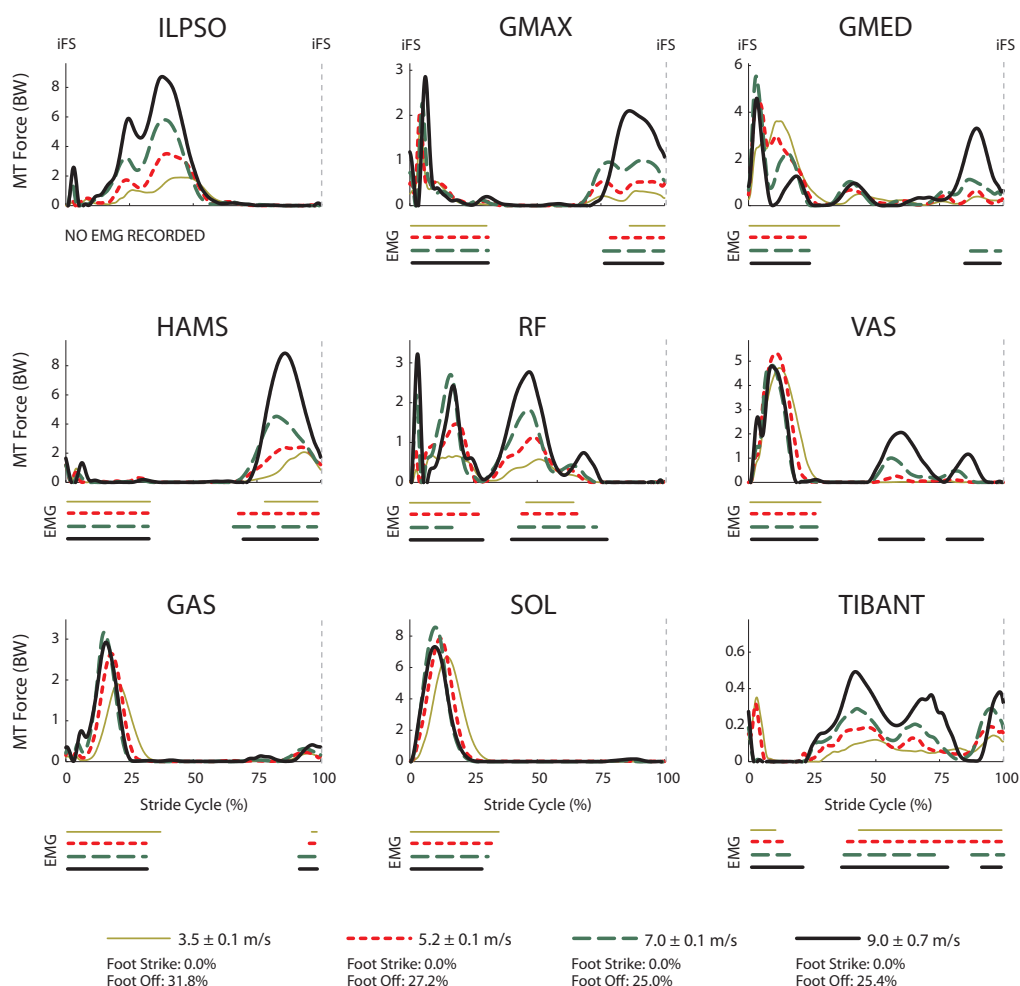


Figure 5.3: Musculotendon forces calculated for each running speed. Horizontal bars shown below each plot indicate the periods of EMG activity recorded for each muscle as determined by TKE filtering of the raw EMG signal. Results were averaged across all trials for all subjects and are shown over a full stride cycle. Forces are normalised by body weight. Muscle symbols appearing in the graphs are: ILPSO (iliacus and psoas combined; no EMG data recorded), GMAX (superior, middle and inferior gluteus maximus), GMED (anterior, middle and posterior compartments of gluteus medius), HAMS (biceps femoris long head, semimembranosus and semitendinosus combined, medial hamstring EMG shown), RF (rectus femoris), VAS (vastus medialis, vastus intermedius and vastus lateralis combined; vastus lateralis EMG shown), GAS (medial and lateral compartments of gastrocnemius combined; medial gastrocnemius EMG shown), SOL (soleus) and TIBANT (tibialis anterior). *iFS* signifies ipsilateral foot-strike.

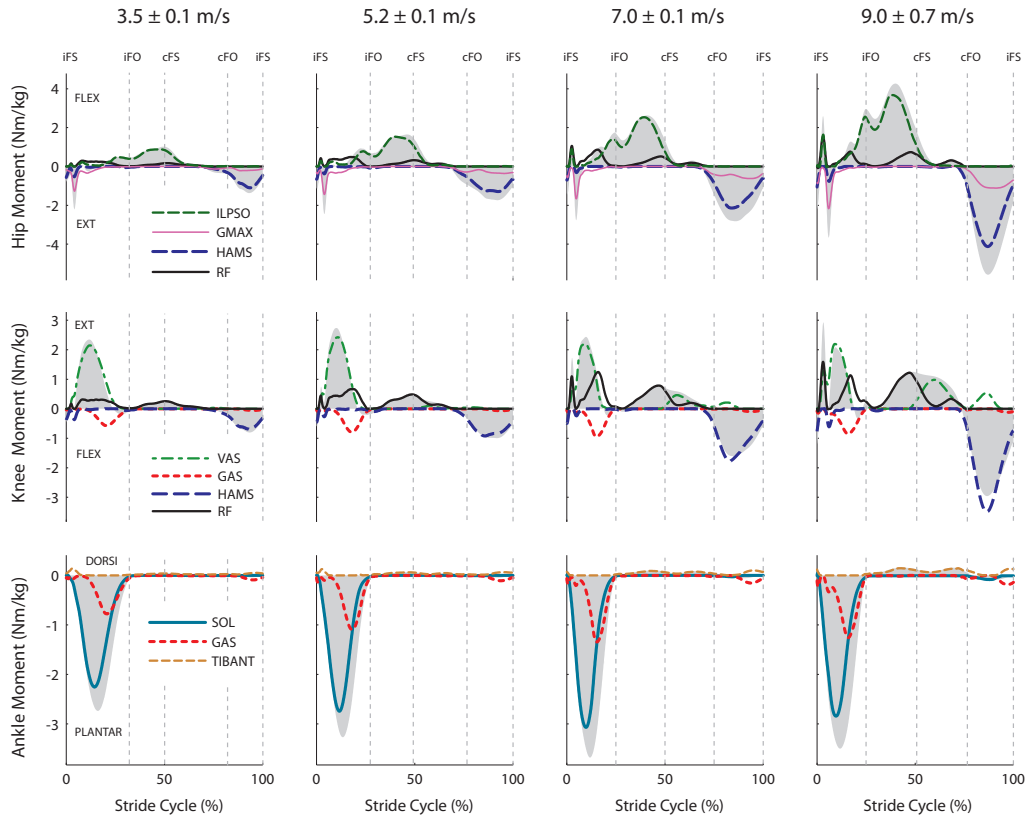


Figure 5.4: Contributions of individual muscles to the net sagittal-plane joint moments (shaded regions) for each running speed. Positive joint moments represent hip flexion, knee extension and ankle dorsiflexion; negative joint moments represent hip extension, knee flexion and ankle plantarflexion. Results were averaged across all trials for all subjects and are plotted for a full stride cycle. Moments are normalised by body mass. Muscle symbols as defined in the caption for 5.3. *iFS*, *iFO*, *cFS* and *cFO* signify ipsilateral foot-strike, ipsilateral foot-off, contralateral foot-strike and contralateral foot-off, respectively.

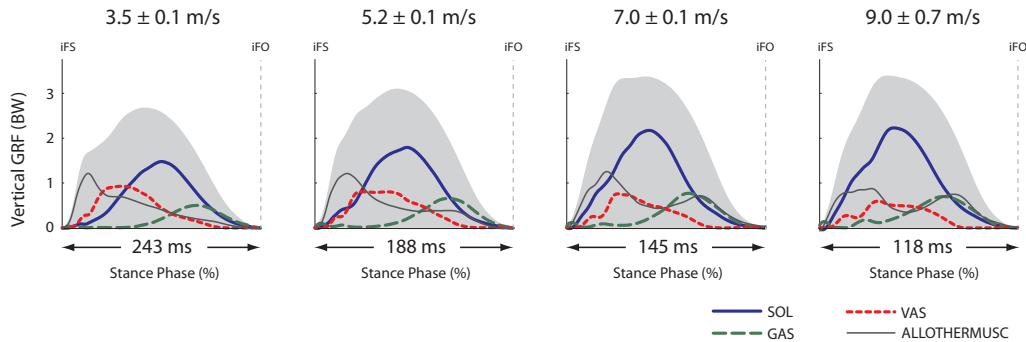


Figure 5.5: Contributions of individual muscles to the net vertical ground reaction force (shaded regions) for each running speed. Positive ground reaction forces are directed upwards. Results were averaged across all trials for all subjects and are shown for the stance phase of the stride cycle. Forces are normalised by body weight. Muscle symbols as defined in the caption for 5.3. ALLOTHERMUSC signifies the contributions of all muscles, except SOL, GAS and VAS. *iFS* and *iFO* signify ipsilateral foot-strike and ipsilateral foot-off, respectively.

this effect was discounted by the high contraction velocities of these muscles.

5.3.4 Muscle function during swing

The mechanical work performed by the hip muscles during swing increased as running speed increased ($p < 0.01$) (Fig. 5.7 and Table 5.1). In particular, ILPSO generated more work at the hip during the first half of swing (linear trend, $R^2 = 0.9457$); GMAX generated more work at the hip in the second half of swing (second-order polynomial trend, $R^2 = 0.9432$); RF absorbed more work at the hip and the knee in the first half of swing (linear trend, $R^2 = 0.9288$); and HAMS absorbed more work at the hip and knee in the second half of swing (second-order polynomial trend, $R^2 = 0.9274$).

The muscles of both the ipsilateral and contralateral legs induced larger accelerations of the ipsilateral hip and knee joints as running speed increased (Fig. 5.8). In the first half of swing, the ipsilateral hip was accelerated into flexion by the ipsilateral ILPSO, and this action was opposed by the contralateral HAMS and GMAX. In the second half of swing, the ipsilateral

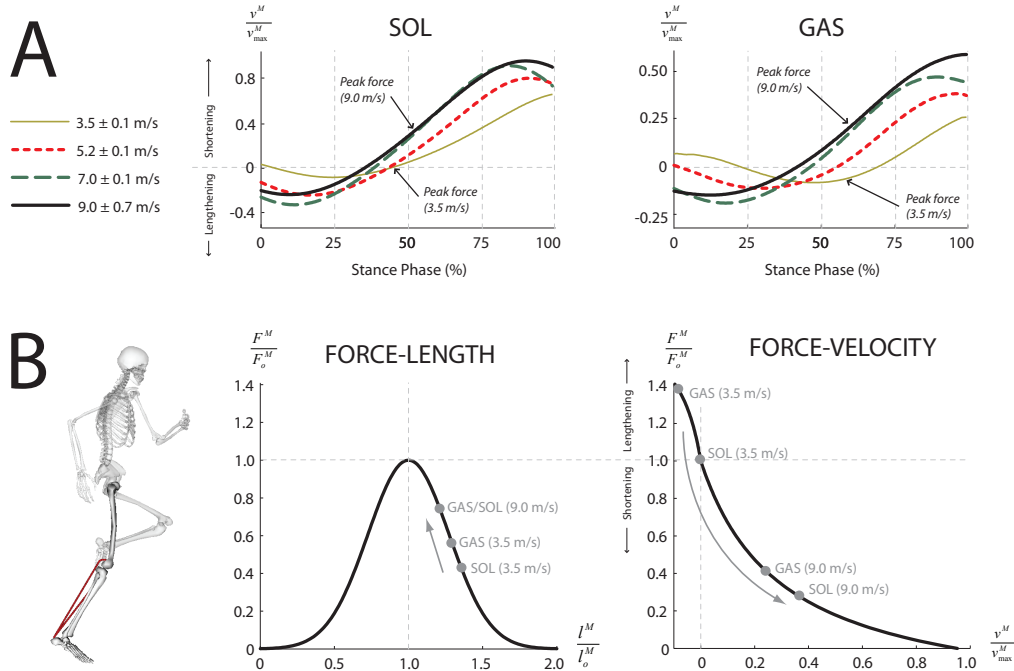


Figure 5.6: (A) Normalised muscle-fibre velocities of the soleus (SOL) and gastrocnemius (GAS) muscles calculated for the stance phase of the stride cycle at each running speed. The time instant of peak force production is labelled for running speeds of 3.5 m/s and 9.0 m/s. (B) Normalised force-length and force-velocity curves for SOL and GAS at running speeds of 3.5 m/s and 9.0 m/s. The force-length curve of muscle was normalised by the muscle's peak isometric force, F_0^M , and its optimal fibre length, l_0^M . The force-velocity curve of muscle was normalised by the muscle's peak isometric force, F_0^M , and its maximum shortening velocity, v_{max}^M . Points are displayed for the instants when the muscles developed their peak forces; see part (A).

hip was accelerated into extension by the ipsilateral HAMS and GMAX, and this action was opposed by the contralateral ILPSO (Fig. 5.8, HIP). Similarly, the ipsilateral knee was accelerated into flexion by the ipsilateral ILPSO during the first half of swing, and this action was opposed by the contralateral HAMS and GMAX. In the second half of swing the ipsilateral knee was accelerated into extension by the ipsilateral GMAX and VAS, and these actions were opposed by the ipsilateral HAMS and contralateral ILPSO (Fig. 5.8, KNEE). ILPSO, HAMS and GMAX contributed to greater hip and knee accelerations as running speed increased ($p < 0.01$), especially between

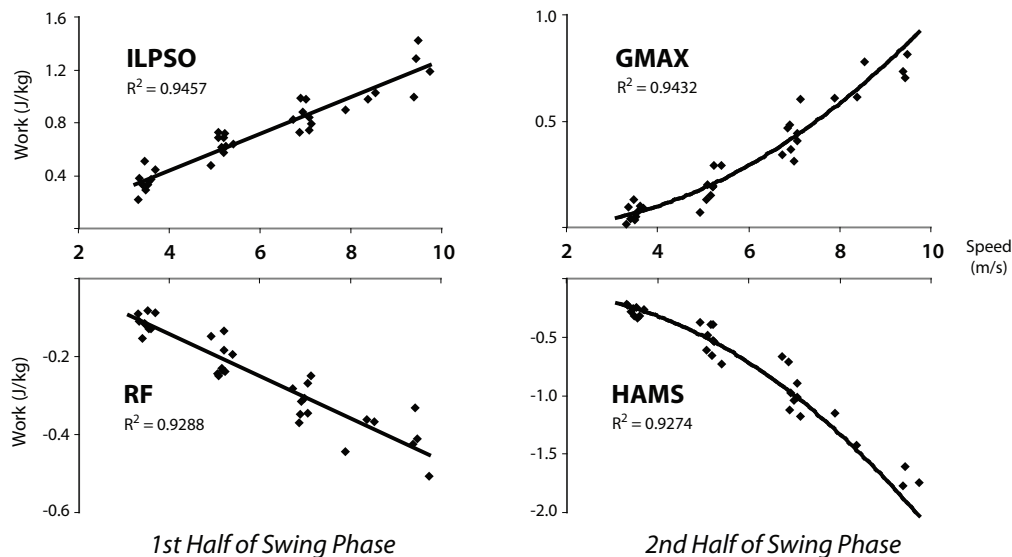


Figure 5.7: Hip muscle work trends for the swing phase of running. Muscle symbols as defined in the caption for 5.3. ILPSO work generation is shown for the first half of swing and follows a linear trend. GMAX work generation is shown for the second half of swing and follows a second-order polynomial trend. RF work absorption is shown for the first half of swing and follows a linear trend. HAMS work absorption is shown for the second half of swing and follows a second-order polynomial trend.

7.0 m/s and 9.0 m/s when these muscles produced an almost two-fold increase in hip and knee-joint acceleration.

5.4 Discussion

The goal of the present study was to better understand how the individual leg muscles coordinate motion of the body segments during running. Our specific aim was to determine the contributions of the individual leg muscles to increases in stride length and stride frequency, and hence running speed. Experimental gait data were combined with a detailed musculoskeletal model of the body to evaluate two hypotheses: **(H1)** *The ankle plantarflexors are mainly responsible for increasing stride length during the stance phase of running;* and **(H2)** *The hip flexors and extensors are mainly responsible for increasing stride frequency during swing.*

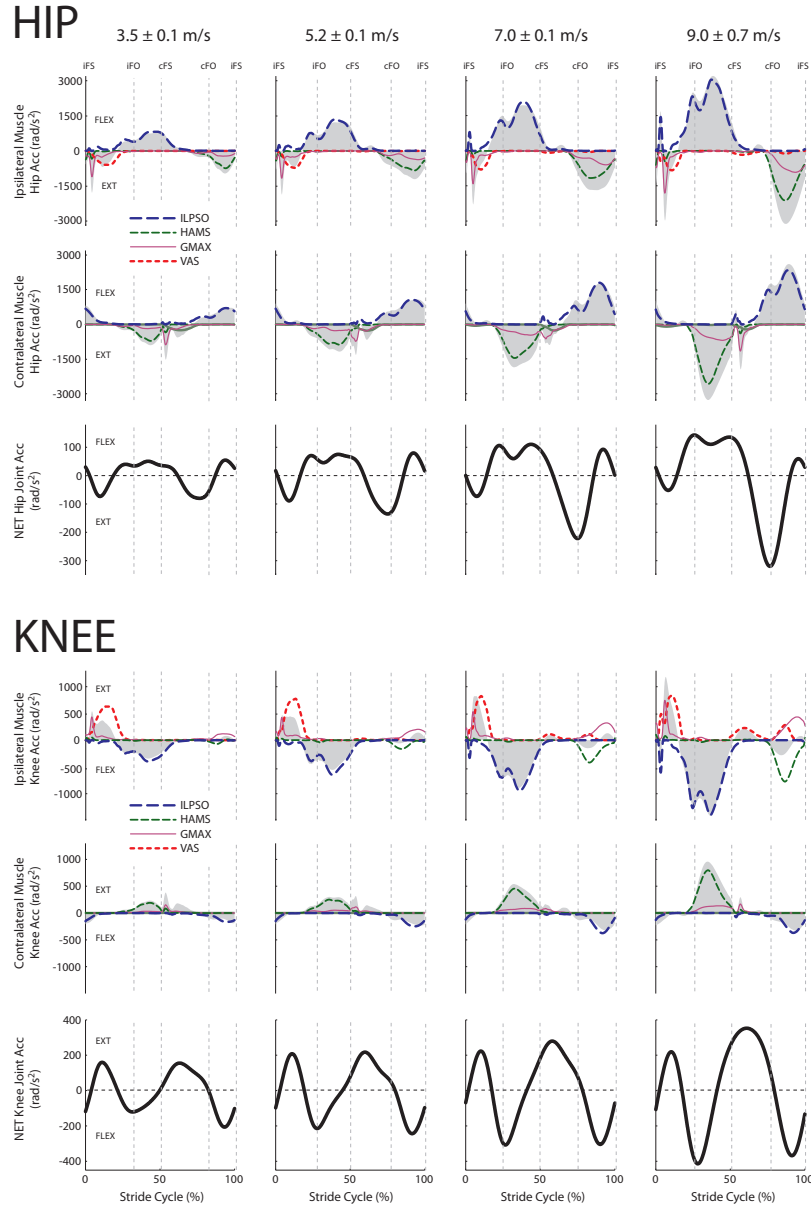


Figure 5.8: Contributions of the individual muscles of the ipsilateral and contralateral legs to the net sagittal-plane angular accelerations of the ipsilateral hip and knee joints. The shaded regions represent the total joint acceleration induced by the ipsilateral- and contralateral-leg muscles, respectively. Results are shown for each running speed. Positive joint accelerations represent hip flexion and knee extension; negative joint accelerations represent hip extension and knee flexion. Results were averaged across all trials for all subjects and are plotted for the full stride cycle. Muscle symbols as defined in the caption for 5.3. *iFS*, *iFO*, *cFS* and *cFO* signify ipsilateral foot-strike, ipsilateral foot-off, contralateral foot-strike and contralateral foot-off, respectively.

Musculoskeletal modelling is a powerful tool for studying muscle function during movement because it allows individual muscle outputs such as length, force and power to be determined non-invasively (Pandy and Andriacchi, 2010). The accuracy of the model used to calculate lower-limb muscle forces during running has been evaluated in a number of previous studies undertaken by various groups, including our own (Erdemir et al., 2007; Hamner et al., 2010; Pandy and Andriacchi, 2010). Further, muscle morphological parameters assumed in the model were updated with the most recent data obtained from a comprehensive cadaver dissection study (Ward et al., 2009).

To verify the convergence of the static optimisation analysis, we compared the inverse dynamic joint moments with the summed muscle moments (i.e., the product of muscle force and moment arm) for each muscle in the model. The average RMS of the difference between the two sets of joint moments was found to be less than 0.05 Nm/kg, with the exception of the transverse plane hip rotation moment (Fig. 5.9). The evident discrepancy between the muscle-computed and inverse-dynamics-computed transverse plane hip moment was most likely attributable to errors in the experimental data (e.g., soft tissue artefact), which is prevalent when investigating fast dynamic activities that involve large muscle contractions (Cappozzo et al., 1996; Akbarshahi et al., 2010). However, for all running speeds, the discrepancy was never greater than 0.5 Nm/kg and hence was not considered to be of any major consequence for evaluating the functional roles of muscles in running. The results from the induced acceleration analysis were also evaluated using the superposition principal (Anderson and Pandy, 2003): the sum of all individual muscle contributions to the vertical ground reaction force and hip- and knee-joint accelerations predicted by the model matched the equivalent experimental data with errors of less than 5% RMS for all running speeds (Fig. 5.10).

To our knowledge, this is the first study to determine the contributions of individual muscle forces to performance-related biomechanical variables, specifically, joint moments, joint accelerations and ground reaction forces across a wide range of human running speeds. Although only sagittal-plane dynamics are reported here, the analysis performed was three-dimensional

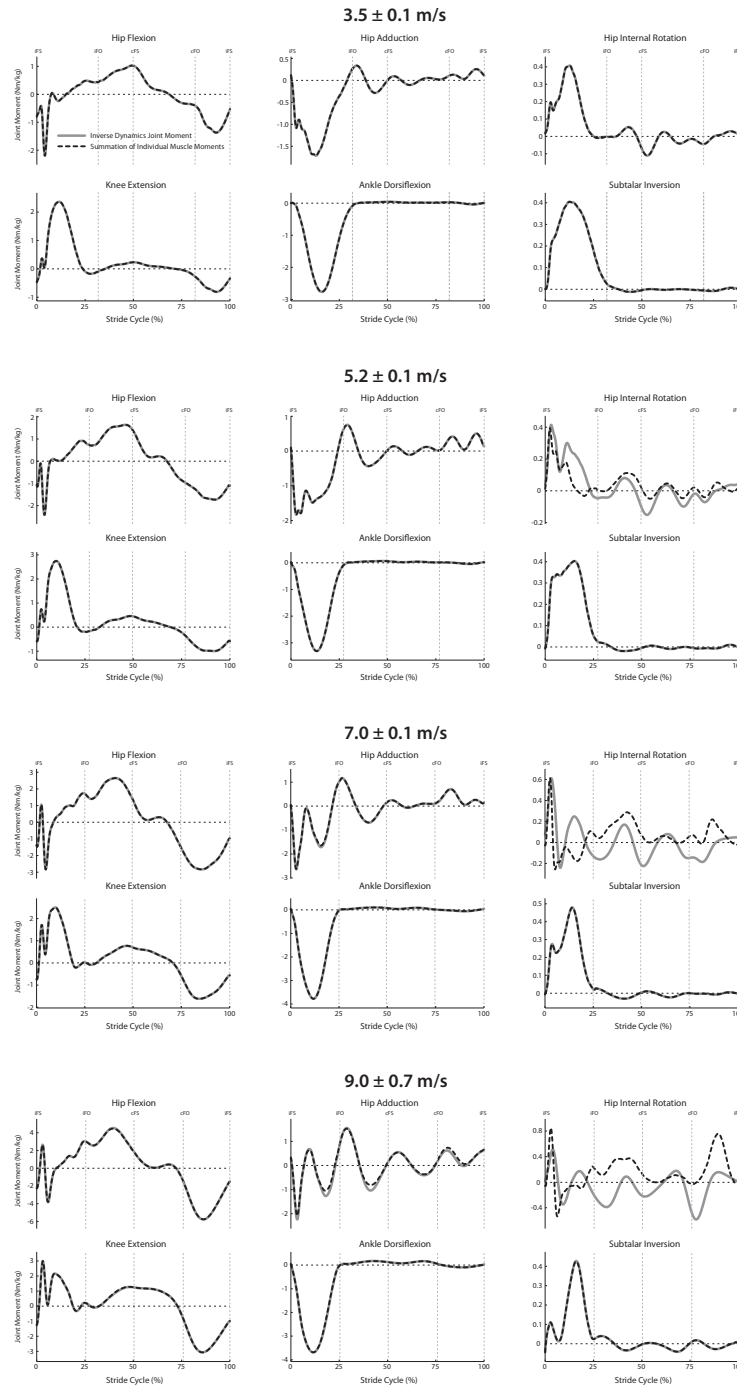


Figure 5.9: Lower-limb joint moments for each running speed calculated from inverse dynamics (solid line) and by summing the individual moment contributions (product of muscle force from static optimisation and moment arm) for every muscle in the model (dashed line).

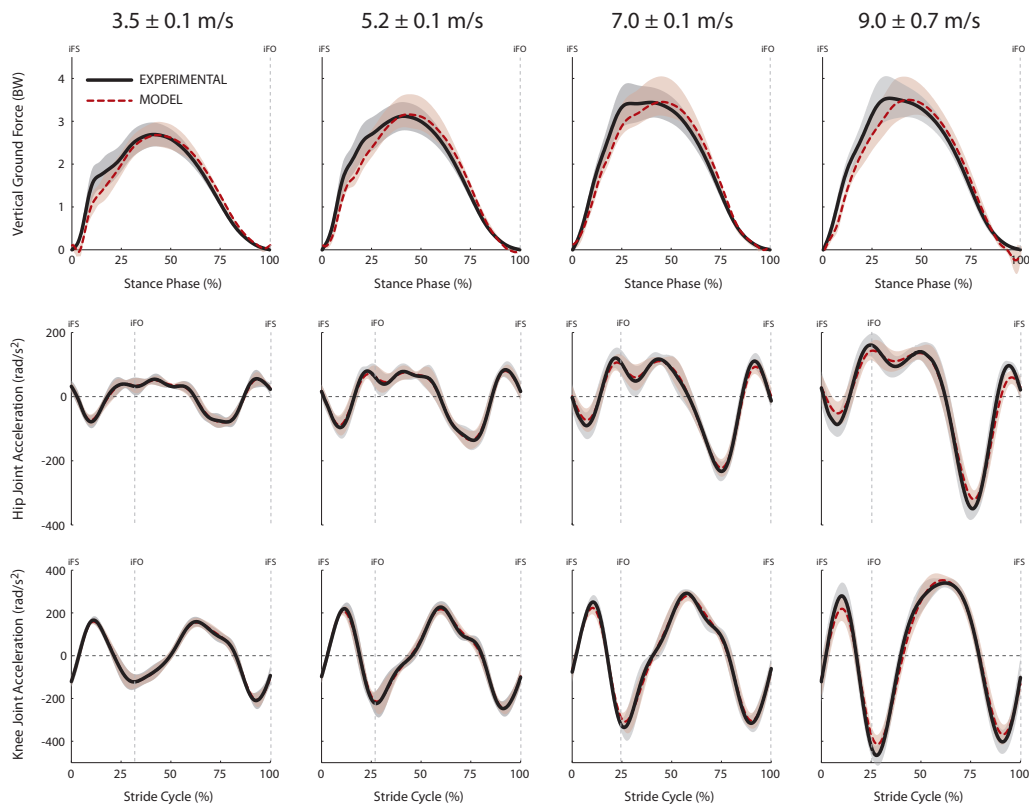


Figure 5.10: *Experimental (solid) and model predicted (dashed) trajectories of the vertical ground reaction force, net sagittal hip joint acceleration and net sagittal knee joint acceleration at all running speeds. The vertical ground reaction force is presented during the stance phase, while the hip and knee joint accelerations are presented for the entire stride cycle. Solid and dashed represent mean values across all subjects, and the shaded regions represent one standard deviation from the mean. iFS and iFO signify ipsilateral foot-strike and ipsilateral foot-off, respectively.*

and included muscle contributions in the coronal and transverse planes as well. This is also the first study to quantify the mechanical work done by the individual leg muscles during running. Previous studies investigating the energetics of running have used inverse dynamics to determine muscular work at the joint level (Novacheck, 1998; Swanson and Caldwell, 2000; Biewener et al., 2004; McIntosh et al., 2006; Devita et al., 2007; Schache et al., 2011a). Calculations of joint work do not account for the contributions of individual muscles, particularly those that cross more than one joint. For example, because the hip joint acts as an energy generator and the knee joint as an energy absorber (Sawicki et al., 2009; Schache et al., 2011a), it is not possible to determine whether a biarticular muscle spanning both of these joints, such as HAMS, is absorbing energy from, or generating energy to, the skeleton. Finally, the results of the present study are based on novel experimental data recorded for overground running. Whilst treadmills enable gait experiments to be performed more easily in a laboratory setting, differences in the kinematics and kinetics of treadmill and overground running have been widely reported, particularly at the higher speeds of running (Nelson et al., 1972; Elliott and Blanksby, 1976; Frishberg, 1983; Nigg et al., 1995; Riley et al., 2008).

5.4.1 Hypothesis 1: The ankle plantarflexors are mainly responsible for increasing stride length during stance.

As running speed increased from 3.5 m/s to 7.0 m/s, SOL and GAS were mainly responsible for increasing stride length by generating higher support forces during ground contact (Figs 5.2A and 5.5). Above 7.0 m/s, however, the peak forces developed by SOL and GAS decreased (Fig. 5.3), while their contributions to the vertical ground force remained roughly the same (Fig. 5.5). The peak forces developed by the ankle plantarflexors decreased at the higher running speeds for two possible reasons. First, the muscles may have been operating at lengths much shorter or longer than the muscles' optimum fibre lengths (Gordon et al., 1966; Woledge et al., 1985;

Close, 1972); and second, the contractile velocities may have been too high to allow the muscles to develop high forces (Katz, 1939; Abbott and Wilkie, 1953; Bahler et al., 1968). The model calculations showed that even though SOL and GAS operated at more favorable positions on their force-length curves as running speed increased, the peak forces that could potentially be developed by these muscles decreased due to their high contraction velocities (Fig. 5.6A). For example, in running at 3.5 m/s SOL developed its peak force while contracting isometrically, whereas in sprinting at 9.0 m/s SOL developed its peak force while shortening at 37% of its maximum shortening velocity. As running speed increased from 3.5 m/s to 9.0 m/s, the force generating capacity of SOL decreased from 100% to 30% of its peak isometric force, while that of GAS reduced from 140% to 40% of its peak isometric force (Fig. 5.6B). The plantarflexors shortened at higher rates as running speed increased because the time available for ground contact diminished (Fig. 5.2B), meaning that these muscles had less time to generate the support forces needed during stance. We conclude that the ability of the ankle plantarflexors to increase stride length is limited when running speed approaches 7.0 m/s. An alternative strategy is therefore needed to increase running speed beyond this mark.

5.4.2 Hypothesis 2: The hip muscles are mainly responsible for increasing stride frequency during swing.

We found that second-order polynomial trends adequately described the relationships between the swing phase work done by the hip-extensor muscles (i.e., GMAX and HAMS) and running speed (Fig. 5.7). Second-order polynomial trends have also been used to describe the relationship between stride frequency and running speed (Mercer et al., 2002). Taken together, these results suggest a causal link between the actions of the hip muscles and stride frequency.

The model calculations showed that stride frequency was increased by increasing the forces generated by the hip-spanning muscles, primarily

ILPSO, GMAX and HAMS, as these muscles contributed significantly to the larger hip- and knee-joint accelerations observed at higher running speeds (Fig. 5.8). Although a given muscle can only generate a moment about a joint that it spans, the same muscle can induce angular accelerations of all the joints in the body, including those not spanned by that muscle. This is a consequence of dynamic coupling, whereby the force applied by a muscle is transmitted to all the body segments simultaneously (Zajac and Gordon, 1989). Indeed, we found that the contralateral leg muscles are just as important as the ipsilateral leg muscles in controlling the accelerations of the ipsilateral hip and knee joints (Fig. 5.8). During the swing phase of running, the ipsilateral HAMS accelerated the ipsilateral knee into flexion and the contralateral knee into extension. The latter result may seem counter-intuitive because HAMS is classified anatomically as a knee flexor and also because the ipsilateral HAMS does not span any of the joints in the contralateral leg. Similarly, the contralateral HAMS accelerated the ipsilateral knee into extension to oppose the knee-flexor acceleration induced by the ipsilateral ILPSO. We note here that although the ILPSO does not span the knee, it nonetheless contributed significantly to knee-joint acceleration. As running speed increased, particularly above 7.0 m/s, the hip muscles played a more substantial role in increasing stride frequency by accelerating the leg more vigorously during swing.

5.4.3 Biological limit to running speed

We now discuss how our findings relate to the biological limits of running speed. Factors that limit the maximum speed of human sprinting have been debated in the literature and various conflicting views have emerged. Some investigators have hypothesised that maximum running speed is limited by the performance of the hip and knee muscles during swing (Chapman and Caldwell, 1983b; van Ingen Schenau et al., 1994). Whilst our findings have revealed significant increases in the accelerations of the lower-limb joints and the work performed by the hip muscles during swing at speeds above 7.0 m/s (Figs 5.3 and 5.8), there is no evidence to suggest that the forces exerted by the hip muscles at the highest running speeds represent thresholds of muscle

performance that cannot be improved. An alternative view is that maximum running speed is limited by the ability of the leg muscles to generate sufficient vertical impulse during stance (Cavagna et al., 1971; Weyand et al., 2000, 2010). Our model calculations are consistent with this idea. We found that the ankle plantarflexors generate the majority of the vertical ground force and that these same muscles are compromised by the adverse contractile conditions present at faster running speeds.

The force-velocity property of muscle, by determining the amount of force a muscle can transmit to the ground during stance, also influences the rate at which the limbs must be swung through and repositioned during swing. This is evidenced by the similar trends visible in the effective vertical ground impulse, a stance phase measurement, and aerial time, a swing phase measurement (Fig. 5.2B). A reduced effective vertical ground impulse decreases the upward acceleration of the center-of-mass, shortens the aerial time and requires the legs to be swung through more quickly (Weyand et al., 2000, 2009). Hence, the plateau in stride length observed above 7.0 m/s, which results from the high contraction velocities of SOL and GAS, means that further increases in running speed can only be achieved by increasing stride frequency. Indeed, at the fastest running speeds we observed virtually no change in the peak vertical ground force (Fig. 5.5), yet stride frequency increased by 25% (Fig. 5.2A) and the work performed by the hip muscles approximately doubled (Fig. 5.7).

We therefore conclude that the fastest running speeds are achieved by increasing stride frequency once the ankle plantarflexors have reached their maximum capacities. This finding has relevance for the design of improved training techniques for runners. If the speed at which the ankle muscles fail to provide a sufficiently large effective vertical impulse can somehow be increased, then the goal of increasing stride frequency could be delayed until a higher running speed is reached, thus improving the overall maximum sprinting speed. This proposition is supported by previous research (Weyand et al., 2000) and could be achieved by improving the strength of the calf musculature under high-velocity contractile conditions, for example, through the use of targeted plyometric-type strength training regimes (Wilson et al., 1993; Kawamori and Haff, 2004; Ozcaldiran and Durmaz, 2008).

5.4.4 Limitations of the study

There are a number of limitations associated with the present study. First, our results apply only to steady-state running, and hence do not reflect the coordination strategies used during the initial burst of acceleration needed to reach a constant speed. Although the continuous acceleration phase of running between 3.5 m/s and 9.0 m/s may exploit different mechanical strategies to that observed by independent steady-state running trials between the same two speeds, practical considerations prevented the collection of acceleration phase running data in the laboratory. For example, subjects required up to 40 m of track to accelerate to maximum speed. Capturing marker-based kinematics and ground reaction forces over this length would require excessive amounts of laboratory equipment. In addition, controlling the acceleration rate of individuals in overground running is almost impossible, whereas steady-state speeds can be more rigorously managed. Indeed, previous musculoskeletal modelling studies investigating human locomotion over a range of speeds have been based on multiple steady-state trials (Liu et al., 2008; Pandy and Andriacchi, 2010). Future work is required to test the assumption that analyses of multiple steady-state trials are equivalent to a continuous acceleration phase in both walking and running.

Second, we assumed the same cost function in calculating muscle forces across all running speeds. At self-selected speeds of walking and running, a minimum muscle-stress criterion yields muscular loading patterns that are consistent with measured EMG activity (Glitsch and Baumann, 1997; Raikova and Prilutsky, 2001). However, minimum muscle stress may not be the most appropriate criterion to use at the fastest running speeds. For example, one objective of sprinting may be to maximise the average horizontal velocity of the center-of-mass throughout the stride cycle, which could be achieved by maximizing muscular effort over time, irrespective of the metabolic cost of transport (Cavagna et al., 1971; Ward-Smith, 1985). However, it is unlikely that such a cost function would apply to running at submaximal speeds. We therefore used the same cost function (i.e., minimum muscle stress) to calculate leg-muscle forces at all running speeds.

We evaluated the sensitivity of muscle force predictions for a single subject using different exponents for the cost function and found no significant differences in the shapes and magnitudes of the predicted muscle forces (Fig. 5.11). These findings are in agreement with Glitsch and Baumann (1997). Future work should be directed at quantifying the performance criteria applicable to running at different speeds and their concomitant effects on model predictions of muscle forces.

Third, activation dynamics was neglected in the formulation of the static optimisation problem posed in this study. Although activation dynamics does not have a significant effect at slow running speeds its role in faster running may be more pronounced (see the paper entitled: *Comparison of different methods for estimating muscle forces in human movement* in Appendix D for a detailed discussion on the implications of using static optimisation to make predictions of muscle force). Nevertheless, the patterns of muscle activations and muscle forces predicted by the model were in agreement with the sequence and timing of measured EMG activity (Fig. 5.11).

Fourth, the musculoskeletal model for each subject was generated by scaling a common generic musculoskeletal model to the subject's anthropometry and hence did not explicitly incorporate the internal subject-specific anatomy present in the athletic population. Elite sprinters are known to possess smaller Achilles tendon moment arms and longer fascicle lengths than the non-elite population, which together, provide the capabilities to generate a larger ground reaction force and impulse during stance (Lee and Piazza, 2009). Such key model parameters can be non-invasively measured in vivo using ultrasound apparatus (Ishikawa and Komi, 2007; Lichtwark et al., 2007), but require a considerable investment in time and equipment to successfully incorporate into existing musculoskeletal models. In addition, several mechanisms that are known to enhance the force generating ability of muscle were not included in the muscle model, which may be important for maximising running performance. Such mechanisms include muscle gearing through shape change (Azizi et al., 2008; Wakeling et al., 2011), stretch induced residual force enhancement (Rassier and Herzog, 2005; Lee and Herzog, 2008), force

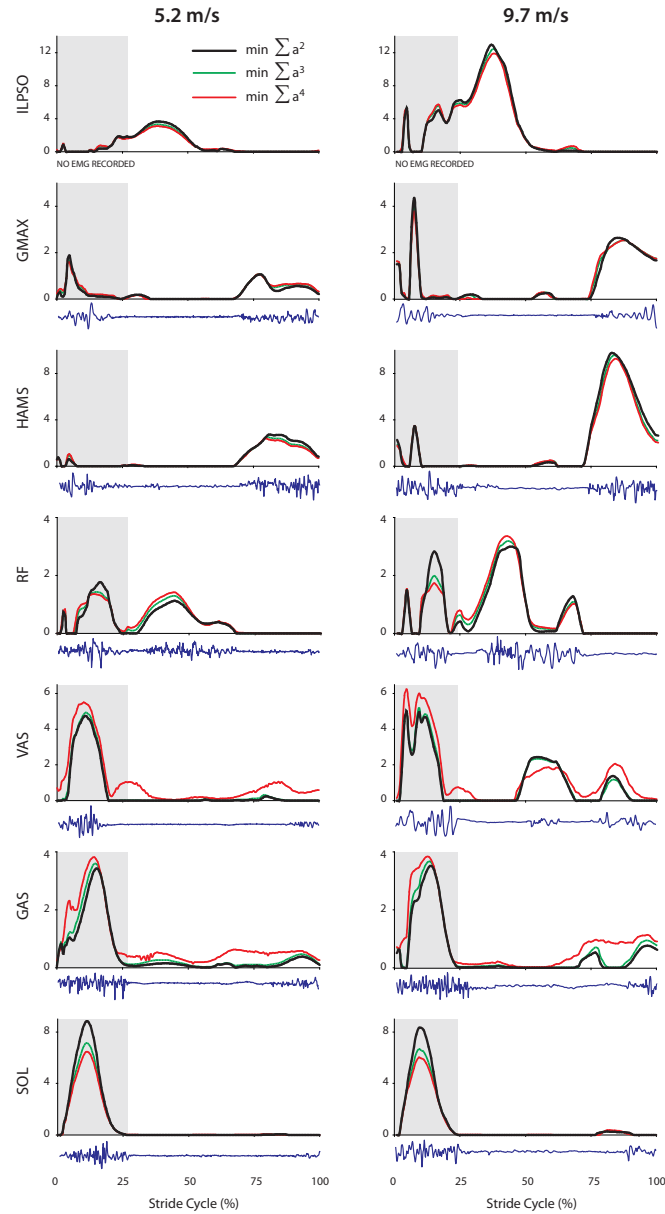


Figure 5.11: Sensitivity of muscle force predictions to the objective function exponent for one representative subject running at 5.2 m/s and 9.7 m/s. Force magnitudes were normalised by body weight. Raw EMG signals measured in the experiment are shown below each plot. Muscle symbols as defined in the caption for 5.3. Because activation dynamics was neglected in the model, there is no time lag between muscle activation and force production; hence at any given time, muscle activations are directly proportional to muscle force.

depression with shortening (Joumaa and Herzog, 2010; McGowan et al., 2010) and complex interactions between muscle and multi-dimensional elastic tissue (e.g., aponeurosis) (Magnusson et al., 2008).

Finally, we assumed that joint moments were satisfied in their entirety by muscle forces alone. It is likely that several non-muscular structures also contribute to the moment exerted about each joint. For example, foot and shoe deformation during ground contact (Webb et al., 1988), the plantar fascia (Kibler et al., 1991), and the anterior cruciate ligament (Hart et al., 2010) all exert moments about the joints they span, but these contributions are likely to be negligible compared to the moments exerted by the muscles.

5.4.5 Summary

The ankle plantarflexors, soleus and gastrocnemius, contribute most significantly to vertical support forces, and hence increases in stride length, during slow and medium-paced running (up to 7.0 m/s). At speeds near 7.0 m/s, the contractile conditions for these muscles deteriorate due to increased shortening velocities, requiring a change in the strategy used by runners to increase their speed still further. The strategy used to increase running speed beyond 7.0 m/s shifts from the goal of increasing stride length to one of increasing stride frequency. This new goal is achieved by the synergistic actions of the ipsilateral and contralateral hip muscles, primarily ILPSO, GMAX and HAMS, accelerating the leg more vigorously through the air and providing the high stride frequencies needed to reach the fastest running speeds possible.

Chapter 6

How leg muscles power human running

This chapter is based on the following work:

- **Dorn, T.W., Lin, Y.C., Schache, A.G., Pandy, M.G. (2012).**
Which muscles power the human running stride?, *American Society of Mechanical Engineers 2012 Summer Bioengineering Conference, June 20 - June 23, 2012, Fajardo, Puerto Rico.*

ABSTRACT

Running is a physically demanding activity that requires explosive muscle power and limb coordination. As the speed of running increases, greater metabolic energy is required in the form of muscle mechanical work to power the motion of the center of mass (external power) and the individual body segments (internal power). The purpose of this study was to quantify the contributions that muscles make to the external and internal powers of the body across a wide range of running speeds. Experimental marker kinematics and ground reaction forces were collected at 3.5 m/s, 5.2 m/s, 7.0 m/s and 9.0 m/s and input into a using computer-based musculoskeletal model. Individual muscle contributions to the external and internal powers were calculated using an induced acceleration analysis and a segment power analysis. In the stance phase, the external power underwent a period of absorption followed by a period of generation, provided by the actions of soleus, gastrocnemius and vasti of the ipsilateral leg, to decelerate the body in early stance and propel the body forward in late stance, whilst continuously supporting the body against gravity. In the swing phase, iliopsoas, gluteus maximus and hamstrings from both legs generated the majority of power to the swing-leg to initially drive it forwards, and then absorbed the majority of power from the swing-leg in preparation for ground contact. As running speeds increased, the muscles exhibited increased external and internal work transfer rates, demonstrating the remarkable energetic demands of running at the fastest speeds possible.

6.1 Introduction

Running is a physically demanding activity that requires explosive muscle power and precise limb coordination. As running speed increases, the energy requirements needed to support the body against gravity, propel the body forward and power the lower limbs all increase (Margaria et al., 1963; van der Walt and Wyndham, 1973; Di Prampero et al., 1993; Arampatzis et al., 2000). This energy is derived from the concentric and eccentric contraction of skeletal muscle in the form of mechanical power and is transferred to the skeleton, influencing its motion (Devita et al., 2008; Schache et al., 2011a).

Mechanical power in human locomotion can be classified as either external or internal (Willems et al., 1995). External power represents the energy involved in moving the whole-body center of mass relative to the environment, and is governed by external forces. With the exception of gravity, external power can only be generated whilst the foot is in contact with the ground. Internal power represents the energy involved in moving the individual body segments relative to the whole-body center of mass, and can be influenced throughout the entire stride cycle. Whereas the calculation of external power is relatively straightforward (i.e., the product of the ground reaction force and center of mass velocity), computing internal power is more complex because it requires a computer model that incorporates the geometrical and inertial properties of each body segment. Determining how individual muscles contribute to the power of a given body segment is complicated further by the phenomena of dynamic coupling, whereby each muscle force contributes to the instantaneous acceleration of all the joints, and hence the instantaneous power of each body segment (Zajac and Gordon, 1989; Zajac et al., 2002).

Segment power analyses developed by Fregly and Zajac (1996) have been used in conjunction with computer-based musculoskeletal models to quantify the transfer of mechanical power between the muscles and segments of the body in human walking (Neptune and Kautz, 2001; Neptune et al., 2004; Neptune and McGowan, 2011). By generating power to a segment, a muscle tends to accelerate the segment in the direction of

its current motion; and conversely, by absorbing power from a segment, a muscle tends to decelerate the segment. In walking, the soleus and vasti have been shown to decelerate trunk progression by absorbing energy from the trunk in the first half of stance, and to propel the trunk forward by delivering energy to it in the second half of stance (Neptune and Kautz, 2001; Neptune et al., 2004). During the swing phase of walking, the transfer of energy between ipsilateral and contralateral lower-limb segments has been found to be important in powering the ipsilateral thigh and shank forward in the first half of swing, and then backward in the second half of swing (Neptune et al., 2004; Sasaki et al., 2008).

In running, only one other study has adopted a segment power analysis to investigate the mechanical power transfer strategies in running (Sasaki and Neptune, 2006). This study reported a significant difference in the function of soleus between walking and running, with all other muscles showing a qualitatively similar functional role to distribute mechanical power among the body segments. Unfortunately, the running speed analysed was very slow (1.96 m/s), so these results can not be generalised over the full range of running speeds. Other studies that have used musculoskeletal models to simulate running have either: (i) computed muscle forces without examining how individual muscles coordinate motion of the lower limbs and the center of mass (Glitsch and Baumann, 1997; Yokozawa et al., 2007; Schache et al., 2010; Chumanov et al., 2011); or (ii) computed muscle forces and their contributions to the accelerations of the lower-limb joints and center of mass, but only for running speeds less than 4 m/s (Hamner et al., 2010; Lin et al., 2011b).

The purpose of this study, therefore, was to determine how individual leg muscles power human running, across a range of speeds, from slow running to maximal sprinting. More specifically the aims were: (i) in the stance phase, to determine how muscles generate external power to support and drive the body forwards; and (ii) in the swing phase, to determine how muscles contribute to the internal segment power of the body segments to coordinate the swinging of the lower limbs. Such a description of lower-limb muscle function will highlight the strategies used by individual muscles to supply the power necessary to run at the fastest speeds possible.

6.2 Methods

Nine habitual runners (5 males, 4 females; age: 27.7 ± 8.0 years; mass 73.1 ± 8.6 kg; height 176 ± 7 cm) volunteered to participate in this study. The study was approved by the Research Ethics Committees of the Australian Institute of Sport and the University of Melbourne. Prior to the commencement of data collection, a test leg was randomly allocated for each participant and designated as the ipsilateral leg (right = 4; left = 5).

6.2.1 Experimental data collection

Overground running data were collected at four target speeds: 3.5 m/s ($n = 9$), 5.0 m/s ($n = 9$), 7.0 m/s ($n = 8$) and 9.0 m/s ($n = 7$). Each subject ran on an indoor 110 m synthetic running track in the Biomechanics Laboratory at the Australian Institute of Sport. Timing gates (Speedlight Telemetry Timing, Swift Performance Equipment, Australia) were used to monitor the steady-state speed of each runner. Verbal feedback was provided to ensure the subject attained the desired target speed. Adequate recovery time was provided between trials to prevent fatigue.

Marker derived kinematics were acquired using a three-dimensional motion analysis system (VICON, Oxford Metrics, Oxford, UK) (see Table 3.1 in Chapter 3). Ground reaction forces were captured on a series of eight force plates (Kistler Instrument Corp., Amherst, NY, USA) and low-pass filtered at 60 Hz using a fourth-order Butterworth filter. Electromyography (EMG) data were collected from 11 lower-limb muscles of the test leg (Noraxon Telemetry 2400T G2, Noraxon USA Inc.): gluteus maximus, gluteus medius, rectus femoris, vastus medialis, vastus lateralis, medial hamstrings, lateral hamstrings, tibialis anterior, medial gastrocnemius, lateral gastrocnemius and soleus (see Table 3.2 in Chapter 3). EMG onset and offset times were determined by applying a Teager-Kaiser Energy (TKE) filter to the raw EMG signal (Li et al., 2007; Solnik et al., 2010). A Gait-Extract Toolbox (freely available from <https://simtk.org/home/c3dtoolbox>) was used to extract and process raw marker trajectories, ground reaction forces, and EMG data into a

format suitable for input into the musculoskeletal model. Refer to Chapter 3 for more details on the experimental protocol.

6.2.2 Musculoskeletal model

A three-dimensional 12 segment, 31 degree-of-freedom musculoskeletal model was used to simulate running (Fig. 6.1A). The head and trunk were lumped into a single rigid body, which articulated about the pelvis via a ball-and-socket joint. The pelvis was free to translate and rotate relative to the surrounding environment. In the lower-limb, each hip was modelled as a ball-and-socket joint, each knee as a translating hinge joint (Seth and Delp, 2009), and each ankle-joint complex as two non-intersecting pure hinge joints. In the upper-limb, each shoulder was modelled as a ball-and-socket joint and each elbow as two non intersecting pure hinge joints. The lower limbs and trunk were actuated by 92 muscle-tendon units, each unit represented as a Hill-type muscle in series with an elastic tendon (Fig. 6.1B and C). The upper limbs were actuated by 10 torque motors to simulate the dynamics of arm swing. The model was implemented in OpenSim and is freely available at <https://simtk.org/home/runningspeeds>.

Five discrete points located on the sole of each foot (Fig. 6.1D) were used to simulate the interaction between the foot and the ground so that ground reaction forces could be generated in the model (see Section 3.2.7). Two ground contact points were located at the heel, two at the metatarsal joint, and one at the end of the toes. During periods of ground contact, the measured center of pressure was used to control the stiffness of each contact point relative to the ground, according to a set of rules that governed the heel-strike, foot-flat and toe-off phases of ground contact (see Section 3.2.7 and in particular, Fig. 3.9). In this way, the ground contact model was naturally adapted to the particular contact pattern (i.e., rearfoot- or forefoot-strike) exhibited by the subjects at each running speed.

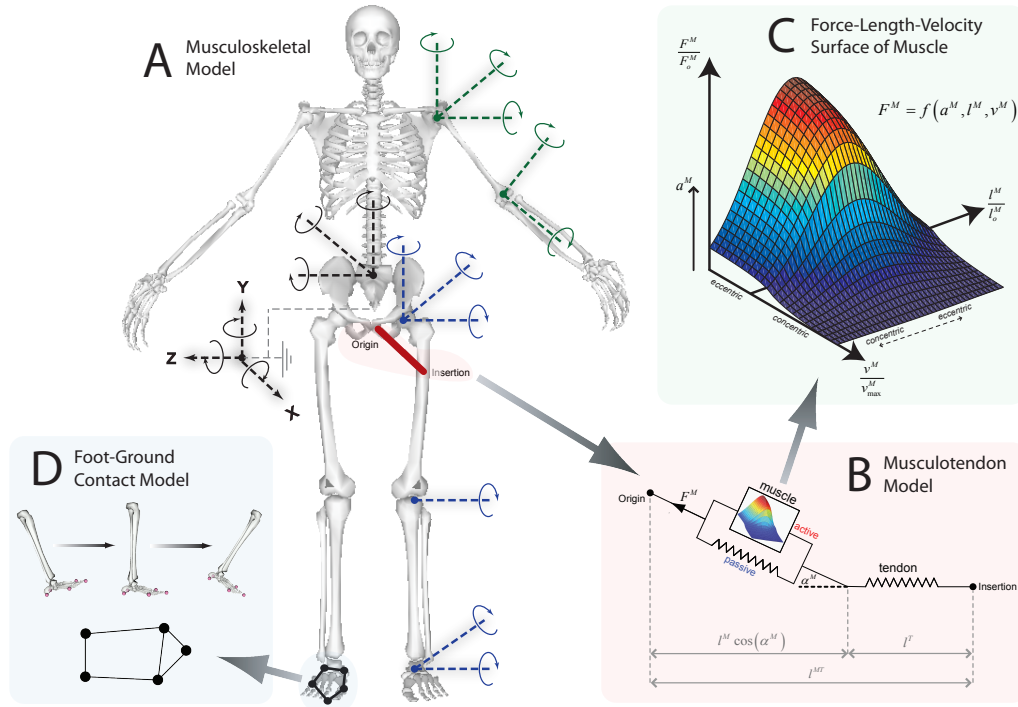


Figure 6.1: Three-dimensional full body musculoskeletal model used in the present study. (A) The skeleton was represented as a multibody linkage containing 31 degrees-of-freedom, driven by 92 musculotendon actuators (lower extremity and trunk) and 10 ideal torque actuators (upper extremity). (B) Each musculotendon actuator was represented as a Hill-type physiological muscle in series with tendon. Muscle fibre length l^M and tendon length l^T were governed by the distance between musculotendon origin and insertion l^{MT} , muscle pennation angle α^M and muscle force F^M . (C) The active force-length-velocity surface of physiological muscle was defined by the muscle's optimal fibre length l_0^M , maximum shortening velocity v_{max}^M and maximum isometric force F_0^M . Active muscle force generation was always constrained to this surface, scaled by the level of muscle activation a^M . (D) Foot-ground contact was assumed to take place at five discrete contact points distributed around the foot.

6.2.3 Model analyses

OpenSim (Delp et al., 2007) was used to perform all analyses (Fig. 6.2). Subject-specific musculoskeletal models were first generated by scaling the generic model according to individual subject anthropometry. Inverse kinematics was performed to minimise the sum of the squared errors between the positions of surface markers on the subject and virtual markers on the model. Muscle forces were computed using inverse dynamics and static optimisation. At each time instant, joint kinematics and ground reaction forces were input into the skeletal model to calculate the net joint moments about each joint. The net joint moments were then decomposed into individual muscle forces by solving an optimisation problem that minimised the sum of the squares of all muscle activations (Crowninshield and Brand, 1981). The optimisation solution was constrained by the force-length-velocity properties assumed for each muscle (Katz, 1939; Gordon et al., 1966; Zajac, 1989) (Fig. 6.1C). For each subject, the timing of the predicted muscle forces was evaluated against EMG recordings obtained from experiment.

An induced acceleration analysis (Section 3.2.7) and state-space segment power analysis (Section 3.2.8) was performed at each time instant to determine the power transferred by individual muscles to the body segments (see Fig. 6.2). For the induced acceleration analysis, gravity and all joint angular velocities were set to zero and an individual muscle force was applied to the model in isolation in order to calculate the muscle's contribution to the ground reaction force and joint angular acceleration. The induced joint angular accelerations were then input into the segment power analysis with the current joint position and velocity of the model to calculate the contribution of each muscle to the instantaneous power of each segment. The internal segment work performed by a given muscle was found by integrating the muscle's contribution to the internal segment power curve with respect to time. Individual muscle contributions to the external power were found by computing the product of the muscle's contribution to the ground reaction force and the velocity of the center of mass of the body. Positive power designates energy generation and negative

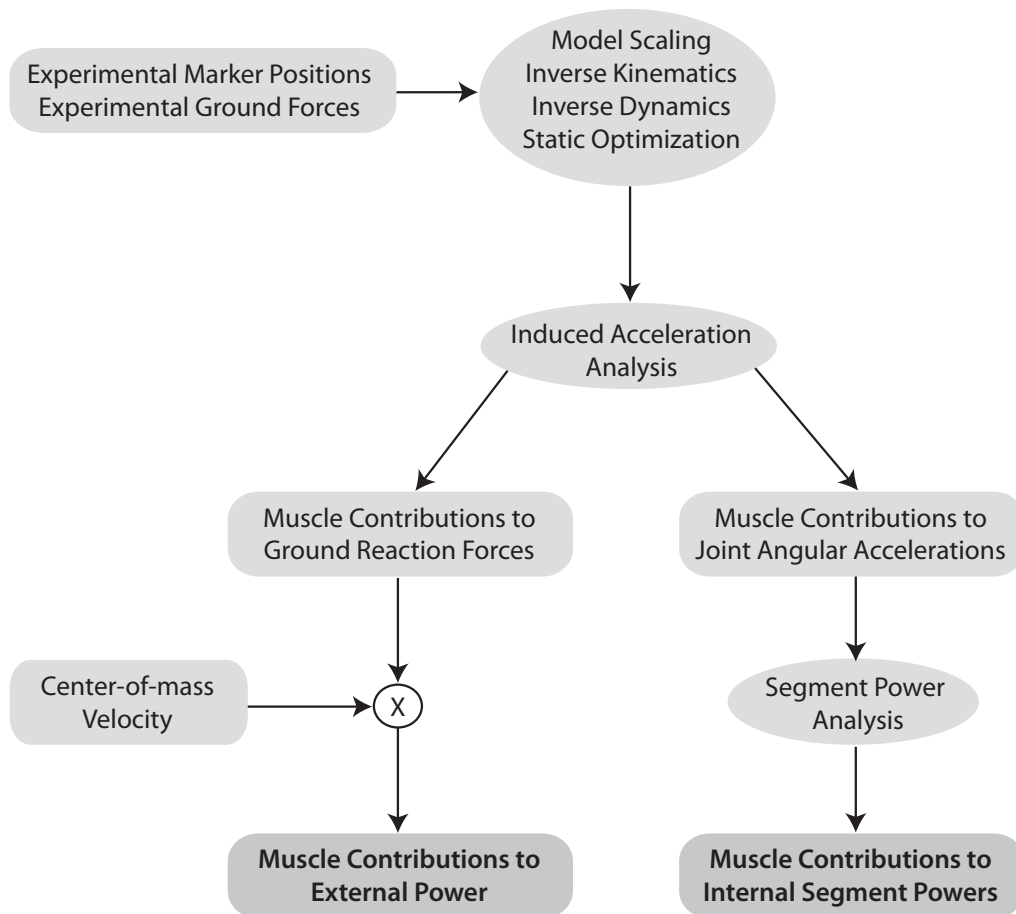


Figure 6.2: Computational pipeline used to calculate individual muscle contributions to: (i) external power; and (ii) internal segment power. Ellipses represent computational analyses and rounded rectangles represent biomechanical variables.

power, energy absorption.

Power contributions were categorised into four segment groups: i) trunk; ii) pelvis; iii) thigh; and iv) shank-foot complex. All trials were analysed over a full stride cycle beginning and ending at ipsilateral foot-strike. Results were time-normalised to a full stride cycle and then averaged across all subjects for each speed. One-way repeated measures analysis of variance (ANOVA) tests were used to identify the muscles that generated (and absorbed) mechanical work to (and from) each segment. When significant F ratios were obtained, *post hoc* pairwise comparisons (paired t-tests) were used to determine differences between each increment in running speed. A conservative significance level of $p < 0.01$ was adopted for all tests.

6.3 Results

Mean running speeds recorded across subjects were 3.5 ± 0.1 m/s (slow running), 5.2 ± 0.1 m/s (medium-paced running), 7.0 ± 0.1 (fast running) and 9.0 ± 0.7 m/s (sprinting) (Table 3.3 in Chapter 3; see also Fig. C.3 in Appendix C). Model predictions of musculotendon force successfully reproduced the net joint torques from inverse dynamics (see Figs C.8 and C.9 from Appendix C) and displayed temporal consistency with experimental EMG data (Fig. 6.3). The summation of model-predicted muscle contributions to the sagittal-plane hip, knee and ankle joint angular accelerations matched the measured net joint accelerations with errors of less than 5% RMS (Fig. 6.4).

Six ipsilateral muscles generated power to the center of mass across all running speeds during stance: SOL, GAS, VAS and RF as major contributors and GMAX and GMED as minor contributors (Fig. 6.5). SOL, VAS and RF decelerated the body horizontally and absorbed external power during the first half of the stance phase, whereas SOL and GAS accelerated the body forwards and generated external power during the second half of stance (Fig. 6.5A). In the vertical direction, the ground reaction force and external power were generated primarily by SOL, GAS

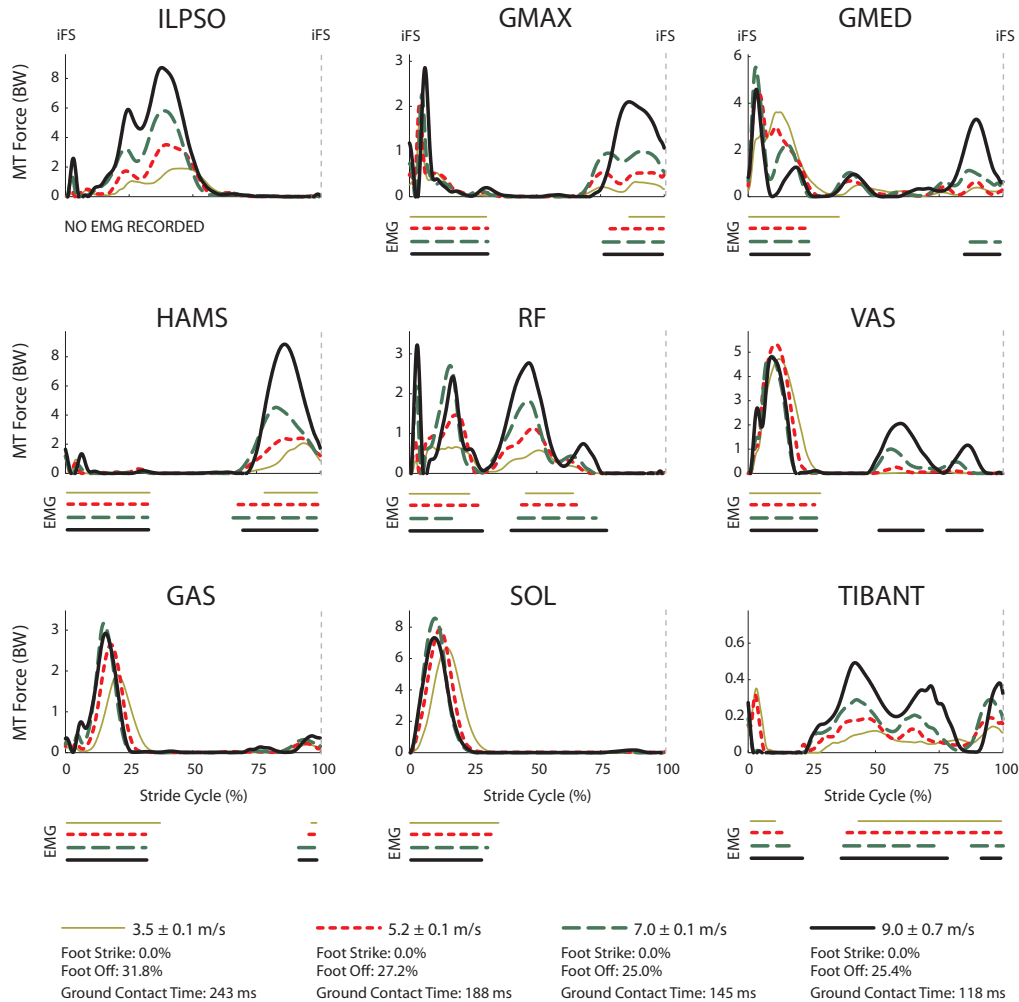


Figure 6.3: Ipsilateral muscle forces calculated for each running speed. Horizontal bars shown below each plot indicate the periods of EMG activity recorded for each muscle. Results were averaged across all trials for all subjects and are shown over a full stride cycle. Muscle symbols appearing in the graphs are: ILPSO (iliacus and psoas combined; no EMG data recorded), GMAX (superior, middle and inferior gluteus maximus), GMED (anterior, middle and posterior compartments of gluteus medius), HAMS (biceps femoris long head, semimembranosus and semitendinosus combined, medial hamstring EMG shown), RF (rectus femoris), VAS (vastus medialis, vastus intermedius and vastus lateralis combined; vastus lateralis EMG shown), GAS (medial and lateral compartments of gastrocnemius combined; medial gastrocnemius EMG shown), SOL (soleus) and TIBANT (tibialis anterior). *iFS* signifies ipsilateral foot-strike.

CHAPTER 6. HOW LEG MUSCLES POWER HUMAN RUNNING

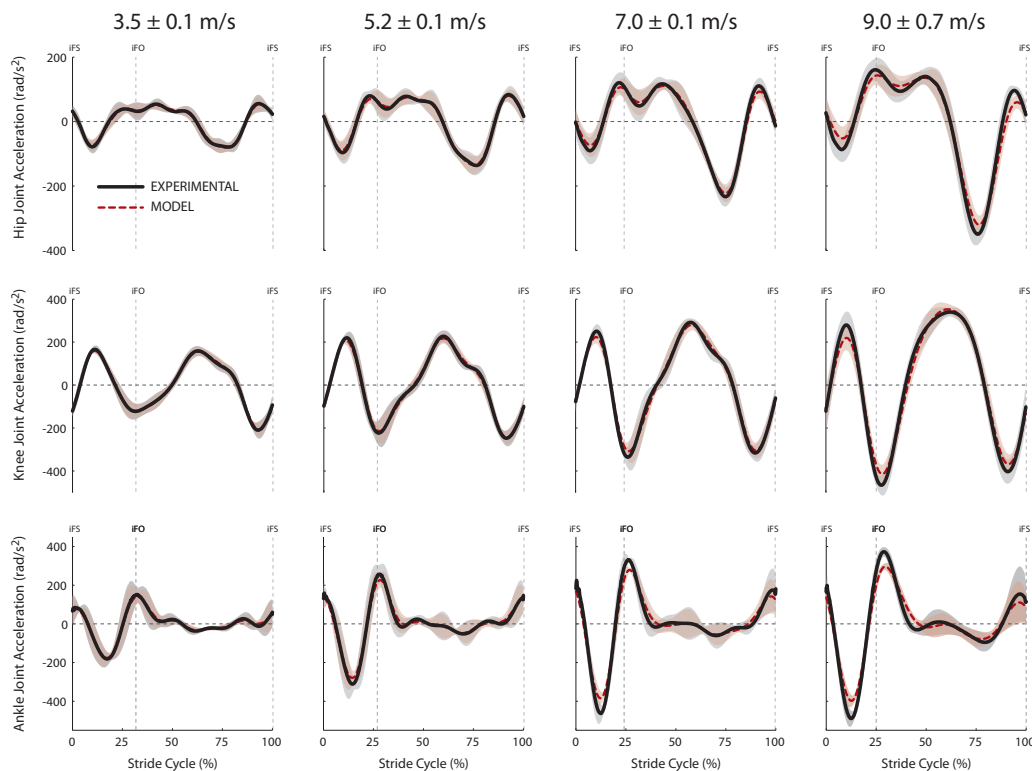


Figure 6.4: *Experimental (solid) and model predicted (dashed) trajectories of the net sagittal-plane hip, knee and ankle joint accelerations at all running speeds. Experimental joint accelerations were calculated by double differentiating the corresponding joint position trajectory (from inverse kinematics) with respect to time. Model predicted joint accelerations were calculated by summing together the individual joint acceleration contributions made by the muscle, gravity and centrifugal forces acting on the model. Mean subject results are presented across the entire stride cycle. Shaded regions represent one standard deviation from the mean. iFS and iFO signify ipsilateral foot-strike and ipsilateral foot-off events, respectively.*

and VAS (Fig. 6.5B). Although the vertical ground force was larger than the fore-aft ground force, the external power generated in the horizontal direction was greater due to the increasingly larger horizontal center of mass velocities associated with faster running speeds.

Five muscles on each of the ipsilateral and contralateral legs generated power to the lower-limb segments during swing: ILPSO, GMAX and HAMS as major contributors, and RF and VAS as minor contributors (Figs 6.6 and 6.7). Unlike the external power, which is comprised entirely by the muscles from the ipsilateral leg, both ipsilateral and contralateral muscles contributed in equal proportions to the internal segment powers of all segments. The ipsilateral ILPSO and contralateral GMAX and HAMS were simultaneously activated to regulate the net power of the trunk, pelvis and thigh segments (Figs 6.6A, 6.6B and 6.7A). More specifically, the ipsilateral ILPSO generated power to the trunk whilst the contralateral GMAX and HAMS absorbed power from this segment (Fig. 6.6A). The opposite was observed for the pelvis and thigh segments: the ipsilateral ILPSO absorbed power from the pelvis and thigh whilst the contralateral GMAX and HAMS generated power to these segments (Figs 6.6B and 6.7A). The shank-foot complex was powered mainly by the ipsilateral ILPSO and HAMS. The ipsilateral ILPSO generated power in the first half of swing, whereas the ipsilateral HAMS absorbed power in the second half of swing.

Running speed was found to have a significant effect on the magnitude of muscle work transferred to the segments (Fig. 6.8). In particular, ILPSO, GMAX and HAMS significantly increased the amount of mechanical work performed on the major segment groups of the skeleton (i.e., ipsilateral leg, contralateral leg, pelvis and trunk) as running speed increased.

6.4 Discussion

The overall goal of the present study was to understand how the lower-limb muscles generate, absorb and transfer power to the skeleton during the stance and swing phases of running, across a wide range of running speeds from 3.5 m/s to 9.0 m/s.

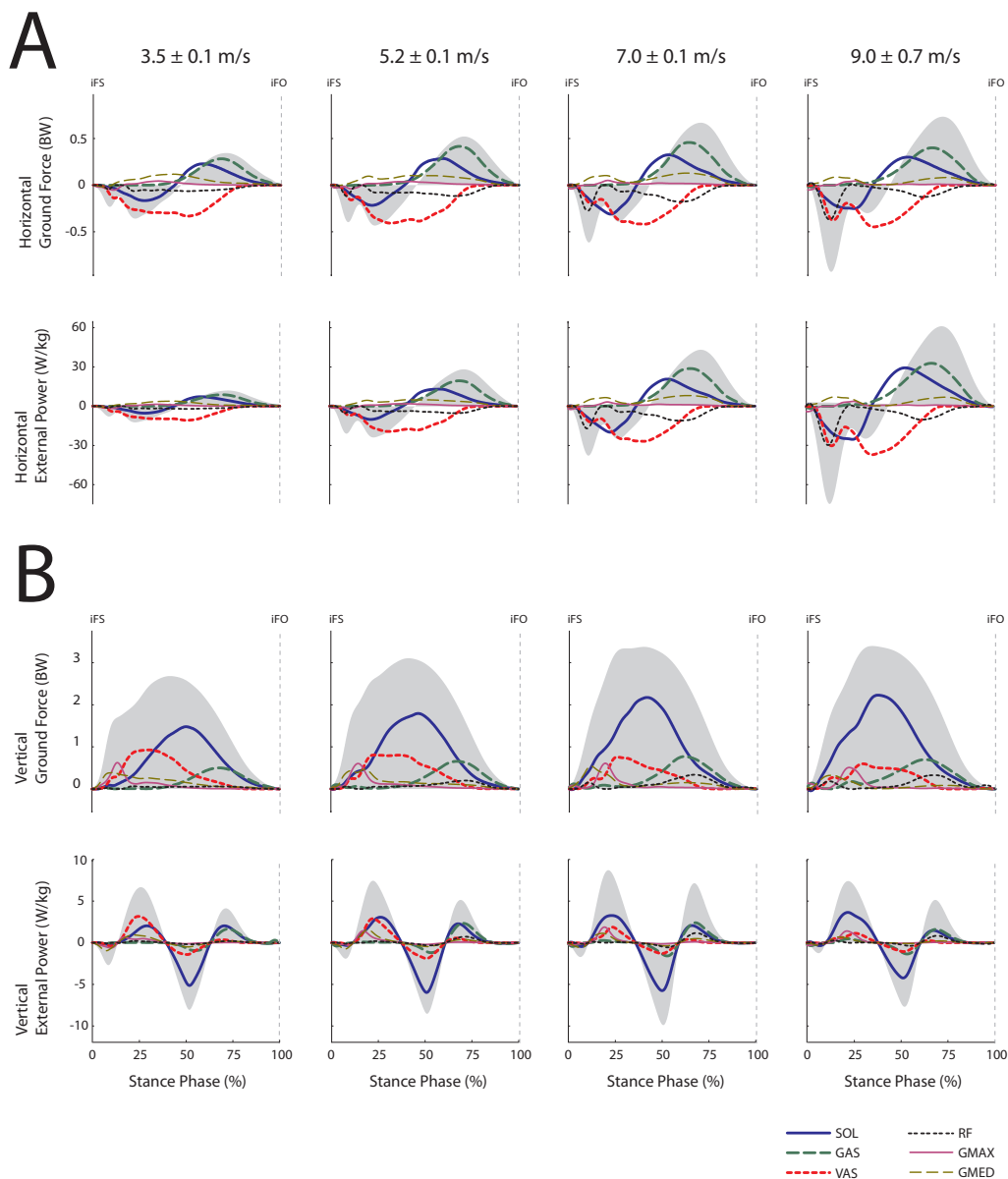


Figure 6.5: Contributions of individual muscles to the net ground reaction force and net external power (shaded regions) in the (A) horizontal direction; and (B) vertical direction. The contribution of a muscle to the net external power was computed as the muscle’s contribution to the ground force multiplied by the center of mass velocity. Similarly, the net external power was computed as the product of the net ground reaction force and the center of mass velocity. Muscle symbols as defined in the caption for Fig. 6.3 and relate to the muscles on the stance-leg, i.e., the leg in contact with the ground.

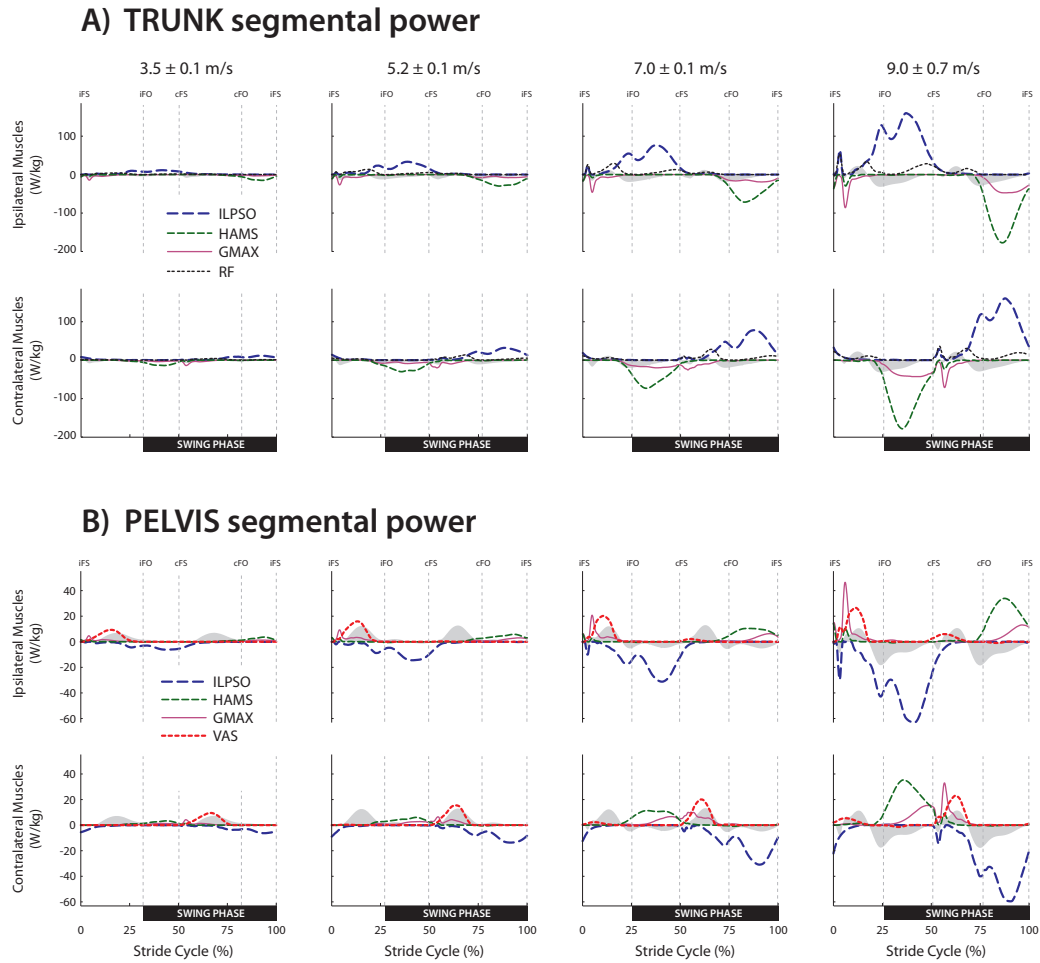


Figure 6.6: Contributions of individual leg muscles to the net segment power (shaded regions) of the TRUNK and PELVIS segments. Results were averaged across all trials for all subjects and are shown over a full stride cycle. Muscle symbols as defined in the caption for Fig. 6.3. *iFS*, *iFO*, *cFS* and *cFO* signify ipsilateral foot-strike, ipsilateral foot-off, contralateral foot-strike and contralateral foot-off, respectively.

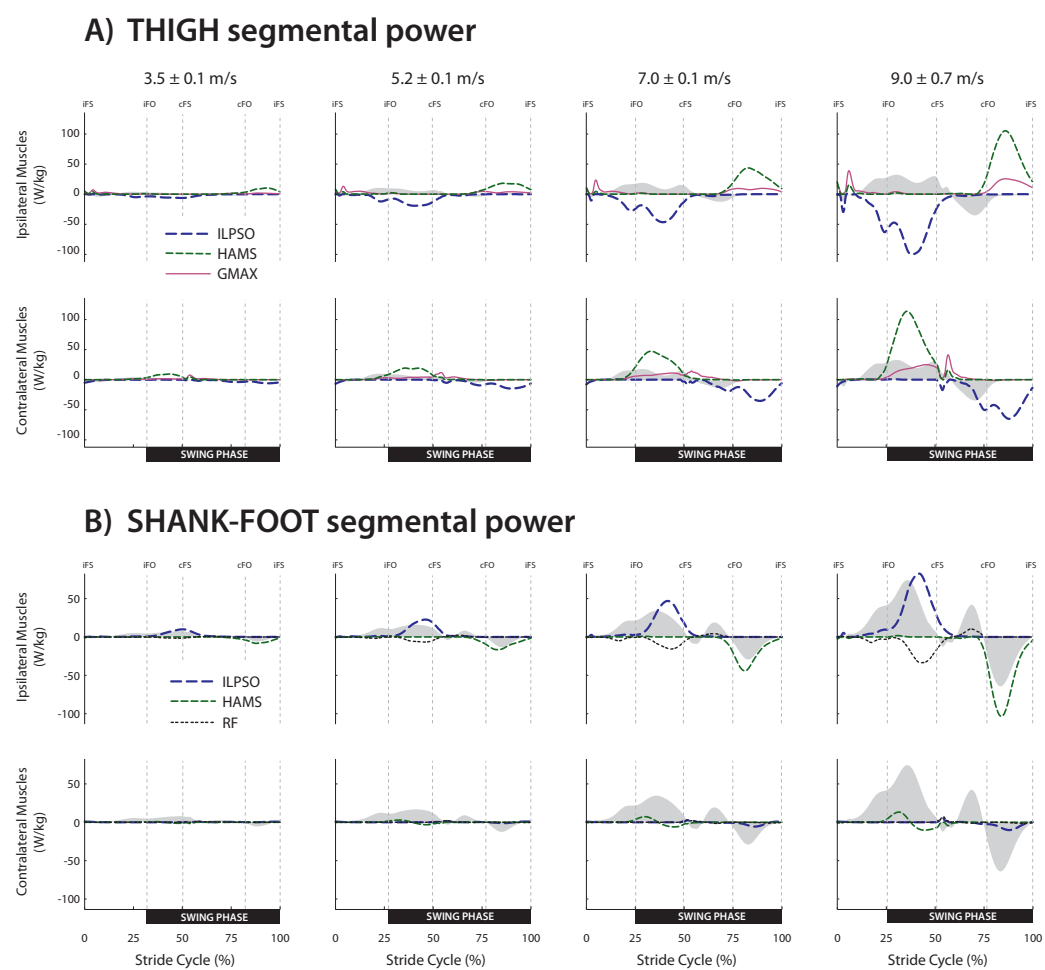


Figure 6.7: Contributions of individual leg muscles to the net segment power (shaded regions) of the THIGH and SHANK-FOOT segments. Results were averaged across all trials for all subjects and are shown over a full stride cycle. Muscle symbols as defined in the caption for Fig. 6.3. *iFS*, *iFO*, *cFS* and *cFO* signify ipsilateral foot-strike, ipsilateral foot-off, contralateral foot-strike and contralateral foot-off, respectively.

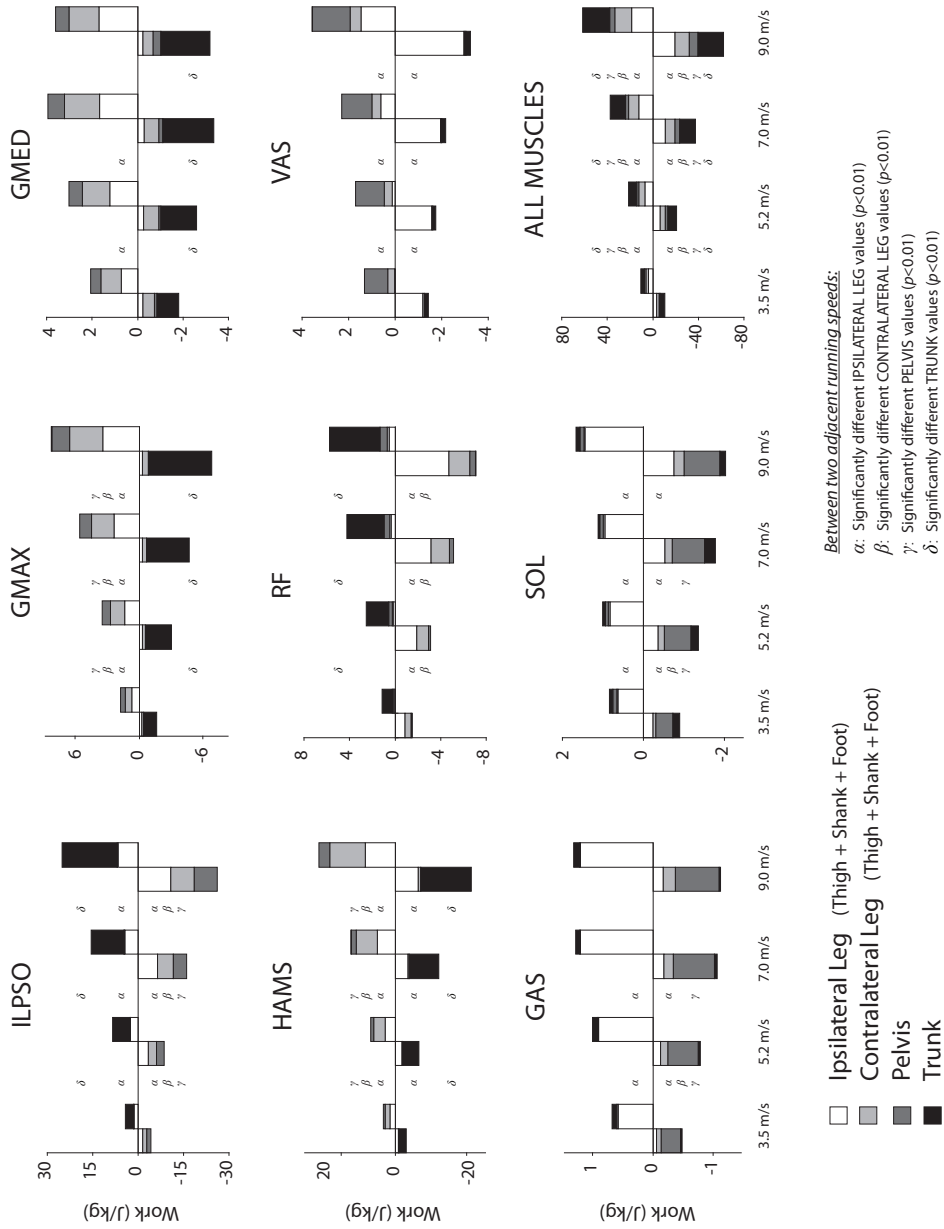


Figure 6.8: Ipsilateral muscle contributions to segmental power over a full stride cycle. Positive work (generation) and negative work (absorption) is shown for each running speed. Results were divided into four segment groups: (i) ipsilateral leg; (ii) contralateral leg; (iii) pelvis; and (iv) trunk. Muscle symbols as defined in the caption for Fig. 6.3.

6.4.1 Muscle contributions to external power during the stance phase

Body external power may only be influenced by the actions of muscles during periods of ground contact because external power is delivered to the center of mass by the ground reaction force. Hence, the muscles that contribute most to the ground reaction force must also be responsible for providing the mechanical power to translate the whole-body center of mass horizontally and vertically (Donelan et al., 2002).

The horizontally-directed external power ultimately determines running speed. Our results show that eccentric contractions by the ipsilateral SOL, VAS and RF in the first half of stance absorb energy from the center of mass and decelerate the body in the fore-aft direction (Fig. 6.5A). In the second half of stance, concentric contractions of the ipsilateral ankle plantarflexors (SOL and GAS) generate almost all the horizontal external power required to propel the body forwards. Thus, increases in running speed are brought about by greater amounts of horizontal external power delivered by SOL and GAS. It is interesting to note, however, that although SOL and GAS developed less force between 7.0 and 9.0 m/s (Fig. 6.3), the overall horizontal external power increased between these two speeds because of the decrease in stance phase duration, which caused SOL to contract at a much higher velocity and generate more power to the skeleton (Figs 6.5 and 6.8). The ankle plantarflexors have been shown to be important muscle groups for propelling the body forward throughout stance in walking (Pandy and Andriacchi, 2010). The findings of the present study suggest that these muscles are also important for powering the body forward in the stance phase of running, up to speeds of 9 m/s.

In the vertical direction, muscle power is required to overcome gravity and accelerate the center of mass upwards to achieve long aerial times and large stride lengths, which are particularly important for running at higher speeds (Ferris et al., 1998; Weyand et al., 2000, 2010). The SOL, GAS and VAS of the ipsilateral leg generate the majority of the vertical ground force, and therefore are largely responsible for accelerating the center of mass upwards. Although large ground forces were recorded in the vertical

direction (up to 3.4 BW for maximal sprinting), the corresponding external power was small due to the relatively small vertical velocity of the center of mass at all running speeds (Fig. 6.5B). Indeed, it has been suggested that a larger vertical center of mass displacement may reduce the economy of running as more muscle energy would then be converted into vertical kinetic energy and potential energy leaving less to contribute directly to horizontal running speed (Williams and Cavanagh, 1987; Heise and Martin, 2001). Minimising vertical external power would therefore appear to be an important requirement for energy-efficient running.

6.4.2 Muscle contributions to internal segment power during the swing phase

Each muscle generates power to or absorbs power from all the body segments at each instant of the stride cycle. This is a direct consequence of dynamic coupling, whereby muscle energy is transmitted through the joints and distributed throughout the skeleton (Zajac and Gordon, 1989). The majority of internal segment power distribution occurred during swing.

The purpose of the swing phase in running is to rapidly power the leg forward before decelerating it in preparation for foot strike (Novacheck, 1998). Although the leg makes up only 15% of total body mass (Winter, 2009), it moves at high speed during running and therefore requires significant energy expenditure. This energy was provided mainly by the hip-spanning muscles, ILPSO, GMAX, HAMS and RF (Fig. 6.7). These muscles have previously been shown to be most active in the swing phase of running, both experimentally (Mann et al., 1986; Gazendam and Hof, 2007; Yu et al., 2008) and in computer-based musculoskeletal models (Glitsch and Baumann, 1997; Hamner et al., 2010; Schache et al., 2011b), so it is intuitive that they contribute significantly to the internal leg-segment power during swing. However, these previous studies only considered the actions of the ipsilateral muscles, overlooking the potential synergies arising from the contralateral muscles. The results of the present study suggest that the simultaneous actions of ILPSO, GMAX, HAMS and RF from both legs are equally important in powering the swing leg into motion. This is

particularly evident in Fig. 6.7A where the ipsilateral ILPSO and contralateral HAMS provide antagonistic power contributions to control the motion of the ipsilateral thigh during swing.

The upper-body segments of the skeleton, i.e., the trunk and pelvis, also need to be powered during the swing phase so that they maintain a smooth sinusoidal motion trajectory (Neptune et al., 2004; Sasaki and Neptune, 2006). For example, the combined mass of the trunk and pelvis segments comprise approximately 70% of total body mass (Winter, 2009), so require considerable energy to generate movement. The trunk and pelvis were powered by the same muscles as the lower limb segments: ILPSO, GMAX, HAMS and RF from both legs (Fig. 6.6). This result, at first glance, may seem to contradict the findings of Sasaki and Neptune (2006), who reported major trunk power contributions by SOL, GAS and VAS; however, these investigators analysed the power contributions only during the stance phase of running, and at an extremely slow speed (1.96 m/s). As running speed increases, the peak forces developed by ILPSO, GMAX, HAMS and RF increased significantly, whereas those developed by SOL, GAS and VAS showed no significant speed effects (see Table 5.1 in Chapter 5). Our results indicate, therefore, that the contributions of SOL, GAS and VAS to trunk segment power are attenuated at the fastest running speeds.

6.4.3 Power transfer between limb segments

All muscle powers developed in the ipsilateral leg were transferred to the contralateral leg to some extent during the running stride cycle. For example, across all running speeds, around 30% of the positive work generated by the ipsilateral GMAX and HAMS was directed to the contralateral leg, and similarly, around 30% of the negative work absorbed by the ipsilateral ILPSO and RF was taken from the contralateral leg (Fig. 6.8). In walking, Neptune et al. (2004) previously showed that the ipsilateral ILPSO, GMAX and HAMS accelerated the legs and trunk forward through power redistribution, which they suggested was a fundamental mechanism for energy management. Our results confirm that the synergistic power transfer by multiple leg muscles is paramount to

maintaining an efficient running economy. It is important to note, however, that even though all lower-limb muscles influenced the motion of all body segments throughout the stride cycle, their net effect on the external power was zero during periods of double-float (where both feet were off the ground). Muscles therefore cannot influence the motion of the whole-body center of mass while the runner is airborne; they can only act to rotate the body segments about the center of mass while both feet are off the ground.

The arm torques from the model contributed to less than 3% of the internal segment power for each segment of the model (not shown). Although, it may seem logical that arm swing dynamics help to generate power to move the upper extremity segments, the light mass of the arms ensured this power contribution to be minimal. Indeed, studies have attributed the benefits of arm swing to counteracting the vertical axis angular momentum generated by the lower limbs, thereby stabilising the rotation of the whole body throughout the stride cycle (Hinrichs, 1987; Hamner et al., 2010). We illustrate that this is indeed the case in Fig. C.32 (middle row) in Appendix C.

6.4.4 Limitations of the study

The limitations of this study all pertain to the calculation of individual muscle forces and are discussed in Section 5.4.4.

6.4.5 Summary

In the stance phase of running, the external power of the body underwent a period of absorption followed by a period of generation, providing the energy to support the body vertically and drive it horizontally forward. SOL, GAS, VAS and RF of the ipsilateral leg contributed most significantly to the external power of the body during stance. During swing, the actions of the ILPSO, GMAX and HAMS from both legs generated the majority of power to the swing leg initially to drive it forwards; these muscles then absorbed the majority of power from the swing leg to prepare it for ground contact. The actions of the ILPSO, GMAX and HAMS from both legs were also responsible for transferring power to the trunk and pelvis to maintain

CHAPTER 6. HOW LEG MUSCLES POWER HUMAN RUNNING

their smooth motion trajectories throughout the stride. As running speeds increased, the individual muscle contributions to the external and internal power increased, in line with experimental evidence that greater metabolic energies are necessary to facilitate faster running speeds. Experimental and model simulation data for one subject are available at <https://simtk.org/home/runningspeeds>.

Chapter 7

Summary and future work

The work presented in this dissertation addresses a variety of theoretical and applied research problems associated with the biomechanics of human running. The dissertation began with the question: “how do leg-muscles synergise to coordinate an efficient running motion?” Despite the fundamental nature of this question, no work to this date has fully quantified the muscle forces and powers transmitted around the skeleton that accelerate and power the body during running, particularly as running speed increases. The computational processes required to calculate such biomechanical variables involve a set of complex systems that together form a mathematical description of the anatomy, physiology and mechanics of the human musculoskeletal system. Of the many disciplines that go into the development of a computer-based musculoskeletal model, the mechanical structure of the skeleton is one of the most important because it exploits the fundamental equations of Newton’s Second Law of Motion to simulate the dynamics of movement.

Computer-based musculoskeletal models that simulate human motion therefore have the ability to predict specific biomechanical variables that cannot be measured in an experiment (i.e., the forces, powers, lengths and velocities developed by individual muscles as well as their contributions to the ground reaction force and lower-limb joint accelerations). In some situations, computer modelling may even be preferred over traditional

“direct experimentation” techniques. For example, the sheer quantity of simultaneous muscle contractions occurring in the body all but eliminates the possibility of performing EMG or invasive buckle transducer type experiments on the leg muscles to estimate muscle loading.

In this dissertation, non-invasive experiments and advanced computer modelling was used to answer fundamental questions about how humans run. Marker derived kinematics, ground reaction forces and EMG data were collected for nine healthy subjects during walking and four speeds of running: 3.5 m/s 5.2 m/s 7.0 m/s and 9.0 m/s. All data were captured in a state-of-the-art biomechanics laboratory containing twenty-two infra-red motion capture cameras to capture experimental marker trajectories, sixteen channels of telemetered EMG to record muscle activity, and eight serially located force plates to measure the external ground reaction forces. This experimental setup made it possible to capture multiple consecutive foot strikes of overground running at all speeds and ensured the highest quality running data possible (Chapter 3). Analysing the data using computer-based musculoskeletal models makes it possible to explore a broad variety of research questions which relate to the synergistic coordination of leg-muscles in running. It also has the potential to provide valuable insight into the mechanics of specific muscle groups, such as the biarticular hamstrings, to investigate the mechanisms of acute musculoskeletal injury, which is prevalent in today’s running population. The reader is referred to two studies (based on the same dataset used in this dissertation) for a detailed discussion of hamstrings mechanics in running (Appendix D):

- **Schache, A.G., Blanch, P.D., Dorn, T.W., Brown, N.A., Rosemond, D., Pandy, M.G. (2011)** Effect of Running Speed on Lower-Limb Joint Kinetics, *Medicine & Science in Sports & Exercise*, 43(7):1260-1271.
- **Schache, A.G., Dorn, T.W., Blanch, P.D., Brown, N.A., Pandy, M.G. (2011)** Mechanics of the human hamstring muscles during sprinting, *Medicine & Science in Sports & Exercise*, In press.

Chapter 4 identified the limitations of simplified foot-ground contact models by examining their effect on predictions of muscle coordination. This was considered an important step towards a description of muscle function in running, particularly because different contact models are capable of providing different interpretations of muscle function. Six different ground contact models were used to predict the individual muscle contributions to the ground reaction force for walking (1.5 m/s) and running (3.5 m/s). Results showed that two factors — the number of foot-ground contact points assumed in the model and the type of kinematic constraint enforced at each point — affect model predictions of muscle coordination.

To assess the muscle coordination strategies in running, it was imperative that an accurate representative ground contact model be developed. This contact model would have to satisfy two criteria to best represent foot-ground contact in reality: (i) describe the time-varying nature of foot-ground contact by assuming a set of time-varying kinematic constraints; and (ii) allow contact to take place around a distributed contact surface of the foot. Of the six contact models tested, only one model fit this criteria and was considered the most realistic. However, this contact model cannot represent a “gold standard” because an individual muscle’s contribution to the ground reaction force cannot be experimentally measured and hence the contact model cannot be rigorously validated. Further work is needed to develop validation techniques for ground contact models so that its predictions can be viewed with the highest of confidence. Nevertheless, for the purposes of this dissertation, the benchmark contact model qualitatively satisfied the criteria for realistic foot-ground contact and was therefore brought into the pipeline of Chapters 5 and 6.

Chapter 5 investigated the mechanical strategies for increasing running speed by calculating the contributions of individual muscles to the vertical ground reaction force (as an analog for stride length) and hip- and knee-joint acceleration (as an analog for stride frequency) at running speeds of 3.5 m/s, 5.2 m/s, 7.0 m/s and 9.0 m/s. For speeds up to 7.0 m/s, the ankle plantarflexors, soleus and gastrocnemius, contributed most significantly to vertical support forces, and hence increases in stride length. At speeds

greater than 7.0 m/s, these muscles shortened at relatively high velocities and had less time to generate the forces needed for support. Thus, above 7.0 m/s the strategy used to increase running speed switched to the goal of increasing stride frequency. The hip muscles, primarily iliopsoas, gluteus maximus and hamstrings, achieved this goal by accelerating the hip and knee joints more vigorously during swing. These findings provide additional insight into how the leg muscles coordinate motion of the lower limbs to improve running performance and have implications for the design of athletic training programs.

Chapter 6 investigated the mechanical strategies for increasing running speed from a power and energy perspective. The contributions of individual muscles to the external center-of-mass power and internal segment power were calculated throughout the stride cycle at running speeds of 3.5 m/s, 5.2 m/s, 7.0 m/s and 9.0 m/s. In the stance phase of running, the actions of SOL, GAS, VAS and RF of the ground-contact-leg underwent a period of power absorption followed by a period of power generation to provide the external power necessary to vertically support and horizontally propel the center-of-mass. In the swing phase, the actions of the ILPSO, GMAX, HAMS and RF from *both* legs generated power to the swing-leg to rapidly drive it forwards, and absorbed power from the swing-leg to prepare it for ground contact. The same hip-muscles, ILPSO, GMAX, HAMS and RF from *both* legs also simultaneously regulated the internal power delivered to the trunk and pelvis to maintain a smooth motion trajectory during the stride. As running speed increased, the contributions of individual muscles to the external and internal power generally increased, in line with experimental evidence showing that greater metabolic energies are necessary to facilitate faster running speeds.

The overall work presented in this dissertation can be expanded in three ways. First, the analyses conducted in Chapters 3, 4 and 5 could be performed with a larger cohort of subjects to increase the statistical confidence in the findings presented. The clinical need to identify population based differences in muscle function (i.e., how does muscle function change with age, weight, height, race, gender, level of training, etc.) can be achieved by collecting running data over a large cross section

of the population. Future work in identifying the differences in muscle coordination between heel-strike and toe-strike runners would also help to explain the predisposition for switching to toe running at faster speeds and have implications in the design of athletic programs geared towards improving running performance. Similarly, simulating the acceleration phase of running using computer-based musculoskeletal models would provide insights into how athletes may most efficiently reach their maximum speed from rest. Such knowledge would prove valuable in adapting current training regimes for improved performance.

Second, specific theoretical or applied problems relating to running biomechanics could be tackled in greater detail. For example, the individual muscle groups prone to musculoskeletal injury would benefit from a rigorous analysis of the computer simulations that predict their force, strain, and power development in running. Apart from the hamstrings muscle, which is by far the most commonly injured muscle in sprinting-based activities (Mendiguchia et al., 2011), other musculoskeletal pathologies such as Achilles Tendonitis (Flynn and Soutas-Little, 1995; McCrory et al., 1999; Azevedo et al., 2009) and Patellofemoral Pain Syndrome (Besier et al., 2009) are active research areas that are just now turning to computer-based musculoskeletal models to offer new insights into how such conditions can be diagnosed and treated.

Finally, it is imperative to evaluate the theoretical findings predicted by computer-based musculoskeletal models in the “real world” (Nigg and Bobbert, 1990; Delecluse et al., 1995; Delecluse, 1997). After all, “real world” scenarios form the motivation for conducting original biomedical research. In order to obtain trust in the results from computer-based musculoskeletal models, these models must first be systematically and thoroughly validated in every regard. Unfortunately, this is currently one of the biggest challenges in computational biomechanics. For example, it is not currently possible to non-invasively measure individual muscle forces *in vivo*. Because these muscle forces ultimately form the basis of all musculoskeletal analyses (e.g., induced acceleration analyses), any inaccuracies will manifest themselves down the analysis pipeline and have the potential to affect the final conclusions made about muscle function in

human locomotion. New and evolving technologies such as ultrasound, Dynamic Magnetic Resonance Imaging (DMRI) and Diffusion Tensor Imaging (DTI) provide dynamic, high resolution experimental apparatus which one day may provide the potential to validate the vast number of parameters contained in computer-based musculoskeletal models as well as their direct outputs.

Who will benefit as a result of using improved, high fidelity musculoskeletal models? For one, the professional athletes around the world who strive to maximise sprinting speed by improving running technique. Incorporating training strategies, as predicted by computer modelling studies will determine the true potential for improving running performance. Similarly, strategies for injury prevention, also suggested by computer modelling studies, could be adopted into regular training practice to investigate whether these approaches have the potential to reduce the frequency of injury. Implementing theoretical findings into the practical domain is pivotal. Because only then will confidence in computer modelling studies grow and be accepted by the wider medical community.

Appendix **A**

Musculoskeletal model

This appendix is concerned with the general equations that describe the generic musculoskeletal model used in this dissertation. This is followed by a detailed description of the joint, muscle and ground contact parameters used within the model.

A.1 Musculoskeletal model equations

The human musculoskeletal system can be represented as a collection of coupled systems, each comprising their own sets of equations and parameters (Fig. A.1).

Rigid body equations of motion: A set of equations, derived from Newton's Second Law of Motion, $F = ma$, which represent the motion of the bones and joints of the skeleton. Specifically, they govern the relationship between the acceleration of each joint, and the generalised forces which need to be applied to generate this acceleration. Inertial parameters of the bones, joint centers and joint axes of rotation are included in the description of the equations of motion. Virtual markers are rigidly attached to the segments of the skeleton, hence their positions in three-dimensional space are also governed by the equations of motion.

Musculoskeletal geometry: A set of muscle insertion and origin points that are rigidly attached to the segments of the skeleton. Their path describes the lines of action and moment arms of each muscle-tendon unit.

Muscle contraction dynamics: A set of equations that describe the force generating capacity of skeletal muscle. Included in the description of muscle contraction dynamics are the physiological force-length and force-velocity relationship of active muscle, as well as the passive mechanical properties of muscle and tendon.

Ground contact model: A set of kinematic constraints that govern the manner in which the foot makes contact with the ground. The ground contact model is a fundamental component of the musculoskeletal model because it allows ground reaction forces to be generated during a simulation. More importantly, it allows the ground reaction force to be decomposed into their individual muscle contributions, thus describing how individual muscles control the acceleration of the center-of-mass.

A.1.1 Rigid body equations of motion

The relationship between the motion of n generalised coordinates q_1, q_2, \dots, q_n and m muscle forces $F_1^M, F_2^M, \dots, F_m^M$ in a musculoskeletal model that interacts with the ground via a set of f foot-contact forces $F_1^E, F_2^E, \dots, F_f^E$ can be expressed in matrix form by its equation of motion (EoM):

$$\ddot{\mathbf{q}} = \mathbf{M}^{-1}(\mathbf{q}) [\mathbf{C}(\mathbf{q}, \dot{\mathbf{q}}) + \mathbf{G}(\mathbf{q}) + \mathbf{S}(\mathbf{q}) \mathbf{F}^M + \mathbf{E}(\mathbf{q}) \mathbf{F}^E] \quad (\text{A.1})$$

where \mathbf{q} , $\dot{\mathbf{q}}$ and $\ddot{\mathbf{q}}$ are vectors of generalised displacements, velocities and accelerations, respectively; \mathbf{M} is the $n \times n$ system mass matrix used to specify the mass and inertial properties of the body segments; \mathbf{C} is a $n \times 1$ generalised force vector due to velocity related centrifugal and Coriolis forces; \mathbf{G} is a $n \times 1$

A.1. MUSCULOSKELETAL MODEL EQUATIONS

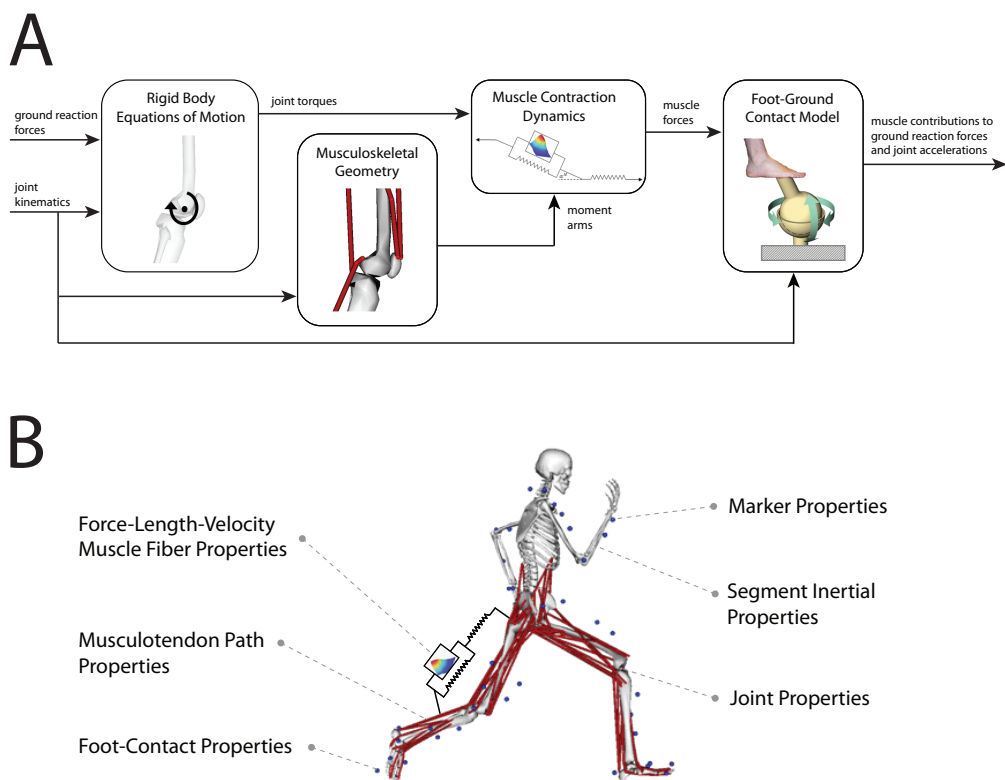


Figure A.1: *Musculoskeletal model properties. (A) Structure of an inverse solution of muscle function in locomotion. (B) Architecture and physiological force producing properties of a single musculotendon actuator.*

generalised force vector due to a uniform gravity field; \mathbf{S} is a $n \times k$ matrix of muscular moment arms that maps a $k \times 1$ vector of musculotendon forces \mathbf{F}^M into a $n \times 1$ vector of generalised forces; \mathbf{E} is a $n \times 3f$ partial velocity matrix that maps a $n \times 3f$ vector of external foot-contact forces \mathbf{F}^E into a $n \times 1$ vector of generalised forces (Pandy, 2001; Lin et al., 2011a).

An important property of the EoM is that the inverted mass matrix \mathbf{M}^{-1} is non-diagonal. Therefore, the biomechanical system is dynamically coupled and all forces that act on the system, e.g., muscle forces, gravitational forces and centrifugal forces — simultaneously contribute to the acceleration of every joint in the body. Another way to understand the phenomena of dynamic coupling is to recognise that any load applied to the musculoskeletal

model is transmitted between adjacent segments through a joint contact (inter-segmental) force.

Another important property of the EoM is its indeterministic nature when solving for muscle forces. Indeterminism arises because the number of muscles m exceeds the number of generalised coordinates n , i.e., ($m > n$) — each joint is spanned by many muscles. Therefore, optimisation is necessary to uniquely solve for individual muscle forces (Pandy and Anderson, 2000; Anderson and Pandy, 2001b; Thelen et al., 2003; Thelen and Anderson, 2006; Seth and Pandy, 2007). Although a variety of optimisation techniques and objective criteria exist to decompose the joint moment into individual muscular contributions, a static optimisation approach that minimises the sum of the squared activations across all muscles is used in this dissertation. The reader is referred to the paper entitled *Comparison of different methods for estimating muscle forces in human movement* in Appendix D for a detailed discussion on the variety of different approaches for predicting muscle forces in computer-based musculoskeletal models.

A.1.2 Musculoskeletal geometry

Each muscle-tendon unit in the model is rigidly attached to at least two body segments. Straight line muscle-tendon paths occur when the muscle inserts on one segment and originates on another segment (e.g., gluteus medius, gluteus minimus and soleus). More complex curved muscle paths occur when intermediate *via points* exist between the insertion and origin of a muscle-tendon unit, to approximate the wrapping of muscle around bone (Garner and Pandy, 2000; Anderson and Pandy, 2001a). For example, at large hip flexion angles, the path of the gluteus maximus wraps around the posterior portion of the pelvis). The path of a muscle determines not only its line of action to the connecting bone, but also its moment arm about the joints that it spans. The moment arm s of a muscle i with respect a to joint j is defined using the tendon excursion method (An et al., 1984):

$$s_j^i = \frac{\partial l_i^{MT}(\mathbf{q})}{\partial q_j} \quad (\text{A.2})$$

where $\partial l_i^{MT}(\mathbf{q})$ is the total musculotendon length from origin to insertion as a function of the set of generalised coordinates of the skeleton \mathbf{q} . The product of moment arm and musculotendon force is equal to the muscle moment of i about joint j .

A.1.3 Muscle contraction dynamics

Muscles are the source of force and power in the body, which are transmitted through their connective tendons to the bones of the skeleton. A muscle connected in series with tendon is modelled as a Hill-type muscle-tendon actuator (Hill, 1938; Zajac, 1989)(Fig. A.2A).

Muscles are modelled as active and passive elements acting in parallel. The active (contractile) element of muscle produces force only when it is activated by neural excitation. Experimental studies using electrical stimuli to activate individual muscle fibres have determined the force-length profile of the underlying sarcomeres to be bell shaped (Page and Huxley, 1963; Gordon et al., 1966; Brown et al., 1984; Edman and Reggiani, 1987; Huxley, 1995, 2008). This suggests an optimal fibre-length, l_o^M , where the muscle is most capable of developing maximum force. As the length of the fibre deviates away from its optimal length, its force generating capacity diminishes. In the mathematical model of muscle, the normalised force-length curve is modelled as a Gaussian function (Thelen, 2003). In addition to force-length characteristics, active muscle also exhibits force-velocity characteristics. Under isometric conditions (zero shortening velocity), a muscle is able to develop maximum force — this capacity diminishes as the shortening velocity increases until a critical maximum shortening velocity, v_{\max}^M , where the muscle fibre is no longer able to sustain tension, even if fully activated. Therefore, the maximum isometric force of muscle, F_o^M , can only be developed when the muscle is: (i) fully activated; (ii) contracting isometrically; and (iii) contracting at its optimal fibre length. It is possible for greater forces than F_o^M to be developed in muscle during eccentric contractions (Katz, 1939; Joyce and Rack, 1969), however eccentric contractions are associated with excessive muscle strains and possible rupture. The level of muscle activation, a , in the model ranges

from 0 (no motor unit recruitment) to 1 (all motor units recruited), and muscle forces are linearly scaled to the activation value. Merging the force-length and force-velocity relationship produces a force-length-velocity surface (Fig. A.2E), which the corresponding muscle force trajectory is constrained to during a simulation.

Passive muscle force is generated as the fibres stretch beyond their slack length (assumed to be equal to the fibre’s optimal length, l_0^M). Passive muscle force is modelled as an exponential spring and is defined to have a nominal strain, ε_0^M , at a tensile force equal to the maximum isometric force, F_o^M .

The pennation angle, α^M , is defined as the orientation of the muscle fibres to the tendon’s line of action. In the mathematical model of muscle, pennation angle is assumed to change with fibre length based on the assumption of constant muscle width w (Anderson and Pandy, 1999).

Tendon is modelled as a hybrid exponential-linear spring (Fig. A.2B), which replicates its typical experimental loading curve (Kuo et al., 2001). Tendon consists of tough bands of fibrous connective tissue, made up of many fibrils that vary in length and thickness. When tensile loading is applied to tendon at the slack length, l_s^T , the initially crimped fibrils straighten, all at different rates, resulting in a region of progressively increasing stiffness, termed the “toe region”. Only when all of the fibrils are taut does the tendon stretch linearly. The tendon is defined to have a nominal strain, ε_0^T , which occurs at a tensile force equal to the maximum isometric force of its connected muscle, F_o^M .

A.1.4 Foot-ground contact model

Contact between the foot and the ground was assumed to take place at five discrete points distributed over the sole of the foot. This contact model, termed the MULTIPOINT contact model is described in further details in Section 3.2.7. Briefly, each contact point is associated with a set of rules that define the linear kinematic constraints in each of the three principal directions. The measured center-of-pressure location at each instant in time determines which phase of stance the foot is in (i.e., initial foot-strike,

A.1. MUSCULOSKELETAL MODEL EQUATIONS

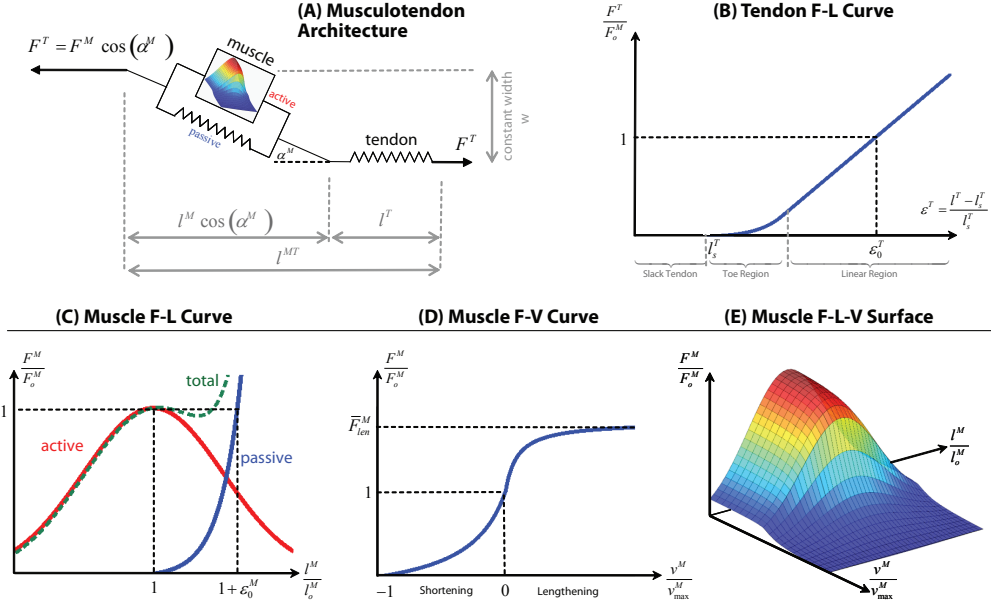
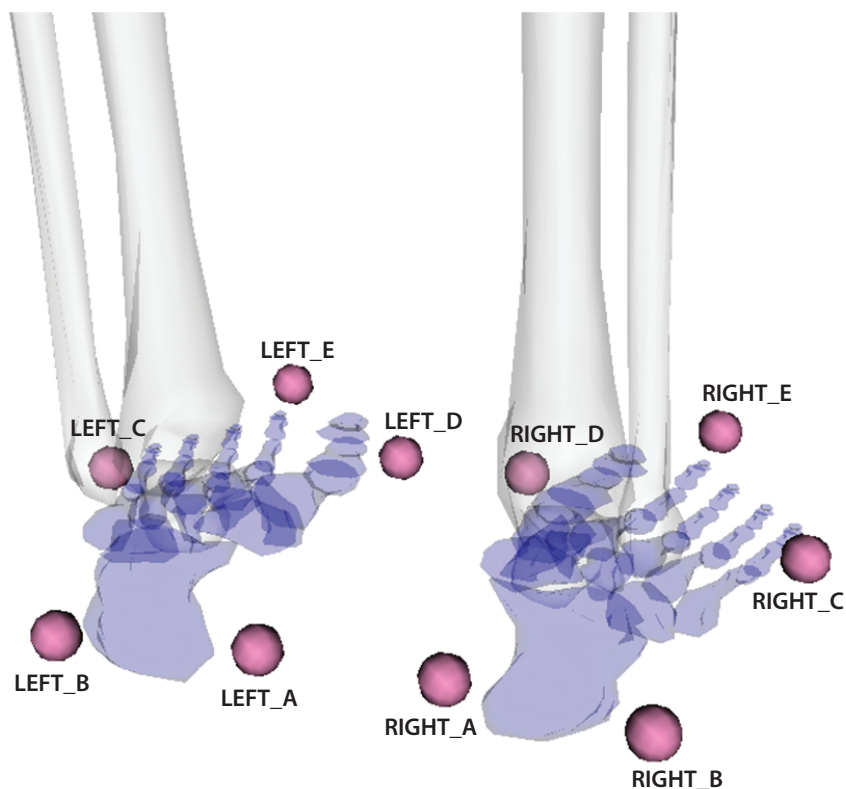


Figure A.2: *Musculotendon properties. Architecture and physiological force producing properties of a single musculotendon actuator. All plots are for a fully activated muscle ($a = 1$). Properties are linearly scaled with activation $0 < a < 1$.*

midfoot stance, or toe-off), thus allowing the kinematic constraints to smoothly transition throughout ground contact. The five contact points were defined by model-based kinematic markers attached to the foot coordinate frame. Although it is possible to scale the contact points to the size of each subject's foot, the same contact points were used across all subjects in this dissertation (Fig. A.3). Subject-specific foot points would require additional markers to be placed on the foot during the static trial (see Section 3.1.3). The contribution of each muscle force to the total ground reaction force was determined by calculating the muscle's contribution to each ground contact point and then summing the contributions across all contact points (Fig. A.4).



Marker Name	Marker Body	Marker Location (m) (X,Y,Z) in Body coordinates
RIGHT_A	calcn_r	(0.01, 0.00, -0.05)
RIGHT_B	calcn_r	(0.00, 0.00, 0.03)
RIGHT_C	calcn_r	(0.135, 0.00, 0.07)
RIGHT_D	calcn_r	(0.205, 0.00, -0.05)
RIGHT_E	calcn_r	(0.275, 0.00, 0.02)
LEFT_A	calcn_l	(0.01, 0.00, 0.05)
LEFT_B	calcn_l	(0.00, 0.00, -0.03)
LEFT_C	calcn_l	(0.135, 0.00, -0.07)
LEFT_D	calcn_l	(0.205, 0.00, 0.05)
LEFT_E	calcn_l	(0.275, 0.00, -0.02)

Figure A.3: Five points distributed over the sole of each foot provided locations for foot-ground contact to occur.

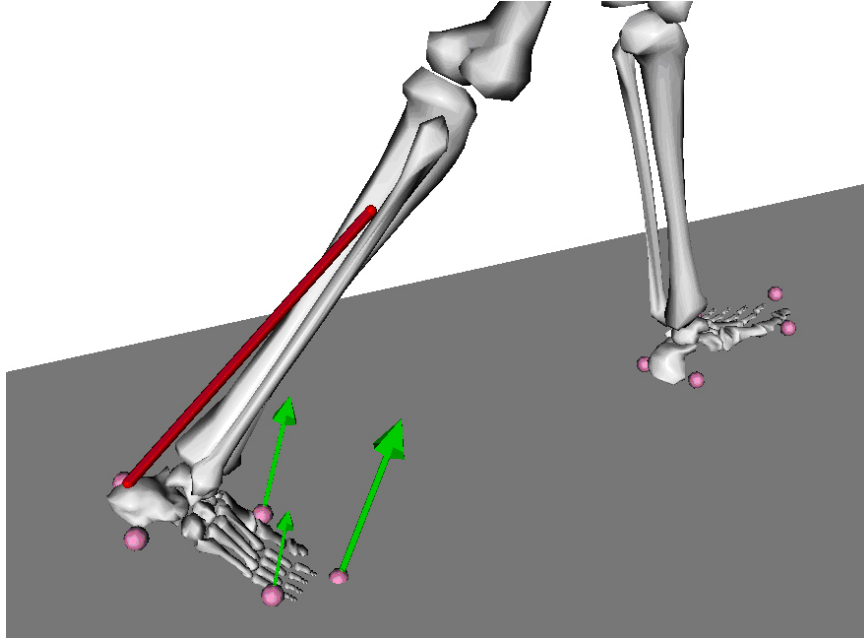


Figure A.4: *The induced ground reaction force at each contact point on the right leg from the soleus during the second half of stance in walking.*

A.2 Musculoskeletal models in this thesis

Two computational models of the lower limbs were used in the studies of in this thesis (Table A.1):

1. Anderson et al. Musculoskeletal Model (Chapter 4)
2. OpenSim Musculoskeletal Model (Chapter 5 and 6)

The modular, compact and open source nature of OpenSim model files (**.osim*) allow models to be easily shared and distributed between researchers. As future studies in running biomechanics may choose to adopt the OpenSim model used in this thesis, the OpenSim model parameters are described here in greater detail (Fig. A.5 and Tables A.2 and A.3).

Table A.1: Description of the two musculoskeletal models used in this thesis. DOF represents degrees of freedom.

ANDERSON*		OPENSIM
Chapter	3	4 and 5
Segments	10 pelvis, torso, femur, tibia, hindfoot, toes	20 pelvis, torso, femur, tibia, talus, toes, calcaneus, humerus, ulna, radius, hand
Total DOF	23 Pelvis/ground: free joint (6DOF) Hip: ball-and-socket joint (3DOF) Knee: pure hinge joint (1DOF) Ankle: universal joint (2DOF) Toes: pure hinge joint (1DOF) Back: ball-and-socket joint (3DOF)	37 (Fig. A.5A, Table A.1) Pelvis/ground: free joint (6DOF) Hip: ball-and-socket joint (3DOF) Knee: translating hinge joint** (1DOF) Ankle: two nonintersecting pure hinges (2DOF) Toes: pure hinge joint (1DOF) Back: ball-and-socket joint (3DOF) Shoulder: ball-and-socket joint (3DOF) Elbow: two nonintersecting pure hinges (2DOF) Wrist: two nonintersecting pure hinges (2DOF)
Locked DOF	2 Toes: pure hinge (1DOF)	6 Toes: pure hinge (1DOF) Wrist: two nonintersecting pure hinges (2DOF)
Actuators	54 muscle-tendon actuators 6 residual pure force/torque actuators	92 muscle-tendon actuators (Fig. A.2B, Table A.3) 6 residual pure force/torque actuators 10 upper-limb torque actuators
Contact***	BALL, UNIVERSAL, HINGE, WELD, SINGLEPOINT and MULTIPOINT	MULTIPOINT

* Anderson, F.C. (1999). A dynamic optimisation solution for a complete cycle of normal gait. The University of Texas at Austin. Ph.D. Thesis.

** Yamaguchi, G.T. and F.E. Zajac, A planar model of the knee joint to characterise the knee extensor mechanism. J Biomech, 1989. 22(1): p. 1-10.

*** Details of the foot-ground contact models are contained in the Methods section of Chapter 4.

Table A.2: Description of the unlocked joint conventions in the *OpenSim* model

Degree-of-freedom	Parent/child Body	Positive convention	Negative convention
PELVIS (Translation X)	GROUND / PELVIS	Anterior	Posterior
PELVIS (Translation Y)		Vertically Up	Vertically Down
PELVIS (Translation Z)		Horizontally Right	Horizontally Left
PELVIS (List)		Right	Left
PELVIS (Rotation)		Left	Right
PELVIS (Tilt)		Posterior	Anterior
HIP (Sagittal)	PELVIS / FEMUR	Flexion Extension	Abduction
HIP (Coronal)		Adduction	External Rotation
HIP (Transverse)		Internal Rotation	External Rotation
KNEE (Sagittal)	FEMUR / TIBIA	Extension	Flexion
ANKLE (Sagittal)		Dorsiflexion	Plantarflexion
ANKLE (Coronal)		Subtalar Inversion	Subtalar Eversion
LUMBAR (Sagittal)	PELVIS / TORSO	Extension	Flexion
LUMBAR (Coronal)		Right Lateral Bending	Left Lateral Bending
LUMBAR (Transverse)		Left Rotation	Right Rotation
SHOULDER (Sagittal)	TORSO / HUMERUS	Flexion	Extension
SHOULDER (Coronal)		Adduction Abduction	External Rotation
SHOULDER (Transverse)		Internal Rotation	External Rotation
ELBOW (Sagittal)	HUMERUS / ULNA	Flexion	Extension
ELBOW (Coronal)		ULNA / RADIUS	Pronation

APPENDIX A. MUSCULOSKELETAL MODEL

Table A.3: *Individual muscles contained in the musculoskeletal model.*

Symbol	Name	Joint	Function	F_0^M
GLUT_MED1	Gluteus Medius (anterior)	Hip	Hip abductor Hip flexor Hip internal rotator	2457
GLUT_MED2	Gluteus Medius (middle)	Hip	Hip abductor	1719
GLUT_MED3	Gluteus Medius (posterior)	Hip	Hip abductor Hip extensor Hip external rotator	1959
GLUT_MIN1	Gluteus Minimus (anterior)	Hip	Hip abductor Hip flexor Hip internal rotator	810
GLUT_MIN2	Gluteus Minimus (middle)	Hip	Hip abductor	855
GLUT_MIN3	Gluteus Minimus (posterior)	Hip	Hip abductor Hip external rotator Hip extensor	969
SEMIMEM	Semimembranosus	Hip, Knee	Hip extensor Hip adductor Knee flexor	3864
SEMITEN	Semitendinosus	Hip, Knee	Hip extensor Hip adductor Knee flexor	1230
BIFEMLH	Biceps Femoris (long head)	Hip, Knee	Hip extensor Hip adductor Knee flexor	2688
BIFEMSH	Biceps Femoris (short head)	Knee	Knee flexor	2412
SAR	Sartorius	Hip, Knee	Hip flexor Hip abductor Knee flexor	468
ADD_LONG	Adductor Longus	Hip	Hip flexor Hip extensor Hip adductor	1881
ADD_BREV	Adductor Brevis	Hip	Hip flexor Hip adductor	1287
ADD_MAG1	Adductor Magnus (superior)	Hip	Hip extensor Hip adductor	1143
ADD_MAG2	Adductor Magnus (middle)	Hip	Hip extensor Hip adductor	1029
ADD_MAG3	Adductor Magnus (inferior)	Hip	Hip extensor Hip adductor	1464

A.2. MUSCULOSKELETAL MODELS IN THIS THESIS

Symbol	Name	Joint	Function	F_0^M
TFL	Tensor Faciae Latae	Hip, Knee	Hip abductor Hip flexor Hip internal rotator	699
PECT	Pectineus	Hip	Hip flexor Hip adductor	798
GRAC	Gracilis	Hip, Knee	Hip flexor Hip adductor Knee flexor	486
GLUT_MAX1	Gluteus Maximus (superior)	Hip	Hip abductor Hip extensor	1719
GLUT_MAX2	Gluteus Maximus (middle)	Hip	Hip extensor	2457
GLUT_MAX3	Gluteus Maximus (inferior)	Hip	Hip extensor	1656
ILIACUS	Illacus	Hip	Hip flexor Hip internal rotator	3219
PSOAS	Psoas	Hip	Hip flexor Hip internal rotator	3339
QUAD_FEM	Quadratus Femoris	Hip	Hip external rotator	1143
GEM	Gemelli	Hip	Hip external rotator	492
PERI	Periformis	Hip	Hip abductor Hip external rotator	1332
RECT_FEM	Rectus Femoris	Hip, Knee	Hip flexor Knee extensor	3507
VAS_MED	Vastus Medialis	Knee	Knee extensor	3882
VAS_INT	Vastus Intermedius	Knee	Knee extensor	4095
VAS_LAT	Vastus Lateralis	Knee	Knee extensor	5613
MED_GAS	Gastrocnemius (medial)	Knee, Ankle	Knee flexor Ankle plantaflexor	4674
LAT_GAS	Gastrocnemius (lateral)	Knee, Ankle	Knee flexor Ankle plantaflexor	2049
SOLEUS	Soleus	Ankle	Ankle plantaflexor	10647
TIB_POST	Tibialis Posterior	Ankle	Ankle plantaflexor Ankle inverter	4764
FLEX_DIG	Flexor Digitorus Longus	Ankle	Ankle plantaflexor Ankle inverter	930
FLEX_HAL	Flexor Hallucis Longus	Ankle	Ankle plantaflexor Ankle inverter	966
TIB_ANT	Tibialis Anterior	Ankle	Ankle dorsiflexor Ankle inverter	2715

APPENDIX A. MUSCULOSKELETAL MODEL

Symbol	Name	Joint	Function	F_0^M
PER.BREV	Peroneus Brevis	Ankle	Ankle plantaflexor Ankle everter	1305
PER.LONG	Peroneus Longus	Ankle	Ankle plantaflexor Ankle everter	2829
PER.TERT	Peroneus Tertius	Ankle	Ankle dorsiflexor Ankle everter	540
EXT.DIG	Extensor Digitorum Longus	Ankle	Ankle dorsiflexor Ankle everter	1536
EXT.HAL	Extensor Hallucis Longus	Ankle	Ankle dorsiflexor Ankle inverter	486
ERCSPN	Erector Spinae	Back	Back extensor Back internal rotator (right) Back external rotator (left) Right lateral bending (right) Left lateral bending (left)	7500
INTOBL	Internal Obliques	Back	Back flexor Back internal rotator (right) Back external rotator (left) Right lateral bending (right) Left lateral bending (left)	2700
EXTOBL	External Obliques	Back	Back flexor Back internal rotator (left) Back external rotator (right) Right lateral bending (right) Left lateral bending (left)	2700

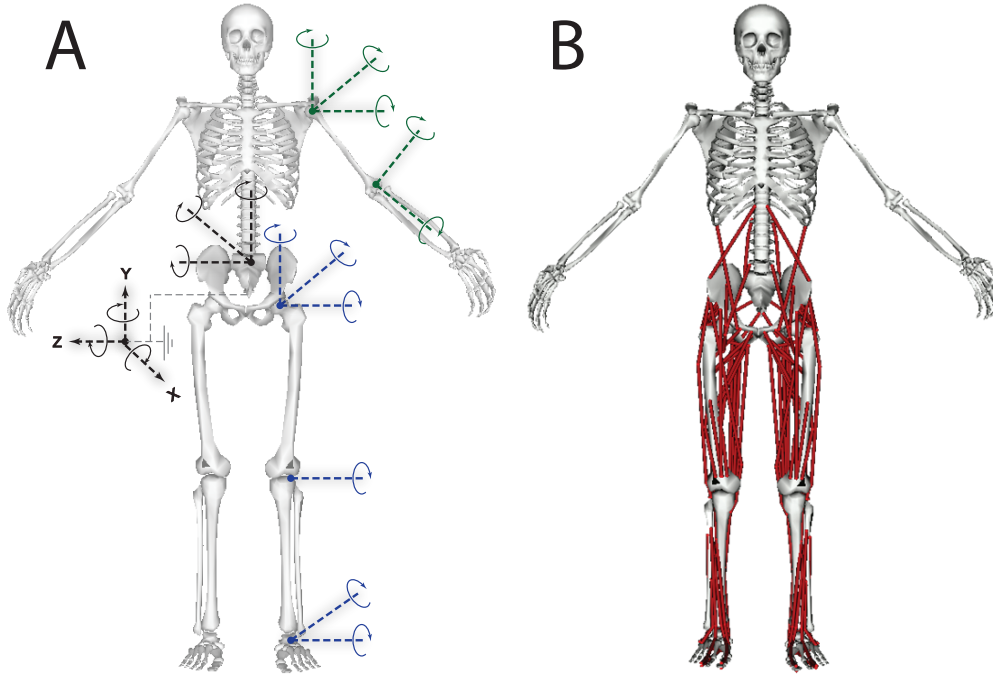


Figure A.5: Joint and muscle geometry. (A) Multibody model of the skeletal system. All unlocked degrees of freedom are shown. Coordinate vectors point in the direction of positive rotation using a right handed coordinate system. (B) 92 musculotendon paths are represented in the musculoskeletal model.

A.3 Reserve actuators and specific tension of muscle

The use of lower-limb reserve actuators in the musculoskeletal model was briefly discussed in Section 3.2.4. Specifically, ideal torque generators were placed at each joint, serving to generate any deficit torque that muscles were unable to achieve during a simulation.

One scenario where reserve actuators would be generating torque would be when muscles alone are incapable of generating the torques required from inverse dynamics. Sprinting requires great amounts of joint torque compared to that of walking, and assuming that muscles are the

APPENDIX A. MUSCULOSKELETAL MODEL

only physiological torque generators present in the musculoskeletal model, an increased maximum isometric force was required to generate a successful simulation. Although a greater torque capacity could also be achieved by increasing the moment arms, modifying the model in this way should generally be avoided because there is a much larger confidence in the accuracy of the muscle moment arms in the model than there is for the maximum isometric forces in the model. This is because leg-muscle moment arms have been directly measured in precise cadaver experiments (Buford et al., 1997; Arnold et al., 2000; Klein Horsman et al., 2007) whereas maximum isometric forces cannot be measured experimentally — rather, they are calculated based the muscle’s physiological cross sectional area (PCSA):

$$F_0^M = PCSA \times \sigma_0^M \quad (\text{A.3})$$

In this equation, σ_0^M is represents the specific tension of muscle, an intrinsic property of muscle that defines the force per unit area (i.e., stress) that the muscle can support. Whereas the PCSA of muscle can be reliably determined from cadaver experiments (Klein Horsman et al., 2007; Ward et al., 2009), the specific tension is difficult to measure and may vary across different muscle groups. Consequently, there is a wide range of reported values for specific tension in the literature, making it difficult to adopt a single value for use in a musculoskeletal model (Kawakami et al., 1995; Fukunaga et al., 1996; Maganaris et al., 2001; Morse et al., 2005, 2008; O’Brien et al., 2010). Therefore, the decision to uniformly increase the maximum isometric force of all muscles in the model is rationalised by the large variability of measured values of muscle specific tension. Increasing the maximum isometric force provides an increased torque generating capability to the model so that the use of reserve actuators are minimised during a simulation. For this dissertation, the maximum isometric forces were uniformly increased three-fold from the original “walking” OpenSim model (Delp et al., 2007).

Reserve actuators should theoretically contribute zero torque to the musculoskeletal model because they do not exist in reality — their

A.3. RESERVE ACTUATORS AND SPECIFIC TENSION OF MUSCLE

existence in musculoskeletal models are merely to allow muscle force optimisations to successfully converge to arbitrarily tight numerical tolerances (i.e., static optimisation, see Section 3.2.4).

Another scenario where reserve actuators may be activated is when muscles spanning joints of greater than one degree-of-freedom (DOF) cannot simultaneously satisfy the desired torques along each axis of rotation. For example, the hamstrings and rectus femoris muscles span both the hip (ball-and-socket joint: 3 DOF) and the knee (hinge joint: 1 DOF). For these muscles to satisfy the joint torques in each of the 4 DOF would require a perfect consistency between the moment arms of the model and the joint kinematics of the trial. Such a numerical consistency is rarely possible, particularly during fast running, hence reserve torques may be required make up the necessary deficit. For the muscles that span joints of more than one DOF, reserve torques were penalised heaviest in the sagittal plane, followed by the coronal plane, and then the transverse plane.

In sprinting, the most dynamic of all human running movements, there was close agreement between the joint moments derived from inverse dynamics and those derived from the model-computed muscle forces except for the hip joint moment in the transverse plane Fig. A.6. The average RMS error between the two joint moments was 0.45 Nm/kg for the transverse plane hip moment (internal/external-rotation) and less than 0.05 Nm/kg for all other joint moments. The discrepancy evident in the transverse plane hip joint moments is most likely attributable to errors in the experimental data. It is well documented that the thigh segment is prone to large amounts of soft tissue artefact (Cappozzo et al., 1996; Akbarshahi et al., 2010), which will most likely be the case when investigating fast dynamic activities that involve large muscle contractions. The non-invasive estimation of transverse plane hip joint kinematics has been shown to be particularly sensitive to this type of experimental error (Schache et al., 2008). Muscles alone, therefore, were incapable of fully satisfying transverse plane hip joint moments derived from potentially noisy kinematics and so transverse plane hip reserve torques were called to made up the difference.

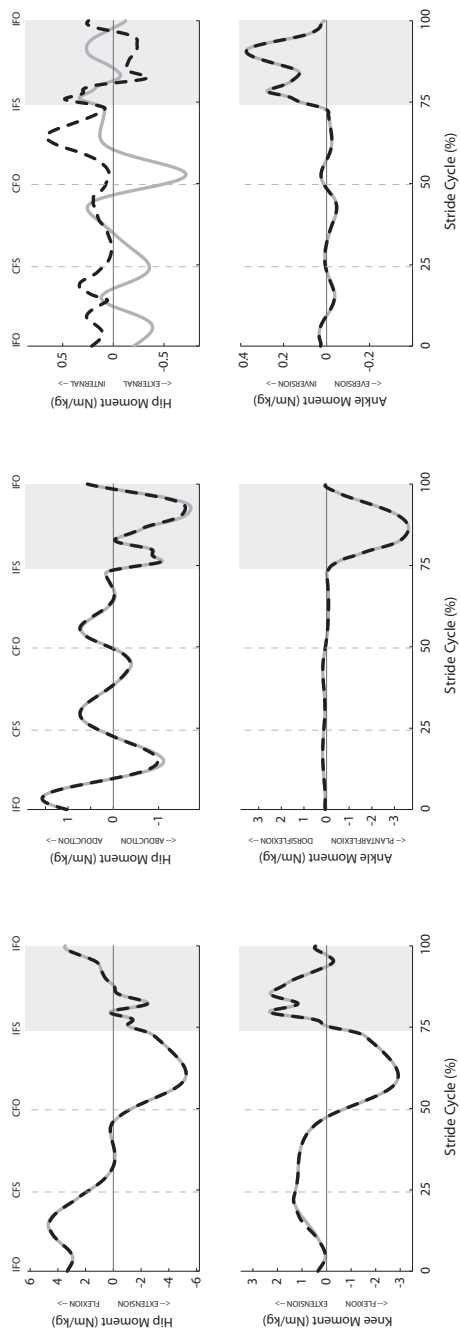


Figure A.6: Group mean lower-limb internal joint moments derived from inverse dynamics (solid grey line) and those derived from the computed muscle forces (dashed black line) across a full stride cycle of sprinting at 9.0 m/s. The light grey shading in each panel indicates the stance phase of the stride cycle. IFO ipsilateral foot-off; IFS contralateral foot-off; CFO contralateral foot-off; IFS ipsilateral foot-strike.

A.4 Pelvic coordinate system

In modelling the coordinate system of the pelvis anatomically, a subject-specific pelvic coordinate system (PCS) is defined from landmarks on the pelvis (Schache et al., 2011a). Typically, the medial-lateral axis is defined by the straight line joining the left and right ASIS markers, the anterior-posterior axis by the straight line joining the SACR marker to the midpoint of the left and right ASIS markers, and the vertical axis by the cross product of the two aforementioned axes. The OpenSim model, however, adopts a more simplified approach to define the PCS: *the joint axis as defined by the zero degree pose is parallel to the global coordinate frame*. This definition results in a sagittal plane offset of approximately 15° between the OpenSim PCS and the anatomical PCS (Fig. A.7). Consequently, the results of hip flexion, pelvic tilt and lumbar extension angles between the two coordinate systems will also differ by 15° . This discrepancy is noted for the purposes of direct comparison of the joint angles between the two kinematic models.

A.5 Hamstring EMG and joint moment paradox

For this dissertation, model-predicted muscle forces calculated from static optimisation were in good temporal agreement with EMG recordings from the same cohort of subjects across all speeds of running except for the hamstrings muscle group, which barely activated in the model in the stance phase despite pronounced EMG activity (see Fig. 5.3 in Chapter 5).

Prior investigations recording the medial and lateral hamstring EMG activity during sprinting have found these hamstring muscles indeed are active during stance (Mann et al., 1986; Mero and Komi, 1987; Jonhagen et al., 1996; Kyrolainen et al., 1999; Kuitunen et al., 2002; Kyrolainen et al., 2005; Yu et al., 2008; Higashihara et al., 2010). Although the relationship between EMG and muscle force for fast dynamic contractions is complicated and affected by many factors (Nigg and Herzog, 2007;

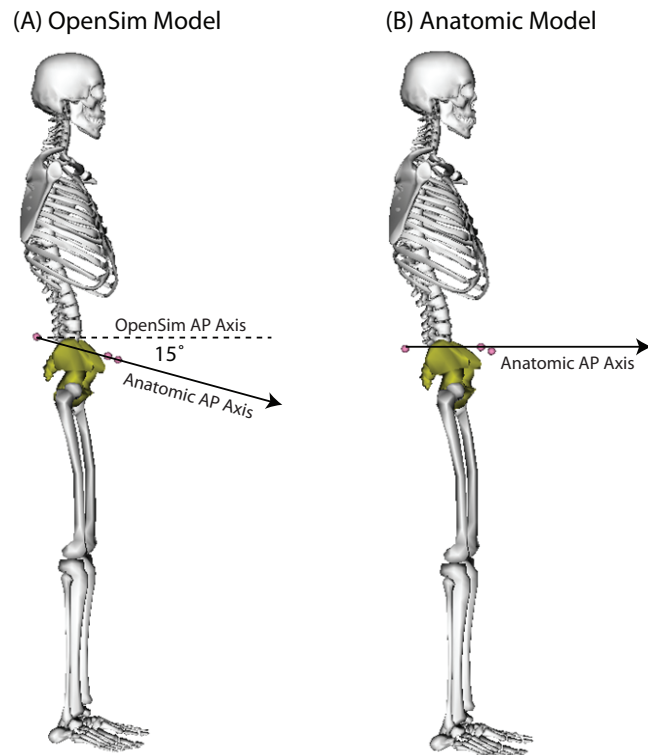


Figure A.7: *OpenSim VS anatomical pelvic coordinate systems*

Disselhorst-Klug et al., 2009), such experimental data would suggest that our stance phase computations of musculotendon force are much less than what would be physiologically expected in reality. It must be noted though that in computer models, the estimation of hamstrings force is a direct consequence of: (i) the hip and knee joint moments calculated during the stride; and (ii) the filter frequency used to filter the measured ground reaction forces.

A.5.1 Hip and knee joint moments

The hip and knee joint moments calculated for running in this dissertation were consistent in shape and magnitude with previous literature (Simpson and Bates, 1990; Arampatzis et al., 1999; Swanson and Caldwell, 2000; Biewener et al., 2004; Yokozawa et al., 2007). In particular, the hip

extensor moment during the stance phase of running is only present for the initial portion of stance (Figs C.9 and C.10 in Appendix C).

The hamstring EMG / joint moment inconsistency is therefore most likely attributable to the computational approach used to calculate muscle forces, i.e., the inability of inverse dynamics-based static optimisation when combined with a minimisation performance criterion to adequately predict antagonistic co-contraction. Evidence for this assertion is provided by Collins (1995), who evaluated the performance of a variety of optimisation algorithms for calculating muscle forces during walking. While the minimisation of the sum of squared muscle activations was not specifically tested, optimisation algorithms that were included were all found to be particularly insensitive to the prediction of antagonistic quadriceps-hamstrings activity during stance. Predicting high levels of hamstrings muscle force during mid-stance when there is a net flexor moment developing at the hip joint and a net extensor moment occurring at the knee joint would not be (from a computational perspective) the most cost effective way to distribute the joint moments across the various lower-limb muscles. Hamstrings muscle force at this time in the stride cycle would likely require the model to compute increased levels of force from the hip flexor and knee extensor muscles so as to counter the mechanical effect of the hamstrings and maintain equality with the inverse dynamics-based joint moments.

Co-contraction of antagonistic muscles can be used to modulate the impedance and thus stability of a joint, which would seem advantageous during the early stance phase in sprinting when the lower-limb is subjected to a high frequency impact force. Rather interestingly, studies have found that people with compromised knee joint stability (i.e., anterior cruciate ligament deficiency) display increased stance phase hamstrings EMG activity during walking and running in comparison to the non-injured side (Hurd and Snyder-Mackler, 2007), as well as in comparison to a group of healthy counterparts (Boerboom et al., 2001; Rudolph et al., 2001). It may therefore be that following foot-strike during sprinting, the hamstrings are active not to counter the external moments generated largely by the ground reaction force (as the results from the studies presented in this thesis would

suggest), but rather to provide alternative functions, such as joint stability and/or proprioception.

A.5.2 Ground reaction force filter frequency

As previously discussed, for hamstrings force to be developed in the musculoskeletal model, a hip extension moment is required. The fore-aft ground reaction force primarily determines the shape and magnitude of the sagittal plane joint moments. Specifically, the hip extensor moment during initial stance is particularly sensitive to the chosen cut-off frequency used to filter the ground reaction force. This sensitivity is well illustrated in Fig. A.8 (2nd row; left panel), where the “burst-like” pattern of the hip extensor moment during early stance is eliminated when a smaller cut-off frequency (e.g., 20 Hz) is applied to the ground reaction force. Furthermore, lower cut-off frequencies to the ground reaction force results in a reduced peak hip and knee joint moment in initial stance (2nd row), as well as the estimated hamstring and gluteus maximus muscle forces (3rd and 4th rows). In this thesis, a 60 Hz cut-off frequency was applied to all trials. If a smaller cut-off frequency was applied (e.g., 20 Hz), this would significantly modify the original shape of the fore-aft ground reaction force, consequently reducing the peak magnitude of the hip extensor moment during initial stance, and also reducing the estimated peak magnitude of the stance phase hamstrings and gluteus maximus muscle forces. Given that we are already suspicious that we have under-estimated the true magnitude of stance phase hamstrings muscle force by disfavoring co-contraction, a filter with a cut-off frequency smaller than 60 Hz would seem undesirable. Moreover, despite a pure hip extensor joint moment in the first 30% of stance when filtering the ground reaction force at 20 Hz, the gluteus maximus — and not the hamstrings — was chosen to primarily satisfy this moment. Computationally, this occurred because: (i) the gluteus maximus has a higher physiological cross sectional area (PCSA) and thus a higher strength (F_0^M) than the hamstrings (Table. A.3); and (ii) the biarticular hamstrings would provide adverse knee flexion moments whereas the gluteus maximus only provided desired hip extension moments.

A.5. HAMSTRING EMG AND JOINT MOMENT PARADOX

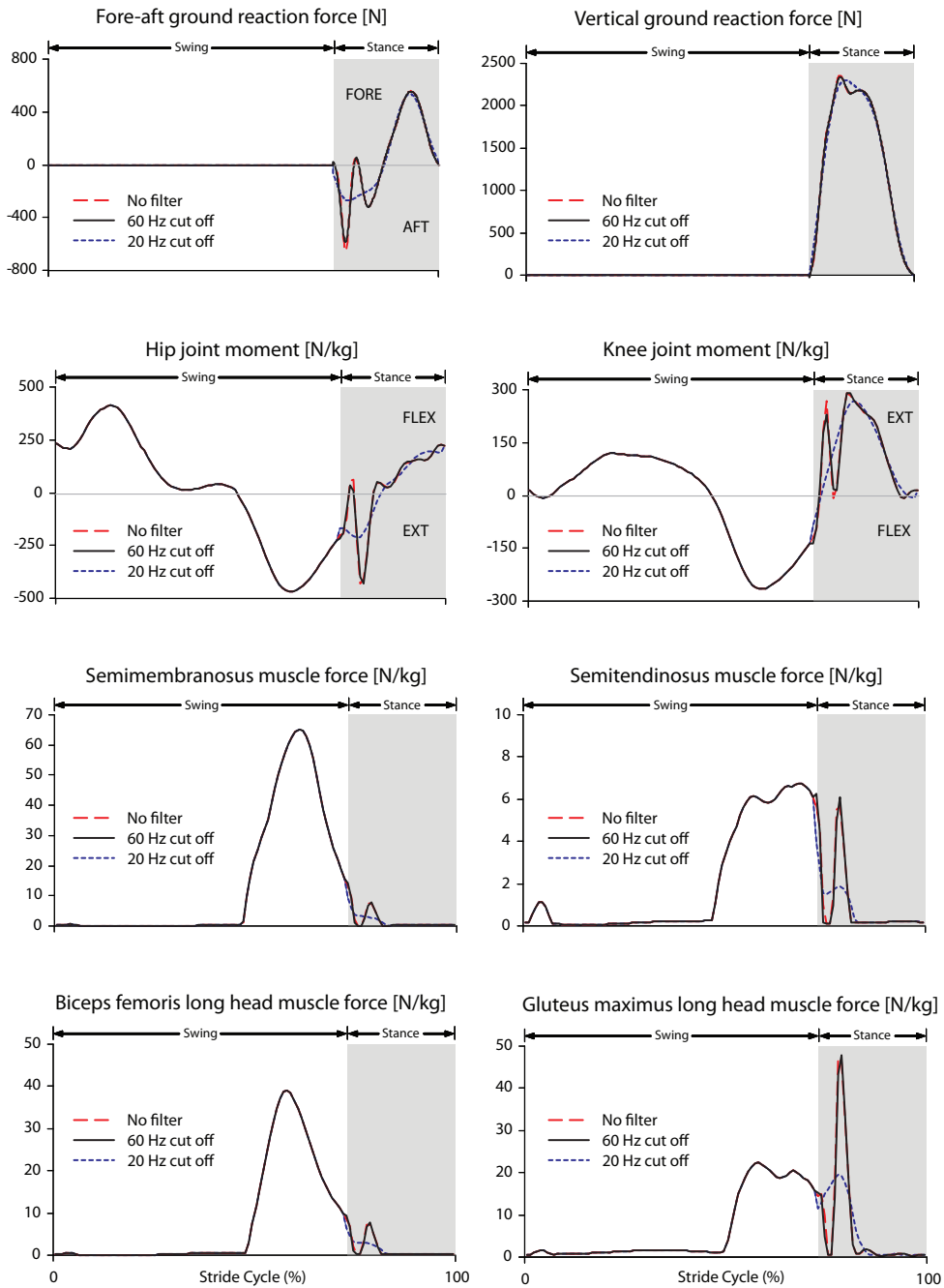


Figure A.8: Effect of hip and knee joint moments and the hamstring musculotendon forces when the ground reaction force is low-pass filtered (4^{th} order Butterworth) at different cut-off frequencies. A sprinting trial is shown for this figure, however, similar patterns exist across all running speeds.

APPENDIX A. MUSCULOSKELETAL MODEL

Appendix **B**

Gait-Extract toolbox

Preprocessing raw experimental gait data from a C3D file is necessary if the data is to be imported into OpenSim because OpenSim requires the experimental marker kinematics and ground reaction forces to be represented as tab delimited data in the OpenSim model's global coordinate system. The Gait-Extract toolbox was designed in MATLAB (The MathWorks, Inc., Natick, MA, USA) to efficiently prepare raw data for input into OpenSim and allows for batch processing in the event of multiple trials. Specifically, the Gait-Extract toolbox performs the following transformations to the raw data:

- Extract the marker kinematics for the experimental marker set
- Extract (and filter) ground reaction forces and moments from all force plates
- Transform marker and force plate data from the laboratory coordinate system to the OpenSim model coordinate system
- Extract (and perform filtering operations to the) EMG data for each muscle in the EMG muscle set
- Detect which leg belongs to each force plate
- Calculate center-of-pressure and vertical free moment
- Crop the extracted data (for example to a full stride cycle)

- Output marker kinematics (*.trc), ground kinetics (*.mot), and EMG (*.mot) tab delimited text files
- Produce trial specific OpenSim XML setup files

The Gait-Extract toolbox is freely available from <https://simtk.org/home/c3dtoolbox> (Fig. B.1).

B.1 Coordinate systems

Because kinematic marker data and ground reaction force data are collected independently by separate devices, they are recorded in their own internally defined coordinate system: VIDEO coordinate system for kinematic markers and FORCEPLATE coordinate system for ground reaction force data (Fig. B.2). Furthermore, the OpenSim model also has its own coordinate system (MODEL), and OpenSim requires all input data to be represented in this frame (Fig. B.2). By defining simple transformation matrices between each of the coordinate systems, the Gait-Extract toolbox automatically transforms the raw data into the MODEL coordinate system and saves the results as a tab-delimited text file (*.mot or *.sto file for further processing in OpenSim).

B.2 Foot detection algorithm

Experimentally recorded ground force data contains no information about which foot it came from. Therefore, it is required for the Gait-Extract toolbox to map each ground force to either the left or right foot. Event tags in the raw C3D file can define the foot-strike and foot-off events for each leg and this information is used to automatically detect the foot-side striking each plate. The algorithm requires the assumption that each foot hits one and only one plate during its entire interval of ground contact. In short, the algorithm cycles through the intervals defined by each set of two consecutive event tags and determines the set of “active” force plates (plates that are recording force during that interval). Combining the active plates with the event information provides enough information to prescribe a foot-side to each time interval.

The screenshot shows the website for the Gait-Extract toolbox project on the SimTK platform. The top navigation bar includes links for Home, About Simtk.org, How to Contribute, Search Simtk.org, News, Create Project, Tim Dorn, Log Out, and My Page. The main content area is titled "C3D Extraction Toolbox Project Overview" and includes a description of the toolbox, its main features, and related projects. A sidebar on the left contains links for Overview, Team, Downloads, Documents, Publications, Public Forums, and Advanced. A sidebar on the right features a Project Lead section for Tim Dorn and a section for Driving Biological Problems.

Overview
 Update
 Statistics
 Geography of use

Team

Downloads

Documents

Publications

Public Forums

Advanced

Downloads & Source Code
[GaitExtractToolbox](#)
 This projects does not store source code in Simtk's Subversion repository.

C3D Extraction Toolbox Project Overview

Description: This toolbox is of benefit to musculoskeletal modellers in the field of biomechanics / bioengineering to assist extracting kinematic, kinetic, and EMG information directly from a C3D file for Matlab manipulation or for input to OpenSim biosimulation software. The scripts can be configured for any laboratory configuration. This software is free without warranty but I do ask for acknowledgement if used in publications. Free download is available with documentation and two examples included.

Main features of this script include:

- Custom markerset extraction
- Foot-plate detection algorithm
- Kinetic extraction (ground reaction forces / moments)
- Center of pressure calculation
- Transformation to customizable model coordinate system
- Custom EMG acquisition & processing tools
- XML file production (for OpenSim)
- Lab customizable

The scripts require Motion Labs C3D Server software (freeware) and XML Toolbox (Marc Molinari)(freeware) which is included with the script download.

Additional C3D software may be useful and these are available at <http://www.c3d.org/c3dapps.html>. Review the included manual for version updates and additions. Please inform me of bugs / suggestions to improve as this will be an ongoing project.

Purpose/Synopsis: Provide a simple and time efficient way to extract raw gait data from a C3D file

Audience: Users interested in extracting kinematic, kinetic and EMG data from C3D files

Long Term Goals and Related Uses: To easily extract data from C3D files

Keywords: [c3d](#), [extract](#), [gait](#), [opensim](#), [simulation](#)
 (Links display other projects with that keyword anywhere in the project.)

Project Lead

[Tim Dorn](#)
[Contact](#)

Driving Biological Problems
 This project is part of [Neuromuscular Biomechanics](#)

Related Projects
[Tim's OpenSim Utilities](#)

Feedback | Simbios | Simbiome | BCR | Our Pledge Your Responsibility

SimTK, the Simulation Toolkit, is a part of the Simbios project funded by the National Institutes of Health through the NIH Roadmap for Medical Research, Grant U54 GM072970. Information on the National Centers for Biomedical Computing can be [obtained here](#).

Figure B.1: Gait-Extract toolbox project website on SimTK (<https://simtk.org/home/c3dtoolbox>).

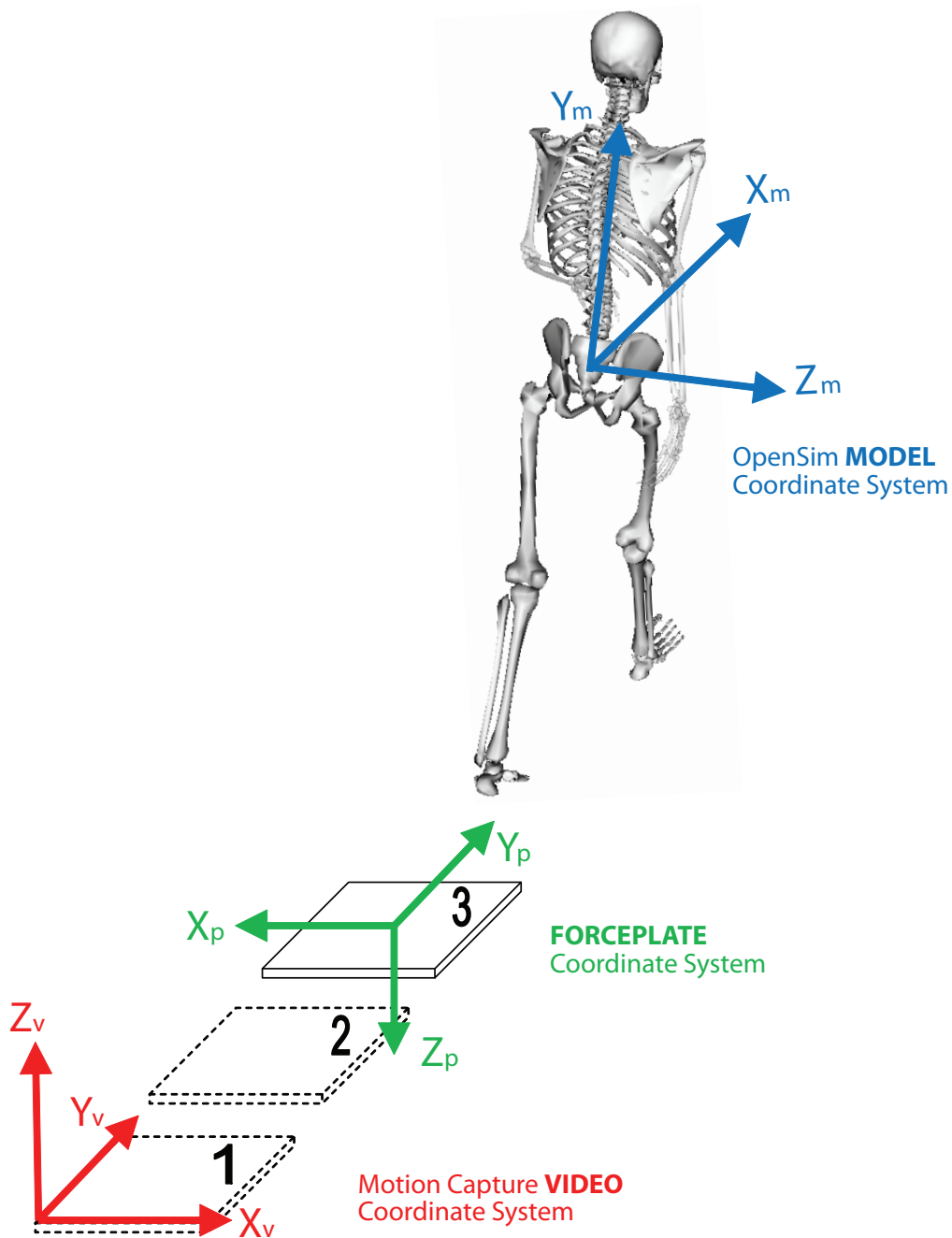


Figure B.2: Marker kinematics and ground reaction force data are captured in their own coordinate systems. Conversion to the MODEL coordinate system is required to proceed.

B.3 Center-of-pressure calculation

The center-of-pressure (CoP) is the single point of ground force application on a force plate. This point can be calculated by performing a moment equilibrium balance about the true origin of the force plate (the exact spatial location where ground reactions are measured from). The center-of-pressure in the *MODEL* coordinate frame can be determined by summing three vectors (Fig. B.3).

1. **Model origin to force plate surface geometric center:** This vector is defined by the geometric center of the force plate corners, as specified in the `FORCE.PLATFORM\CORNERS` field of the C3D file. These values are originally expressed in the *VIDEO* coordinate frame for each force plate and should be correctly setup prior to data capture. The Gait-Extract toolbox converts this vector into the *MODEL* coordinate frame.
2. **Force plate surface geometric center to force plate true origin:** Because of slight inconsistencies in the manufacturing process, each force plate measures a force and moment about a different true origin, which can be slightly offset from the geometric center of the plate surface. This vector between the true origin and the center of the force plate is determined by the manufacturer during individual calibrations and is specified in the `FORCE.PLATFORM\ORIGIN` field in the C3D file. The Gait-Extract toolbox converts this vector into the *MODEL* coordinate frame.
3. **Force plate true origin to center-of-pressure:** The center-of-pressure location with respect to the force plate's true origin (in the force plate's coordinate frame) is calculated by performing a moment balance. The Gait-Extract toolbox converts this vector into the *MODEL* coordinate frame.

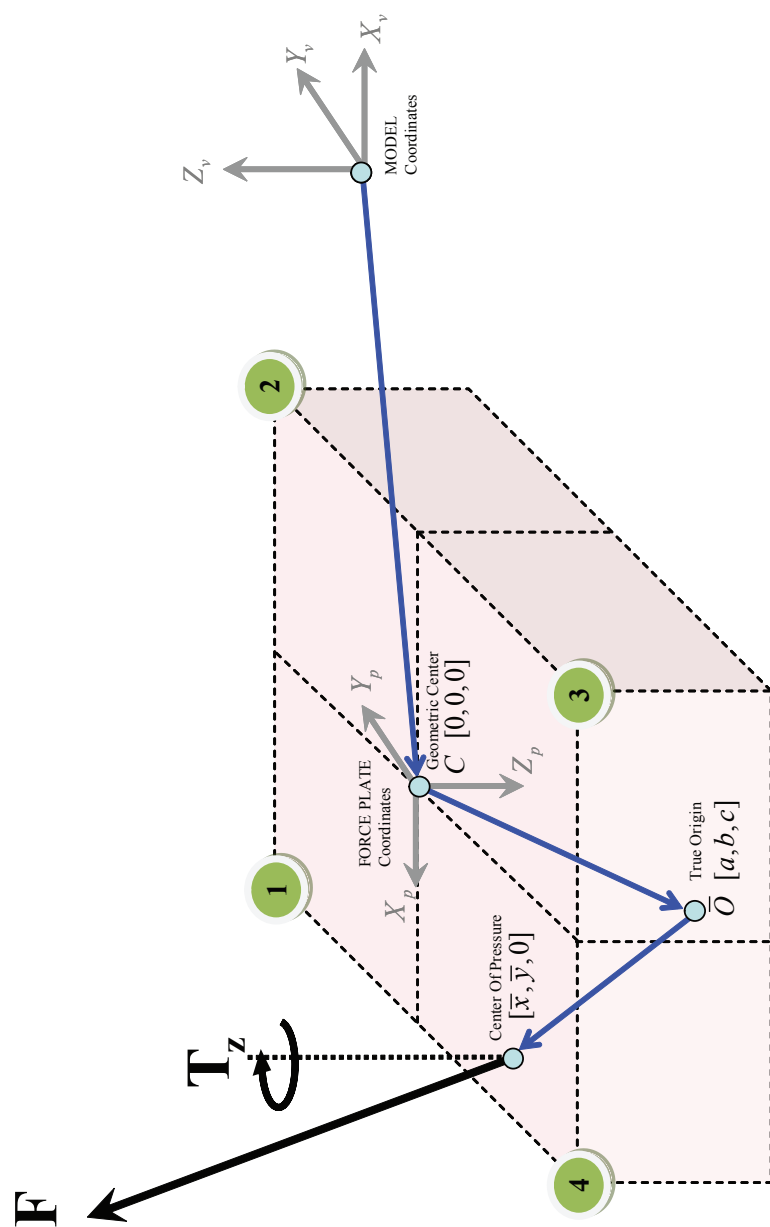


Figure B.3: Calculation of the center-of-pressure. All coordinates shown are in the force plate coordinate system.

B.3. CENTER-OF-PRESSURE CALCULATION

Taking moments about the force plate's true origin:

$$\begin{bmatrix} M_x \\ M_y \\ M_z \end{bmatrix} = \begin{bmatrix} 0 & c & \bar{y} - b \\ -c & 0 & -(\bar{x} - a) \\ -(\bar{y} - b) & \bar{x} - a & 0 \end{bmatrix} \begin{bmatrix} F_x \\ F_y \\ F_z \end{bmatrix} + \begin{bmatrix} 0 \\ 0 \\ T_z \end{bmatrix} \quad (\text{B.1})$$

$$\begin{bmatrix} M_x \\ M_y \\ M_z \end{bmatrix} = \begin{bmatrix} (\bar{y} - b)F_z + cF_y \\ -cF_x - (\bar{x} - a)F_z \\ (\bar{x} - a)F_y - (\bar{y} - b)F_x + T_z \end{bmatrix} \quad (\text{B.2})$$

These three equations have three unknowns: (\bar{x}, \bar{y}, T_z) . T_z represents a vertical free moment about the center-of-pressure. Solving for the three unknowns:

$$\bar{x} = -\frac{(M_y + cF_x)}{F_z} + a \quad (\text{B.3})$$

$$\bar{y} = -\frac{(M_x + cF_y)}{F_z} + b \quad (\text{B.4})$$

$$T_z = M_z - (\bar{x} - a)F_y + (\bar{y} - b)F_x \quad (\text{B.5})$$

Noises in the measured ground reaction forces and moments will manifest themselves in the CoP calculation. Furthermore, since the CoP is calculated by dividing by the vertical GRF, it is most sensitive at early and late stance where the vertical GRF is low. It is here that discontinuities (or spikes) can occur (Fig. B.4). Applying a Butterworth filter to eliminate the discontinuities would not be ideal because the filter would modify the entire CoP trajectory, which is based on accurate ground force measurements. A CoP spike reduction algorithm was developed to filter out only the discontinuities in the first and last few frames of stance. The algorithm performs successive passes of the first and last few frames of CoP during stance, and looks for rapid discontinuities (successive frames of opposing CoP gradients). Where discontinuities occur, the ‘‘spike’’ magnitude is reduced by a factor of a half until the curve becomes smooth. Fig. B.4

illustrates the effect of the filter on the calculated anterior CoP during the stance phase of walking.

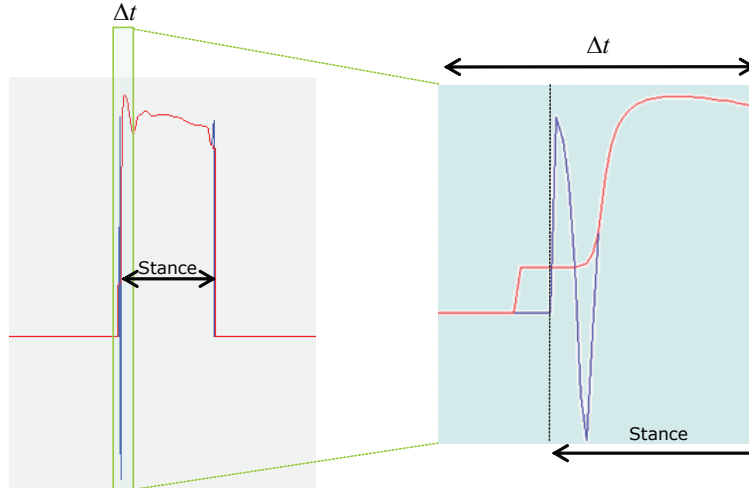


Figure B.4: *Center-of-pressure enhancement. Discontinuities (or spikes) can occur in early and late stance due to low vertical ground reaction forces. The blue line represents the standard CoP calculation. The red line represents the corrected CoP trajectory after CoP spike filter.*

B.4 EMG processing

Raw EMG data were processed using the Teager-Kaiser Energy (TKE) operator (Li et al., 2007; Solnik et al., 2010). Unlike traditional Butterworth filters (Lloyd and Besier, 2003; Buchanan et al., 2004), the TKE operator has been shown to better highlight the onset/offset of motor unit activity. The discrete TKE operator at time n is defined as:

$$TKE[x(n)] = x^2(n) - x(n+1)x(n-1) \quad (\text{B.6})$$

Being an energy operator, the output of the TKE operator considers both the instantaneous frequency and amplitude response of a signal. When a motor unit action potential fires, it is usually accompanied by an instantaneous increase in signal amplitude and frequency, hence its suitability for analysis using the TKE operator (Li et al., 2007). Fig. B.5

illustrates the differences between the TKE and Butterworth filters for a typical raw EMG signal. Under conditions where the level of motor unit firing is weak, signal to noise ratios may become very low and make EMG onset/offset detection difficult using a Butterworth filter. In contrast, the TKE operator clearly identifies on/off regions of muscle activity.

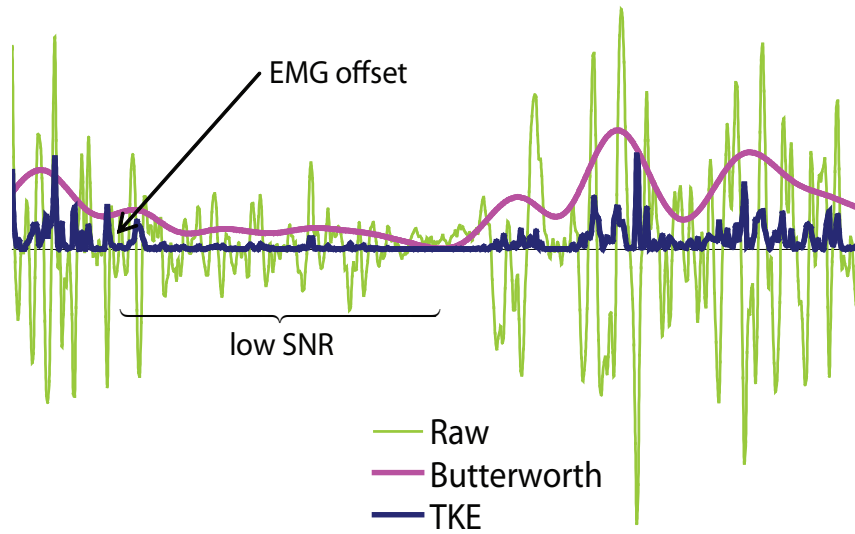


Figure B.5: Comparison of EMG filters. Raw EMG (green); bandpass filtered EMG (25Hz–40Hz) using a 4th order Butterworth filter (pink); and TKE filtered EMG (blue).

APPENDIX B. GAIT-EXTRACT TOOLBOX

Appendix C

Modelling results: Quick reference

This appendix contains a comprehensive set of modelling results during self-selected walking (1.5 m/s) and four speeds of running (3.5 m/s, 5.2 m/s, 7.0 m/s and 9.0 m/s). The majority of results presented in this section were not directly used in answering the research objectives of this dissertation; nevertheless, they represent a valuable dataset which may be used for future reference. For referencing data in this appendix that do not appear in publications resulting from this thesis, please cite this dissertation:

Dorn T.W. (2011). Computational modelling of lower-limb muscle function in human running. Department of Mechanical Engineering, The University of Melbourne, Australia.

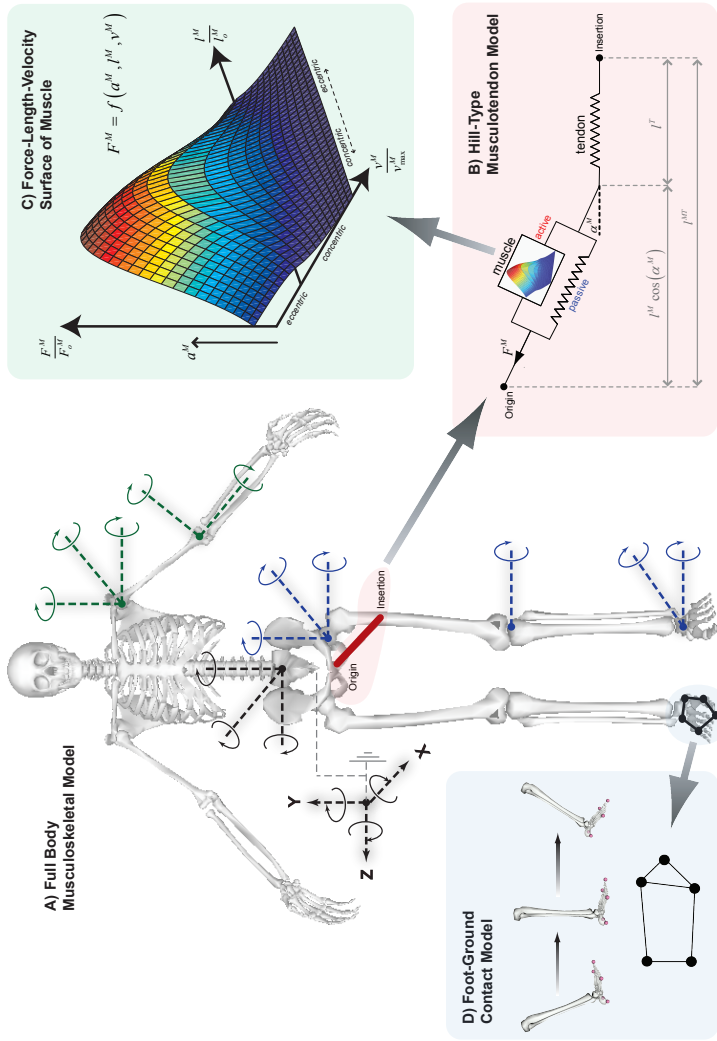


Figure C.1: The three-dimensional OpenSim musculoskeletal model used in this dissertation. (A) The skeleton was represented as a multibody linkage containing 31 degrees-of-freedom, driven by 92 musculotendon actuators (lower extremity and trunk) and 10 ideal torque actuators (upper extremity). (B) Each musculotendon actuator was represented as a Hill-type physiological muscle in series with tendon. Muscle fibre length l^M and tendon length l^T were governed by the distance between musculotendon origin and insertion l^{MT} , muscle pennation angle α^M and muscle force F^M . (C) The active force-length-velocity surface of physiological muscle was defined by the muscle's optimal fibre length l_0^M , maximum shortening velocity v_{max}^M and maximum isometric force F_0^M . Active muscle force generation was constrained to this surface at all times depending on the current value of the muscle fibre length l^M , velocity v^M and activation a^M . (D) Contact model of Lin et al. (2011a) used to model foot-ground interaction. Contact was assumed to take place at five discrete contact points distributed over the foot.

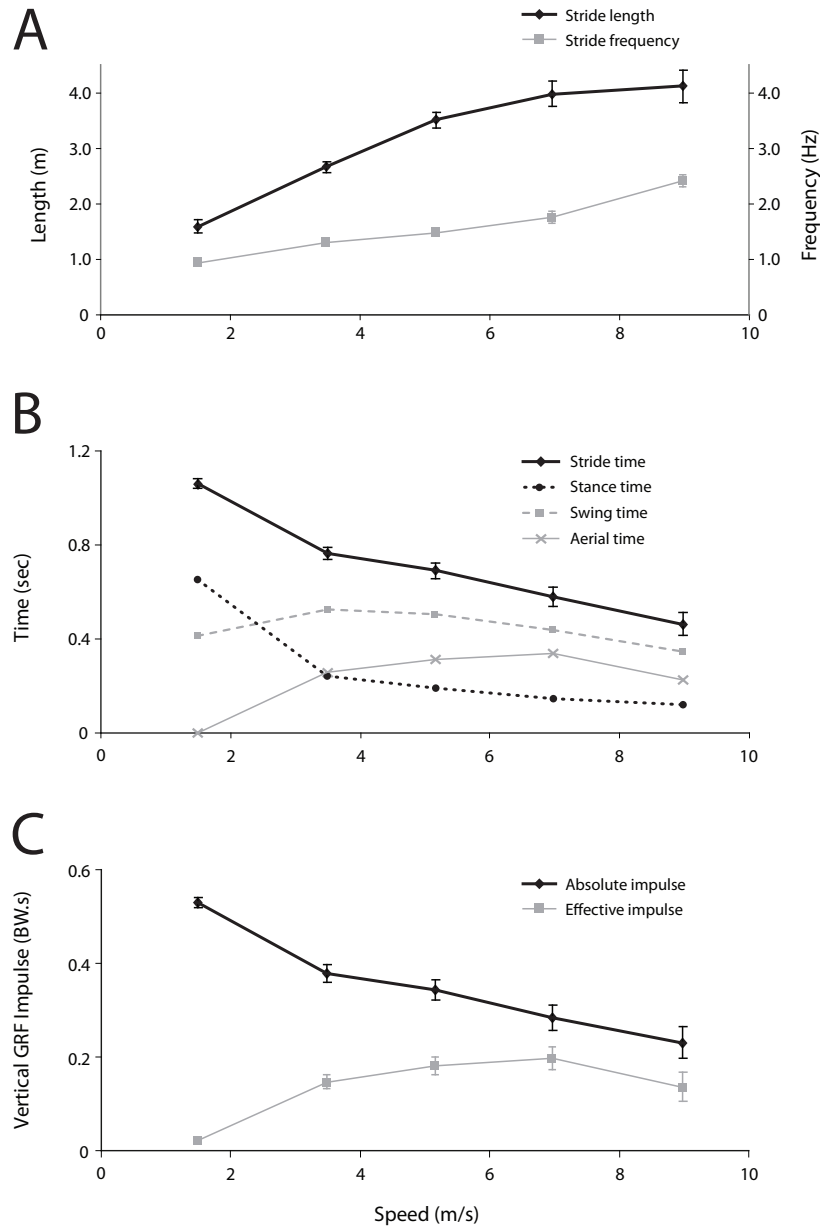


Figure C.2: (A) Stride length and frequency at each speed of locomotion. (B) Stance time, swing time, aerial time and stride time at each speed of locomotion. Stance time plus the swing time equals the stride time. Aerial time is the part of swing time when both feet are off the ground. (C) Absolute and effective vertical ground force impulse at each speed of locomotion. Absolute impulse was calculated from the area underneath the vertical ground reaction force. Effective impulse was calculated from the area bounded by the vertical ground reaction force and the horizontal line representing one bodyweight. Error bars represent 1SD of variance from the mean.

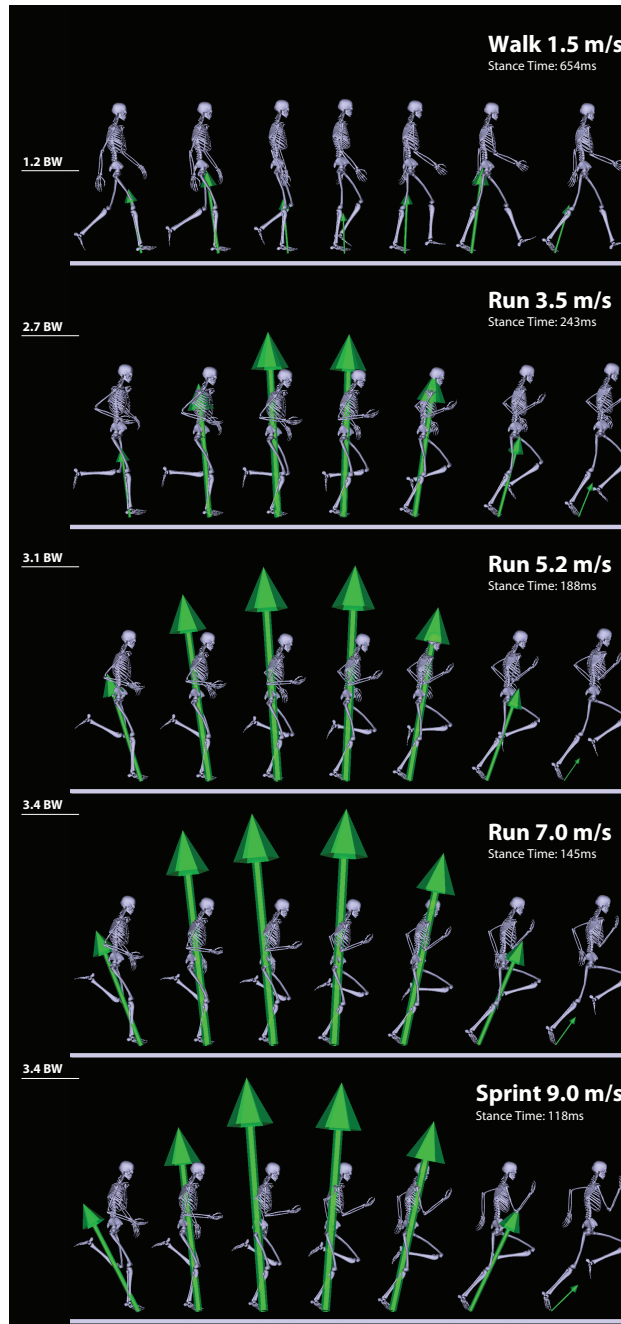


Figure C.3: *Sagittal view of the joint kinematics and ground reaction forces across the stance phase for one representative subject at each speed of locomotion. Snapshots were taken at equal intervals of stance with the right leg in contact with the ground. The vertical scale represents peak magnitudes of the vertical ground reaction force measured in body weight (BW).*

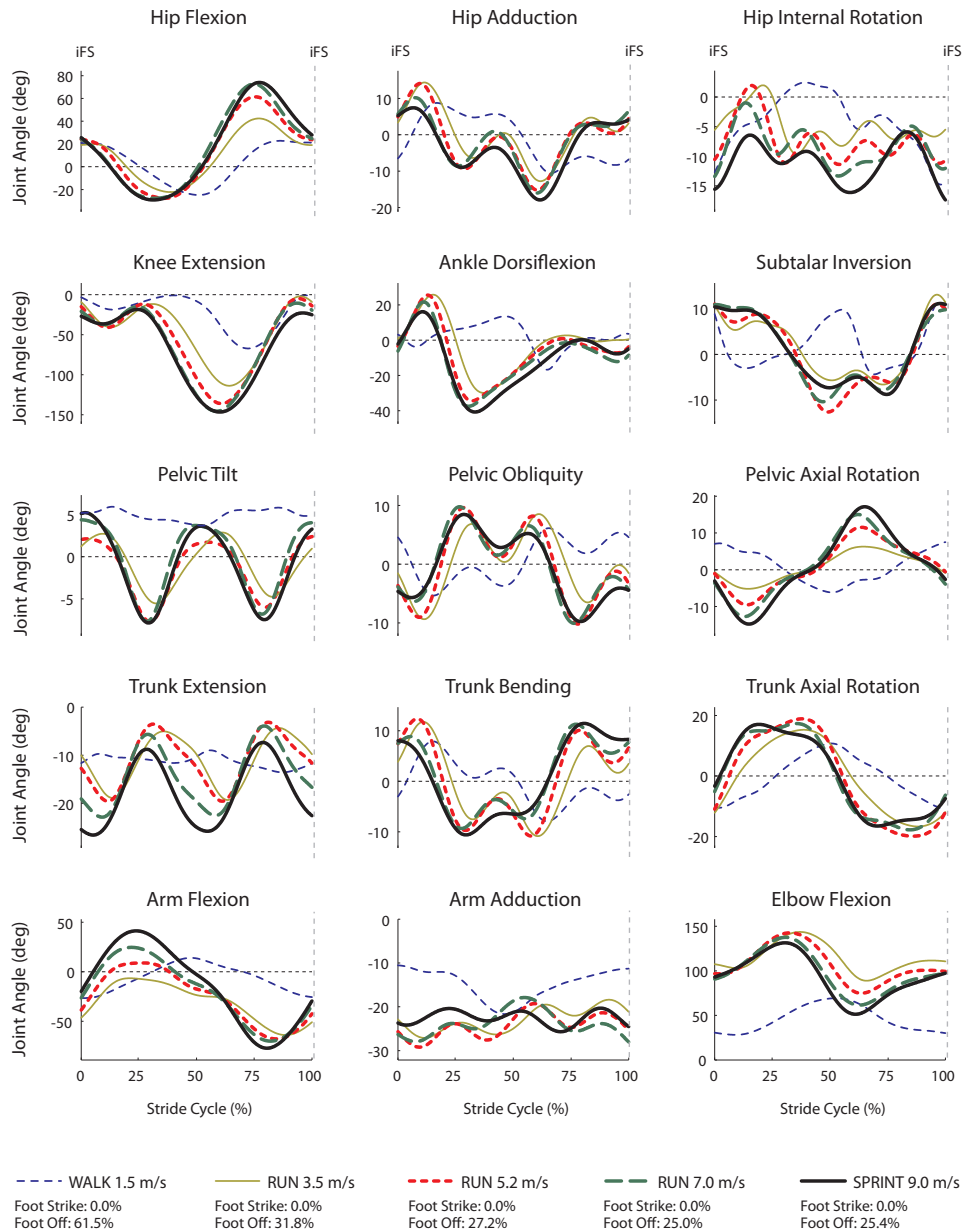


Figure C.4: Joint angles for lower and upper extremities at each speed of locomotion. Positive joint angles are specified in the plot subtitles. Positive pelvis joint angles are in anterior tilt, clockwise obliquity and left axial rotation for the right foot. Positive trunk joint angles are in extension, right bending and left axial rotation for the right foot. Positive leg joint angles are in hip flexion, hip adduction, hip internal rotation, knee extension, ankle dorsiflexion and subtalar inversion. Results were averaged across all trials for all subjects and are shown over a full stride cycle. *iFS* represents ipsilateral foot-strike.

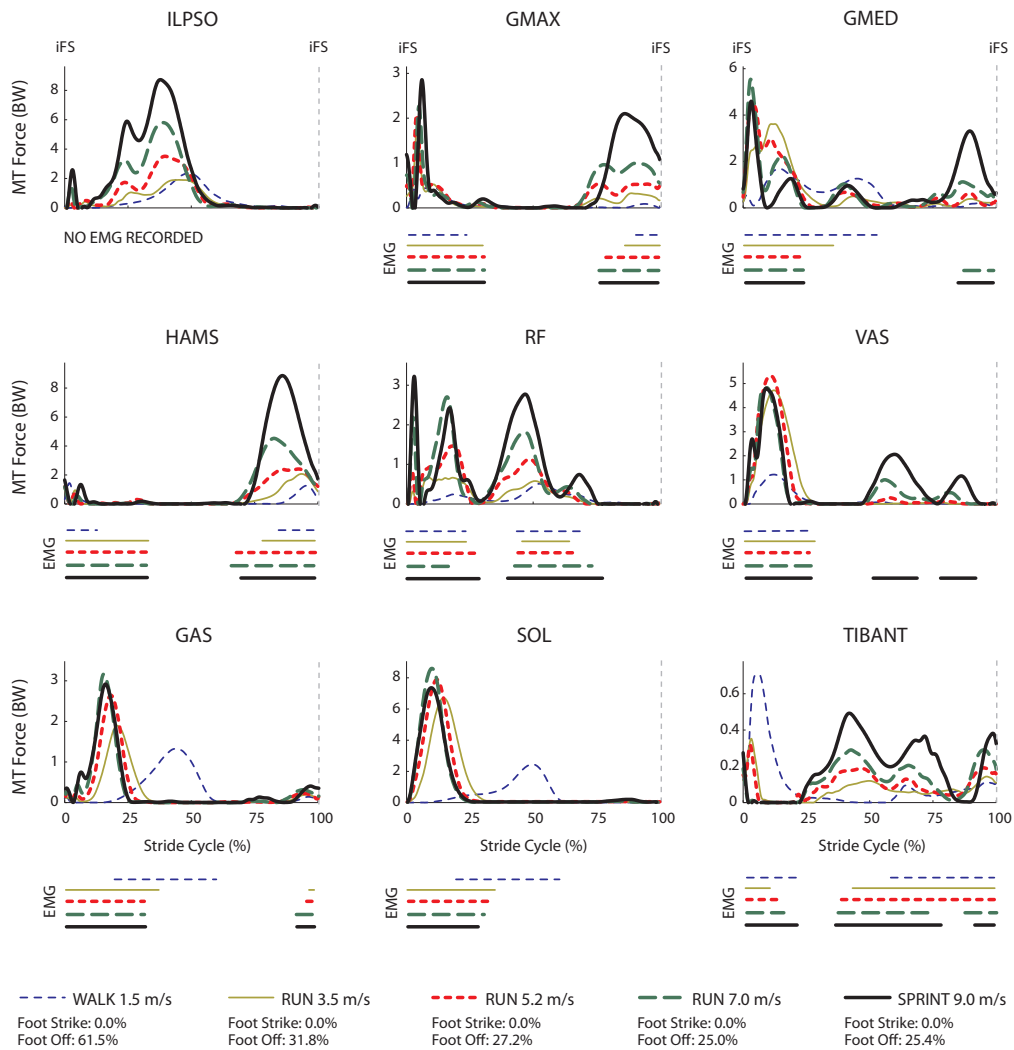


Figure C.5: Musculotendon force at each speed. Horizontal bars beneath each plot indicate the periods of EMG activity recorded for each muscle as determined by filtering the raw EMG signal with a Teager-Kaiser Energy (TKE) filter. Results were averaged across all trials for all subjects and shown over a full stride cycle. Muscle symbols appearing in the graphs are: ILPSO (iliacus and psoas combined; no EMG data recorded), GMAX (superior, middle and inferior gluteus maximus), GMED (anterior, middle and posterior compartments of gluteus medius), HAMS (biceps femoris long head, semimembranosus and semitendinosus combined; medial hamstring EMG shown), RF (rectus femoris), VAS (vastus medialis, vastus intermedius and vastus lateralis combined; vastus lateralis EMG shown), GAS (medial and lateral compartments of gastrocnemius combined; medial gastrocnemius EMG shown), SOL (soleus) and TIBANT (tibialis anterior). *iFS* represents ipsilateral foot-strike.

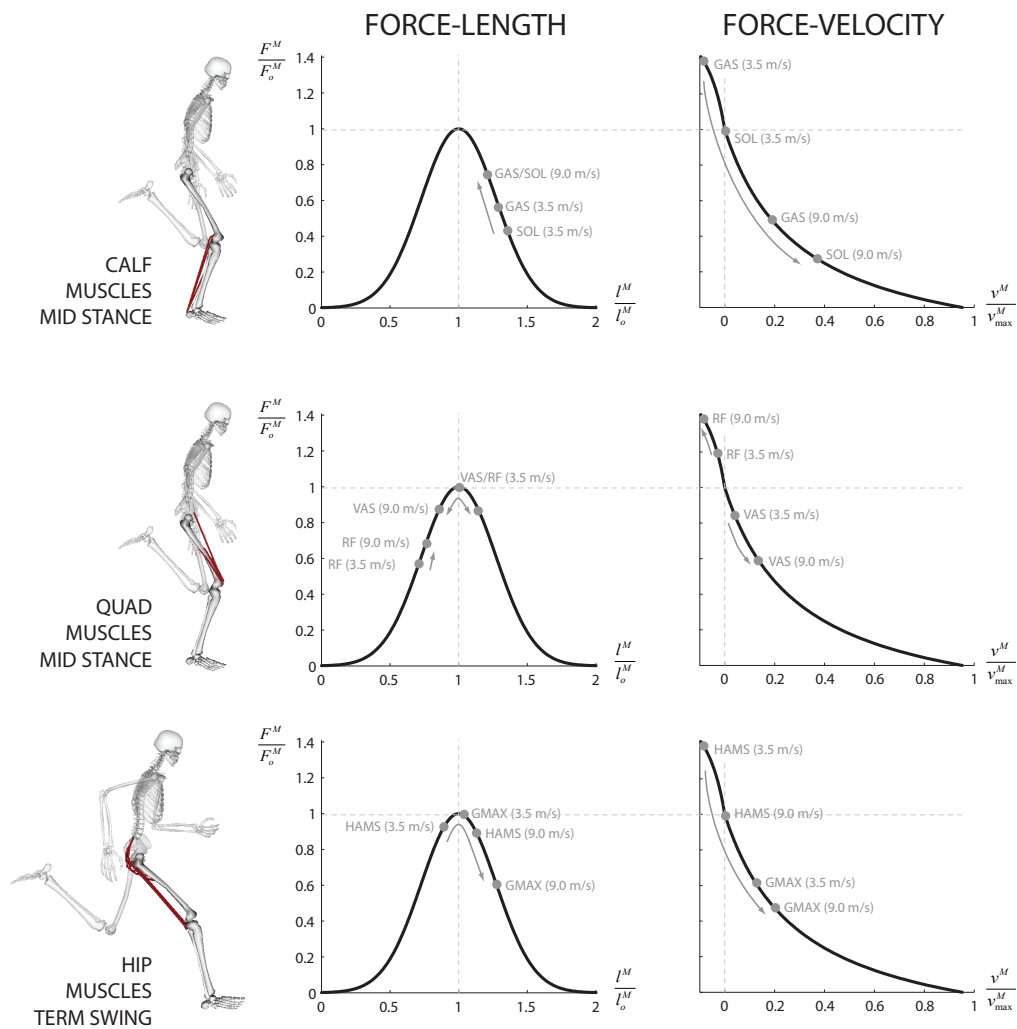


Figure C.6: Normalised force-length and force-velocity operating points at the time of maximum force production during the running stride cycle. Results are shown for the calf, quadricep and hip muscle groups at running speeds of 3.5 m/s and 9.0 m/s.

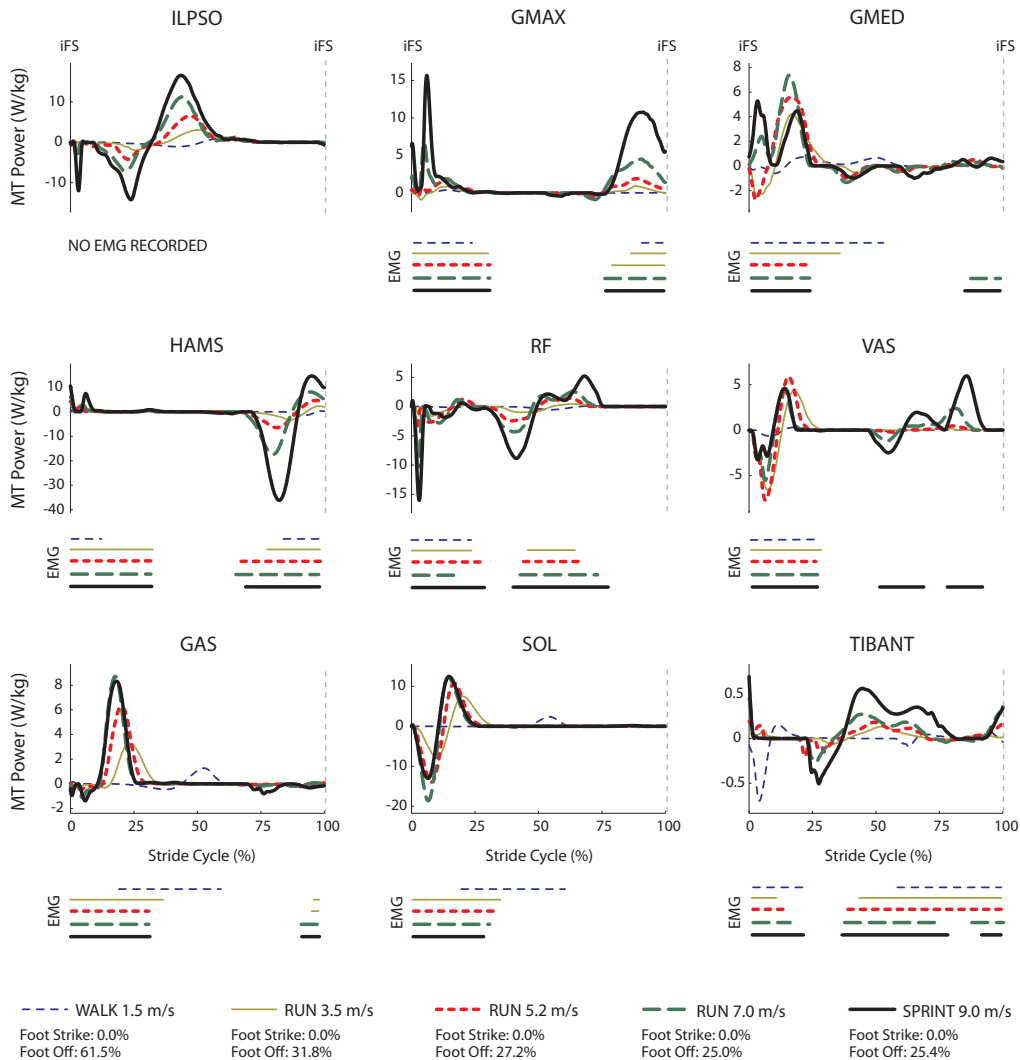


Figure C.7: Musculotendon power at each speed of locomotion. Horizontal bars beneath each plot indicate the periods of EMG activity recorded for each muscle as determined by filtering the raw EMG signal with a Teager-Kaiser Energy (TKE) filter. Results were averaged across all trials for all subjects and are shown over a full stride cycle. Muscle symbols as defined in the caption for Fig. C.5 . *iFS* represents ipsilateral foot-strike.

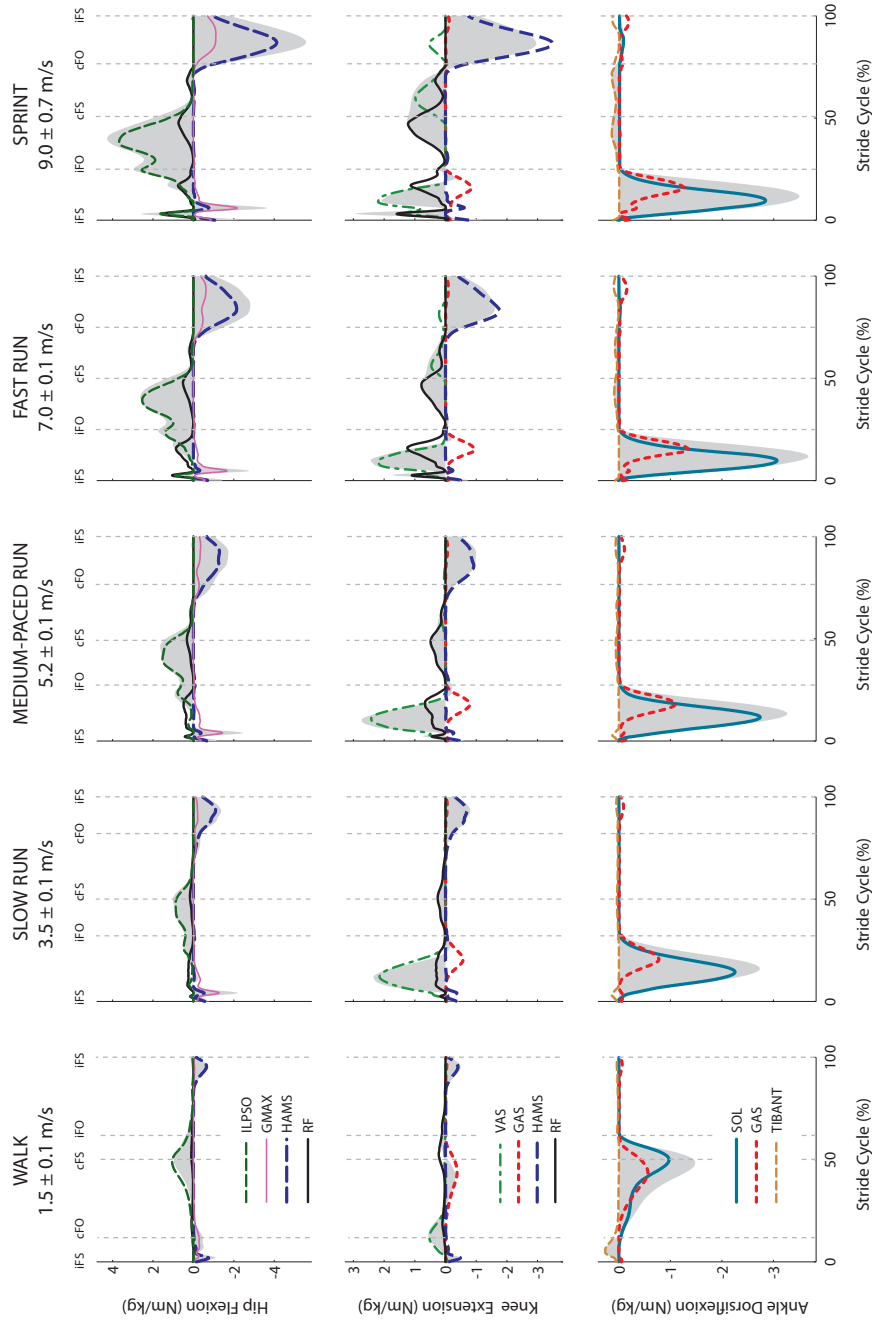


Figure C.8: Contributions of individual muscles to the net sagittal plane joint moments (shaded regions) for each speed of locomotion. Positive joint moments represent hip flexion, knee extension and ankle dorsiflexion; negative joint moments represent hip extension, knee flexion and ankle plantarflexion. Results were averaged across all trials for all subjects and are shown over a full stride cycle. Muscle symbols as defined in the caption for Fig. C.5 . iFS, iFO, cFS and cFO represent ipsilateral foot-strike, ipsilateral foot-off, contralateral foot-strike and contralateral foot-off respectively.

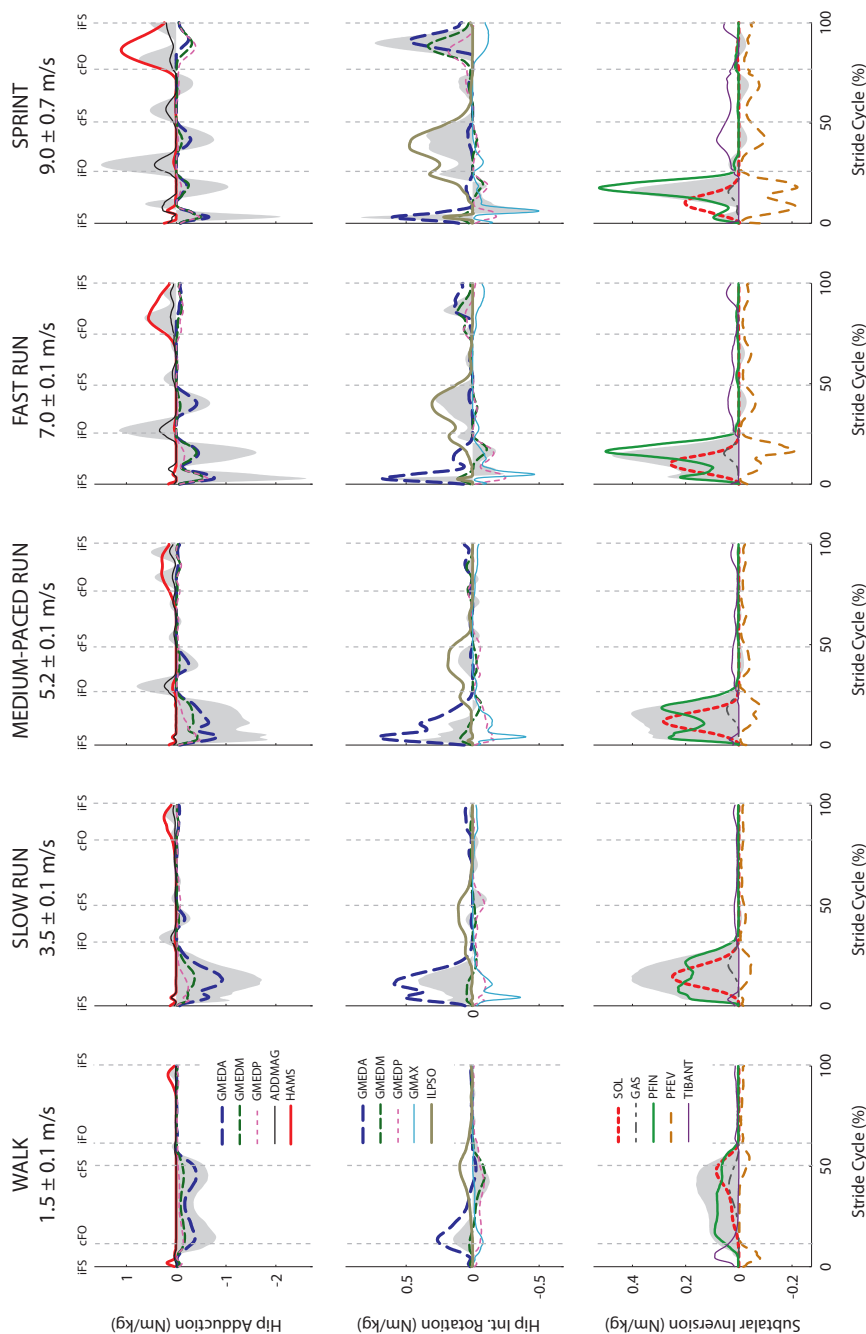


Figure C.9: Contributions of individual muscles to the net coronal and transverse plane joint moments (shaded regions) for each speed of locomotion. Positive joint moments represent hip adduction, hip internal rotation and subtalar inversion, negative joint moments represent hip abduction, hip external rotation and subtalar eversion. Results were averaged across all trials for all subjects and are shown over a full stride cycle. Muscle symbols appearing in the graphs are: GMED (gluteus medius anterior/middle/posterior), ADDMAG (adductor magnus), HAMS (biceps femoris long head, semimembranosus and semitendinosus combined), GMAX (gluteus maximus), ILPSO (iliacus and psoas combined), SOL (soleus), GAS (medial and lateral compartments of gastrocnemius combined), PFIN (tibialis posterior, flexor digitorum longus, flexor hallucis longus and extensor hallucis longus combined), PFEV (peroneus brevis, peroneus longus and extensor digitorum longus combined) and TIBANT (tibialis anterior).

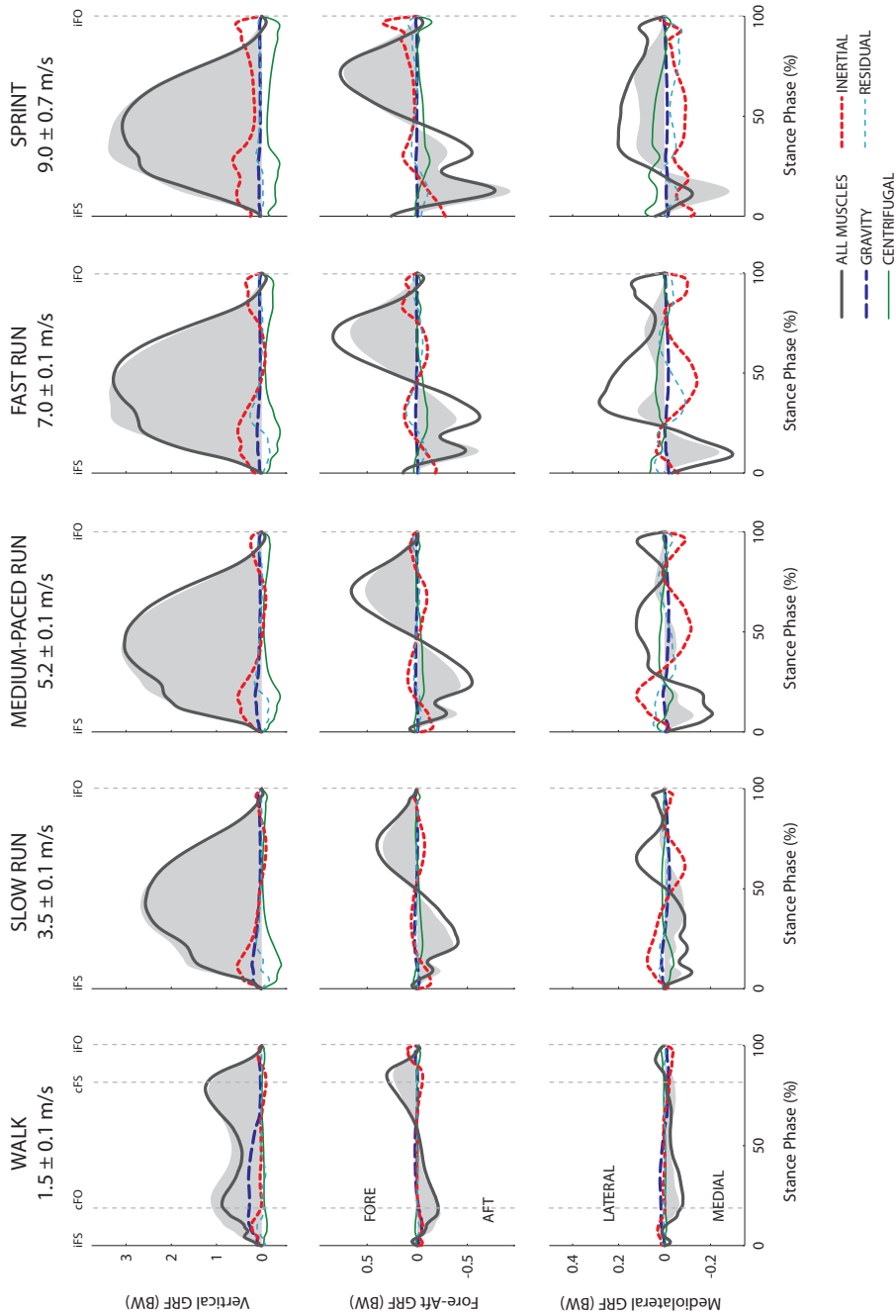


Figure C.11: Contributions of action force groups to the net ground reaction force (shaded regions) in the anterior-posterior, vertical and mediolateral directions for each speed of locomotion. Positive ground reaction forces are directed anteriorly, upward and laterally (for a right leg); negative ground reaction forces are directed posteriorly, downward and medially (for a right leg). Results were averaged across all trials for all subjects and are shown over the stance phase. Symbols appearing in the graphs are: ALL MUSCLES (sum of all muscles), GRAVITY (gravity forces), CENTRIFUGAL (centrifugal forces), INERTIAL (superposition error) and RESIDUAL (residual forces).

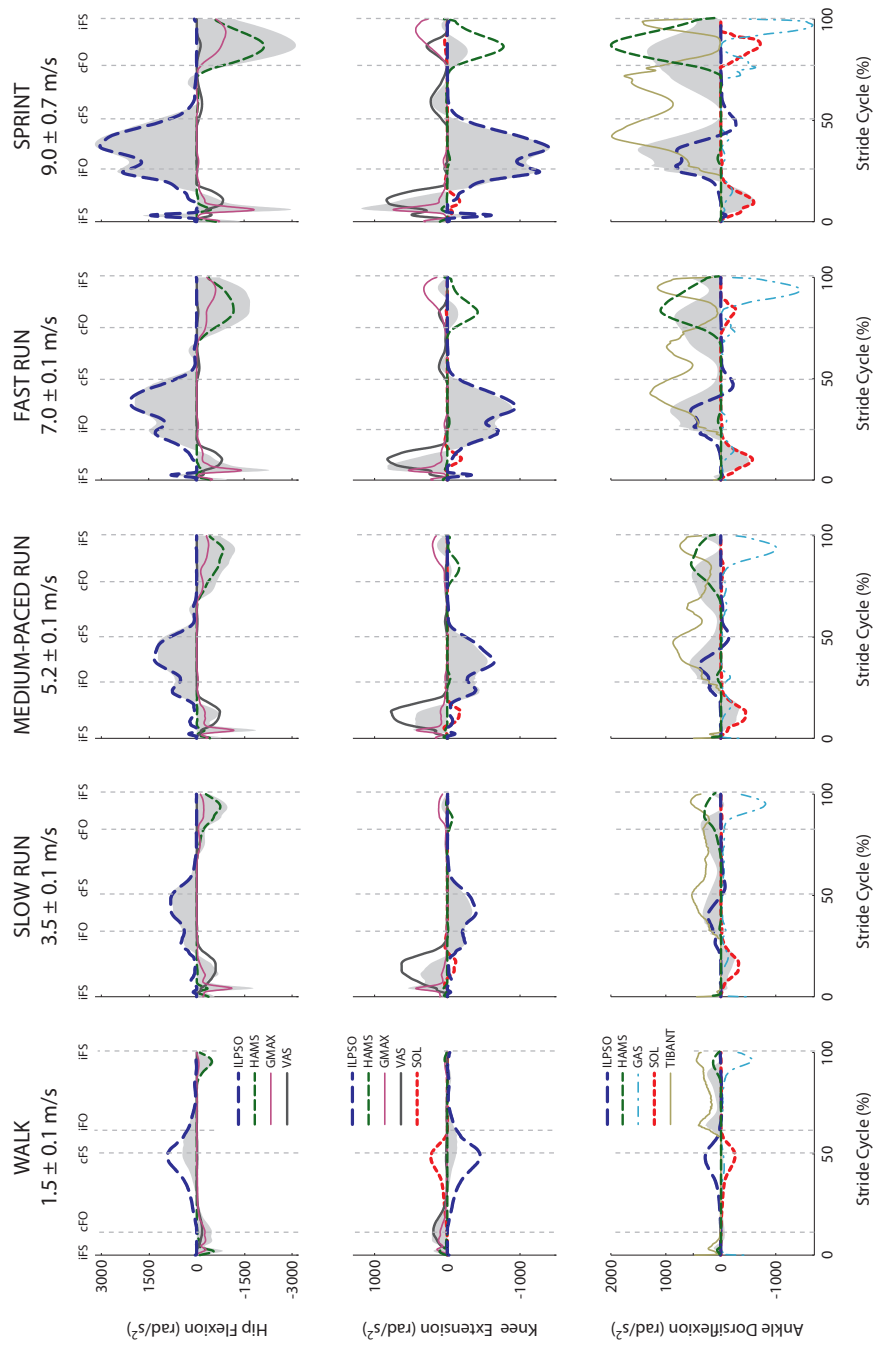


Figure C.12: Contributions of individual ipsilateral-leg muscles to the total ipsilateral-leg induced sagittal joint angular acceleration (shaded regions) of the hip, knee and ankle for each speed of locomotion. Positive joint angular accelerations represent hip flexion, knee extension and ankle dorsiflexion; negative joint angular accelerations represent hip extension, knee flexion and ankle plantarflexion. Results were averaged across all trials for all subjects and are shown over a full stride cycle. Muscle symbols as defined in the caption for Fig. C.5 .

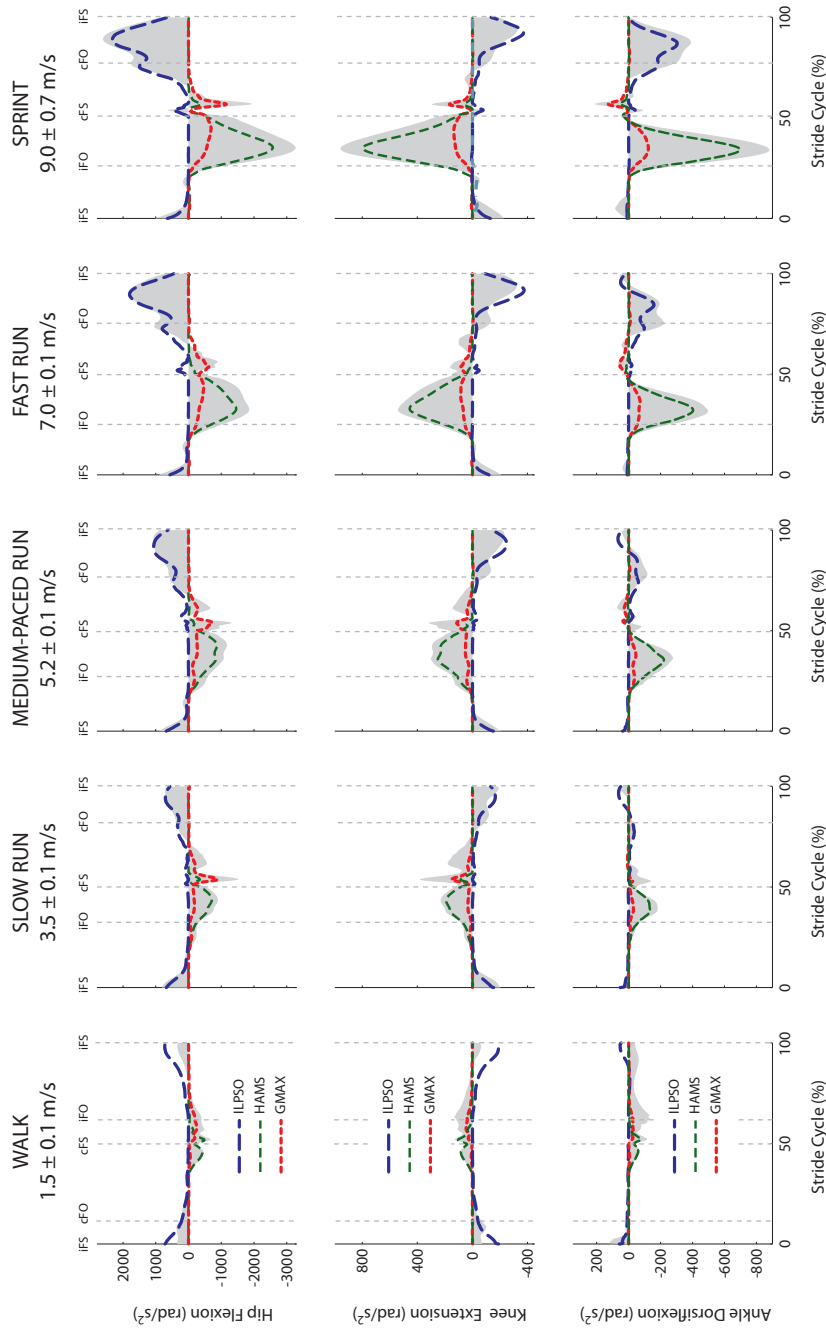


Figure C.13: Contributions of individual contralateral-leg muscles to the total contralateral-leg induced sagittal joint angular acceleration (shaded regions) of the hip, knee and ankle for each speed of locomotion. Positive joint angular accelerations represent hip flexion, knee extension and ankle dorsiflexion; negative joint angular accelerations represent hip extension, knee flexion and ankle plantarflexion. Results were averaged across all trials for all subjects and are shown over a full stride cycle. Muscle symbols as defined in the caption for Fig. C.5 .

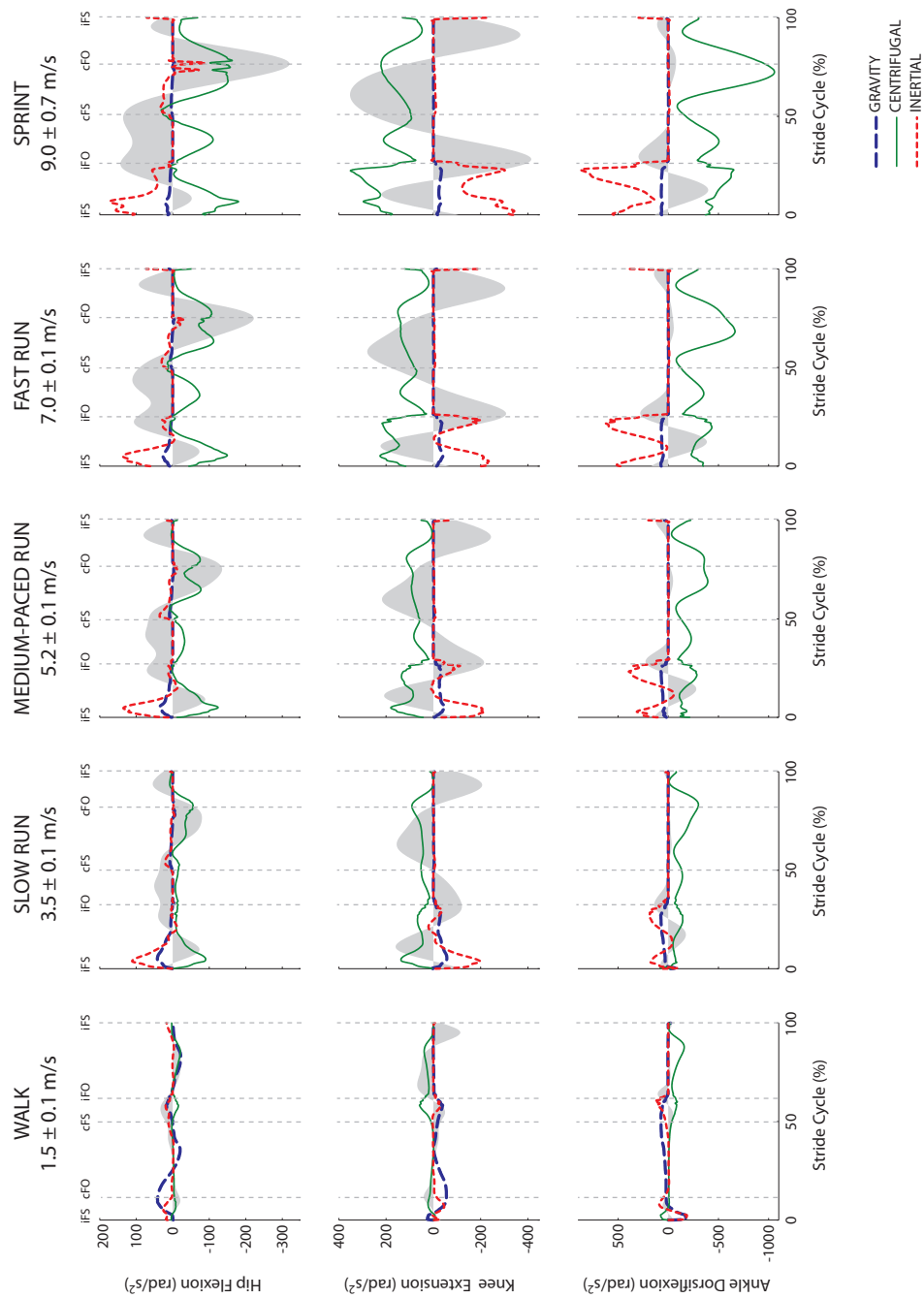


Figure C.14: Contributions of action force groups to the total sagittal joint angular acceleration (shaded regions) of the hip, knee and ankle for each speed of locomotion. Positive joint angular accelerations represent hip flexion, knee extension and ankle dorsiflexion; negative joint angular accelerations represent hip extension, knee flexion and ankle plantarflexion. Results were averaged across all trials for all subjects and are shown over a full stride cycle. Action force symbols as defined in the caption for Fig. C.12 .

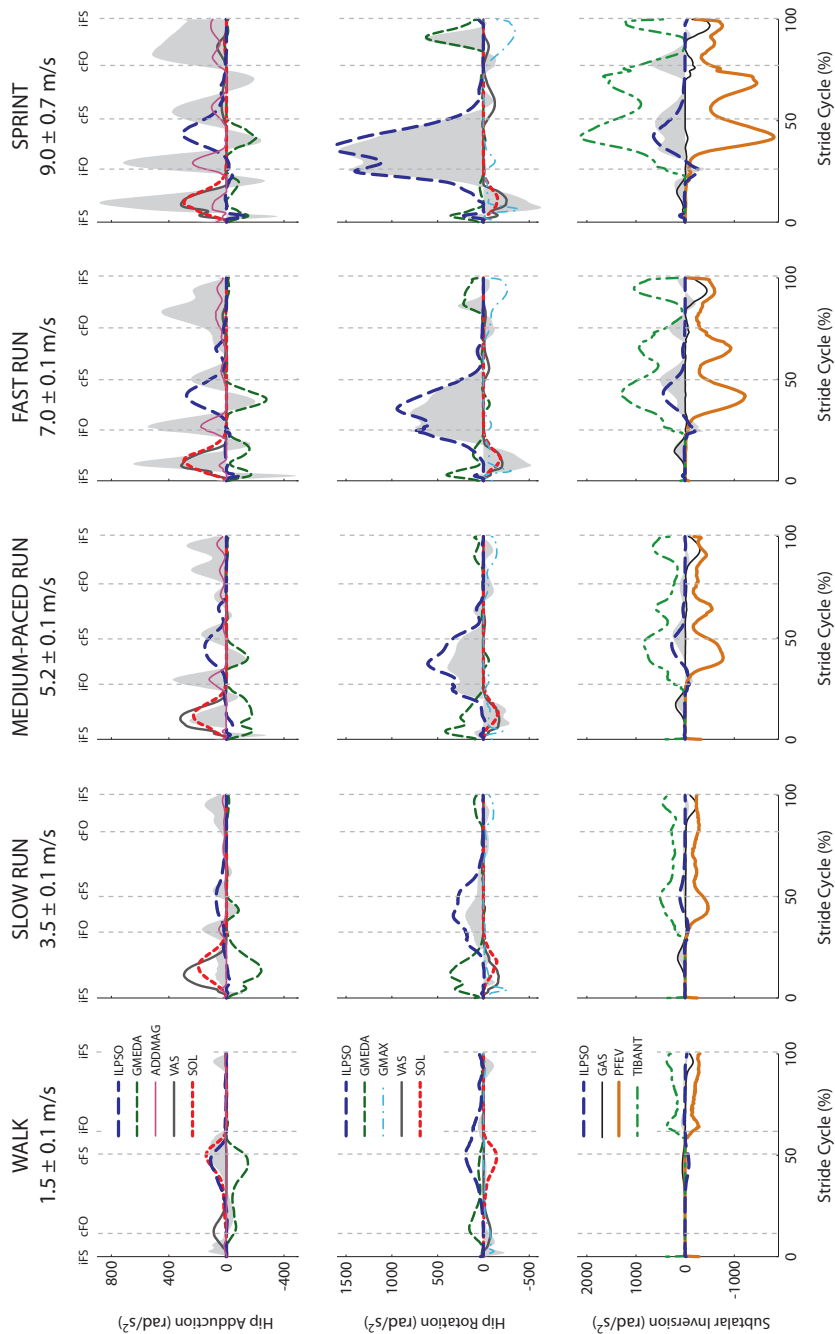


Figure C.15: Contributions of individual ipsilateral-leg muscles to the total ipsilateral-leg induced coronal and transverse plane joint angular acceleration (shaded regions) for each speed of locomotion. Positive joint moments represent hip adduction, hip internal rotation and subtalar inversion; negative joint moments represent hip abduction, hip external rotation and subtalar eversion. Results were averaged across all trials for all subjects and are shown over a full stride cycle. Muscle symbols as defined in the caption for Fig. C.5.

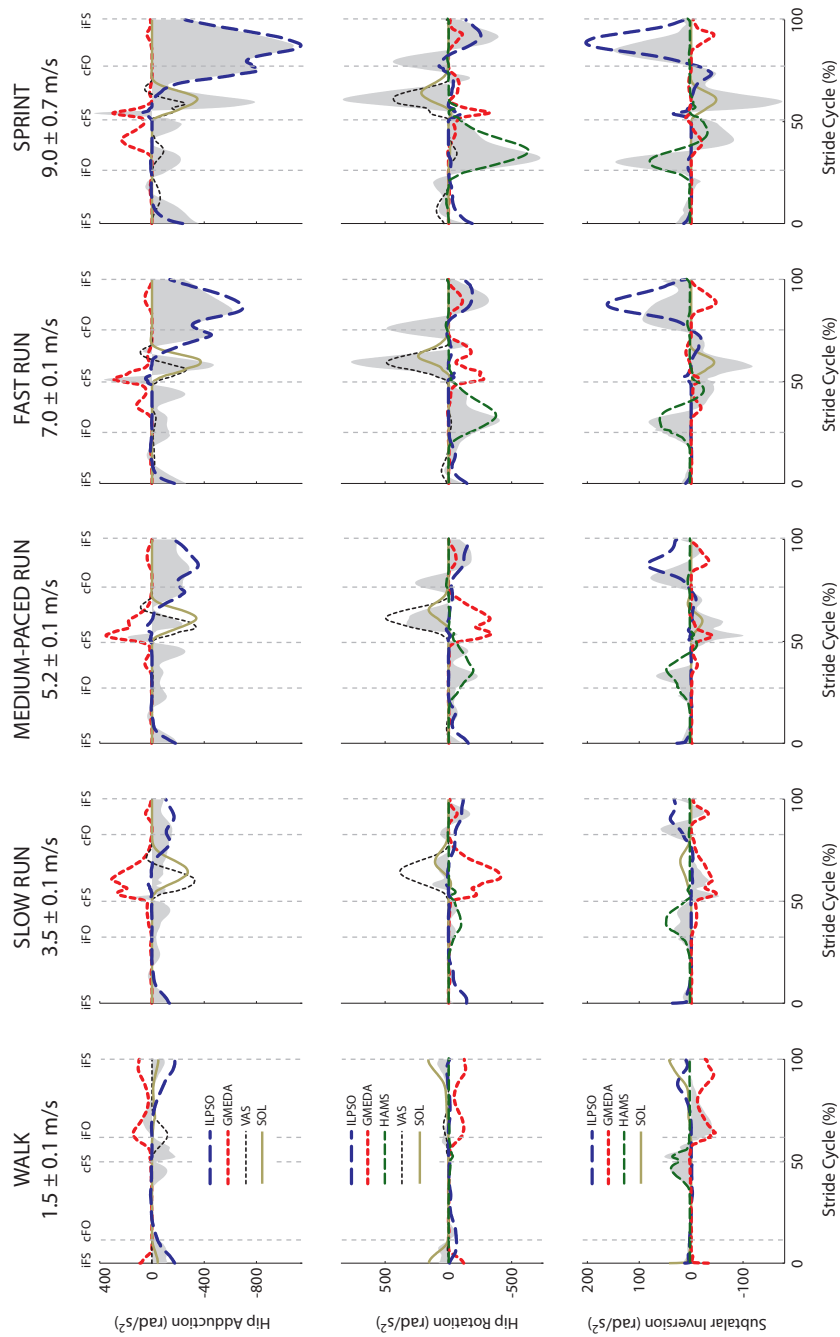


Figure C.16: Contributions of individual contralateral-leg muscles to the total contralateral-leg induced coronal and transverse plane joint angular acceleration (shaded regions) for each speed of locomotion. Positive joint moments represent hip adduction, hip internal rotation and subtalar inversion; negative joint moments represent hip abduction, hip external rotation and subtalar eversion. Results were averaged across all trials for all subjects and are shown over a full stride cycle. Muscle symbols as defined in the caption for Fig. C.5.

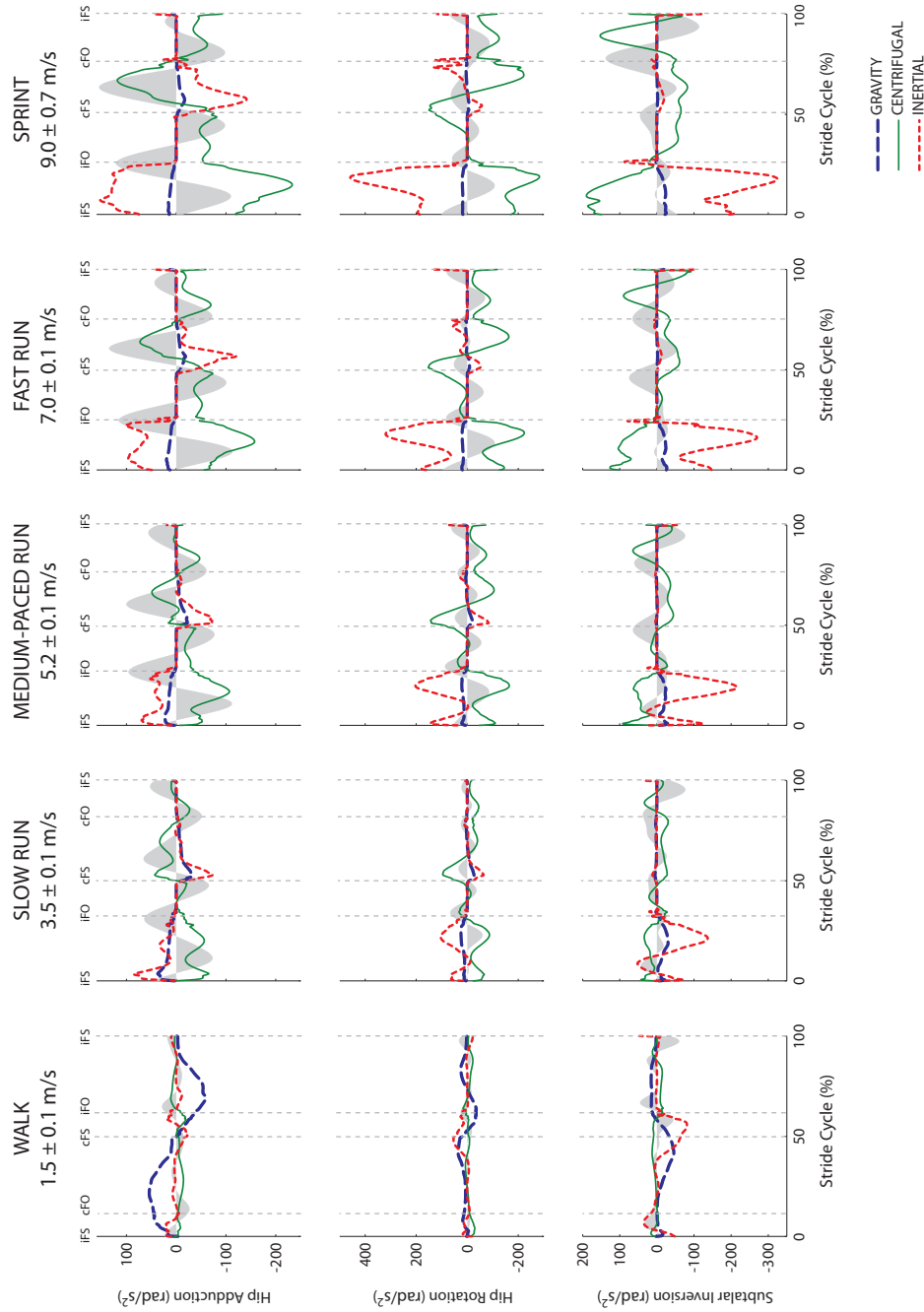
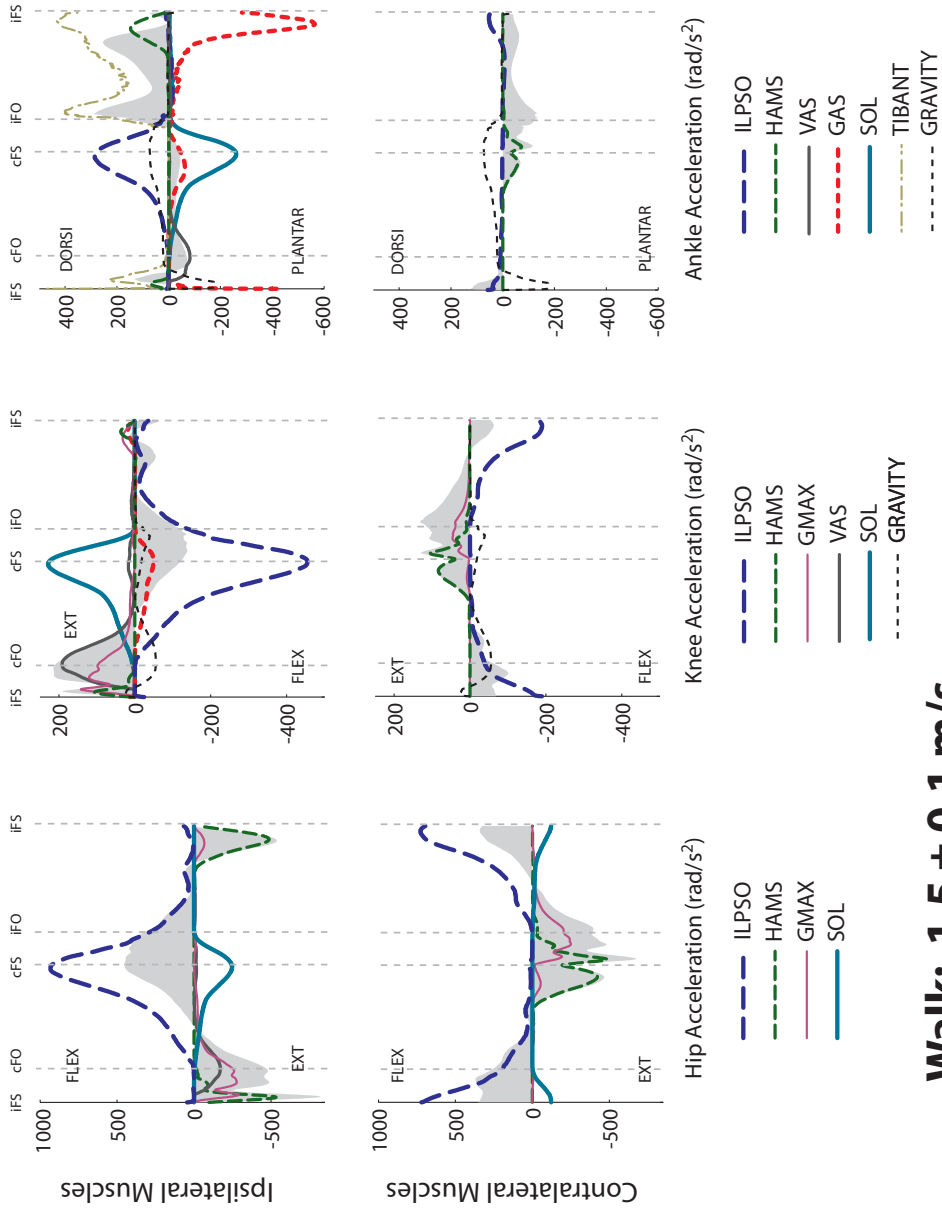


Figure C.17: Contributions of action force groups to the total coronal and transverse plane joint angular acceleration (shaded regions) for each speed of locomotion. Positive joint moments represent hip adduction, hip internal rotation and subtalar inversion; negative joint moments represent hip abduction, hip external rotation and subtalar eversion. Results were averaged across all trials for all subjects and are shown over a full stride cycle. Action force symbols as defined in the caption for Fig. C.12 .



Walk: 1.5 ± 0.1 m/s

Figure C.18: Contributions of individual ipsilateral (top) and contralateral (bottom) leg muscles to the net ipsilateral (top shaded region) and contralateral (bottom shaded region) joint angular accelerations during walking at 1.5 m/s. Results were averaged across all trials for all subjects and are shown over a full stride cycle. Muscle symbols as defined in the caption for Fig. C.5 .

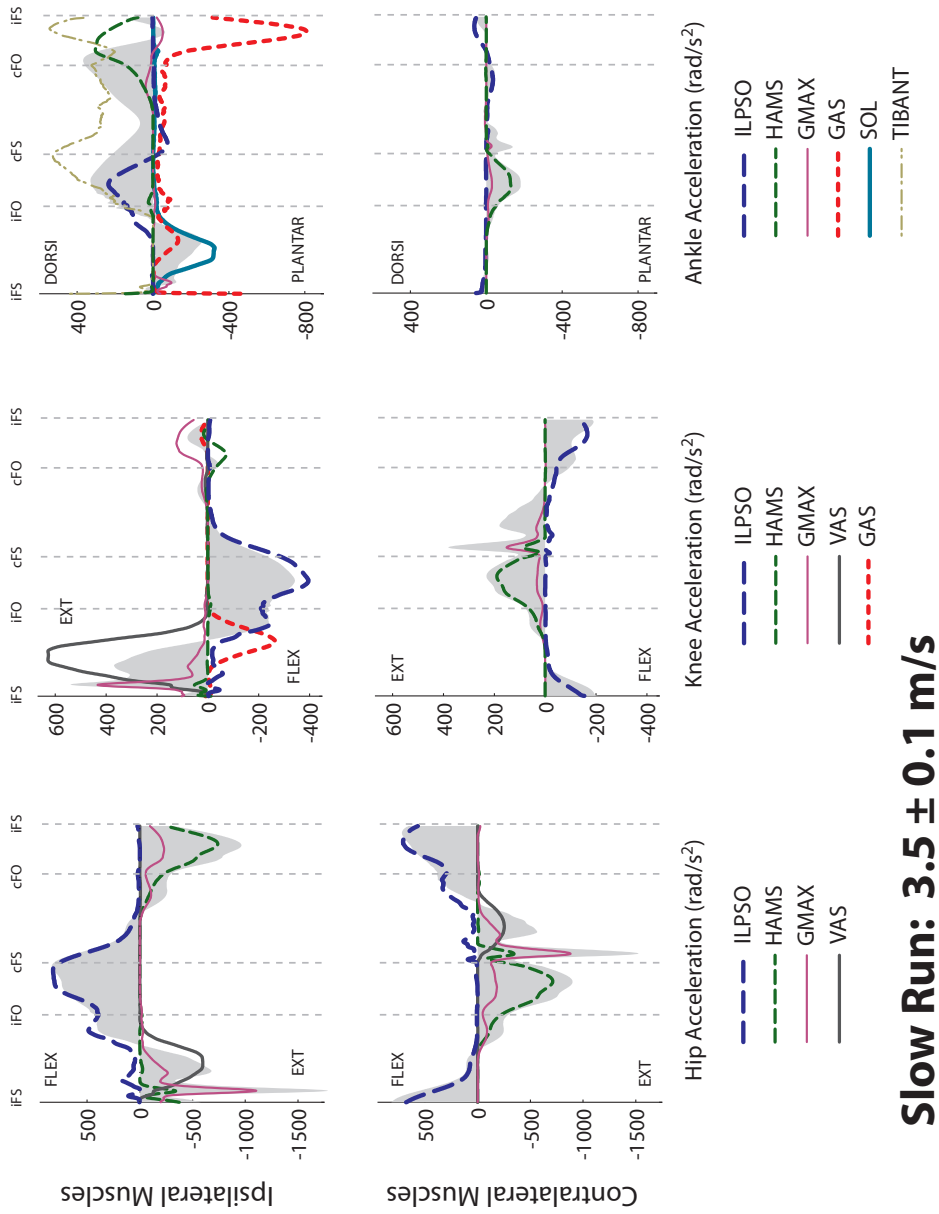
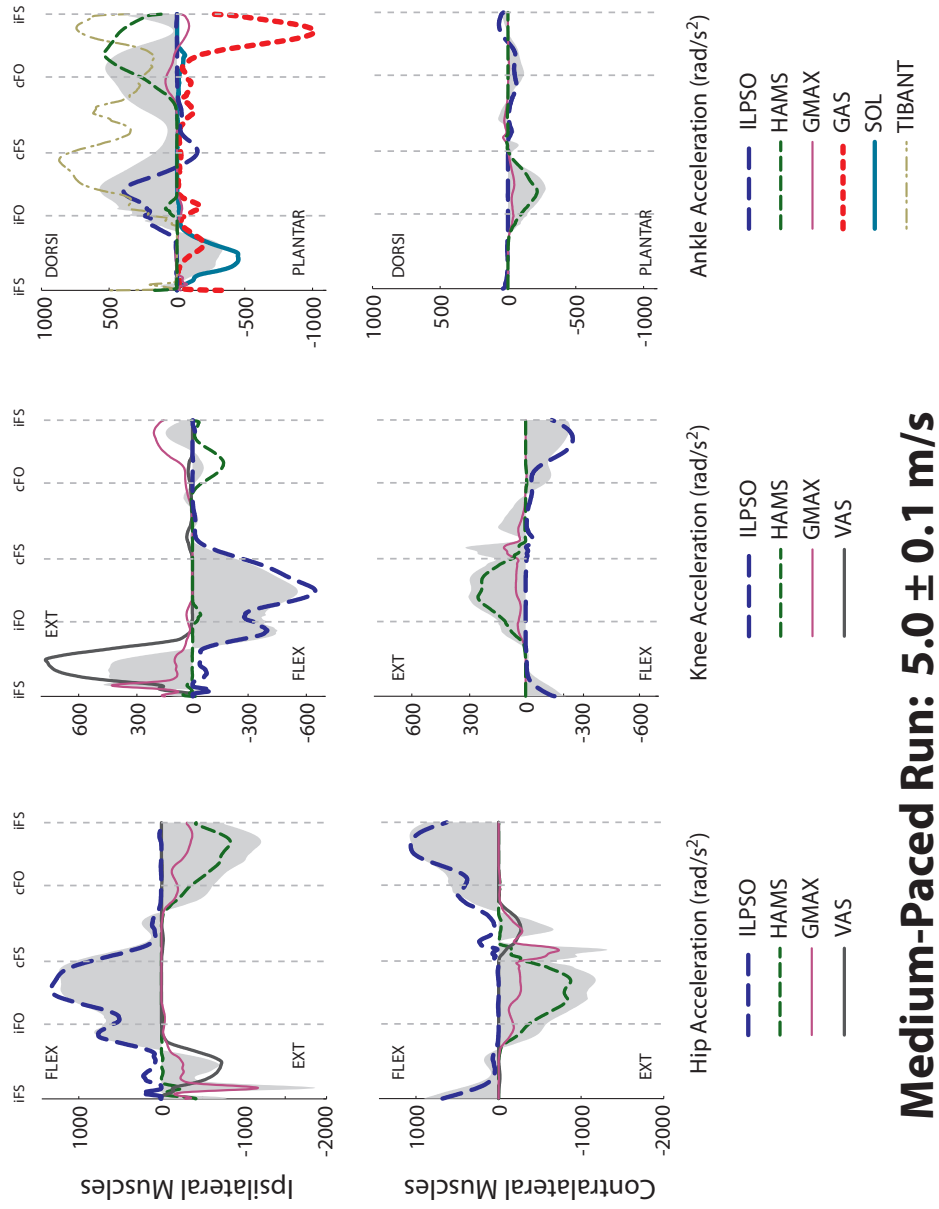
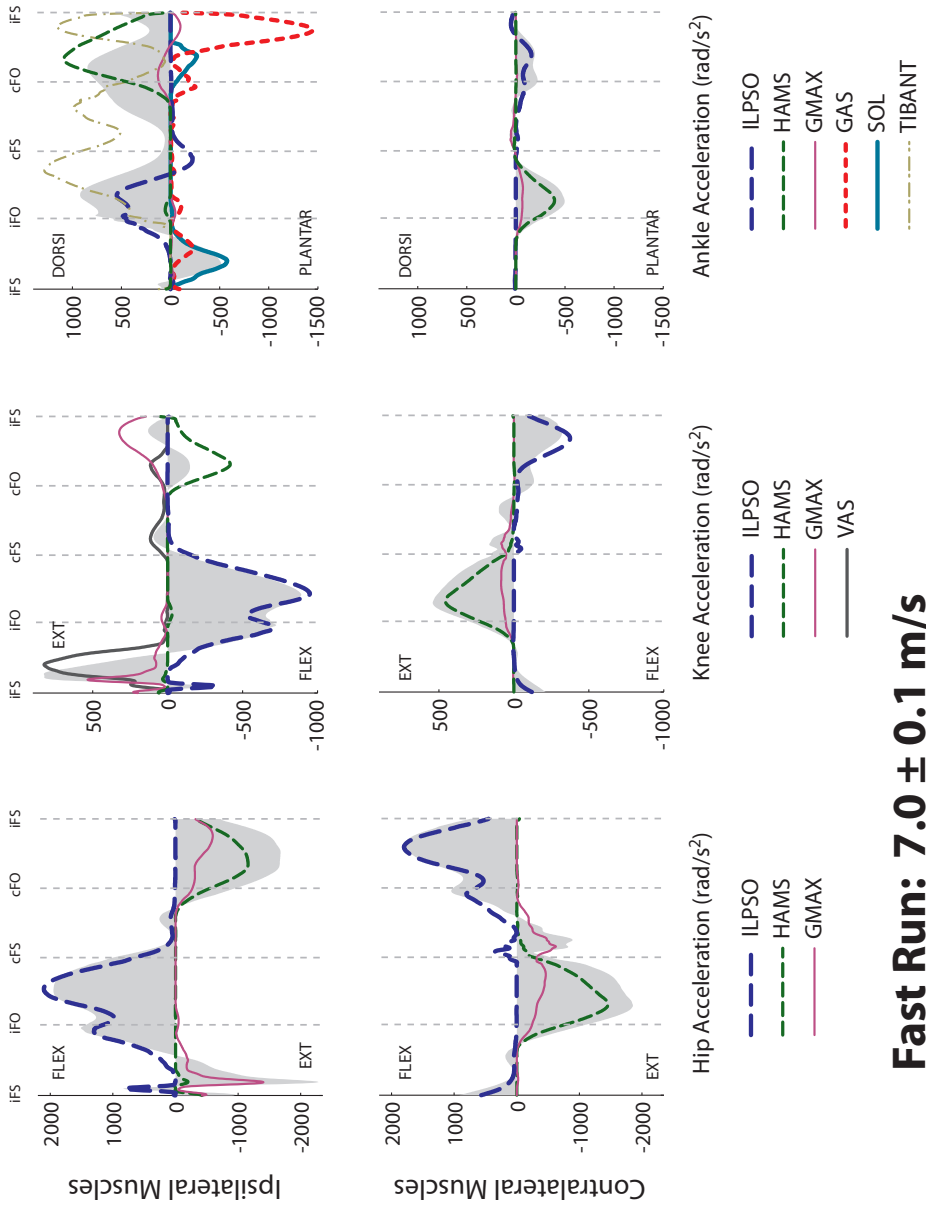


Figure C.19: Contributions of individual ipsilateral (top) and contralateral (bottom) leg muscles to the net ipsilateral (top shaded region) and contralateral (bottom shaded region) joint angular accelerations during running at 3.5 m/s. Results were averaged across all trials for all subjects and are shown over a full stride cycle. Muscle symbols as defined in the caption for Fig. C.5 .



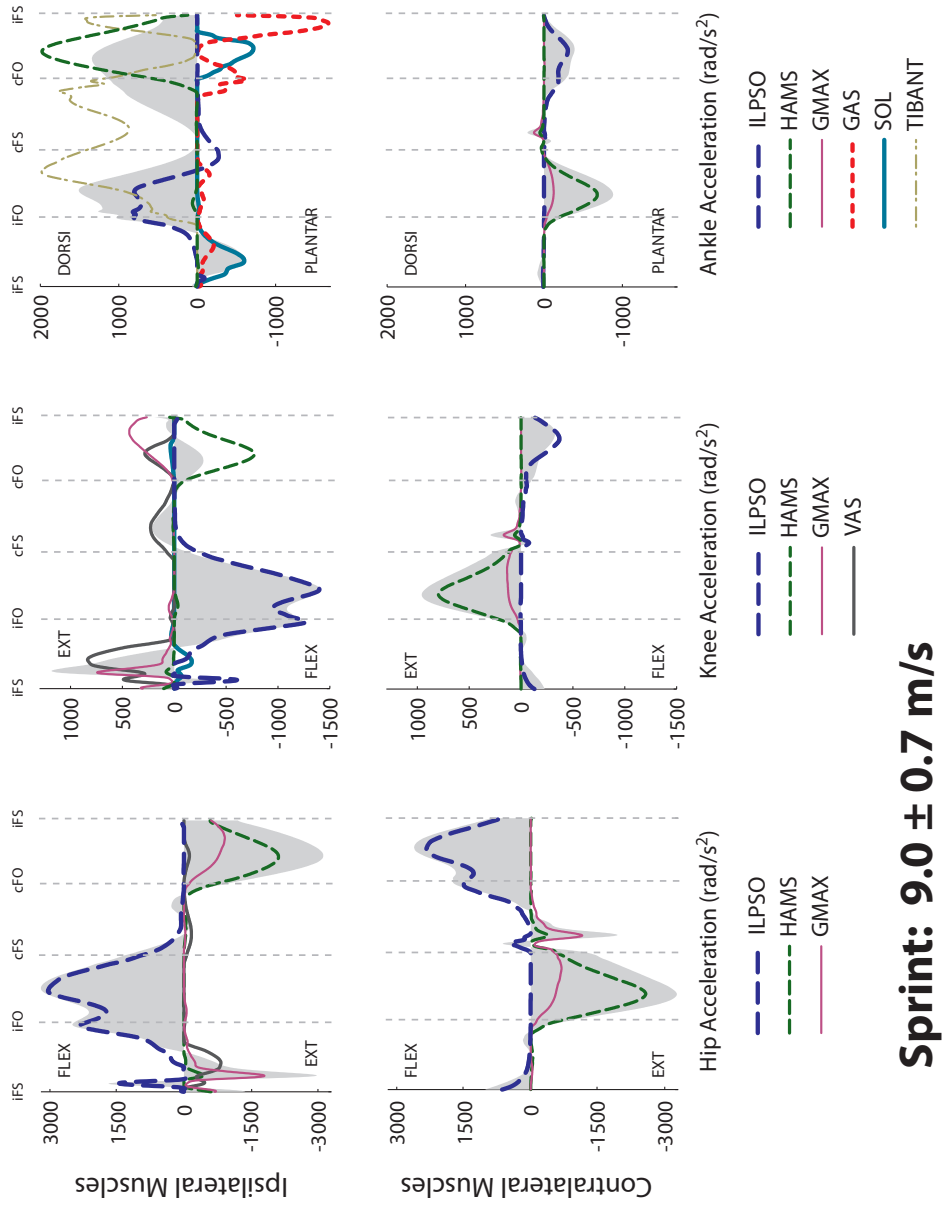
Medium-Paced Run: 5.0 ± 0.1 m/s

Figure C.20: Contributions of individual ipsilateral (top) and contralateral (bottom) leg muscles to the net ipsilateral (top shaded region) and contralateral (bottom shaded region) joint angular accelerations during running at 5.2 m/s. Results were averaged across all trials for all subjects and are shown over a full stride cycle. Muscle symbols as defined in the caption for Fig. C.5 .



Fast Run: 7.0 ± 0.1 m/s

Figure C.21: Contributions of individual ipsilateral (top) and contralateral (bottom) leg muscles to the net ipsilateral (top shaded region) and contralateral (bottom shaded region) joint angular accelerations during running at 7.0 m/s. Results were averaged across all trials for all subjects and are shown over a full stride cycle. Muscle symbols as defined in the caption for Fig. C.5 .



Sprint: 9.0 ± 0.7 m/s

Figure C.22: Contributions of individual ipsilateral (top) and contralateral (bottom) leg muscles to the net ipsilateral (top shaded region) and contralateral (bottom shaded region) joint angular accelerations during sprinting at 9.0 m/s. Results were averaged across all trials for all subjects and are shown over a full stride cycle. Muscle symbols as defined in the caption for Fig. C.5 .

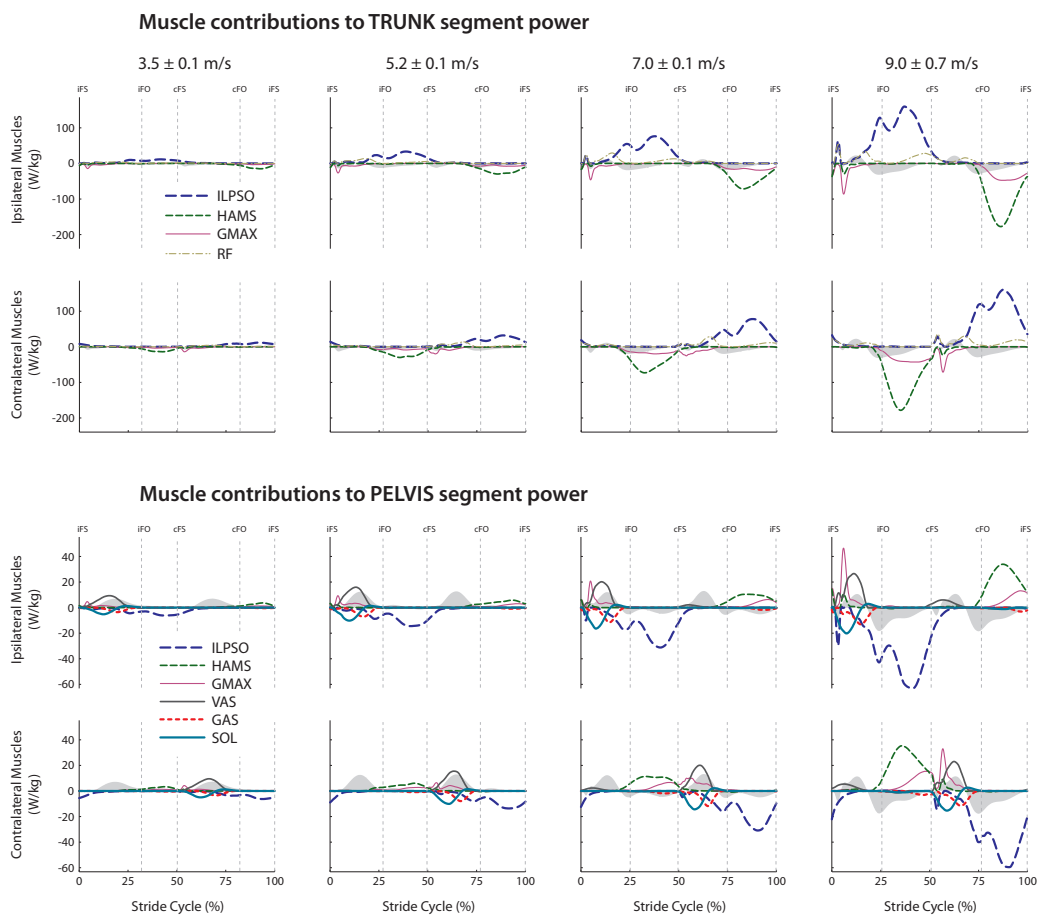


Figure C.23: Contributions of individual leg muscles to the net segment power (shaded regions) of the TRUNK and PELVIS segments. Refer to Section 3.2.6 for how net segment power was calculated. Results were averaged across all trials for all subjects and are shown over a full stride cycle. Muscle symbols as defined in the caption for Fig. C.5 .

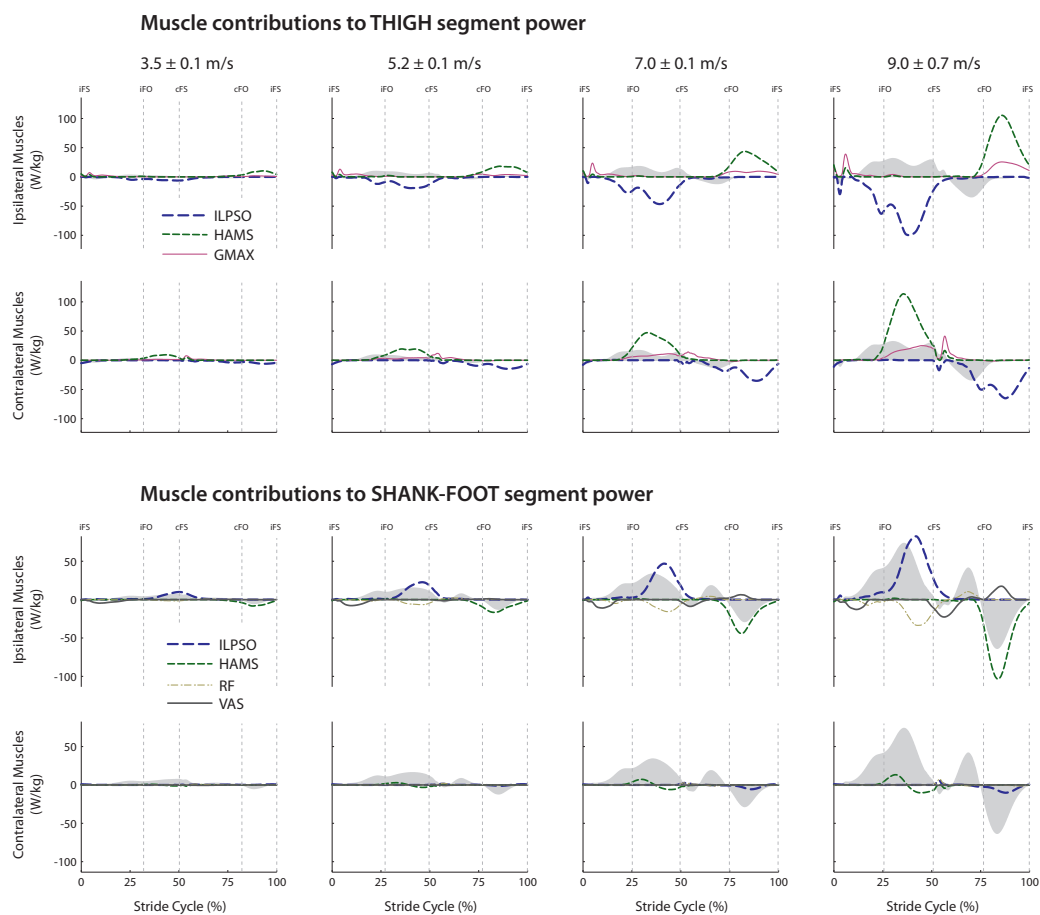


Figure C.24: Contributions of individual leg muscles to the net segment power (shaded regions) of the THIGH and SHANK-FOOT segments. Refer to Section 3.2.6 for how net segment power was calculated. Results were averaged across all trials for all subjects and are shown over a full stride cycle. Muscle symbols as defined in the caption for Fig. C.5

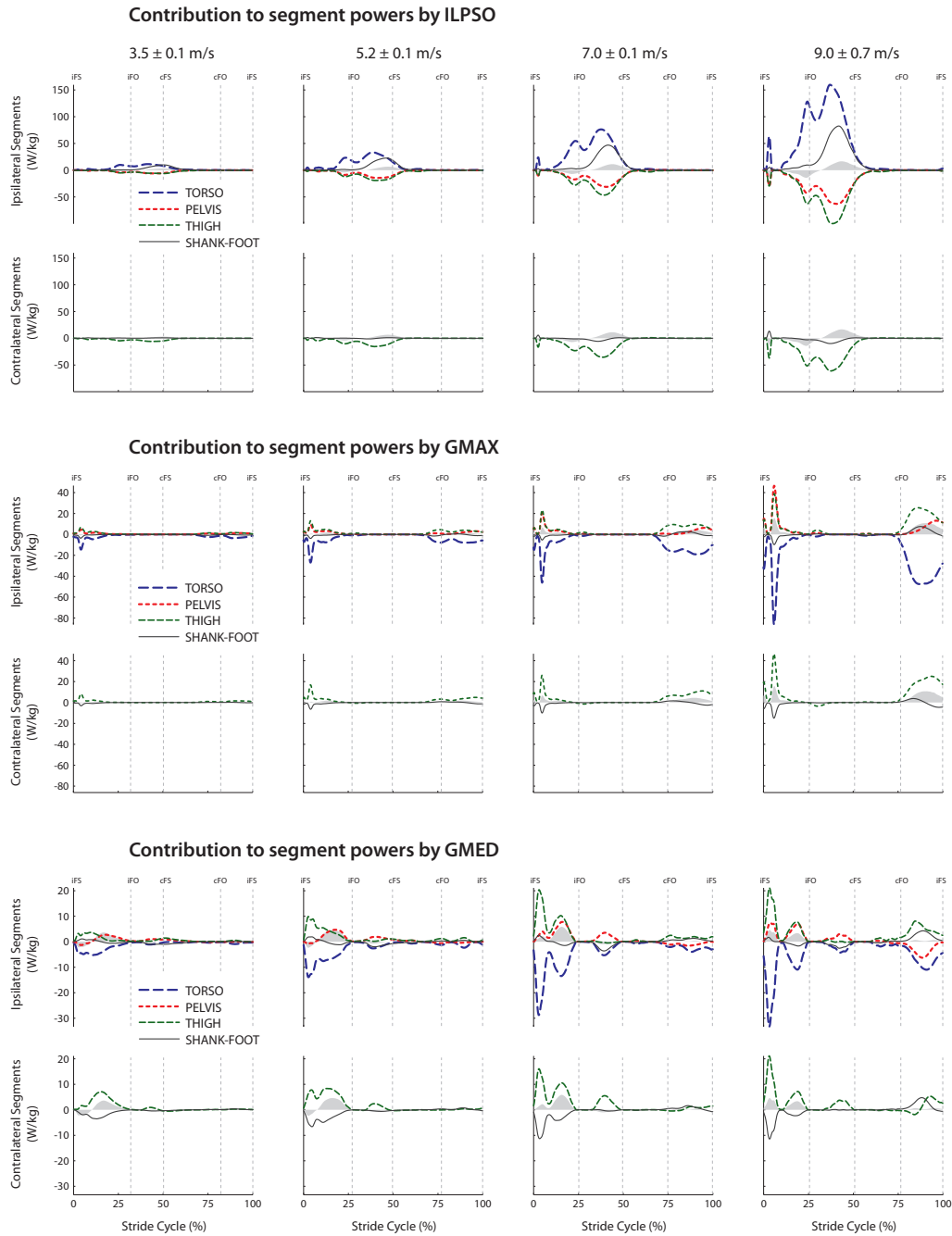


Figure C.25: Distribution of net muscle power from ILPSO, GMAX and GMED (shaded regions) to the segments of the body. Refer to Section 3.2.6 for how net muscle power was calculated. Results were averaged across all trials for all subjects and are shown over a full stride cycle.

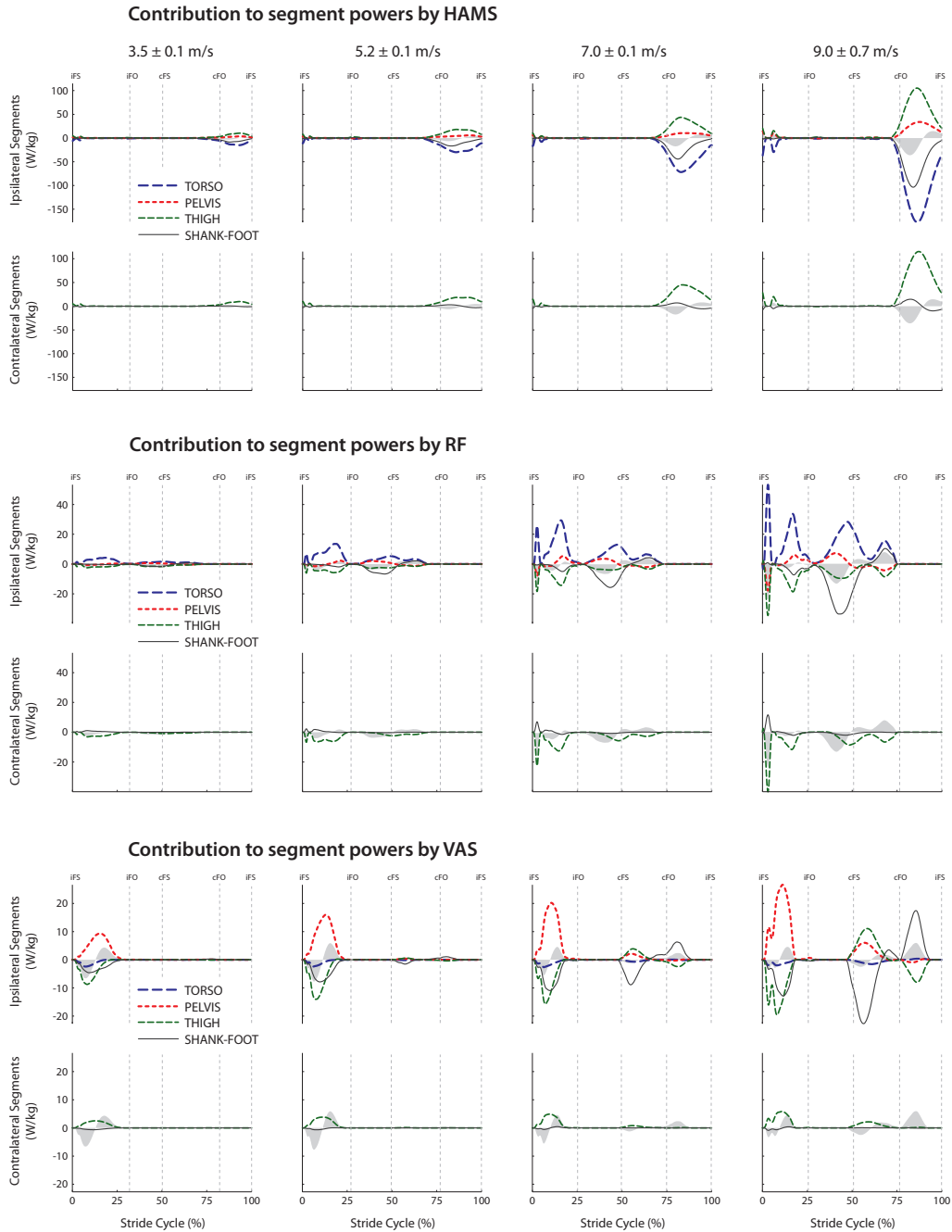


Figure C.26: *Distribution of net muscle power from HAMS, RF and VAS (shaded regions) to the segments of the body. Refer to Section 3.2.6 for how net muscle power was calculated. Results were averaged across all trials for all subjects and are shown over a full stride cycle.*

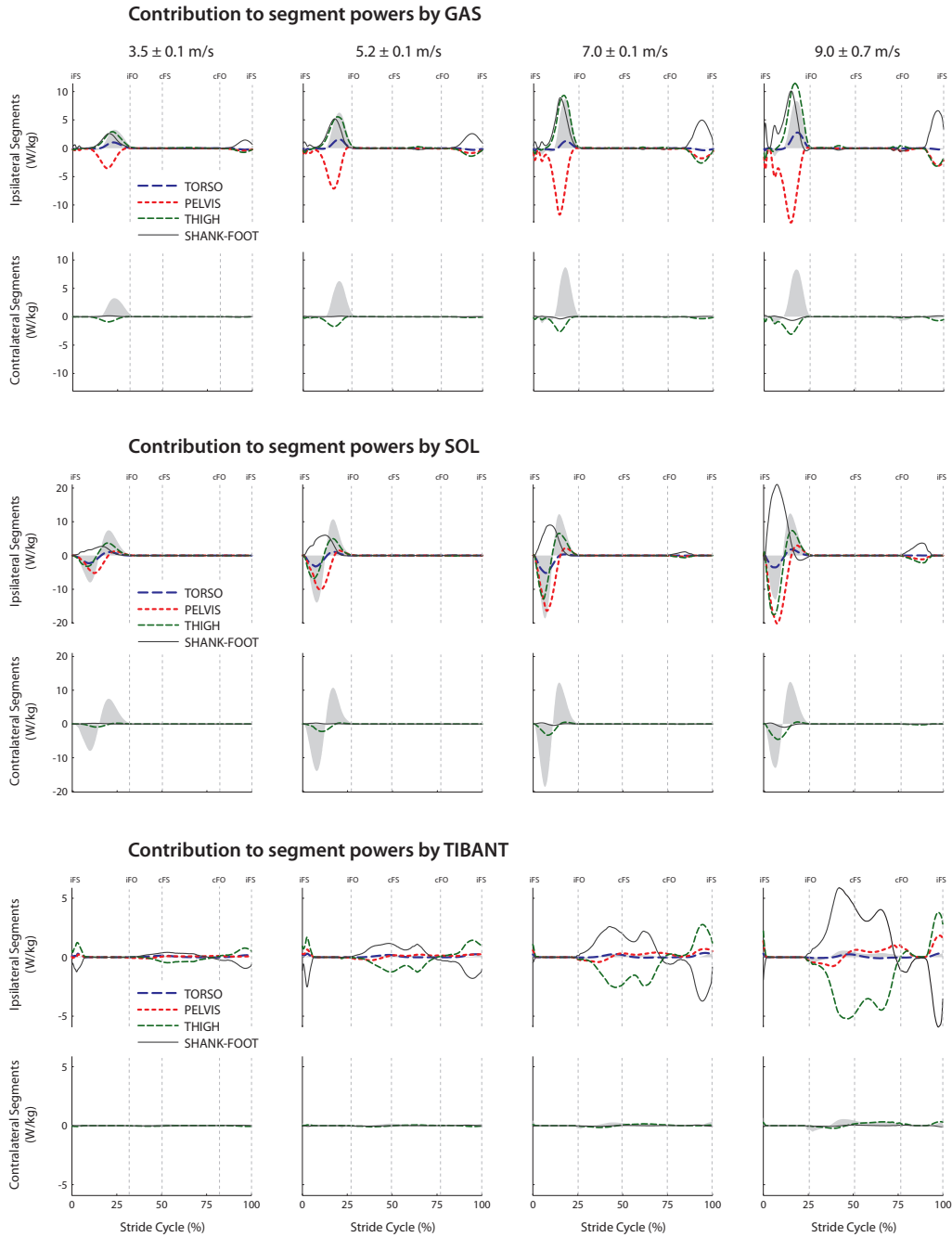


Figure C.27: *Distribution of net muscle power from GAS, SOL and TIBANT (shaded regions) to the segments of the body. Refer to Section 3.2.6 for how net muscle power was calculated. Results were averaged across all trials for all subjects and are shown over a full stride cycle.*

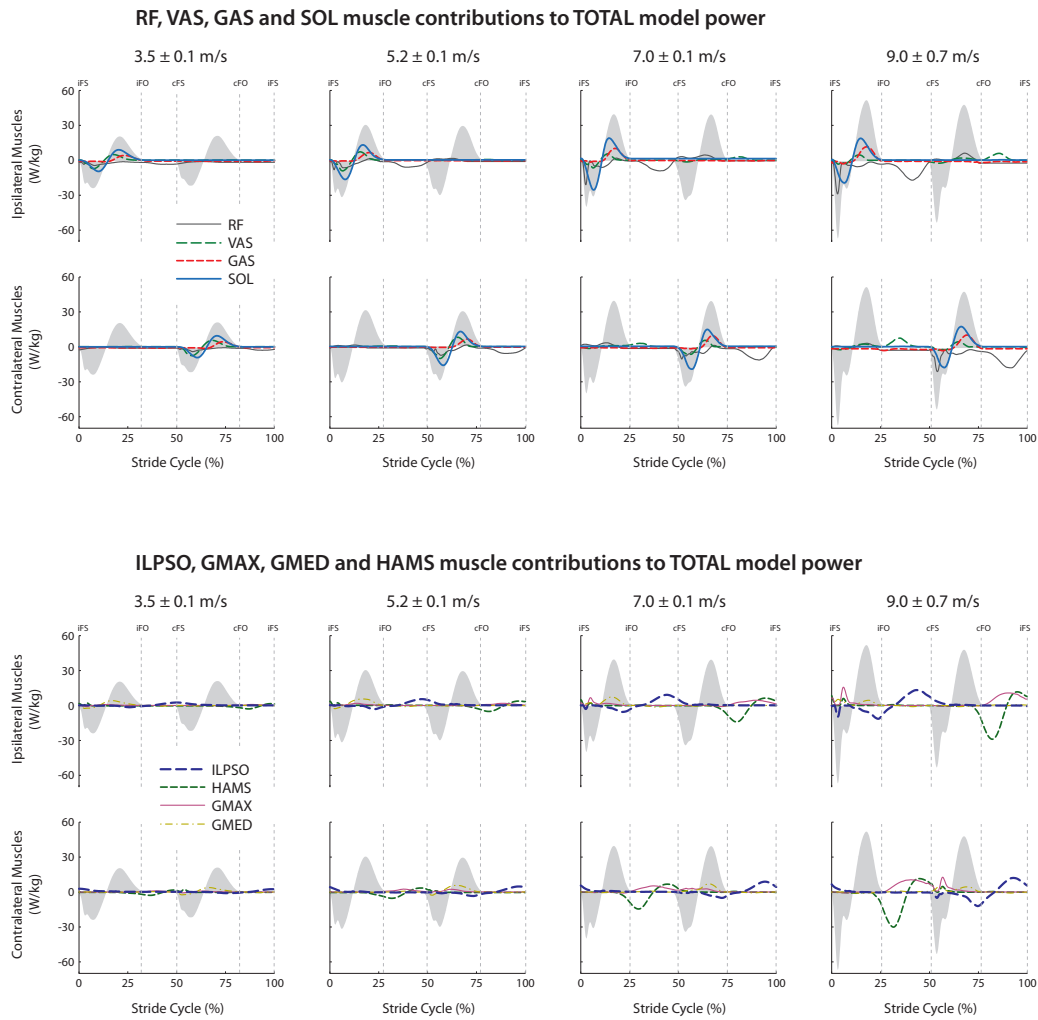


Figure C.28: Contribution of individual muscle powers to the total model power (shaded regions). (A) Contribution of RF, VAS, GAS and SOL; (B) Contribution of ILPSO, HAMS, GMAX and GMED. Results were averaged across all trials for all subjects and are shown over a full stride cycle. Muscle symbols as defined in the caption for Fig. C.5 .

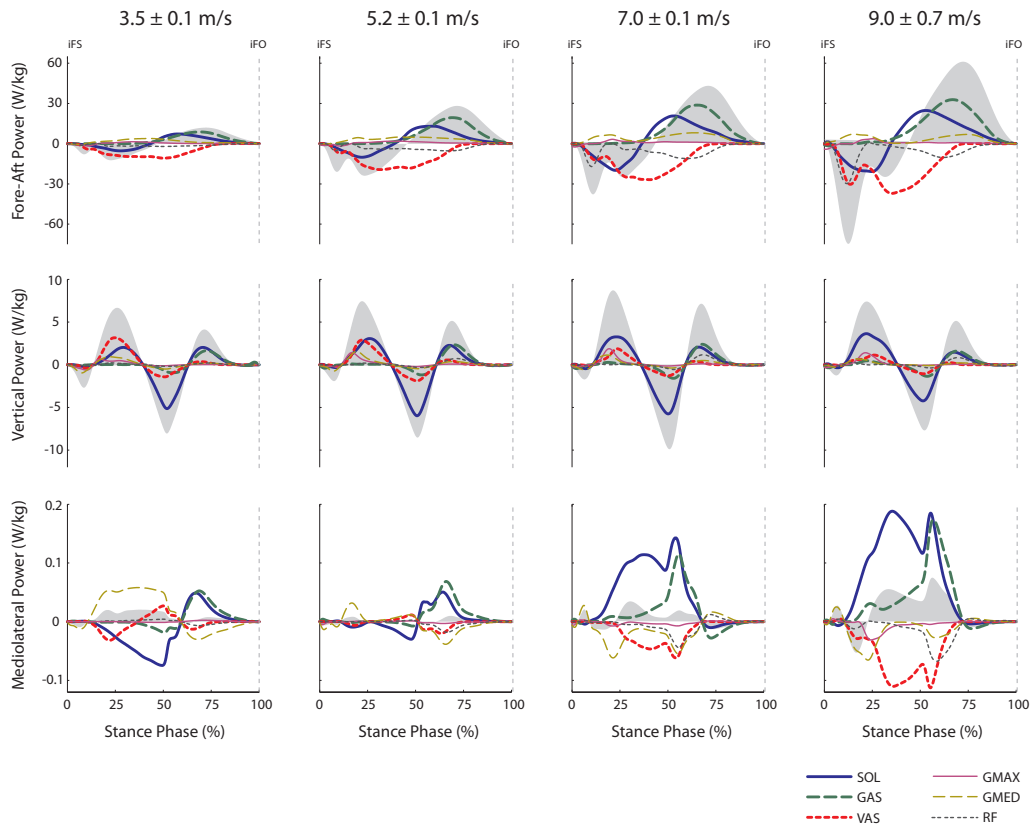


Figure C.29: Contribution of individual muscles to the fore-aft, vertical and mediolateral components of total model power (shaded regions). Each component of power was computed as the product of the same component of ground reaction force and center-of-mass velocity. Muscle symbols as defined in the caption for Fig. C.5 .

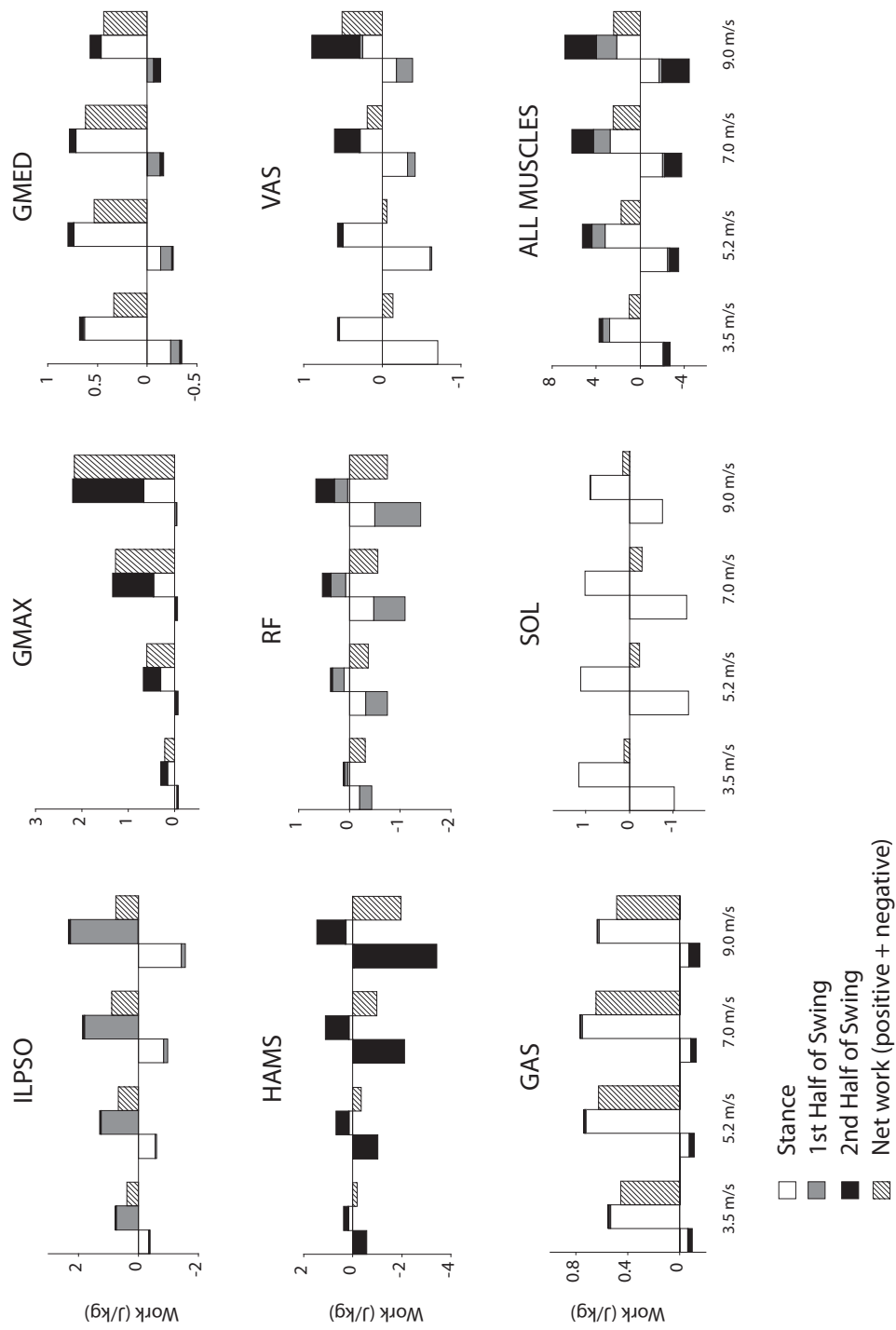


Figure C.30: Work done by individual ipsilateral-leg muscles over a full stride cycle. Positive work (generation), negative work (absorption) and net work is shown for each running speed. For the bar plots displaying positive and negative work, results were further split into (i) stance; and (ii) first half of swing; and (iii) second half of swing. Mid-swing was defined as half way between ipsilateral foot off and ipsilateral foot strike. Muscle symbols as defined in the caption for Fig. C.5 .

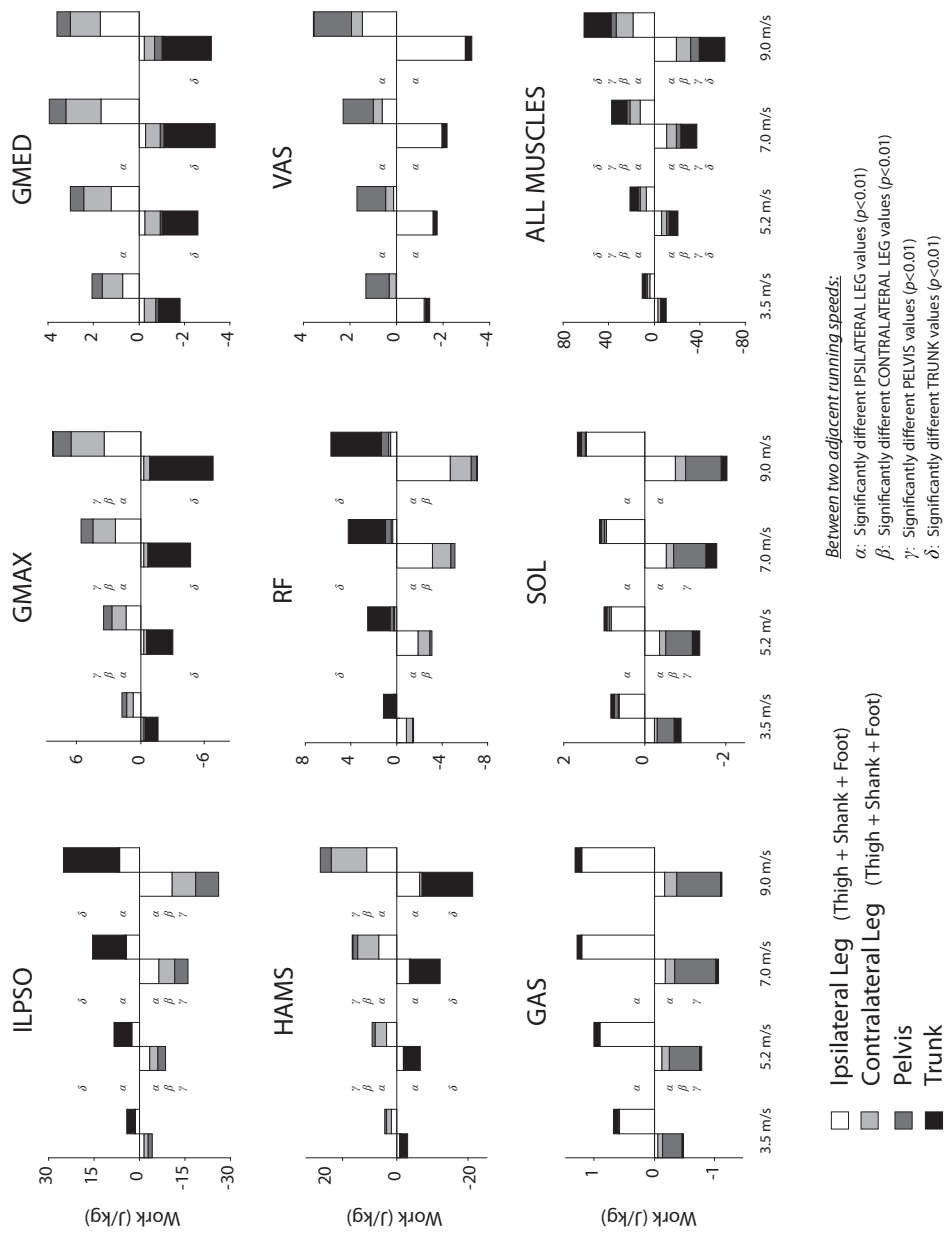


Figure C.31: Work generated to and absorbed from limb segments by ipsilateral-leg muscles over a full stride cycle. Positive work (generation) and negative work (energy absorption) is shown for each running speed. Results were divided into four segment groups: (i) ipsilateral leg; (ii) contralateral leg; (iii) pelvis; and (iv) trunk. Muscle symbols as defined in the caption for Fig. C.5 .

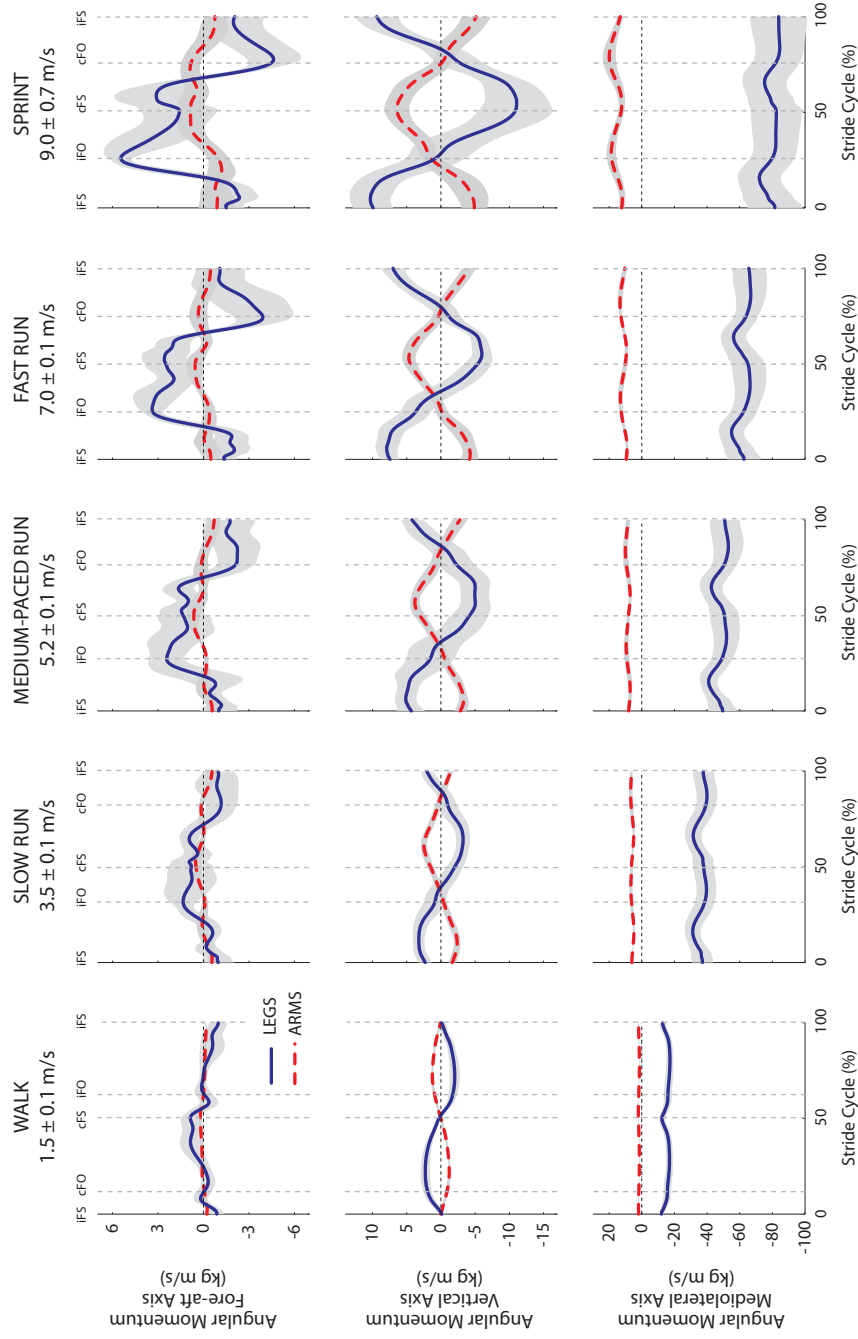


Figure C.32: Angular momentum of all leg segments (solid line) and arm segments (dashed line) computed about the horizontal axis (X), vertical axis (Y) and mediolateral axis (Z) passing through the whole-body center-of-mass. Results were averaged across all trials for all subjects and are shown over a full stride cycle for each speed of locomotion.

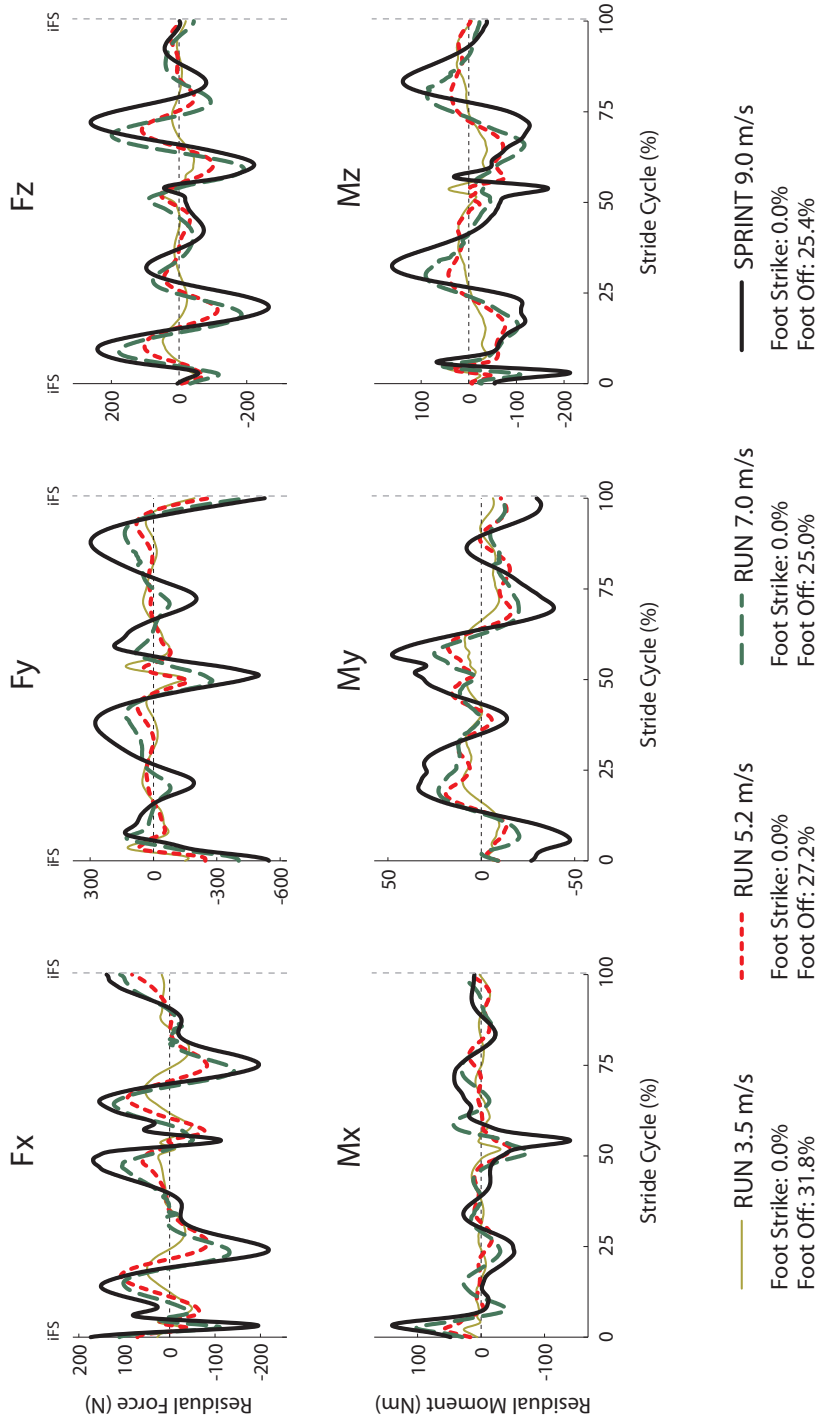


Figure C.33: Residual forces (top) and moments (bottom) between the pelvis and external environment for each running speed. X = anterior/posterior direction; Y = vertical direction; Z = medial/lateral direction. Results were averaged across all trials for all subjects.

Appendix **D**

Supplementary publications

This appendix contains a set of co-authored supplementary publications related to but not directly part of this dissertation:

Peer-reviewed journal articles

- **Lin, Y.C., Dorn, T.W., Schache, A.G., Pandy, M.G. (2011).** Comparison of different methods for estimating muscle forces in human movement, *Journal of Engineering in Medicine*, In press.
- **Schache, A.G., Blanch, P.D., Dorn, T.W., Brown, N.A., Rosemond, D., Pandy, M.G. (2011).** Effect of Running Speed on Lower-Limb Joint Kinetics, *Medicine & Science in Sports & Exercise*, 43(7):1260-1271.
- **Schache, A.G., Dorn, T.W., Blanch, P.D., Brown, N.A., Pandy, M.G. (2011).** Mechanics of the human hamstring muscles during sprinting, *Medicine & Science in Sports & Exercise*, In press.

Conference proceedings

- **Dorn, T.W., Lin, Y.C., Pandy, M.G. (2011).** Estimates of leg-muscle function in human gait depend on how foot-ground contact is modeled, *International Society of Biomechanics: Technical group on Computer Simulation in Biomechanics - 13th Biennial International Symposium, June 30 - July 2, 2011, Leuven, Belgium.*
- **Dorn, T.W., Schache, A.G., Pandy, M.G. (2011).** Biomechanical strategies for increasing running speed, *23rd International Society of Biomechanics Congress, July 3 - July 7, 2011, Brussels, Belgium.*
- **Dorn, T.W., Schache, A.G., Pandy, M.G. (2011).** Muscle coordination of human sprinting, *23rd International Society of Biomechanics Congress, July 3 - July 7, 2011, Brussels, Belgium.*
- **Dorn, T.W., Lin, Y.C., Schache, A.G., Pandy, M.G. (2012).** Which muscles power the human running stride?, *American Society of Mechanical Engineers 2012 Summer Bioengineering Conference, June 20 - June 23, 2012, Fajardo, Puerto Rico.*

Comparison of Different Methods For Estimating Muscle Forces In Human Movement

*Proc IMechE, Part H:
J Engineering in Medicine*
0(0) 1–10
© The Author(s) 2011
Reprints and permissions:
sagepub.co.uk/journalsPermissions.nav
DOI: 10.1177/0954411911429401
pjh.sagepub.com


Yi-Chung Lin¹, Tim W. Dorn¹, Anthony G. Schache¹ and Marcus G. Pandy¹

Abstract

The aim of this study was to compare muscle-force estimates derived for human locomotion using three different methods commonly reported in the literature: static optimisation (SO), computed muscle control (CMC) and neuromusculoskeletal tracking (NMT). In contrast with SO, CMC and NMT calculate muscle forces dynamically by including muscle activation dynamics. Furthermore, NMT utilises a time-dependent performance criterion, wherein a single optimisation problem is solved over the entire time interval of the task. Each of these methods was used in conjunction with musculoskeletal modelling and experimental gait data to determine lower-limb muscle forces for self-selected speeds of walking and running. Correlation analyses were performed for each muscle to quantify differences between the various muscle-force solutions. The patterns of muscle loading predicted by the three methods were similar for both walking and running. The correlation coefficient between any two sets of muscle-force solutions ranged from 0.46 to 0.99 ($p < 0.001$ for all muscles). These results suggest that the robustness and efficiency of static optimisation make it the most attractive method for estimating muscle forces in human locomotion.

Keywords

Inverse dynamics, forward dynamics, joint torque, gait biomechanics, walking, running, motion simulation

Date received: ; accepted:

Introduction

Accurate knowledge of muscle forces is essential for characterising muscle function and for developing new methods for treating patients with movement disorders.¹ Because direct measurement of muscle forces in vivo is not possible, joint kinematic and ground reaction force data from gait analysis experiments are often used in conjunction with musculoskeletal modelling to predict muscle forces non-invasively.^{2,3}

One of the main challenges in applying computational modelling is the muscle-moment redundancy problem.⁴ Because each joint is spanned by several muscles, a net joint moment can be produced by an infinite number of muscle recruitment solutions. Inverse and forward-dynamics techniques have been widely used to solve this indeterminate problem.^{2,3} The inverse-dynamics method uses the experimental joint kinematics and ground reaction force data as input to a musculoskeletal model to calculate the net joint moments applied

about each joint. The muscle-moment redundancy problem is then solved at each time instant using static optimisation to minimise a given performance criterion (e.g. sum of squares of muscle activations^{2,5,6}). While static optimisation is computationally efficient, it is not designed to incorporate time-dependent muscle properties such as the time delay in the transformation of neural excitation to muscle activation (i.e. muscle activation dynamics), or time-dependent performance criteria such as minimum muscular effort⁷⁻⁹ or minimum metabolic energy consumption.¹⁰

¹Dept of Mechanical Engineering, University of Melbourne, Parkville, AUSTRALIA

Corresponding author:

Marcus G. Pandy, Ph.D., Department of Mechanical Engineering, University of Melbourne, Parkville, Victoria 3010, Australia.
Phone + 61 3 8344 4054; Fax + 61 3 8344 4290
Email: pandym@unimelb.edu.au

In contrast, the forward-dynamics method uses neural excitation signals as inputs to a model of the neuromusculoskeletal system. The equations representing muscle activation dynamics, muscle contraction dynamics and body-segmental dynamics are integrated simultaneously to predict the resulting joint motion. Dynamic optimisation or optimal control has been used to predict joint motion and ground reaction forces in walking by minimising the muscle metabolic energy consumed over a full stride cycle.^{10,11} Unfortunately, the vast computation time needed to converge to a solution makes this approach practically infeasible.^{10,11} Computed muscle control (CMC)^{12,13} and neuromusculoskeletal tracking (NMT)⁸ are two recent approaches designed for generating forward-dynamics simulations of movement more efficiently. Both methods use feedback control theory to generate a stable simulation while including muscle activation dynamics to account for the time delay in muscle-force development. Although CMC and NMT are conceptually similar, they differ in the approach used to solve the muscle-moment redundancy problem. Whereas the CMC method uses static optimisation to resolve the muscle redundancy problem at each instant along the movement trajectory (see Figure 1 in Thelen and Anderson¹²), NMT solves the same problem dynamically by minimising a time-dependent performance criterion over the entire period of the task (see equation (11) in Seth and Pandey⁸).

Anderson and Pandey⁶ quantitatively compared lower-limb muscle forces obtained from static and

dynamic optimisation solutions of normal walking and found no significant differences between these two approaches. They concluded that static optimisation provides reasonable predictions of muscle forces when accurate joint moments are available, and suggested that the use of the more time-consuming dynamic optimisation approach is less justified. This conclusion, however, was based on simulated gait data rather than actual gait measurements. It is also unclear whether this finding applies to motor tasks characterised by more rapid joint movements such as running. Although a number of studies have used both inverse and forward-dynamics methods to study muscle function during running,¹⁴⁻¹⁸ none of these studies have conducted a quantitative comparison of the muscle-force solutions obtained from these two methods.

The overall goal of the present study was to compare muscle-force estimates derived for human locomotion using three different methods commonly reported in the literature: static optimisation (SO), CMC and NMT. Muscle-actuated simulations of walking and running were generated for a single subject by combining musculoskeletal modelling and biomechanical gait experiments. In contrast to the study by Anderson and Pandey,¹⁰ muscle forces were calculated using measurements of joint motion and ground reaction forces as inputs to each method. The specific aim of this paper is to determine the extent to which inclusion of muscle activation dynamics and/or a time-dependent performance criterion influences predictions of lower-limb muscle forces for walking and running.

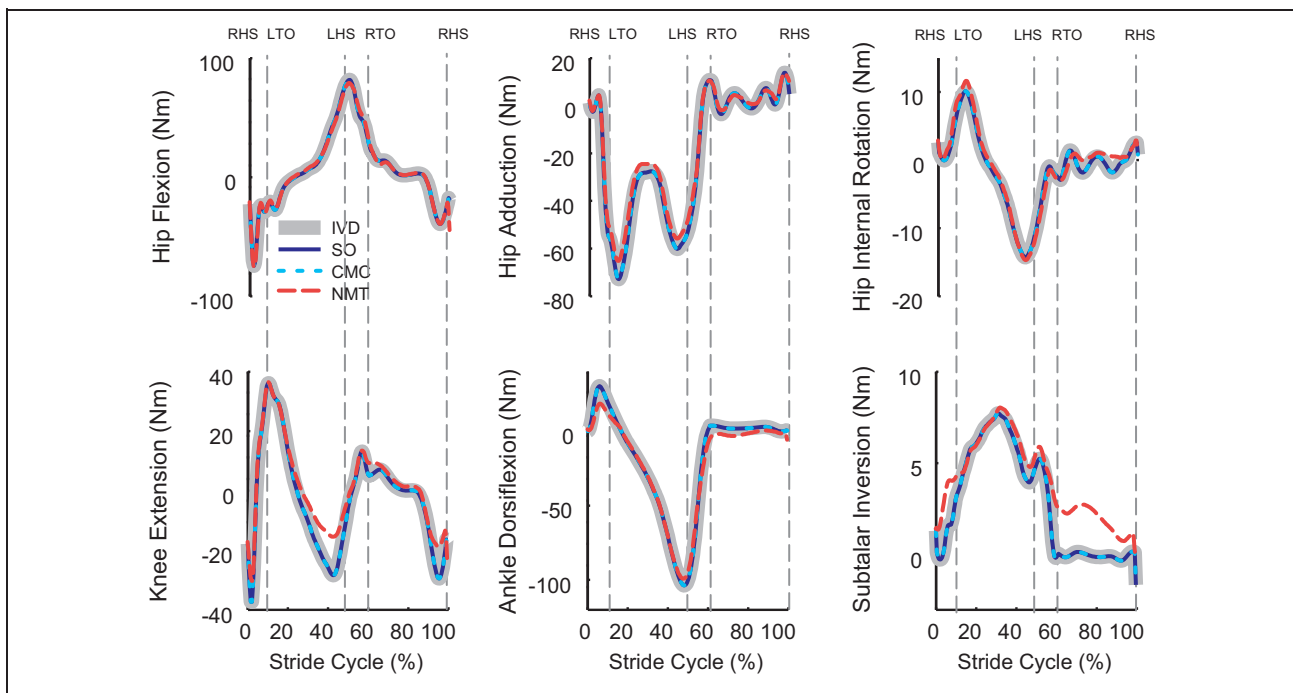


Figure 1. Comparison of net joint moments computed from IVD and net joint moments resulting from three muscle-force solutions (SO, CMC and NMT) for walking at the preferred speed.

Methods

Gait experiments

Data were collected from one healthy female adult (age: 25 years; height: 177 cm; mass: 64 kg) in the Biomechanics Laboratory at the Australian Institute of Sport. The subject provided informed written consent after approval was obtained from the relevant institutional ethics committees. Marker-derived kinematic data were acquired using a three-dimensional motion analysis system (Vicon, Oxford Metrics, Oxford, UK). Small reflective markers (14 mm) were mounted on the trunk and both lower limbs. Marker trajectories were recorded using 22 optical infrared cameras sampling at 250 Hz as the subject walked and ran at her preferred speeds (walking: 1.61 m/s; running: 3.48 m/s) along a synthetic track. A fourth-order Butterworth low-pass filter (4 Hz) was used to smooth the marker trajectories. Ground reaction forces were measured simultaneously using eight force plates (Kistler Instrument Corp., Amherst, New York, USA) arranged in series along the track. The force plate data were low-pass filtered with a fourth-order Butterworth filter (60 Hz) to remove high-frequency noise. Surface electrodes were placed on the subject's right leg to record electromyographic (EMG) activity from seven muscles: gluteus maximus, gluteus medius, medial hamstrings, vastus lateralis, rectus femoris, medial gastrocnemius and soleus.

Inverse and forward-dynamics methods

SO, CMC and NMT were each implemented separately in the calculation of lower-limb muscle forces (Table 1). SO decomposes the net joint moments into individual muscle forces by minimising a time-independent performance criterion at each time instant. In the present study, SO was implemented by minimising the sum of the squares of all muscle activations at each instant of the stride cycle, and the calculated value of each muscle force was subject to physiological constraints according to its force-length-velocity properties.⁶

CMC produces a forward simulation of the prescribed task by using a proportional-integral controller to track the joint angular accelerations measured from a gait experiment.¹² The required set of neural excitations is found by solving a static optimisation problem that minimises the sum of the squares of all muscle

activations at each instant of the task. Time-dependent performance criteria are therefore not incorporated in the formulation of the CMC problem; however, the effects of muscle activation dynamics are taken into account by performing a forward integration of the system equations using muscle excitations as inputs to the model (Table 1).

NMT combines feedback linearization with optimal control theory to track the net joint moments obtained from an inverse-dynamics analysis.⁸ Although NMT is similar to CMC in that both methods implement muscle activation dynamics to solve a tracking problem, the NMT method minimises the sum of the squares of all muscle activations and the sum of squares of the joint torque tracking errors over the entire time interval of the task. Thus, the NMT method requires two sets of predefined weightings (one for minimising joint-torque tracking errors, and another for minimising muscle activation) in its time-dependent performance criterion to balance between joint torque tracking and the minimisation of muscle activation, whereas the SO and CMC methods treat the minimisation of joint-torque tracking errors as an equality constraint in the formulation of the optimisation problem. The NMT method is therefore able to account for the effects of both muscle activation dynamics and a time-dependent performance criterion in estimating muscle forces during movement (Table 1).

Musculoskeletal modelling

A 10-segment, 23-degree-of-freedom musculoskeletal model was used to determine lower-limb muscle forces for one complete stride cycle of both walking and running.¹⁹ The head, arms and torso were modelled as a single rigid body, which articulated with the pelvis via a ball-and-socket joint. Each hip was modelled as a ball-and-socket joint, each knee as a hinge joint, each ankle-subtalar complex as a universal joint and each metatarsal joint as a hinge. A subject-specific model of the skeleton was generated by scaling the anthropometric properties of each segment according to the subject's height and weight. The model was actuated by 54 Hill-type muscle-tendon units.²⁰ The force-producing properties, attachment sites and paths of all muscle-tendon units used in the model were based on data reported by Anderson and Pandy.¹⁹

Muscle-force calculations

Joint angles and net joint moments for walking and running were computed prior to calculation of lower-limb muscle forces. An inverse-kinematics analysis was performed by solving a weighted least-squares optimisation problem²¹ to determine the joint angles in the model that most accurately reproduced the measured marker coordinates. A single set of optimal joint angles

Table 1. Comparison of SO, CMC and NMT.

Algorithm	Muscle activation dynamics	Time-dependent performance criterion
SO	×	×
CMC	√	×
NMT	√	√

was then applied to the musculoskeletal model in conjunction with force plate data to compute the net moments exerted about the lower-limb joints.

Lower-limb muscle forces for both walking and running were determined by applying the SO, CMC and NMT algorithms to the musculoskeletal model. Eight major muscles were selected for comparison across the three sets of muscle-force solutions (F^{SO} , F^{CMC} and F^{NMT}): SOL (soleus), GAS (medial and lateral portions of GAS combined), VAS (vastus medialis, vastus intermedius and vastus lateralis combined), GMAX (gluteus maximus), GMED (anterior and posterior portions of gluteus medius combined), HAMS (medial and lateral portions of hamstrings combined) and ILPSO (iliacus and psoas combined). A correlation coefficient (R) between any two of the solutions was calculated for each muscle. The significance (p -value) of each correlation was also computed.

AQ1

Results

CMC accurately reproduced the sagittal-plane net joint moments computed from inverse dynamics (IVD) for both tasks with a root-mean-square (RMS) difference of less than 1 Nm, but larger variability was evident in the frontal and transverse-plane joint moments (Figures 1 and 2, compare CMC with IVD). For example, an RMS difference of 8 Nm was observed in the hip internal rotation moment generated for running (Figure 2). The NMT algorithm was also able to track the patterns

of all net joint moments computed from IVD for both walking and running with an RMS difference of less than 15 Nm (Figures 1 and 2, compare NMT with IVD). Similar to the CMC results, greater variability was found in the hip internal rotation moment for running compared with the other joint moments (Figure 2). In contrast to the forward-dynamics techniques, SO successfully reproduced the net joint moments in all three planes computed from IVD for both walking and running with an RMS difference of less than 1 Nm (Figures 1 and 2, compare SO with IVD).

Muscle-force patterns predicted by all three methods for walking and running were consistent with the sequence and timing of EMG measured for the subject (Figures 3 and 4). Muscle-force estimates derived from any two methods were similar for walking, with R values ranging from 0.46 to 0.99 (Figure 5). The CMC and NMT solutions for RF muscle force exhibited the least correlation with $R = 0.46$. The NMT solution showed that RF reached its peak value in the first half of the stance, whereas the CMC solution indicated that the peak force for this muscle occurred in the second half of the stance. For running, the correlation between any two muscle-force solutions was similar to that found in walking, with R values ranging from 0.51 to 0.99 (Figure 5). However, an increase in the speed of locomotion improved the correlation between the CMC and NMT solutions for RF force significantly, with $R = 0.77$ obtained for this muscle in running. All correlations were significant with $p < 0.001$.

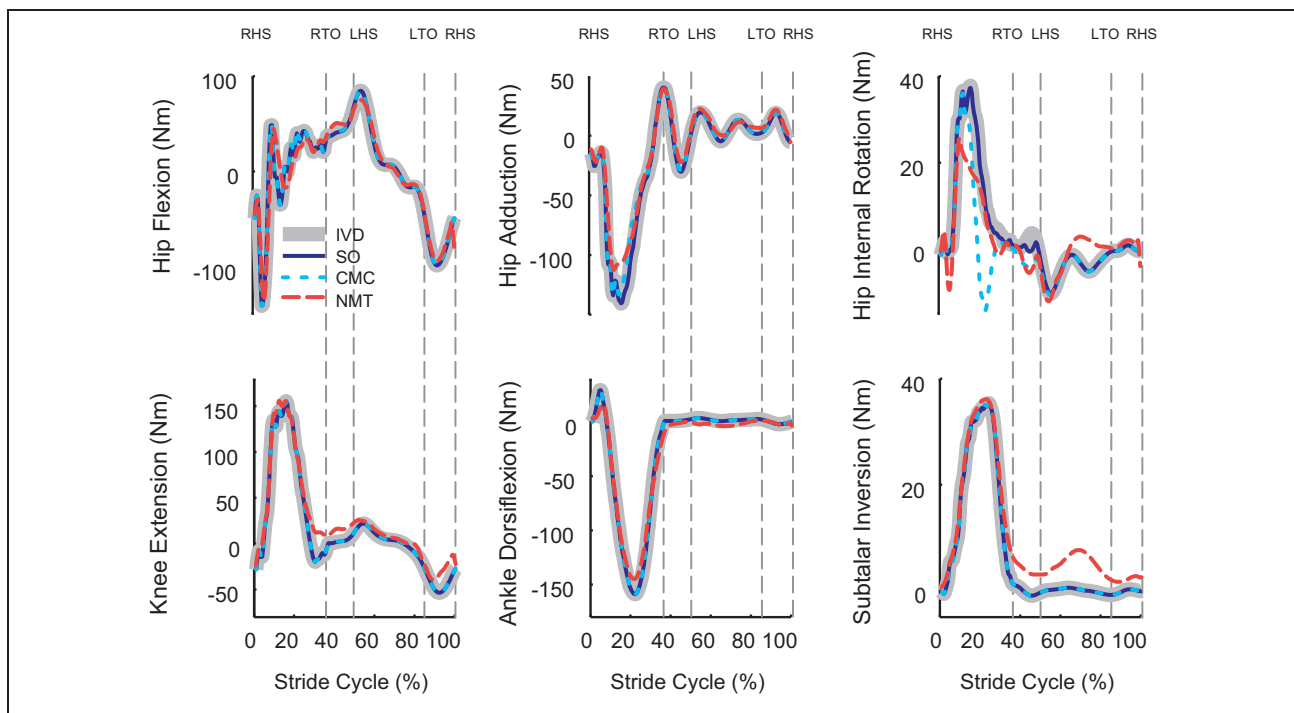


Figure 2. Comparison of net joint moments computed from IVD and net joint moments resulting from three muscle-force solutions (SO, CMC and NMT) for running at the preferred speed.

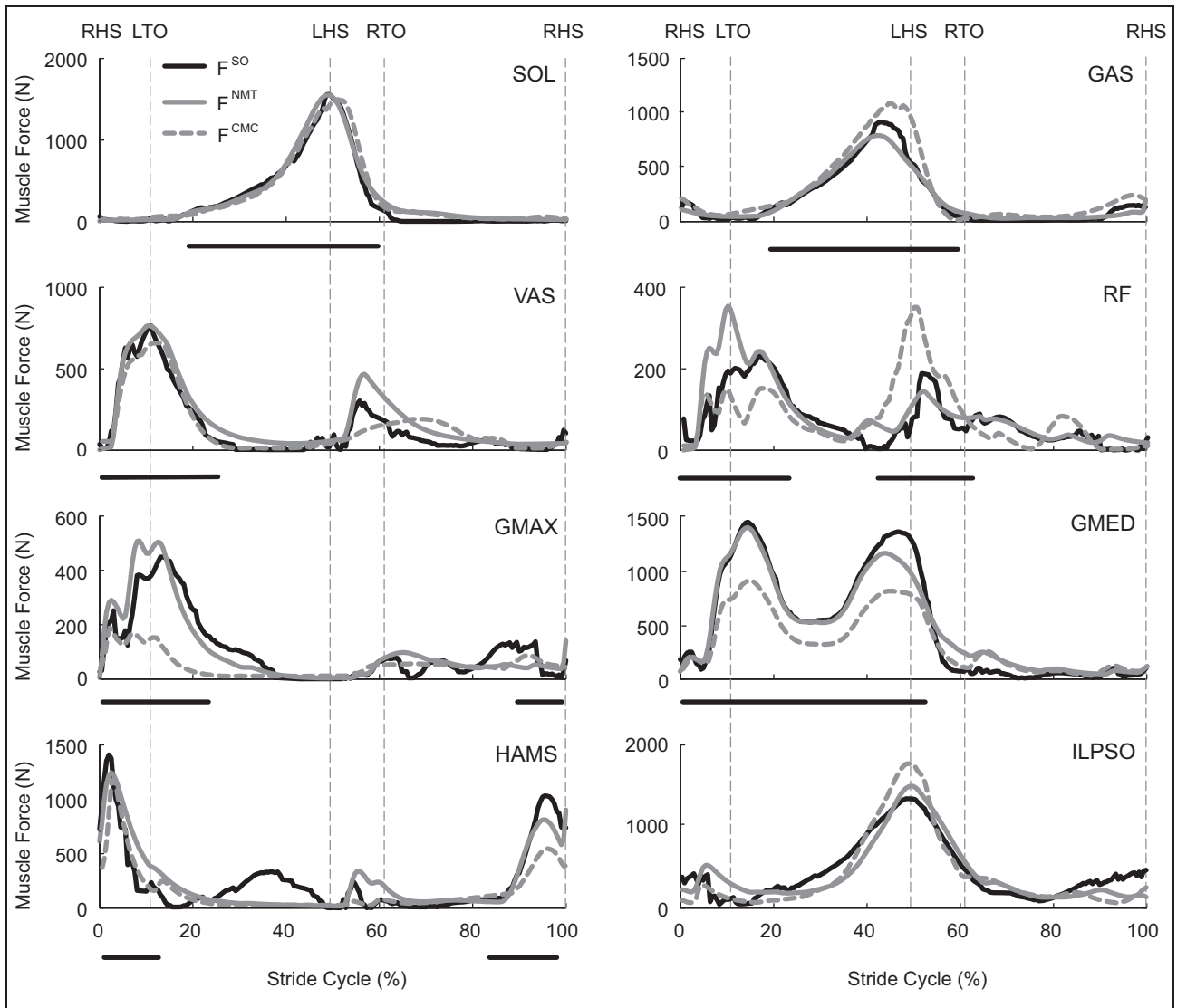


Figure 3. Comparison of three sets of muscle-force solutions (F^{SO} , F^{CMC} and F^{NMT}) for walking at the preferred speed. The horizontal bars indicate the periods of EMG activity recorded for the subject. No EMG data were recorded for ILPSO.

Discussion

This study compared muscle-force estimates obtained for walking and running using three different methods commonly reported in the literature: SO, CMC and NMT. The patterns of muscle forces predicted by these methods were similar for both walking (Figure 3) and running (Figure 4), suggesting that muscle-force calculations are not significantly influenced by the inclusion of either muscle activation dynamics or a time-dependent performance criterion.

The current analysis was associated with a number of limitations. First, the results are based on data obtained from only one subject because the aim was to compare muscle-force estimates derived from different optimisation methods rather than study the functional roles of muscles during gait. Nonetheless, the joint kinematics and ground reaction forces measured for

both walking and running were well within the normal ranges reported in the literature. Furthermore, the EMG data recorded for our subject were consistent with speed-matched EMG reported by others (e.g. compare EMG bars in Figures 3 and 4 with the results at '5 km/h' and '12 km/h' presented by Cappellini et al.²² in their Figure 1). The reader is directed to a recent study by Pandy and Andriacchi³ for a detailed discussion of muscle function in walking and running.

Second, two simulation environments were used when calculating muscle forces for walking and running. In ideal circumstances, all muscle-force calculations would have been performed in a single simulation environment. However, this was not feasible in the present study because the CMC and NMT methods could not be implemented in the same simulation environment: the NMT method was available only in Matlab (The Mathworks Inc., Natick, Massachusetts,

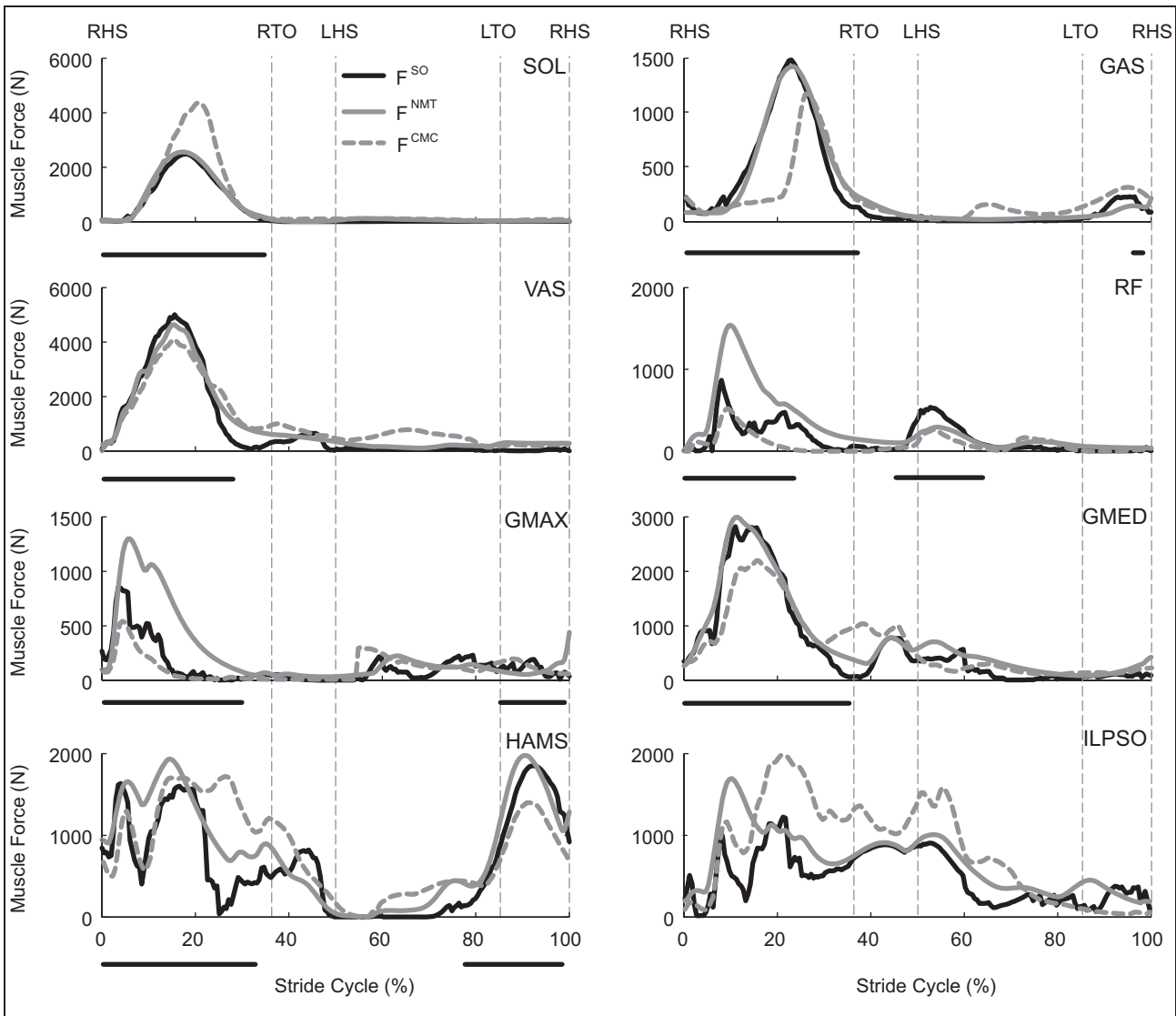


Figure 4. Comparison of three sets of muscle-force solutions (F^{SO} , F^{CMC} and F^{NMT}) for running at the preferred speed. The horizontal bars indicate the periods of EMG activity recorded for the subject. No EMG data were recorded for ILPSO.

USA), and the CMC method could be accessed only through OpenSim.²³ Consequently, muscle-force calculations were performed by implementing the SO and NMT methods in Matlab using a musculoskeletal model developed by Anderson and Pandy,¹⁰ whereas the CMC method was implemented in OpenSim using a model developed by Delp et al.²⁴ While the structure of the skeletal system was identical in both models, the muscle-tendon architecture (i.e. the geometry and mechanical properties of the muscle-tendon units) was different. The OpenSim model²⁴ was actuated by 92 muscle-tendon units, whereas the model developed by Anderson and Pandy¹⁰ was actuated by 54 muscle-tendon units. Although both models included all the major muscle groups of the lower limb, the OpenSim model divided each muscle group into several distinct sub-regions. Details of the force-producing properties

of the muscles included in these models (i.e. maximum isometric force and the corresponding muscle-fibre length, tendon rest length, maximum shortening velocity, etc.) have been reported previously.^{19,23,24} To evaluate the influence of these model differences on the calculated values of muscle forces, we re-solved the walking problem by implementing the SO method in both Matlab and OpenSim. Figure 6 shows that the patterns of muscle loading obtained in Matlab and OpenSim are similar, indicating that muscle-force calculations are not significantly influenced by the simulation environment used. While differences in the magnitudes of the muscle-force estimates are evident in Figure 6, the similarities in the time histories of muscle loading suggests that the two simulation environments will yield a consistent set of predictions for lower-limb muscle function. Finally, the results obtained in the

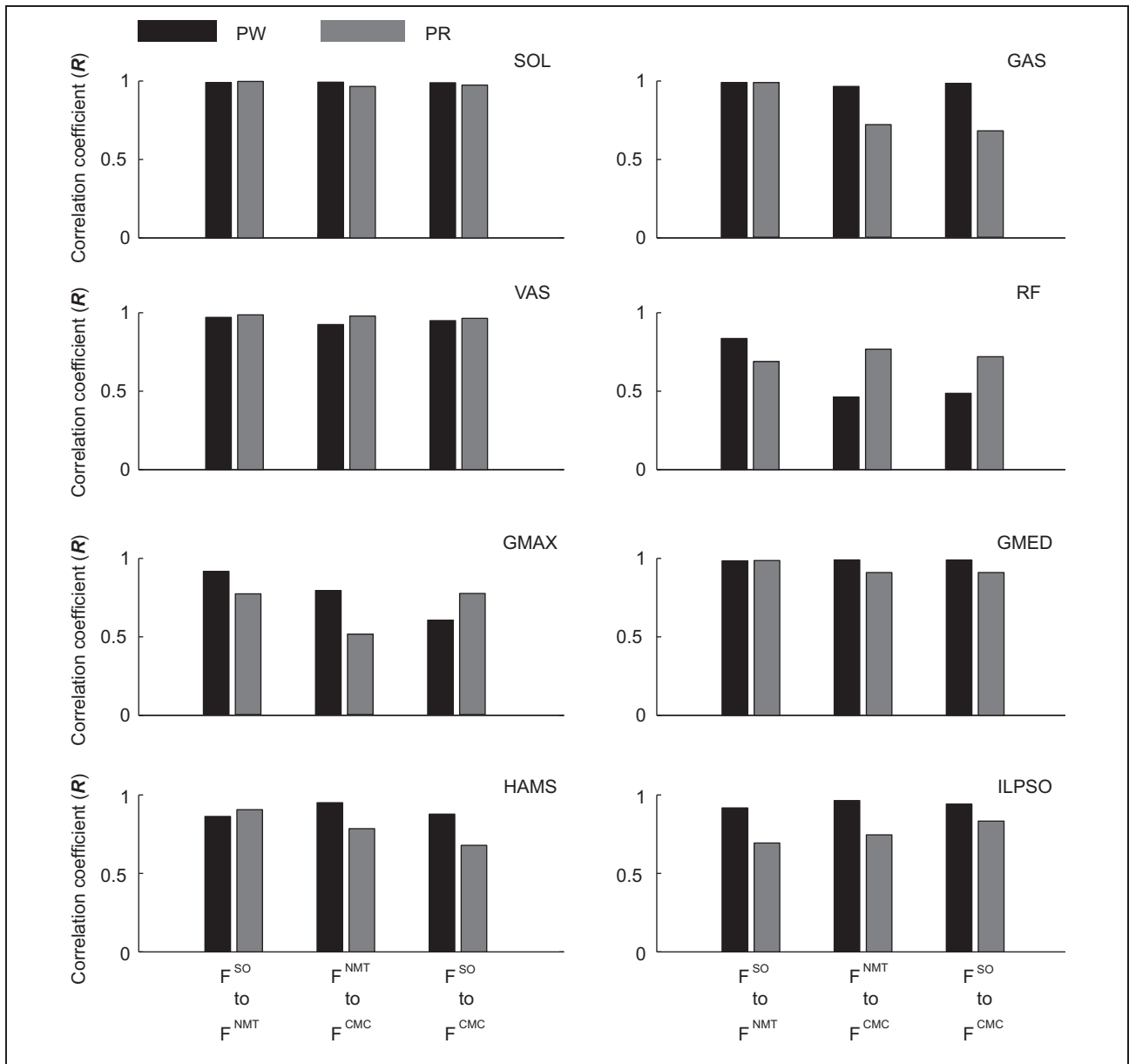


Figure 5. The correlations between the three sets of muscle-force solutions: F^{SO} , F^{CMC} and F^{NMT} . The walking and running results were presented in black and grey bars, respectively.

present study may not be applicable to faster speeds of running (i.e. beyond 3.5 m/s) or to ballistic movements such as vertical jumping, where the influence of muscle activation dynamics may be more pronounced.

Differences in muscle-force estimates obtained from IVD and forward dynamics methods can arise from one or more of the following factors:

- the performance criterion assumed;
- errors obtained in tracking biomechanical gait data, for example, joint angular accelerations and joint torques;
- the inclusion of muscle activation dynamics in the formulation of the optimisation problem.

Previous studies have shown that the performance criterion can significantly influence predictions of muscle forces in human movement.^{2,4} All three methods implemented in the present study minimised the sum of squares of muscle activations. The main difference was that the SO and CMC methods solved a series of separate optimisation problems, one at each time instant during the stride cycle, whereas the NMT method solved just one problem over the entire duration of the task (Table 1). Both CMC and NMT reproduced the net joint torques measured for walking and running (Figure 1), suggesting that differences in muscle-force estimates obtained from SO and CMC are due to the influence of muscle activation dynamics, whereas

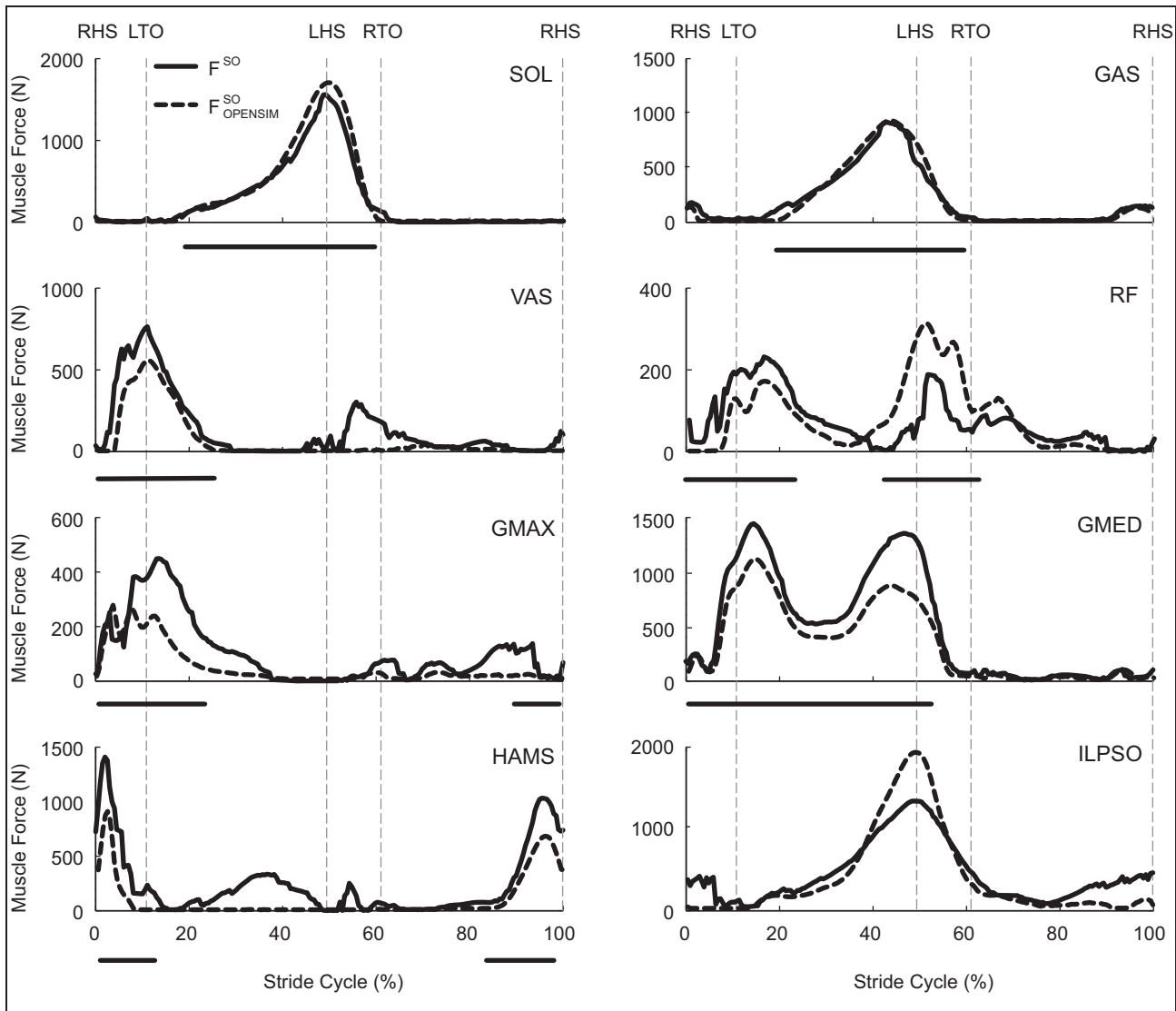


Figure 6. Comparison of two sets of SO solutions (F^{SO} and $F^{SO}_{OPENSIM}$) for walking at the preferred speed. The curve F^{SO} is the same as the curve labeled F^{SO} in Figure 3. The curve $F^{SO}_{OPENSIM}$ was calculated by implementing the SO method in OpenSim using a model developed by Delp et al.²⁴ The horizontal bars indicate the periods of EMG activity recorded for the subject. No EMG data were recorded for ILPSO.

differences obtained from CMC and NMT are due to the influence of a time-dependent performance criterion (see Table 1). The fact that SO and CMC produced similar results suggests that muscle activation dynamics does not have a significant influence on model predictions of muscle forces. It was also found that CMC and NMT produced similar results, which indicates that muscle-force solutions are also not heavily influenced by the presence of a time-dependent performance criterion. Taken together, these findings suggest that valid estimates of muscle forces in walking and running may be obtained by implementing static optimisation alone.

Accuracy, robustness and efficiency are three major considerations when selecting the most suitable method for calculating muscle forces during human movement, especially when large numbers of subjects are involved.

Accuracy refers to the ability of a method to produce valid estimates of muscle forces. Because non-invasive measurement of muscle forces is not possible, model predictions of muscle forces are often validated against EMG measurements of muscle activity. While the temporal patterns of muscle forces calculated for both walking and running were consistent with measurements of muscle EMG, no data are available to directly validate the magnitudes of the predicted muscle forces.

Robustness refers to the ability of a method to produce accurate estimates of muscle forces, even when small changes are introduced into the model and/or the experimental data. Because the process of numerical integration is prone to accumulation of error over time, forward-dynamics methods are inherently less robust than IVD methods. For example, forward integration

of the equations of motion of the neuromusculoskeletal system may progress more slowly, or even terminate, when certain model parameters or user-defined inputs (e.g. integration parameters and tracker weightings) are improperly perturbed. In this study, greater joint-torque tracking errors were evident in the NMT solution (Figures 1 and 2), which resulted directly from the selection of the weighting parameters. Weighting the importance of minimising joint torque errors more heavily will adversely affect the minimisation of muscular effort; and conversely, a heavier weighting on the importance of minimising muscular effort will adversely affect the minimisation of joint torque errors. An optimisation approach is needed to refine the selection of the weighting parameters in the NMT method.

Efficiency refers to the preparation time needed to implement a particular method as well as the computational (CPU) time required to simulate a prescribed task. In this study, static optimisation was approximately five times more efficient than the CMC and NMT methods with respect to actual CPU time. Furthermore, the preparation time for static optimisation was considerably less than that required for the CMC and NMT methods, because the latter two methods required many user-defined inputs to be prescribed prior to implementation. For example, finding an optimal set of weightings that reduces the overall tracking errors in a stable manner and minimises muscular effort simultaneously is not trivial, especially when dealing with non-linear dynamical systems of high dimension.⁸

Whereas the static optimisation method possesses several advantages in relation to accuracy, robustness and efficiency, it may not always be the most appropriate method for calculating muscle forces in human movement. In particular, it is recommended that caution be taken when static optimisation is used to calculate muscle forces under the following circumstances.

1. In ballistic tasks such as jumping¹⁹ and sprint cycling,²⁵ muscle activation dynamics act to prevent a muscle from being activated instantaneously in response to a neural excitation signal. Although the results of the present study suggest that muscle activation dynamics may be neglected when calculating muscle forces for walking and slower speeds of running, the delay between muscle excitation and muscle activation may be important in ballistic-type movements. In the absence of muscle activation dynamics, a static optimisation minimisation criterion will favour a muscle with a larger maximum isometric force because of its potential to contribute to the required joint moment. As a result, static optimisation solutions may yield muscle activation patterns that are inconsistent with measured EMG.
2. In tasks that inherently involve a time-dependent performance criterion. For example, the performance criterion of maximum-height jumping can be characterised by the vertical height achieved by the centre of mass.¹⁹ Sprint running is another example where the time-dependant performance criteria may be defined by maximising muscular power generation^{26, 27} or vertical ground impulse²⁸ over the entire stride cycle. Because a time-independent performance criterion cannot accurately model the goal of such tasks, muscle activation patterns predicted by static optimisation may be inconsistent with measured EMG.

To summarise, the results of the present study suggest that muscle activation dynamics and time-dependent performance criteria do not significantly affect calculations of muscle forces obtained for walking and running. Because all three methods (SO, CMC and NMT) produce similar results, the robustness and efficiency of static optimisation make it the most attractive method for estimating muscle forces in human locomotion.

Funding

Financial support was provided in part by the Australian Research Council under Discovery Projects grants DP0772838, DP0878705 and DP1095366; by the National Health and Medical Research Council under grant 508966; and by a VESKI Innovation Fellowship awarded to M.G.P.

References

1. Tsirakos D, Baltzopoulos V and Bartlett R. Inverse optimization: functional and physiological considerations related to the force-sharing problem. *Crit Rev Biomed Engng* 1997; 25: 371–407.
2. Erdemir A, McLean S, Herzog W and Van den Bogert AJ. Model-based estimation of muscle forces exerted during movements. *Clin Biomech (Bristol, Avon)* 2007; 22: 131–154.
3. Pandy MG and Andriacchi TP. Muscle and joint function in human locomotion. *Ann Rev Biomed Engng* 2010; 12: 401–433.
4. Crowninshield RD. Use of optimization techniques to predict muscle forces. *J Biomech* 1979; 12: 627.
5. An KN, Kaufman KR and Chao EYS. Physiological considerations of muscle force through the elbow joint. *J Biomech* 1989; 22: 1249–1256.
6. Anderson FC and Pandy MG. Static and dynamic optimization solutions for gait are practically equivalent. *J Biomech* 2001; 34: 153–161.
7. Pandy MG, Garner BA and Anderson FC. Optimal control of non-ballistic muscular movements: a constraint-based performance criterion for rising from a chair. *Trans ASME, J Biomech Engng* 1995; 117: 15–26.
8. Seth A and Pandy MG. A neuromusculoskeletal tracking method for estimating individual muscle forces in human movement. *J Biomech* 2007; 40: 356–366.

9. Menegaldo LL, De Toledo Fleury, A and Weber HI. A 'cheap' optimal control approach to estimate muscle forces in musculoskeletal systems. *J Biomech* 2006; 39: 1787–1795.
10. Anderson FC and Pandy MG. Dynamic optimization of human walking. *Trans ASME, J Biomech Engng* 2001; 123: 381–390.
11. Davy DT and Audu ML. A dynamic optimization technique for predicting muscle forces in the swing phase of gait. *J Biomech* 1987; 20: 187–201.
12. Thelen DG and Anderson FC. Using computed muscle control to generate forward dynamic simulations of human walking from experimental data. *J Biomech* 2006; 39: 1107–1115.
13. Thelen DG, Anderson FC and Delp SL. Generating dynamic simulations of movement using computed muscle control. *J Biomech* 2003; 36: 321–328.
14. Chumanov ES, Heiderscheidt BC and Thelen DG. The effect of speed and influence of individual muscles on hamstring mechanics during the swing phase of sprinting. *J Biomech* 2007; 40: 3555–3562.
15. Glitsch U and Baumann W. The three-dimensional determination of internal loads in the lower extremity. *J Biomech* 1997; 30: 1123–1131.
16. Hamner SR, Seth A and Delp SL. Muscle contributions to propulsion and support during running. *J Biomech* 2010; 43: 2709–2716.
17. Schache AG, Kim HJ, Morgan DL and Pandy MG. Hamstring muscle forces prior to and immediately following an acute sprinting-related muscle strain injury. *Gait Posture* 2010; 32: 136–140.
18. Yokozawa T, Fujii N and Ae M. Muscle activities of the lower limb during level and uphill running. *J Biomech* 2007; 40: 3467–3475.
19. Anderson FC and Pandy MG. A dynamic optimization solution for vertical jumping in three dimensions. *Comput Methods Biomech Biomed Engng* 1999; 2: 201–231.
20. Zajac FE. Muscle and tendon: properties, models, scaling, and application to biomechanics and motor control. *Crit Rev Biomed Engng* 1989; 17: 359–411.
21. Lu TW and O'Connor JJ. Bone position estimation from skin marker co-ordinates using global optimisation with joint constraints. *J Biomech* 1999; 32: 129–134.
22. Cappellini G, Ivanenko YP, Poppele RE and Lacquaniti F. Motor patterns in human walking and running. *J Neurophysiol* 2006; 95: 3426–3437.
23. Delp SL, Anderson FC, Arnold AS, et al. OpenSim: open-source software to create and analyze dynamic simulations of movement. *IEEE Trans Biomed Engng* 2007; 54: 1940–1950.
24. Delp SL, Loan JP, Hoy MG, et al. An interactive graphics-based model of the lower extremity to study orthopaedic surgical procedures. *IEEE Trans Biomed Engng* 1990; 37: 757–767.
25. Martin JC, Brown NA, Anderson FC and Spirduso WW. A governing relationship for repetitive muscular contraction. *J Biomech* 2000; 33: 969–974.
26. Cavagna GA, Komarek L and Mazzoleni S. The mechanics of sprint running. *J Physiol* 1971; 217: 709–721.
27. Ward-Smith AJ. A mathematical theory of running, based on the first law of thermodynamics, and its application to the performance of world-class athletes. *J Biomech* 1985; 18: 337–349.
28. Weyand PG, Sternlight DB, Bellizzi MJ and Wright S. Faster top running speeds are achieved with greater ground forces not more rapid leg movements. *J Appl Physiol* 2000; 89: 1991–1999.

Effect of Running Speed on Lower Limb Joint Kinetics

ANTHONY G. SCHACHE¹, PETER D. BLANCH², TIM W. DORN¹,
NICHOLAS A. T. BROWN³, DOUG ROSEMOND³, and MARCUS G. PANDY¹

¹Department of Mechanical Engineering, University of Melbourne, Victoria, AUSTRALIA; ²Department of Physical Therapies, Australian Institute of Sport, Belconnen, ACT, AUSTRALIA; and ³Department of Biomechanics and Performance Analysis, Australian Institute of Sport, Belconnen, ACT, AUSTRALIA

ABSTRACT

SCHACHE, A. G., P. D. BLANCH, T. W. DORN, N. A. T. BROWN, D. ROSEMOND, and M. G. PANDY. Effect of Running Speed on Lower Limb Joint Kinetics. *Med. Sci. Sports Exerc.*, Vol. 43, No. 7, pp. 1260–1271, 2011. **Purpose:** Knowledge regarding the biomechanical function of the lower limb muscle groups across a range of running speeds is important in improving the existing understanding of human high performance as well as in aiding in the identification of factors that might be related to injury. The purpose of this study was to evaluate the effect of running speed on lower limb joint kinetics. **Methods:** Kinematic and ground reaction force data were collected from eight participants (five males and three females) during steady-state running on an indoor synthetic track at four discrete speeds: 3.50 ± 0.04 , 5.02 ± 0.10 , 6.97 ± 0.09 , and 8.95 ± 0.70 m·s⁻¹. A standard inverse-dynamics approach was used to compute three-dimensional torques at the hip, knee, and ankle joints, from which net powers and work were also calculated. A total of 33 torque, power, and work variables were extracted from the data set, and their magnitudes were statistically analyzed for significant speed effects. **Results:** The torques developed about the lower limb joints during running displayed identifiable profiles in all three anatomical planes. The sagittal-plane torques, net powers, and work done at the hip and knee during terminal swing demonstrated the largest increases in absolute magnitude with faster running. In contrast, the work done at the knee joint during stance was unaffected by increasing running speed, whereas the work done at the ankle joint during stance increased when running speed changed from 3.50 to 5.02 m·s⁻¹, but it appeared to plateau thereafter. **Conclusions:** Of all the major lower limb muscle groups, the hip extensor and knee flexor muscles during terminal swing demonstrated the most dramatic increase in biomechanical load when running speed progressed toward maximal sprinting. **Key Words:** GAIT BIOMECHANICS, INVERSE DYNAMICS, JOINT TORQUE, JOINT POWER, HAMSTRING MUSCLE

Knowledge regarding the biomechanical function of the lower limb muscle groups across a range of running speeds is important in improving existing understanding of human high performance as well as in aiding in the identification of factors that might be related to injury. A common approach for quantifying the biomechanical function of lower limb muscle groups during running is inverse dynamics, which is the process of determining the lower limb joint moments of force (or torques) on the basis of measured joint kinematics, ground reaction forces, and segmental inertial properties (38). The primary

parameters of interest include (a) torques, (b) net powers (product of the torque and angular velocity about a joint), and (c) work (area under the net power vs time curve). When interpreted together, these parameters provide insight into the biomechanical causes of the observed movement pattern; more specifically, whether lower limb muscle groups are acting concentrically and generating energy or are acting eccentrically and absorbing energy.

Many studies have computed torques, net powers, and/or work done at the lower limb joints during running (1,3,5,7–9, 12,16,20,23,30,33,37,40) and sprinting (5,6,13,19–22,29,34). Although these studies have provided much insight into the biomechanical function of the lower limb muscle groups across a range of running speeds for adult humans, they are not without limitations. First, most studies have evaluated only certain phases of the stride cycle; specifically, either the stance (3,5–8,12,16,21,23,30) or swing phase (9,13,33,34). Second, many studies have either obtained data for a single speed (6,8,12,13,16,19,21,22,29,34,37) or have obtained data across a range of speeds but have not included maximal sprinting (3,7,30,33,40). Third, almost all studies have used a two-dimensional approach focusing exclusively on sagittal-plane dynamics (1,3,5–9,12,13,19–22,29,30,33,34,37,40). However, an understanding of non-sagittal-plane dynamics is also likely to be important. Both Glitsch and Baumann (16)

Address for correspondence: Anthony G. Schache, Ph.D., Department of Mechanical Engineering, The University of Melbourne, Victoria 3010, Australia; E-mail: anthony@unimelb.edu.au.

Submitted for publication June 2010.

Accepted for publication November 2010.

Supplemental digital content is available for this article. Direct URL citations appear in the printed text and are provided in the HTML and PDF versions of this article on the journal's Web site (www.acsm-msse.org).

0195-9131/11/4307-1260/0

MEDICINE & SCIENCE IN SPORTS & EXERCISE®

Copyright © 2011 by the American College of Sports Medicine

DOI: 10.1249/MSS.0b013e3182084929

and McClay and Manal (23) demonstrated that, during an almost planar movement such as running, the lower limb joints are associated with significant three-dimensional torques, especially in the frontal plane. Furthermore, Stefanyshyn et al. (32) found a relationship between frontal-plane knee joint dynamics during running and risk of injury. Although these studies highlight the potential importance of non-sagittal-plane dynamics during running, data from both Glitsch and Baumann (16) and McClay and Manal (23) are limited to the stance phase of the stride cycle and a single speed of running only. In view of these limitations, further research is needed to generate a more complete analysis regarding the effects of increasing running speed on lower limb joint kinetics.

Many lower limb muscles that play an important role during running have specific actions that are not limited to a single anatomical plane. For example, in addition to being a strong hip extensor, the gluteus maximus muscle also has a large capacity for producing hip external rotation (11,26). Similarly, the rectus femoris and biceps femoris muscles have been shown to be capable of inducing both sagittal- and frontal-plane hip motion (18). Consequently, running is likely to be fundamentally governed by coordinated synchronous muscle activity in all three anatomical planes, which would suggest that any investigation into the biomechanics of running ideally should be approached from a three-dimensional perspective.

The aim of the current study was twofold: first, to use an inverse-dynamics approach to quantify the three-dimensional torques at the lower limb joints across the entire stride cycle during overground running; and second, to determine the effect of increasing running speed on the magnitude of the torques, net powers, and work done at the lower limb joints.

METHODS

Participants. Eight participants (five males and three females) were recruited from running-based sports, such as track and field ($n = 7$) and Australian Rules football ($n = 1$). Participants had a mean \pm SD age of 27.0 ± 7.8 yr, a mean \pm SD height of 176.2 ± 8.1 cm, and a mean \pm SD body mass of 73.0 ± 8.6 kg. At the time of testing, all participants had been free from any musculoskeletal injury likely to adversely affect their running mechanics for at least a 6-month period. The study was approved by the Human Research Ethics Committee at The University of Melbourne and The Australian Institute of Sport, and all participants gave their written informed consent before testing.

Instrumentation. All testing took place on an indoor 110-m synthetic running track in the Biomechanics Laboratory at the Australian Institute of Sport. Kinematic data were acquired using a three-dimensional motion analysis system (VICON; Oxford Metrics Ltd., Oxford, United Kingdom) with 22 cameras sampling at a rate of 250 Hz. The measurement volume had a length, width, and height of 15, 1.3, and 2.2 m, respectively, and was situated approximately 80 m along the 110-m running track allowing ample distance for

acceleration and deceleration. The calibration error for the measurement volume was estimated to be no greater than 1 mm for all cameras. Eight large ($900 \times 600\text{-mm}^2$) Kistler force plates (Kistler Instrument Corp., Amherst, NY) sampling at a rate of 1500 Hz were used to capture ground reaction force data. All force plates were embedded in the floor of the laboratory and were covered with a piece of the synthetic running track to disguise their location to the participants, thus preventing any force plate targeting. The eight force plates were situated immediately adjacent to each other (thereby expanding a total length of 7.2 m) and were located at the center of the calibrated measurement volume.

Procedures. A four-segment, hierarchical, biomechanical model (pelvis, left thigh, left shank, and left foot) was used in this study. Each lower limb joint (hip, knee, and ankle) was modeled as a ball-and-socket joint described by three angles. To define the model, small reflective markers were mounted on each participant's pelvis and left lower limb (see Figure, Supplemental Digital Content 1, Marker setup for experimental data collection, <http://links.lww.com/MSS/A80>). Specifically, an elastic strap (~ 4 cm wide) was tightly secured around the pelvis. A light thermoplastic triangular plate containing four reflective markers (i.e., three markers positioned along the superior border and one marker positioned at the inferior apex) was attached to the back of the strap. The strap was placed on the pelvis such that the triangular plate was mounted on the sacrum with the middle superior marker overlying the midpoint between the two posterior superior iliac spines. A 10-cm-long thermoplastic bar, which contained two markers fixed to either end, was mounted on the lateral aspect of the thigh. Single markers were affixed to the anterior and distal aspects of the thigh, both the superior and inferior aspects of the anteromedial shaft of the tibia, the mid and lateral aspects of the shank, the inferoposterior aspect of the heel, as well as the medial and lateral midfoot. To establish joint centers and define segmental anatomical coordinate systems, additional "calibration" markers were also affixed to the following locations: left and right anterior superior iliac spines, medial and lateral femoral condyles, medial and lateral malleoli, the superoposterior aspect of the heel, and on the forefoot at the junction between the second and third metatarsophalangeal joints.

For testing, the participants wore standard athletic shorts and running sandals (NIKE Strapranner IV Beaverton, Oregon) that allowed adequate exposure of the foot for marker placement (see Figure, Supplemental Digital Content 1, Marker setup for experimental data collection, <http://links.lww.com/MSS/A80>). Data collection commenced with the recording of several anthropometric parameters, which included height, body mass, and pelvic width. Markers were then placed on each participant's pelvis and left lower limb as described above. A static trial was collected with the participant standing in the anatomical position, after which the "calibration" markers were removed. A dynamic calibration trial was then collected. The participant stood on his/her right lower limb and performed three continuous isolated flexion-extension motions of the left

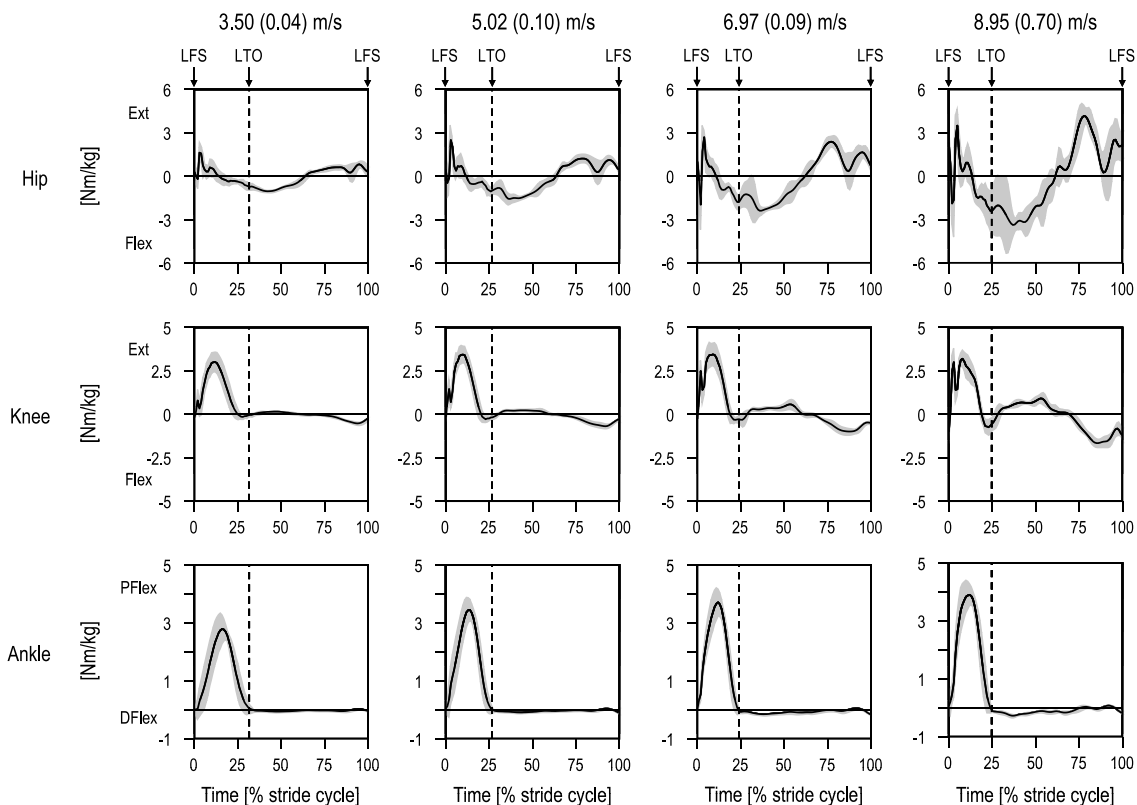


FIGURE 1—Sagittal-plane torques developed about the hip (*top panels*), knee (*middle panels*), and ankle (*bottom panels*) joints across the full stride cycle for the left lower limb (left foot strike to left foot strike) for the four discrete running speeds. Data represent the group mean (*solid black line*) \pm one SD (*gray shading*). The running speeds of 3.50, 5.02, and 6.97 $\text{m}\cdot\text{s}^{-1}$ contain data for eight subjects, whereas the running speed of 8.97 $\text{m}\cdot\text{s}^{-1}$ contains data for seven subjects. The *dashed vertical line* indicates the average time (% stride cycle) of toe-off for each speed condition. Ext, extension; Flex, flexion; PFlex, plantarflexion; DFlex, dorsiflexion; LFS, left foot strike; LTO, left toe-off.

knee through a range of 0° to 90° . The participant was required to keep the left thigh as stationary as possible throughout the duration of the motion so as to minimize thigh-marker soft tissue artifact as much as possible.

Before commencing the running trials, all participants completed a warm-up consisting of repeated walking and slow jogging trials to familiarize themselves with the experimental conditions. Data were collected at the following running speeds: 3.5, 5.0, and 7.0 $\text{m}\cdot\text{s}^{-1}$ and maximum sprinting. For practical reasons, the order of running speeds was incremental rather than randomized. The slower speeds of running provided a graduated warm-up before performing the maximum sprinting trials. For each trial, participants were instructed to maintain a steady-state speed throughout the calibrated measurement volume. There were no restrictions placed on acceleration and deceleration distances. Running speed was recorded using timing gates (Speedlight Telemetry Timing; Swift Performance Equipment, Walcol, Australia) positioned 20 m apart at each end of the calibrated measurement volume. Participants were provided with feedback after each running trial to reproduce the desired running speeds. For the prescribed speed conditions, participants performed repeated trials until a single trial was obtained whereby the measured speed was within $\pm 5\%$ of the desired speed.

Adequate recovery time was provided between speed increments so as to avoid the effects of fatigue. Seven participants completed all running speed conditions, whereas one participant did not complete the maximum sprinting condition.

Data analysis. Marker trajectories were filtered using Woltring's (39) general cross-validators quintic smoothing spline with a predicted mean squared error of 15 mm. Both the static and dynamic calibration trials were used to reconstruct the anatomical coordinate systems for each body segment in the hierarchical biomechanical model. The hip joint center was defined using the approach described by Harrington et al. (17) and was reconstructed relative to the pelvic tracking markers (triangular sacral plate) in the dynamic trials. The knee joint center was defined as the midpoint between the medial and lateral femoral condyle markers and was reconstructed relative to the shank tracking markers in the dynamic trials. The dynamic calibration task (i.e., an open-chain isolated knee flexion–extension motion) was used to determine the orientation of the mediolateral axis of the femoral anatomical coordinate system (or knee joint flexion–extension axis) based on a previously described numerical approach (28). The ankle joint center was defined as the midpoint between the medial and lateral malleoli markers and was reconstructed relative to the shank tracking

markers in the dynamic trials. Full details regarding the anatomical coordinate systems for each body segment can be found elsewhere (27).

Only trials containing a valid foot strike for the left leg (i.e., foot strike occurred well within the boundaries of a single force plate) were analyzed. In the instance that a given trial contained more than one valid foot strike on a force plate for the left leg (e.g., as occurred for the slower running speeds), then the stride cycle closest to the center of the calibrated measurement volume was chosen. A standard inverse-dynamics approach was used to calculate the internal torques developed by the lower limb joints (38). Segmental inertial parameters were taken from de Leva (10). Ground reaction force data were not filtered during the inverse-dynamics process. The center of pressure location and vertical free torque were calculated using the ground reaction forces, torques, and calibration measurements from the relevant force plate. Ground reaction forces and the vertical free torque were then applied directly to the foot segment at the center of pressure location, and three-dimensional joint torques were calculated from the ground up (38). All torques were expressed in a nonorthogonal reference frame or joint coordinate system (27). For each joint, power was calculated as the product of the net torque and angular velocity. Because power is a scalar quantity, only the net power at each lower limb joint was computed. The amount of positive and negative work done at the hip, knee, and ankle joints at distinct phases throughout the stride cycle was calculated by integrating the relevant portion of the power-versus-time curve (i.e., area under the curve) (37). All torque, power, and work data for each participant were normalized by dividing by body mass. Bodybuilder software (VICON; Oxford Metrics Ltd.) was used to perform all computations.

Discrete torque, power, and work variables were extracted from the data set for statistical analysis. Various maxima and minima points that were readily identifiable on the torque and power profiles at the hip, knee, and ankle joints for each participant at each running speed were chosen for analysis. Also, 10 distinct phases in the stride cycle, where it was evident that continuous positive or negative work was being done at the lower limb joints for all running speeds, were identified and chosen for analysis (see Figure, Supplemental Digital Content 2, the 10 distinct periods of continuous positive or negative work done at the lower limb joints identified across the stride cycle for all running speeds, <http://links.lww.com/MSS/A81>). (see Figure, Supplemental Digital Content 1, Marker setup for experimental data collection, <http://links.lww.com/MSS/A80>). A total of 33 torque, power, and work variables were statistically analyzed. One-way repeated-measures ANOVA tests were used to determine which of the dependent variables were significantly affected by running speed. When significant *F* ratios were obtained, *post hoc* pairwise comparisons (paired *t*-test) were used to determine differences between each of the running speeds. A conservative level of significance was set at $P < 0.008$ for all tests, which was determined by applying a Bonferroni

correction to a significance level of $P < 0.05$ (i.e., a total of six *post hoc* pairwise comparisons were performed per dependent variable). To generate a complete data set for purposes of statistical analyses, data for one participant for the maximum sprinting speed were imputed using a mean substitution (15). For each dependent variable, data for this participant were assumed to equal the mean of the sample of available data ($n = 7$) for the maximum sprinting condition. This approach was considered reasonable given that, for each ANOVA, the extent of missing data was small (i.e., limited to a single-speed condition for one participant only). The statistical association between running speed and work done at the lower limb joints was also computed. Second-order polynomial trend lines were fitted to the data for all work variables that were identified from the data set and corresponding coefficient of determination (R^2) values were calculated. Linear trend lines were explored, but they yielded lower R^2 values.

RESULTS

The mean \pm SD running speeds were 3.50 ± 0.04 , 5.02 ± 0.10 , 6.97 ± 0.09 , and 8.95 ± 0.70 $\text{m}\cdot\text{s}^{-1}$. The mean \pm SD magnitudes for the various discrete variables extracted from the data, as well as the results from statistical testing, are displayed in Table 1. Overall, a significant speed effect ($P < 0.008$) was observed for 29 of the 33 variables, with the absolute magnitude of these 29 variables increasing with faster running. *Post hoc* tests revealed that not all running speed conditions were significantly different from each other. Only 12 of the 29 variables were found to display significant increases in absolute magnitude for all running speed increments (variables indicated with gray shading in Table 1). All of these 12 variables related specifically to the biomechanical function of the hip and knee joints during swing.

The normalized mean \pm SD sagittal-plane torques developed about the hip, knee, and ankle joints across the full stride cycle for each running speed condition are presented in Figure 1. At the hip joint, a flexion torque developed for a short period immediately after foot strike, which was a consequence of the rapid increase in magnitude of the fore-aft component of the ground reaction force. An extension torque then developed about the hip during the first half of stance before becoming flexion again during the latter half of stance. The hip flexion torque continued during the first half of swing. Finally, a hip extension torque developed during the last half of swing. At the knee joint, an extension torque occurred for the majority of stance, which was followed by a small flexion torque just before toe-off. A knee extension torque then developed again during the first half of swing, whereas a knee flexion torque developed during the first half of swing, whereas a knee flexor torque developed during the last half of swing. At the ankle joint, a large plantarflexion torque occurred during stance, which peaked around midstance and decreased by toe-off. The torque at the ankle joint during swing was minimal. As running speed increased, the characteristic profiles of the sagittal-plane

TABLE 1. Mean ± SD magnitudes for the torque, power and work variables.

Variable	Speed 1 (n = 8)	Speed 2 (n = 8)	Speed 3 (n = 8)	Speed 4 (n = 7)	Effect Size (Partial η^2)
	3.50 ± 0.04 m·s ⁻¹	5.02 ± 0.10 m·s ⁻¹	6.97 ± 0.09 m·s ⁻¹	8.95 ± 0.70 m·s ⁻¹	
Hip					
$T_{\text{Peak extension initial stance}}$ (N·m·kg ⁻¹)*	2.02 ± 0.36 ^{3,4}	2.95 ± 1.08	3.18 ± 0.85 ¹	4.09 ± 0.69 ¹	0.68
$T_{\text{Peak flexion initial swing}}$ (N·m·kg ⁻¹)*	-1.09 ± 0.06 ^{2,3,4}	-1.69 ± 0.25 ^{1,3,4}	-2.59 ± 0.35 ^{1,2,4}	-4.30 ± 0.87 ^{1,2,3}	0.92
$T_{\text{Peak extension terminal swing}}$ (N·m·kg ⁻¹)*	0.91 ± 0.17 ^{2,3,4}	1.41 ± 0.22 ^{1,3,4}	2.45 ± 0.46 ^{1,2,4}	4.18 ± 1.26 ^{1,2,3}	0.89
$T_{\text{Peak abduction stance}}$ (N·m·kg ⁻¹)*	2.00 ± 0.26 ³	2.42 ± 0.80	3.10 ± 0.65 ¹	3.29 ± 1.10	0.50
$T_{\text{Peak internal rotation stance}}$ (N·m·kg ⁻¹)*	0.49 ± 0.17 ⁴	0.56 ± 0.20	0.70 ± 0.28	0.99 ± 0.54 ¹	0.59
$P_{\text{Peak absorption terminal stance}}$ (W·kg ⁻¹)*	-2.15 ± 0.83 ^{2,3,4}	-5.56 ± 2.25 ^{1,4}	-11.83 ± 5.29 ^{1,4}	-22.93 ± 9.76 ^{1,2,3}	0.81
$P_{\text{Peak generation initial swing}}$ (W·kg ⁻¹)*	3.80 ± 0.95 ^{2,3,4}	7.55 ± 1.63 ^{1,3,4}	15.16 ± 3.45 ^{1,2,4}	29.01 ± 13.06 ^{1,2,3}	0.81
$P_{\text{Peak absorption midswing}}$ (W·kg ⁻¹)*	-1.77 ± 0.88 ^{2,3,4}	-3.98 ± 1.29 ^{1,4}	-7.05 ± 2.75 ¹	-23.45 ± 15.06 ^{1,2}	0.68
$P_{\text{Peak generation terminal swing}}$ (W·kg ⁻¹)*	3.40 ± 0.95 ^{2,3,4}	7.46 ± 3.06 ^{1,3,4}	17.41 ± 5.39 ^{1,2,4}	41.06 ± 9.42 ^{1,2,3}	0.94
$W_{\text{Negative work done terminal stance}}$ (J·kg ⁻¹)*	-0.16 ± 0.13 ^{3,4}	-0.23 ± 0.14 ⁴	-0.46 ± 0.22 ¹	-0.69 ± 0.26 ^{1,2}	0.78
$W_{\text{Positive work done initial swing}}$ (J·kg ⁻¹)*	0.42 ± 0.11 ^{2,3,4}	0.74 ± 0.18 ^{1,3,4}	1.10 ± 0.23 ^{1,2,4}	1.67 ± 0.52 ^{1,2,3}	0.87
$W_{\text{Negative work done midswing}}$ (J·kg ⁻¹)*	-0.10 ± 0.05 ^{2,3,4}	-0.19 ± 0.08 ^{1,3,4}	-0.38 ± 0.14 ^{1,2}	-0.89 ± 0.47 ^{1,2}	0.71
$W_{\text{Positive work done terminal swing}}$ (J·kg ⁻¹)*	0.31 ± 0.10 ^{2,3,4}	0.65 ± 0.27 ^{1,3,4}	1.22 ± 0.28 ^{1,2,4}	2.28 ± 0.71 ^{1,2,3}	0.91
Knee					
$T_{\text{Peak extension midstance}}$ (N·m·kg ⁻¹)	3.12 ± 0.56	3.52 ± 0.51	3.59 ± 0.63	3.55 ± 0.38	0.29
$T_{\text{Peak extension initial swing}}$ (N·m·kg ⁻¹)*	0.17 ± 0.02 ^{2,3,4}	0.30 ± 0.07 ^{1,3,4}	0.64 ± 0.24 ^{1,2,4}	1.01 ± 0.26 ^{1,2,3}	0.88
$T_{\text{Peak flexion terminal swing}}$ (N·m·kg ⁻¹)*	-0.53 ± 0.09 ^{2,3,4}	-0.71 ± 0.13 ^{1,3,4}	-1.08 ± 0.16 ^{1,2,4}	-1.76 ± 0.28 ^{1,2,3}	0.96
$T_{\text{Peak abduction stance}}$ (N·m·kg ⁻¹)*	0.65 ± 0.30 ⁴	0.99 ± 0.49	1.54 ± 0.59	1.42 ± 0.39 ¹	0.50
$T_{\text{Peak external rotation stance}}$ (N·m·kg ⁻¹)*	-0.20 ± 0.08 ^{3,4}	-0.32 ± 0.09	-0.30 ± 0.11 ¹	-0.43 ± 0.11 ¹	0.51
$P_{\text{Peak absorption initial stance}}$ (W·kg ⁻¹)*	-15.69 ± 4.80 ³	-18.67 ± 6.55 ³	-26.73 ± 7.72 ^{1,2}	-28.70 ± 9.61	0.53
$P_{\text{Peak generation terminal stance}}$ (W·kg ⁻¹)*	7.72 ± 1.93 ^{3,4}	11.04 ± 3.06	13.03 ± 3.26 ¹	15.91 ± 5.06 ¹	0.58
$P_{\text{Peak absorption initial swing}}$ (W·kg ⁻¹)*	-1.67 ± 0.34 ^{2,3,4}	-3.21 ± 0.97 ^{1,3,4}	-7.15 ± 2.48 ^{1,2,4}	-13.95 ± 3.00 ^{1,2,3}	0.92
$P_{\text{Peak absorption terminal swing}}$ (W·kg ⁻¹)*	-4.61 ± 0.61 ^{2,3,4}	-8.50 ± 2.22 ^{1,3,4}	-18.30 ± 3.59 ^{1,2,4}	-37.15 ± 7.20 ^{1,2,3}	0.95
$W_{\text{Negative work done initial stance}}$ (J·kg ⁻¹)	-0.74 ± 0.26	-0.78 ± 0.28	-0.83 ± 0.28	-0.60 ± 0.24	0.32
$W_{\text{Positive work done terminal stance}}$ (J·kg ⁻¹)	0.41 ± 0.13	0.44 ± 0.13	0.39 ± 0.16	0.34 ± 0.10	0.21
$W_{\text{Negative work done initial swing}}$ (J·kg ⁻¹)*	-0.19 ± 0.04 ^{2,3,4}	-0.39 ± 0.10 ^{1,3,4}	-0.71 ± 0.17 ^{1,2,4}	-1.21 ± 0.26 ^{1,2,3}	0.93
$W_{\text{Negative work done terminal swing}}$ (J·kg ⁻¹)*	-0.41 ± 0.04 ^{2,3,4}	-0.77 ± 0.16 ^{1,3,4}	-1.31 ± 0.23 ^{1,2,4}	-2.07 ± 0.27 ^{1,2,3}	0.97
Ankle					
$T_{\text{Peak plantarflexion midstance}}$ (N·m·kg ⁻¹)*	2.94 ± 0.35 ^{2,3,4}	3.55 ± 0.39 ¹	3.77 ± 0.44 ¹	4.00 ± 0.42 ¹	0.74
$T_{\text{Peak inversion stance}}$ (N·m·kg ⁻¹)*	0.24 ± 0.12 ^{3,4}	0.31 ± 0.17	0.61 ± 0.20 ¹	0.63 ± 0.15 ¹	0.63
$T_{\text{Peak external rotation stance}}$ (N·m·kg ⁻¹)	-0.25 ± 0.11	-0.31 ± 0.05	-0.32 ± 0.08	-0.38 ± 0.13	0.32
$P_{\text{Peak absorption initial stance}}$ (W·kg ⁻¹)*	-7.77 ± 2.60 ^{2,3,4}	-14.42 ± 3.81 ^{1,3,4}	-23.79 ± 6.39 ^{1,2}	-34.20 ± 13.27 ^{1,2}	0.82
$P_{\text{Peak generation terminal stance}}$ (W·kg ⁻¹)*	16.09 ± 2.09 ^{2,3,4}	27.25 ± 4.99 ^{1,3,4}	37.10 ± 6.55 ^{1,2}	46.98 ± 9.50 ^{1,2}	0.89
$W_{\text{Negative work done initial stance}}$ (J·kg ⁻¹)*	-0.46 ± 0.16 ^{2,3,4}	-0.69 ± 0.19 ¹	-0.85 ± 0.18 ¹	-0.83 ± 0.21 ¹	0.65
$W_{\text{Positive work done terminal stance}}$ (J·kg ⁻¹)*	1.00 ± 0.10 ^{2,3,4}	1.30 ± 0.19 ¹	1.38 ± 0.20 ¹	1.44 ± 0.21 ¹	0.69

Gray shaded rows indicate variables that displayed significant increases in absolute magnitude for all running speed increments.

* Significant speed effect ($P < 0.008$).

¹ Significantly different from running speed 1 ($P < 0.008$).

² Significantly different from running speed 2 ($P < 0.008$).

³ Significantly different from running speed 3 ($P < 0.008$).

⁴ Significantly different from running speed 4 ($P < 0.008$).

η^2 , eta-squared; P , power; T , torque; W , work.

torques remained consistent (Fig. 1). However, the maxima and minima points on the curves increased in absolute magnitude (Table 1). Of the seven variables extracted from the sagittal-plane torques, only peak knee extension torque during midstance was not found to display a significant speed effect. A significant increase in absolute magnitude for all running speed increments was shown by four variables: peak hip flexion torque during initial swing, peak hip extension torque during terminal swing, peak knee extension torque during initial swing, and peak knee flexion torque during terminal swing. When running speed changed from 3.50 to 8.95 m·s⁻¹, these variables increased in absolute magnitude by 3.21 N·m·kg⁻¹ (3.94-fold), 3.27 N·m·kg⁻¹ (4.59-fold), 0.84 N·m·kg⁻¹ (5.94-fold), and 1.23 N·m·kg⁻¹ (3.32-fold), respectively.

The normalized mean ± SD frontal-plane torques developed about the hip, knee, and ankle joints across the full

stride cycle for each running speed condition are presented in Figure 2. At the hip joint, an abduction torque rapidly developed after foot strike that persisted for the majority of stance, after which an adduction torque developed just before toe-off. During swing, the frontal-plane torque at the hip fluctuated between small adduction and abduction torques. An adduction torque occurred during the final stages of swing, which continued through to the instant of foot strike. At the knee joint, an abduction torque developed during the first half of stance. For slower running speeds (3.50 and 5.02 m·s⁻¹), an abduction torque persisted until toe-off, but for faster running speeds (6.97 and 8.95 m·s⁻¹), an adduction torque developed at midstance and at toe-off. The frontal-plane torque at the knee joint was minimal for most of swing before a small abduction torque occurred just before foot strike. At the ankle joint, an inversion torque developed throughout initial and midstance, after which a

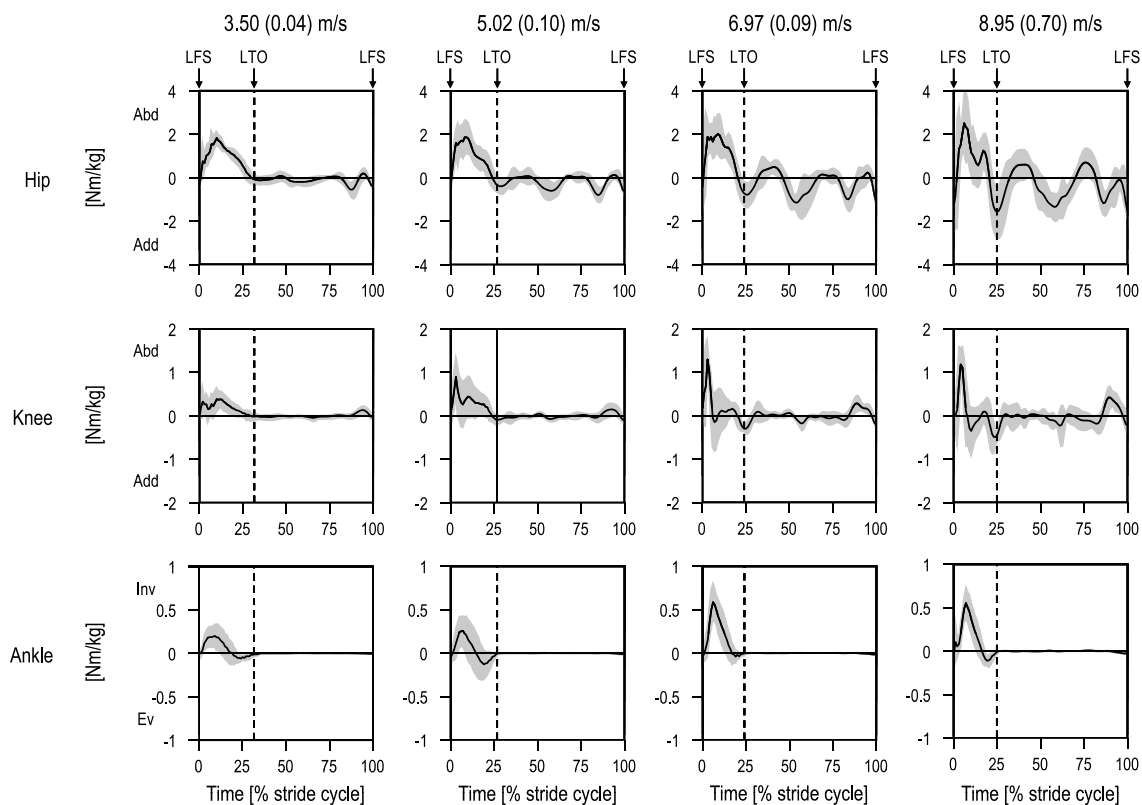


FIGURE 2—Frontal-plane torques developed about the hip (*top panels*), knee (*middle panels*), and ankle (*bottom panels*) joints across the full stride cycle for the left lower limb (left foot strike to left foot strike) for the four discrete running speeds. Data represent the group mean (*solid black line*) \pm one SD (*gray shading*). The *dashed vertical line* indicates the average time (% stride cycle) of toe-off for each speed condition. LFS: left foot-strike; LTO: left toe-off; Abd, abduction; Add, adduction; Ev, eversion; Inv, inversion.

small eversion torque developed during terminal stance. The peak magnitudes of the frontal-plane torques during stance all displayed a significant speed effect (Table 1). Peak hip abduction torque during stance, peak knee abduction torque during stance, and peak ankle inversion torque during stance increased by $1.29 \text{ N}\cdot\text{m}\cdot\text{kg}^{-1}$ (1.65-fold), $0.77 \text{ N}\cdot\text{m}\cdot\text{kg}^{-1}$ (2.18-fold) and $0.39 \text{ N}\cdot\text{m}\cdot\text{kg}^{-1}$ (2.63-fold), respectively, when running speed changed from 3.50 to $8.95 \text{ m}\cdot\text{s}^{-1}$.

The normalized mean \pm SD transverse-plane torques developed the hip, knee, and ankle joints across the full stride cycle for each running speed condition are presented in Figure 3. After an initial external rotation hip joint torque at foot strike, an internal rotation torque developed during initial stance, whereas an external rotation torque developed during terminal stance. The transverse-plane torque at the hip joint then fluctuated during initial and midswing before an external rotation torque developed during terminal swing. At the knee joint, an external rotation torque developed during stance, especially for faster running speeds. A degree of variability across participants was evident for the slower running speeds. At the ankle joint, an external rotation torque developed during stance. The peak magnitudes of the transverse-plane torques during stance displayed a significant speed effect at the hip and knee joints but not at the ankle (Table 1). Peak hip internal rotation torque during stance and peak knee external rotation torque during

stance increased in absolute magnitude by $0.5 \text{ N}\cdot\text{m}\cdot\text{kg}^{-1}$ (2.02-fold) and $0.23 \text{ N}\cdot\text{m}\cdot\text{kg}^{-1}$ (2.15-fold), respectively, when running speed changed from 3.50 to $8.95 \text{ m}\cdot\text{s}^{-1}$.

The normalized mean \pm SD net powers developed about the hip, knee, and ankle joints across the full stride cycle for each running speed condition are presented in Figure 4. At the hip, small bursts of power generation tended to occur during the first half of stance, especially at faster running speeds. From midstance onward, continuous phases in the hip joint power profile were clearly identifiable. Power was absorbed during terminal stance, generated during initial swing, then absorbed again during midswing, and finally generated during terminal swing. At the knee, power was absorbed during the first half of stance and generated during the latter half of stance. Power was also absorbed during terminal stance, generated during initial swing. At the ankle, power was absorbed during the first half of stance and then generated for the remainder of stance. All 10 variables extracted from the lower limb joint powers displayed a significant speed effect (Table 1). However, a significant increase in absolute magnitude for all running speed increments was only demonstrated by four variables: peak hip joint power generation during initial swing, peak hip joint power generation during terminal swing, peak knee joint power absorption during initial swing, and peak knee joint power absorption during terminal swing. When running speed

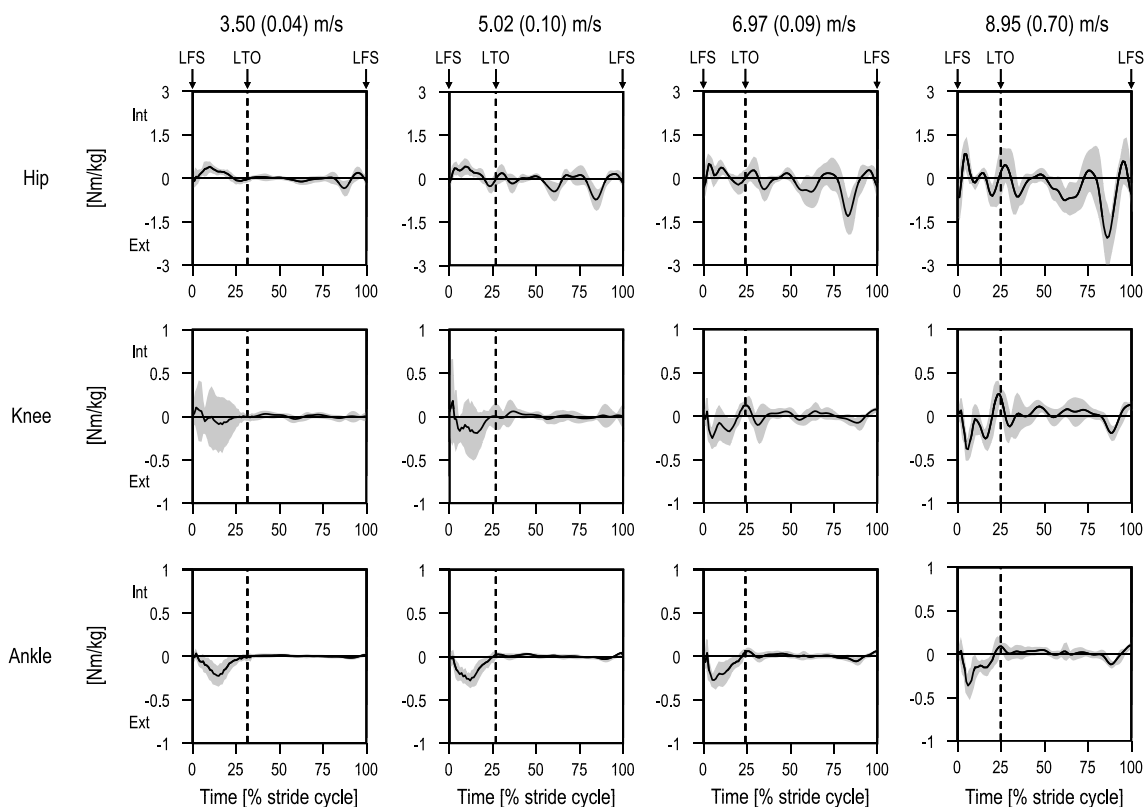


FIGURE 3—Transverse-plane torques developed about the hip (*top panels*), knee (*middle panels*), and ankle (*bottom panels*) joints across the full stride cycle for the left lower limb (left foot strike to left foot strike) for the four discrete running speeds. Data represent the group mean (*solid black line*) \pm one SD (*gray shading*). The *dashed vertical line* indicates the average time (% stride cycle) of toe-off for each speed condition. LFS: left foot-strike; LTO: left toe-off; Ext, external rotation; Int, internal rotation.

changed from 3.50 to 8.95 $\text{m}\cdot\text{s}^{-1}$, these variables increased in absolute magnitude by 25.21 $\text{W}\cdot\text{kg}^{-1}$ (7.63-fold), 37.66 $\text{W}\cdot\text{kg}^{-1}$ (12.08-fold), 12.28 $\text{W}\cdot\text{kg}^{-1}$ (8.35-fold), and 32.54 $\text{W}\cdot\text{kg}^{-1}$ (8.06-fold), respectively.

Data for the amount of work done at the lower limb joints are contained in Table 1. The hip and ankle were found to be predominantly energy generators because the amount of positive work done over the stride cycle exceeded the amount of negative work done. Conversely, the knee joint was predominantly an energy absorber. The work done at the hip increased significantly with faster running. For example, the largest absolute change occurred during terminal swing, where the amount of positive work increased by 1.97 $\text{J}\cdot\text{kg}^{-1}$ (7.35-fold) when running speed changed from 3.50 to 8.95 $\text{m}\cdot\text{s}^{-1}$. At the knee, the total work done during stance was relatively invariant across running speed conditions, whereas the negative work done during initial swing and terminal swing increased in absolute magnitude by 1.02 $\text{J}\cdot\text{kg}^{-1}$ (6.37-fold) and 1.66 $\text{J}\cdot\text{kg}^{-1}$ (5.05-fold), respectively, when running speed changed from 3.50 to 8.95 $\text{m}\cdot\text{s}^{-1}$. At the ankle, the total work done during stance increased by 0.53 $\text{J}\cdot\text{kg}^{-1}$ (1.36-fold) from 3.50 to 5.02 $\text{m}\cdot\text{s}^{-1}$, but then increased by only 0.28 $\text{J}\cdot\text{kg}^{-1}$ (1.14-fold) thereafter.

When second-order polynomial trend lines were fitted to the data for each of the work variables, very little association was found between running speed and the work

done at the knee joint during initial stance (work = $0.019 \times \text{speed}^2 - 0.223 \times \text{speed} - 0.179$; $R^2 = 0.10$) and terminal stance (work = $-0.002 \times \text{speed}^2 + 0.012 \times \text{speed} + 0.403$; $R^2 = 0.04$). Moderate associations occurred between running speed and the work done at the hip joint during terminal stance (work = $-0.007 \times \text{speed}^2 - 0.014 \times \text{speed} - 0.023$; $R^2 = 0.56$) and midswing (work = $-0.031 \times \text{speed}^2 + 0.249 \times \text{speed} - 0.605$; $R^2 = 0.74$) as well as at the ankle joint during initial stance (work = $0.013 \times \text{speed}^2 - 0.238 \times \text{speed} + 0.197$; $R^2 = 0.44$) and terminal stance (work = $-0.017 \times \text{speed}^2 + 0.288 \times \text{speed} + 0.220$; $R^2 = 0.50$). The strongest associations with running speed were found for the positive work done at the hip during initial swing ($R^2 = 0.83$) and terminal swing ($R^2 = 0.87$) and for the negative work done at the knee during initial swing ($R^2 = 0.89$) and terminal swing ($R^2 = 0.94$; Fig. 5).

DISCUSSION

The purpose of the current study was to evaluate the effect of running speed on lower limb joint kinetics to determine which biomechanical variables were most influenced by speed approaching maximal sprinting. Kinematic and ground reaction force data were collected from eight participants while running at four discrete speeds: $3.50 \pm 0.04 \text{ m}\cdot\text{s}^{-1}$, $5.02 \pm 0.10 \text{ m}\cdot\text{s}^{-1}$, $6.97 \pm 0.09 \text{ m}\cdot\text{s}^{-1}$, and

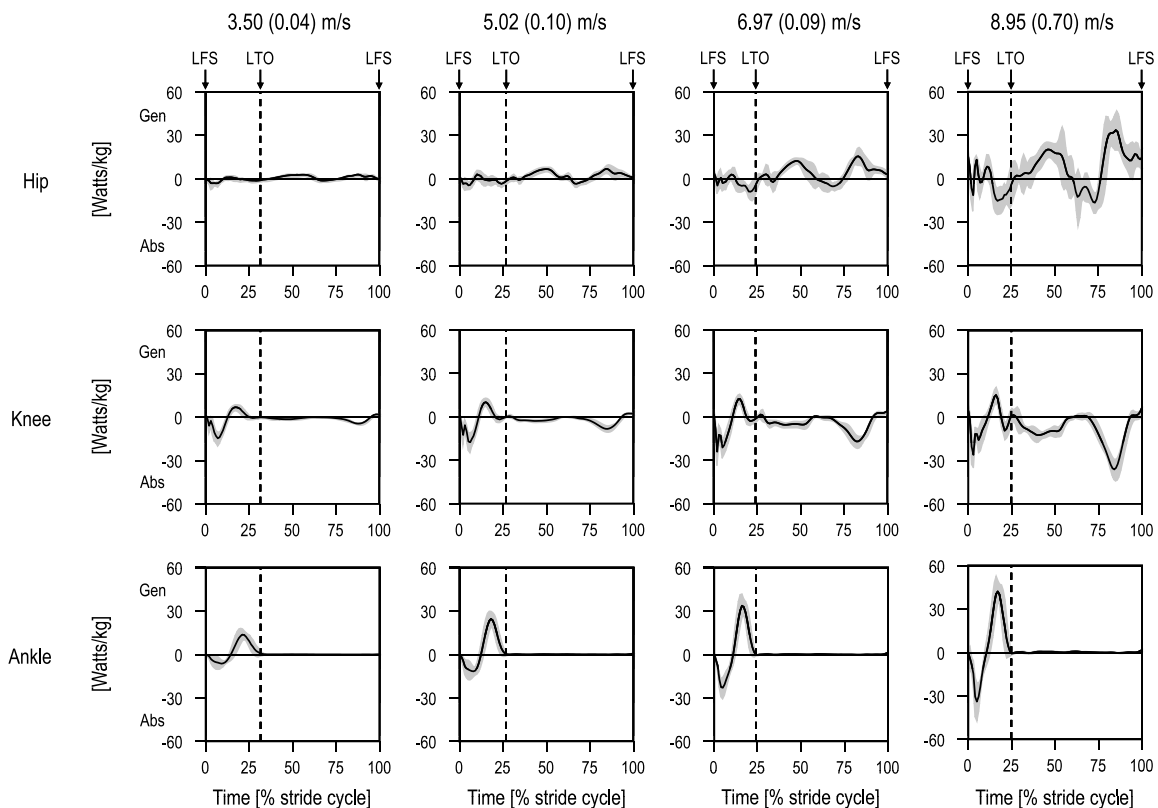


FIGURE 4—Net powers developed about the hip (*top panels*), knee (*middle panels*), and ankle (*bottom panels*) joints across the full stride cycle for the left lower limb (left foot strike to left foot strike) for the four discrete running speeds. Data represent the group mean (*solid black line*) \pm one SD (*gray shading*). The *dashed vertical line* indicates the average time (% stride cycle) of toe-off for each speed condition. LFS: left foot-strike; LTO: left toe-off; Abs, absorption; Gen, generation.

$8.95 \pm 0.70 \text{ m}\cdot\text{s}^{-1}$. A standard inverse-dynamics approach was used to compute the three-dimensional torques at the lower limb joints, from which net powers and work were also calculated. The torques developed about the hip, knee, and ankle joints during running displayed identifiable profiles in all three anatomical planes (Figs. 1–3). Several interesting findings were revealed from the data. First, the

variables that displayed the largest increases in absolute magnitude with faster running were the sagittal-plane torques, net powers, and work done at the hip and knee joints during terminal swing (Table 1; Figs. 1, 4, and 5). Second, the peak extension torque and work done at the knee joint during stance were found to be unaffected by increasing running speed (Table 1). Third, whereas the work done at the ankle

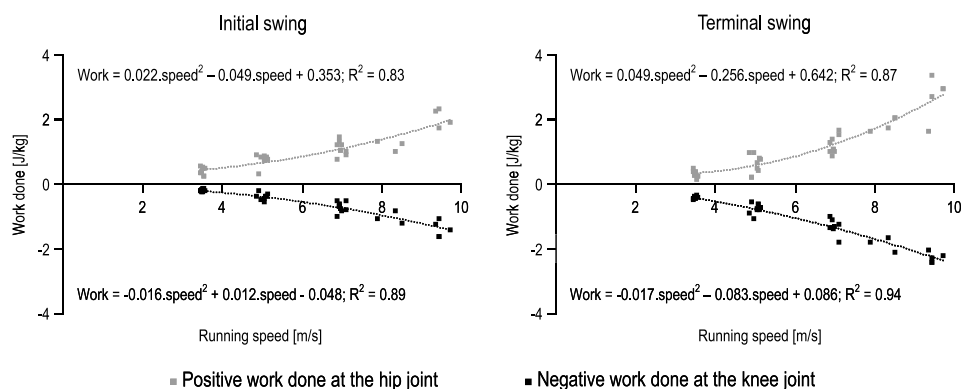


FIGURE 5—Work done at the hip and knee joints during initial swing (*left panel*) and terminal swing (*right panel*) with increasing running speed. The scatter plots contain data for each participant (*filled boxes*) for each speed condition as well as the second-order polynomial trend lines fitted to the data (*dotted lines*). Data for the positive work done at the hip joint are indicated in *gray*, whereas data for the negative work done at the knee joint are indicated in *black*. During initial swing, energy is generated at the hip joint primarily by the hip flexor muscles at the same time as energy is absorbed at the knee joint primarily by the knee extensor muscles. During terminal swing, energy is generated at the hip joint primarily by the hip extensor muscles at the same time as energy is absorbed at the knee joint primarily by the knee flexor muscles. Note that with increasing running speed, the gradient of the trend lines becomes steeper for the work done at the hip and knee joints during terminal swing when compared to initial swing.

joint during stance significantly increased when running speed changed from 3.50 to 5.02 m·s⁻¹, it seemed to plateau when running speed progressed beyond 5.02 m·s⁻¹ (Table 1). These results have important implications for lower limb muscle function with faster running. For example, when running speed progressed beyond 6.97 m·s⁻¹, a substantial increase in biomechanical load occurred for the hip flexor and extensor muscles during swing compared with the knee extensor and ankle plantar-flexor muscles during stance. Furthermore, of all the major lower limb muscle groups, the hip extensor and knee flexor muscles during terminal swing demonstrated the most dramatic increase in biomechanical load with faster running.

There are several limitations associated with the methods used in the present study that need to be acknowledged. First, an inverse-dynamics approach was used to calculate lower limb joint torques during running. Although inverse dynamics as well as subsequent net power and work done calculations are well-accepted biomechanical analyses, such an approach is limited in its ability to provide quantitative information regarding muscle function, as a given torque can be produced by an infinite combination of muscle forces. Second, as skin markers were used to measure lower limb kinematics, it is likely that estimates of segment velocity and acceleration were associated with a degree of error due to soft tissue artifact, particularly for the thigh as running speed increased. Some of the large fluctuations in the computed hip joint torques during swing for the faster speeds of running may therefore be attributable to this error. To minimize soft tissue artifact as much as possible, two main strategies were taken: (a) thigh tracking markers were restricted to areas that have been shown to be associated with lesser amounts of soft tissue artifact, such as the anterolateral aspect of the distal third of the thigh (2,31); and (b) a hierarchical biomechanical model was used in this study, whereby the pelvic tracking markers were used to reconstruct the hip joint center and the shank tracking markers were used to reconstruct the knee joint center. The thigh tracking markers (which are likely prone to the largest amounts of soft tissue artifact) were therefore only used to reconstruct the additional anatomical location that was required, together with the hip and knee joint centers, to define the femoral anatomical coordinate system. Third, given the large amount of data collected and analyzed in this study, the sample size was restricted to eight participants. It is therefore possible that some of the variables that showed a significant effect for speed but did not display significant increases in absolute magnitude for all running speed increments on *post hoc* testing may have done so with a larger sample size (e.g., peak ankle joint power absorption and generation during stance). However, it is not expected that a larger sample size would alter the main conclusions from this study, which were also based on the evident associations between work done at the lower limb joints and running speed. Fourth, the sample analyzed in this study was somewhat heterogenous, composed of both male and female participants recruited from two alternative running-

based sports. Finally, only a single trial was analyzed per speed condition for each participant. It is acknowledged that it would have been ideal to have analyzed several trials per speed condition for each participant. However, the criteria for a successful trial were that the participant achieved a running speed within 5% of the desired speed and also achieved a valid foot strike on a single force plate for the test leg. It often took several attempts to obtain a single successful trial for a given speed condition, especially for the faster speeds of running. Consequently, in an effort to collect all data within a reasonable time frame and avoid the potential confounding effect of fatigue, the study was limited to a single trial per speed condition for each participant.

When comparing data in the present study with that reported by previous researchers, there are many factors that must be taken into account. These factors include (i) running speeds tested; (ii) the particular region of the running task that has been evaluated, such as the acceleration versus steady-state speed regions; (iii) differences in the biomechanical model used, such as definitions of joint center locations; (iv) the sampling rate used to capture data; (v) the filtering technique applied to the data; (vi) the process used to normalize the data; and (vii) the reference frame used to express the components of the net torque vector at each of the joints, specifically, laboratory reference frame, proximal segment reference frame, distal segment reference frame, or nonorthogonal reference frame (i.e., joint coordinate system). Various combinations of these factors will explain any observed differences between the data from the current study compared with previous studies.

With the above factors in mind, data from the present study display reasonable quantitative consistency with previous data in the literature. Ae et al. (1) measured sagittal-plane torques and net powers at the lower limb joints across the full stride cycle from five skilled male sprinters running at 2.68, 3.89, 6.52, 7.86, and 9.59 m·s⁻¹. Unfortunately, the study of Ae et al. (1) is only available in abstract format, and thus, very limited data are actually presented. Also, a two-dimensional approach was taken; thus, only sagittal-plane torques were evaluated. Despite these issues, data that are available in Ae et al. (1) are in agreement with the present study. For example, during terminal swing for sprinting at 9.59 m·s⁻¹, Ae et al. (1) computed a peak hip extension torque of ~3.5 N·m·kg⁻¹, a peak knee flexion torque of ~2.0 N·m·kg⁻¹, and a peak knee power absorption of ~35.0 W·kg⁻¹. These peak magnitudes are all quantitatively consistent with equivalent data from the current study (Table 1).

Other studies have reported sagittal-plane torques and net powers at the lower limb joints across a range of running speeds but have obtained data only for a certain phase of the stride cycle, specifically, either the stance (3,5) or the swing phase (33). In a study of 13 runners, Arampatzis et al. (3) reported peak stance knee extension torques ranging from 2.57 ± 0.46 to 2.98 ± 0.37 N·m·kg⁻¹ (1.16-fold increase) and peak stance ankle plantarflexion torques ranging from

2.79 ± 0.42 to 3.43 ± 0.49 $\text{N}\cdot\text{m}\cdot\text{kg}^{-1}$ (1.23-fold increase) when running speed changed from 3.55 ± 0.19 to 6.59 ± 0.24 $\text{m}\cdot\text{s}^{-1}$. These relative increases in magnitude were similar to the present study, where the peak stance knee extension and ankle plantarflexion torques increased by 1.15-fold and 1.36-fold, respectively, when running speed changed from 3.50 to 6.97 $\text{m}\cdot\text{s}^{-1}$ (Table 1). Belli et al. (5) measured sagittal-plane torques and net powers at the lower limb joints from nine middle-distance runners at running speeds of 4.0 , 6.0 , and 8.9 $\text{m}\cdot\text{s}^{-1}$. When comparing results to the current study, one notable difference is that Belli et al. (5) found the peak stance knee extension torque to increase (1.57-fold) with faster running. This discrepancy might be explained by differences in running technique for middle-distance runners versus sprinters. Swanson and Caldwell (33) measured net powers during swing at the hip and knee joints for 12 male athletes while running on a level treadmill at 4.47 and 7.61 $\text{m}\cdot\text{s}^{-1}$. Net powers from the current study for running speeds of 5.02 and 6.97 $\text{m}\cdot\text{s}^{-1}$ (Table 1) were between 1.5- and 3.3-fold greater than that reported by Swanson and Caldwell (33). It is possible that these differences are a consequence of contrasting experimental conditions: data from Swanson and Caldwell (33) were collected during treadmill running, whereas data from this study were obtained during overground running.

The profiles of the computed torques and net powers at the lower limb joints from this study also display good qualitative consistency with previous findings in the literature. With respect to the sagittal-plane torques, the profiles from the current study are near identical with those presented by Ae et al. (1), which, to our knowledge, is the only previous study to have presented torques at the hip, knee, and ankle joints across the full stride cycle for a range of running speeds. With respect to net powers, four distinct phases of power absorption and generation were identified in the current study at the hip joint (i.e., terminal stance power absorption, initial swing power generation, midswing power absorption, terminal swing power generation) and the knee joint (i.e., initial stance power absorption, terminal stance power generation, initial swing power absorption, terminal swing power absorption) (Fig. 4), which is consistent with previous studies (1,6,19,33,34,37). For the ankle joint, two distinct phases of power absorption and generation were identified in the current study (i.e., initial stance power absorption and terminal stance power generation) (Fig. 4), which is also in agreement with that from other studies (1,3,5,6,8,19,23,37). However, the profile of the hip joint power during initial stance is less consistent across the literature. In this study, a variable or burstlike pattern was found to exist, particularly for the faster speeds of running (Fig. 4). Whereas other researchers (1,6,19,37) have observed a similar profile to the current study, Belli et al. (5) found a distinct phase of continuous power generation at the hip during the initial stance.

Despite being a predominantly planar motion, this study demonstrated that the torques at the lower limb joints during

running do contain appreciable three-dimensional components. Identifiable profiles were evident in all planes; however, some variability across participants was evident in the frontal- and transverse-plane torques developed about the knee joint (Figs. 2 and 3) during stance at the running speeds of 3.50 and 5.02 $\text{m}\cdot\text{s}^{-1}$. This result suggests that participants displayed a degree of variability in the posture of their knee joint with respect to the ground reaction force in the frontal and transverse planes for the slower speeds of running. Although two previous studies also have reported three-dimensional torques at the lower limb joints during running (16,23), both were limited to stance phase data and a single speed of running only. Furthermore, Glitsch and Baumann (16) obtained data for a single subject only, whereas McClay and Manal (23) did not evaluate the hip joint. To our knowledge, no previous study has provided a complete description of the three-dimensional torques at the hip, knee, and ankle joints across a broad spectrum of running speeds. Data contained in Table 1 and Figures 1–3 are therefore important in terms of providing reference values for future studies to use for comparative purposes.

Of all the biomechanical variables evaluated in this study, the work done at the lower limb joints conveys the most critical information regarding muscle function (38). Positive work is work done during a concentric contraction, which represents a flow of energy from the muscles to the limbs (energy generation), whereas negative work is work done during an eccentric contraction, which represents a flow of energy from the limbs to the muscles (energy absorption). Given the significance of work done at the lower limb joints for understanding muscle function, the association between work and running speed was computed for all the periods in the stride cycle where it was evident that a continuous portion of positive or negative work was performed. A total of 10 periods were identified across all running speeds (Table 1; see Figure, Supplemental Digital Content 2, the 10 distinct periods of continuous positive or negative work done at the lower limb joints identified across the stride cycle for all running speeds, <http://links.lww.com/MSS/A81>). The strongest associations between work and running speed were found for the hip and knee joints during initial swing and terminal swing (Fig. 5). In contrast, the work done at the knee joint during stance was relatively invariant with running speed, whereas the work done at the ankle joint increased between 3.50 and 5.02 $\text{m}\cdot\text{s}^{-1}$ but then changed very little thereafter (Table 1). Such results are generally consistent with that previously reported in the literature by Ae et al. (1). Knowledge regarding the work done at the lower limb joints with faster running therefore has important implications for both swing and stance phase leg muscle function.

During the initial swing, the hip flexor muscles were found to generate energy at the same time as the knee extensor muscles absorbed energy, whereas during terminal swing the hip extensor muscles were found to generate energy at the same time as the knee flexor muscles absorbed

energy (Figs. 4 and 5). These findings provide insights into the function of the major biarticular muscles of the thigh, specifically, the rectus femoris and hamstring muscles (9). Such muscles have been proposed to act as “energy straps” by harnessing the energy from a moving body segment and transferring that energy to the next adjacent joint (24). Energy exchange via the rectus femoris may occur at two points in the stride cycle: (a) during terminal stance, where energy is absorbed at the hip and simultaneously generated at the knee; and (b) during initial swing, where energy is absorbed at the knee and simultaneously generated at the hip. However, the energy exchange occurring during initial swing is likely to be more critical, as it was found to have a far greater sensitivity to increasing running speed. During terminal stance, the energy absorbed at the hip displayed only a moderate association with running speed ($R^2 = 0.56$), whereas the energy generated at the knee displayed no association with running speed ($R^2 = 0.04$). Energy exchange via the hamstring muscles may occur during terminal swing, where energy is absorbed at the knee and simultaneously generated at the hip. On the basis of these results, it is speculated that, as running speed is progressed toward maximal sprinting, a dramatic increase in biomechanical load is likely imparted onto the rectus femoris and hamstring muscles during initial swing and terminal swing, respectively. It has been well documented that rectus femoris and hamstring muscle strain injuries are common in sports that involve repetitive bouts of sprinting, such as Australian Rules football (25) and soccer (4,14). The sensitivity of the work done at the hip and knee joints during initial swing and terminal swing to increasing running speed may potentially offer a biomechanical explanation for these clinical observations. Future studies using computer-based musculoskeletal modeling techniques to quantify the function of individual muscles with increasing speeds of running are needed to further explore these hypotheses.

In contrast to swing, it seems that the work done by the leg extensor muscles during stance changes very little when running speed is progressed beyond $5.02 \text{ m}\cdot\text{s}^{-1}$. Although the positive work done at the hip joint by the extensor muscles during early stance was not quantified, it is not

anticipated that doing so would change this general conclusion. Such results can be used to identify the mechanisms by which humans run faster. There are two basic ways to increase running speed: one can push on the ground harder (i.e., increase stride length) and/or one can push on the ground more frequently (i.e., increase stride frequency). Data from the present study indicate that, to achieve speeds above $5.02 \text{ m}\cdot\text{s}^{-1}$, runners become increasingly reliant on more frequent ground contacts of similar force rather than more forceful ground contacts. However, it is important to note that this observation cannot be used to make definitive conclusions regarding the biomechanical limitation to maximal sprinting. On the basis of the experimental data reported by Weyand et al. (35,36), the ultimate limit to maximal sprinting would seem to be related to how hard and quickly a runner can push on the ground. More specifically, these researchers found that top speed was obtained when the impulse responsible for elevating the body against gravity (force applied normal to the ground multiplied by stance time) reduced to the minimum levels necessary to provide enough time to swing the leg into position for the next step (36). As running speed increases, stance time eventually becomes too short to allow the forces developed by the leg extensor muscles to reach their contractile maximums (35).

In summary, this study measured three-dimensional torques, net powers, and work done at the lower limb joints across a broad spectrum of running speeds. The results provide insights into the underlying biomechanical causes of the observed movement patterns at the hip, knee, and ankle joints during running. Of all the major lower limb muscle groups, the hip extensor and knee flexor muscles during terminal swing demonstrated the most dramatic increase in biomechanical load when running speed progressed toward maximal sprinting.

Funding for this project was provided by the Physiotherapy Research Foundation Tagged Sports Physiotherapy Australia Research Grant (T08-THE/SPA(1)018), an Australian Research Council Discovery Grant (DP0772838), and a VESKI Innovation Fellowship.

The authors have no conflicts of interest.

The results of the present study do not constitute endorsement by the American College of Sports Medicine.

REFERENCES

1. Ae M, Miyashita K, Yokoi T, Hashihara Y. Mechanical power and work done by the muscles of the lower limb during running at different speeds. In: Jonsson B, editor. *Biomechanics X-B*. Champaign (IL): Human Kinetics; 1987. p. 895–9.
2. Akbarshahi M, Schache AG, Fernandez JW, Baker R, Banks S, Pandy MG. Non-invasive assessment of soft-tissue artifact and its effect on knee joint kinematics during functional activity. *J Biomech*. 2010;43:1292–301.
3. Arampatzis A, Bruggemann GP, Metzler V. The effect of running speed on leg stiffness and joint kinetics in human running. *J Biomech*. 1999;32:1349–53.
4. Arnason A, Gudmundsson A, Dahl HA, Johannsson E. Soccer injuries in Iceland. *Scand J Med Sci Sports*. 1996;6:40–5.
5. Belli A, Kyrolainen H, Komi PV. Moment and power of lower limb joints in running. *Int J Sports Med*. 2002;23:136–41.
6. Bezodis IN, Kerwin DG, Salo AIT. Lower-limb mechanics during the support phase of maximum-velocity sprint running. *Med Sci Sports Exerc*. 2008;40(4):707–15.
7. Biewener AA, Farley CT, Roberts TJ, Temaner M. Muscle mechanical advantage of human walking and running: implications for energy cost. *J Appl Physiol*. 2004;97:2266–74.
8. Buczek FL, Cavanagh PR. Stance phase knee and ankle kinematics and kinetics during level and downhill running. *Med Sci Sports Exerc*. 1990;22(5):669–77.
9. Chapman AE, Caldwell GE. Factors determining changes in lower limb energy during swing in treadmill running. *J Biomech*. 1983;16:69–77.
10. de Leva P. Adjustments to Zatsiorsky–Seluyanov’s segment inertia parameters. *J Biomech*. 1996;29:1223–30.
11. Delp SL, Hess WE, Hungerford DS, Jones LC. Variation of

- rotation moment arms with hip flexion. *J Biomech.* 1999;32:493–501.
12. DeVita P, Skelly WA. Intrasubject variability of lower extremity joint moments of force during the stance phase of running. *Hum Mov Sci.* 1990;9:99–115.
 13. Dillman CJ. A kinetic analysis of the recovery leg during sprint running. In: Cooper JM, editor. *Selected Topics on Biomechanics: Proceedings of the C. I. C. Symposium on Biomechanics, Indiana University, 1970.* Chicago (IL): Athletic Institute; 1971. p. 137–65.
 14. Ekstrand J, Hagglund M, Walden M. Injury incidence and injury patterns in professional football: the UEFA injury study. *Br J Sports Med.* 2011;45(7):553–8.
 15. El-Masri MM, Fox-Wasylyshyn SM. Missing data: an introductory conceptual overview for the novice researcher. *Can J Nurs Res.* 2005;37:156–71.
 16. Glitsch U, Baumann W. The three-dimensional determination of internal loads in the lower extremity. *J Biomech.* 1997;30:1123–31.
 17. Harrington ME, Zavatsky AB, Lawson SE, Yuan Z, Theologis TN. Prediction of the hip joint centre in adults, children, and patients with cerebral palsy based on magnetic resonance imaging. *J Biomech.* 2007;40:595–602.
 18. Hunter BV, Thelen DG, Hhaher YY. A three-dimensional biomechanical evaluation of quadriceps and hamstrings muscle function using electrical stimulation. *IEEE Trans Neural Syst Rehabil Eng.* 2009;17:167–75.
 19. Johnson MD, Buckley JG. Muscle power patterns in the mid-acceleration phase of sprinting. *J Sports Sci.* 2001;19:263–72.
 20. Kuitunen S, Komi PV, Kyrolainen H. Knee and ankle stiffness in sprint running. *Med Sci Sports Exerc.* 2002;34(1):166–73.
 21. Mann R, Sprague P. A kinetic analysis of the ground leg during sprint running. *Res Q Exercise Sport.* 1980;51:334–48.
 22. Mann RV. A kinetic analysis of sprinting. *Med Sci Sports Exerc.* 1981;13(5):325–8.
 23. McClay I, Manal K. Three-dimensional kinetic analysis of running: significance of secondary planes of motion. *Med Sci Sports Exerc.* 1999;31(11):1629–37.
 24. Novacheck TF. The biomechanics of running. *Gait Posture.* 1998;7:77–95.
 25. Orchard JW. Intrinsic and extrinsic risk factors for muscle strains in Australian football. *Am J Sports Med.* 2001;29:300–3.
 26. Pandy MG, Lin Y-C, Kim HJ. Muscle coordination of mediolateral balance in normal walking. *J Biomech.* 2010;43:2055–64.
 27. Schache AG, Baker R. On the expression of joint moments during gait. *Gait Posture.* 2007;25:440–52.
 28. Schache AG, Baker R, Lamoreux LW. Defining the knee joint flexion-extension axis for purposes of quantitative gait analysis: an evaluation of methods. *Gait Posture.* 2006;24:100–9.
 29. Simonsen EB, Thomsen L, Klausen K. Activity of mono- and biarticular leg muscles during sprint running. *Eur J Appl Physiol Occup Physiol.* 1985;54:524–32.
 30. Simpson KJ, Bates BT. The effects of running speed on lower extremity joint moments generated during the support phase. *Int J Sport Biomech.* 1990;6:309–24.
 31. Stagni R, Fantozzi S, Cappello A, Leardini A. Quantification of soft tissue artefact in motion analysis by combining 3D fluoroscopy and stereophotogrammetry: a study on two subjects. *Clin Biomech.* 2005;20:320–9.
 32. Stefanyshyn DJ, Stergiou P, Lun VM, Meeuwisse WH, Worobets JT. Knee angular impulse as a predictor of patellofemoral pain in runners. *Am J Sports Med.* 2006;34:1844–51.
 33. Swanson SC, Caldwell GE. An integrated biomechanical analysis of high speed incline and level treadmill running. *Med Sci Sports Exerc.* 2000;32(6):1146–55.
 34. Vardaxis V, Hoshizaki TB. Power patterns of the leg during the recovery phase of the sprinting stride for advanced and intermediate sprinters. *Int J Sport Biomech.* 1989;5:332–49.
 35. Weyand PG, Sandell RF, Prime DNL, Bundle MW. The biological limits to running speed are imposed from the ground up. *J Appl Physiol.* 2010;108:950–61.
 36. Weyand PG, Sternlight DB, Bellizzi MJ, Wright S. Faster top running speeds are achieved with greater ground forces not more rapid leg movements. *J Appl Physiol.* 2000;89:1991–9.
 37. Winter DA. Moments of force and mechanical power in jogging. *J Biomech.* 1983;16:91–7.
 38. Winter DA. *Biomechanics and Motor Control of Human Movement.* New York (NY): John Wiley & Sons, Inc.; 2009. p. 370.
 39. Woltring HJ. A Fortran package for generalised, cross-validatory spline smoothing and differentiation. *Adv Eng Software.* 1986;8:104–7.
 40. Yokozawa T, Fujii N, Ae M. Muscle activities of the lower limb during level and uphill running. *J Biomech.* 2007;40:3467–75.

Mechanics of the Human Hamstring Muscles during Sprinting

ANTHONY G. SCHACHE¹, TIM W. DORN¹, PETER D. BLANCH², NICHOLAS A. BROWN³,
and MARCUS G. PANDY¹

¹Department of Mechanical Engineering, University of Melbourne, Victoria, AUSTRALIA; ²Department of Physical Therapies, Australian Institute of Sport, Belconnen ACT, AUSTRALIA; and ³Department of Biomechanics and Performance Analysis, Australian Institute of Sport, Belconnen ACT, AUSTRALIA

ABSTRACT

SCHACHE, A. G., T. W. DORN, P. D. BLANCH, N. A. BROWN, and M. G. PANDY. Mechanics of the Human Hamstring Muscles during Sprinting. *Med. Sci. Sports Exerc.*, Vol. 44, No. 4, pp. 00–00, 2012. **Purpose:** An understanding of hamstring mechanics during sprinting is important for elucidating why these muscles are so vulnerable to acute strain-type injury. The purpose of this study was twofold: first, to quantify the biomechanical load (specifically, musculotendon strain, velocity, force, power, and work) experienced by the hamstrings across a full stride cycle; and second, to determine how these parameters differ for each hamstring muscle (i.e., semimembranosus (SM), semitendinosus (ST), biceps femoris long head (BF^{LH}), biceps femoris short head (BF^{SH})). **Methods:** Full-body kinematics and ground reaction force data were recorded simultaneously from seven subjects while sprinting on an indoor running track. Experimental data were integrated with a three-dimensional musculoskeletal computer model comprised of 12 body segments and 92 musculotendon structures. The model was used in conjunction with an optimization algorithm to calculate musculotendon strain, velocity, force, power, and work for the hamstrings. **Results:** SM, ST, and BF^{LH} all reached peak strain, produced peak force, and performed much negative work (energy absorption) during terminal swing. The biomechanical load differed for each hamstring muscle: BF^{LH} exhibited the largest peak strain, ST displayed the greatest lengthening velocity, and SM produced the highest peak force, absorbed and generated the most power, and performed the largest amount of positive and negative work. **Conclusions:** As peak musculotendon force and strain for BF^{LH}, ST, and SM occurred around the same time during terminal swing, it is suggested that this period in the stride cycle may be when the biarticular hamstrings are at greatest injury risk. On this basis, hamstring injury prevention or rehabilitation programs should preferentially target strengthening exercises that involve eccentric contractions performed with high loads at longer musculotendon lengths. **Key Words:** RUNNING BIOMECHANICS, MUSCLE FORCE, MUSCLE FUNCTION, MUSCLE INJURY, MUSCULOSKELETAL MODELING

Acute strain-type injuries to lower limb skeletal muscles have a high incidence rate in many popular sports, such as soccer (13) and rugby (15), and can create considerable cost in lost training and competition time. Of these injuries, the hamstring muscles are by far the most frequently involved (13,15). Although sports participation can involve a variety of skills that can potentially load the hamstrings (e.g., kicking, twisting, jumping), it has been reported that the majority of hamstring muscle strain-type injuries occur while the athlete is running at maximal or

close to maximal speeds (4). A complete understanding of the biomechanical function of the hamstring muscles during sprinting is therefore required to aid in the development of rehabilitation and prevention strategies that are targeted to the mechanism of injury.

Most studies to date have measured EMG activity and/or have applied an inverse dynamics approach to evaluate hamstring muscle function during sprinting. For example, studies involving recordings of EMG activity have found the hamstrings to be active from midswing until terminal stance (7,21,23,25,26,35,45). Some of these studies have reported peak activity to occur during terminal swing (21,26,45), whereas others have found it to occur during stance (23,25). Studies have also made inferences about hamstring muscle function during sprinting from net lower limb joint moments and powers calculated using standard inverse dynamics (32,35,43). Such studies have shown a hip extensor moment to be present from midswing until early stance, along with a knee flexor moment during terminal swing, implying that considerable load is likely imparted onto the hamstrings.

Although EMG- and/or inverse dynamics-based analyses have provided some important insights, the ability of these approaches to quantify the biomechanical load experienced

Address for correspondence: Anthony G. Schache, B. Physio.(Hons), Ph.D., Department of Mechanical Engineering, University of Melbourne, Victoria 3010, Australia; E-mail: anthony@unimelb.edu.au.

Submitted for publication June 2011.

Accepted for publication September 2011.

Supplemental digital content is available for this article. Direct URL citations appear in the printed text and are provided in the HTML and PDF versions of this article on the journal's Web site (www.acsm-mssse.org).

0195-9131/12/4404-0000/0

MEDICINE & SCIENCE IN SPORTS & EXERCISE®

Copyright © 2011 by the American College of Sports Medicine

DOI: 10.1249/MSS.0b013e318236a3d2

by a given muscle during a functional motor task is limited in two main ways. First, the human musculoskeletal system is mechanically redundant. Many muscles cross each joint, and so a net joint moment can be satisfied by an infinite combination of muscle forces. Biarticular muscles such as the hamstrings span two joints—the hip and the knee—and so contribute to the net moments exerted about both joints simultaneously. It is therefore not possible to discern the actions of individual muscles from net joint moments alone (29). Second, EMG recordings primarily establish whether a muscle is active or not. Determining muscle force from EMG data alone is not a straightforward process, particularly for fast dynamic activities like sprinting. This is because many factors influence the relation that may exist between the EMG signal and the force developed by a muscle, including (but not limited to) muscle length, muscle fatigue, elastic properties of the musculotendon unit, contraction type, contraction velocity, as well as the level of contribution provided by synergistic muscles (12). Furthermore, the risk of crosstalk when recording EMG data from muscles that lie near each other can never be entirely avoided. One way to overcome these limitations is via advanced musculoskeletal modeling.

Models of the musculoskeletal system can be particularly advantageous for investigating the mechanics of a specific muscle group, such as the hamstrings (6,7,33–35,39,40,43,45). This is because musculoskeletal models have the capacity to estimate several additional and potentially significant parameters. For example, by including detailed anatomical information, such models allow musculotendon length to be estimated (35,40,43,45). This parameter is likely to be of particular relevance in the context of acute muscle strain-type injuries because animal-based experimental evidence exists demonstrating that the amount of musculotendon strain that occurs during repeated eccentric contractions is highly related to the severity of the subsequent muscle damage (28). Furthermore, it is possible to integrate musculoskeletal models with mathematical optimization routines to estimate additional parameters, such as musculotendon force, power, and work done, which are otherwise unmeasurable by noninvasive means (29). Musculoskeletal modeling is therefore a commonly used tool for studying the biomechanics of human movement, and it has proven to be a powerful method for advancing current understanding of muscle function (29,47).

Published research involving the application of musculoskeletal models to specifically evaluate hamstring muscle function during sprinting already exists (6,7,33–35,39,40,43,45). Some studies have focused on hamstring kinematics during sprinting and have found the peak length of the musculotendon unit to occur during terminal swing just before foot-strike (34,35,40,43,45). Peak length is approximately 10% greater than that assumed during an upright stance pose, and it does not seem to vary significantly as running is progressed from submaximal to maximal speeds (40). Other studies have estimated additional parameters

such as hamstrings muscle force, power, and work done (6,7,33,39). These parameters, in contrast to musculotendon length, have all been shown to steadily increase with speed. For instance, an increase in running speed from 80% to maximum was associated with an increase in net hamstring muscle force and energy absorption during terminal swing of 1.4-fold and 1.9-fold, respectively (6). Unfortunately, however, studies to date that have quantified hamstrings muscle force, power, and work done during sprinting have collected data using a treadmill (6,7,39), evaluated the swing phase of the stride cycle only (6,39), obtained data for a single subject only (33,39), or modeled the hamstring muscle complex as a single unit (33). A more complete analysis of the biomechanical load experienced by the hamstrings during overground sprinting is therefore required.

In the present study, a three-dimensional (3D) musculoskeletal computer model was used in conjunction with subject-specific experimental data to study the mechanics of the hamstring muscles during human sprinting. The aim of the study was twofold: first, to quantify the biomechanical load (specifically, musculotendon strain, velocity, force, power, and work) experienced by the hamstrings across a full stride cycle during overground sprinting; and second, to determine how the biomechanical load differs for each individual hamstring muscle (i.e., semimembranosus (SM), semitendinosus (ST), biceps femoris long head (BF^{LH}), biceps femoris short head (BF^{SH})).

METHODS

Subjects. Seven subjects (five males and two females) volunteered to participate in this study. Subjects had a mean \pm age of 26.6 ± 8.3 yr, a mean \pm SD height of 177.9 ± 5.6 cm, and a mean \pm SD body mass of 74.4 ± 8.2 kg. All subjects were experienced sprinters and, at the time of testing, were not experiencing any musculoskeletal injury likely to adversely affect their sprinting mechanics. Subjects were not specifically excluded if they had a history of an acute hamstring muscle strain-type injury. Four of the subjects had never suffered a hamstring injury, whereas two subjects had a history of bilateral hamstring injuries and one subject had a history of a unilateral hamstring injury. The study was approved by the Human Research Ethics Committee at The University of Melbourne and The Australian Institute of Sport, and all participants gave their written informed consent before testing.

Experimental data collection. Data collection took place on an indoor 110-m synthetic running track in the Biomechanics Laboratory at the Australian Institute of Sport. Kinematic data were recorded using a 3D motion analysis system (VICON; Oxford Metrics Ltd., Oxford, United Kingdom) with 22 cameras sampling at 250 Hz. The measurement volume had a length, width, and height of 15, 1.3, and 2.2 m, respectively, and was situated approximately 80 m along the 110-m running track, providing ample distance for acceleration and deceleration. Ground reaction

force (GRF) data were recorded via eight large (900 × 600 mm) force plates (Kistler Instrument Corp., Amherst, NY), sampling at 1500 Hz. Force plates were embedded in the laboratory floor and were covered with individual pieces of the synthetic running track to disguise their actual location. The force plates were embedded immediately adjacent to each other (thereby expanding a total length of 7.2 m) and were situated in the center of the measurement volume. GRF data were low-pass filtered using a fourth-order Butterworth filter with a cutoff frequency of 60 Hz before data processing. Hamstring EMG activity was recorded using a telemetered system (Noraxon Telemetry 2400 G2; Noraxon USA, Inc., Scottsdale, AZ) at a sampling rate of 1500 Hz. To facilitate the precise determination of onset and offset times, a Taeger–Kaiser energy operator was applied to the raw EMG signal to increase the detection accuracy of the EMG burst boundaries (27,36).

For each subject, one lower limb was designated as the side to be tested (or lower limb of interest) for purposes of the study. This lower limb was the left side for four subjects and the right side for three subjects. Subjects wore athletic shorts and running sandals (Nike Strapranner IV, Beaverton, OR) for testing. Running sandals were used rather than conventional running shoes to allow exposure of the foot for marker placement. This decision was based on studies demonstrating that shoe-mounted markers do not seem capable of providing a true reflection of underlying foot motion (11,37). Standard anthropometric parameters (i.e., height and body mass) were initially measured. Bipolar silver/silver chloride surface electrodes with a 10-mm-diameter contact area and a fixed interelectrode distance of 20 mm (Nicolet Biomedical, Memphis, TN) were mounted on the posterior aspect of the thigh in accordance with SENIAM recommendations (20). For the medial hamstrings, surface electrodes were positioned on the midpoint of a line connecting the ischial tuberosity and medial tibial epicondyle, whereas for the lateral hamstrings, surface electrodes were positioned on the midpoint of a line connecting the ischial tuberosity and the lateral tibial epicondyle. A ground electrode (3M Health Care, St. Paul, MN) was placed over the proximal end of the anteromedial shaft of the tibia. A total of 50 small (14 mm) reflective markers were mounted at specific anatomical locations on each subject's whole body, and a static trial was captured with the subject assuming a neutral pose. After the static trial, subjects were provided with sufficient time to warm-up (repeated strides of increasing speed) after which they performed maximal sprinting. Sprinting speed was measured using timing gates (Speedlight Telemetry Timing; Swift Performance Equipment, Queensland, Australia), which were located 20 m apart at either end of the measurement volume. A single representative trial containing valid force plate contacts for a complete stride cycle for the designated lower limb of interest (i.e., initial foot-strike and toe-off for the ipsilateral limb, followed by foot-strike and toe-off for the contralateral limb, followed by another foot-strike and toe-off for the ipsilateral limb) was recorded and analyzed for each subject.

Musculoskeletal model. A generic musculoskeletal model was accessed from OpenSim (10). The skeleton was represented by a 3D 12-segment, 11-degree-of-freedom linkage (Fig. 1A). The head and torso were lumped together and represented as a single rigid body (i.e., the trunk), which articulated with the pelvis via a ball-and-socket joint located approximately at the third lumbar vertebra (2,3). For the lower limbs, each hip was modeled as a ball-and-socket joint, each knee as a translating hinge joint (44), and each ankle complex as two nonintersecting pure hinge joints (11). All degrees-of-freedom for the trunk-to-pelvis and lower limb joints were actuated by a total of 92 musculotendon structures (Fig. 1B), each represented as a Hill-type muscle in series with the tendon (46) (Fig. 1C). Muscle lines of action in the musculoskeletal model were identical with those of Hamner et al. (17). For the upper limb, each shoulder was modeled as a ball-and-socket joint and each elbow as two nonintersecting hinge joints (22). The upper limb joints were actuated by 10 pure torque motors to model the dynamics of arm swing.

Subject-specific musculoskeletal models were then generated in OpenSim (10) by scaling the generic model according to individual subject anthropometry. Specifically, individual segment scale factors were calculated using the ratio of the distances between two markers on the segment during the static standing calibration trial and the distances between the same two markers on the musculoskeletal model. These scale factors were then used to scale segment lengths, segment inertial properties, and muscle attachment points (10).

Joint kinematics across the entire stride cycle was computed by performing an inverse kinematic analysis, which minimized the sum of the squared differences between the positions of virtual markers on the musculoskeletal model and those placed on the subject. Resulting joint kinematics were passed into a residual reduction algorithm (10). This algorithm refined the estimates obtained from inverse kinematics to improve their dynamic consistency with the recorded GRF data. All lower limb joint moments were computed via an inverse dynamics approach. A static optimization algorithm (3) was used to calculate individual musculotendon forces taking into account the prescribed force–length–velocity properties for each musculotendon structure in the model (Table 1 outlines the values used for each of the hamstring muscles). Specifically, the muscular load sharing problem was solved for each time point in the stride cycle by minimizing a performance criterion as well as satisfying the equality of the sum of individual muscular moments (i.e., force multiplied by moment arm for each muscle) to the joint moments obtained from the inverse dynamics analysis. The performance criterion applied in the present study was to minimize the sum of the square of muscle activations (3). This particular performance criterion was chosen for three main reasons. First, this criterion has been used by previous researchers to estimate lower limb muscle forces during walking (2,3,9), running (16,29), and sprinting (6,7,39). Second, it has been demonstrated that the

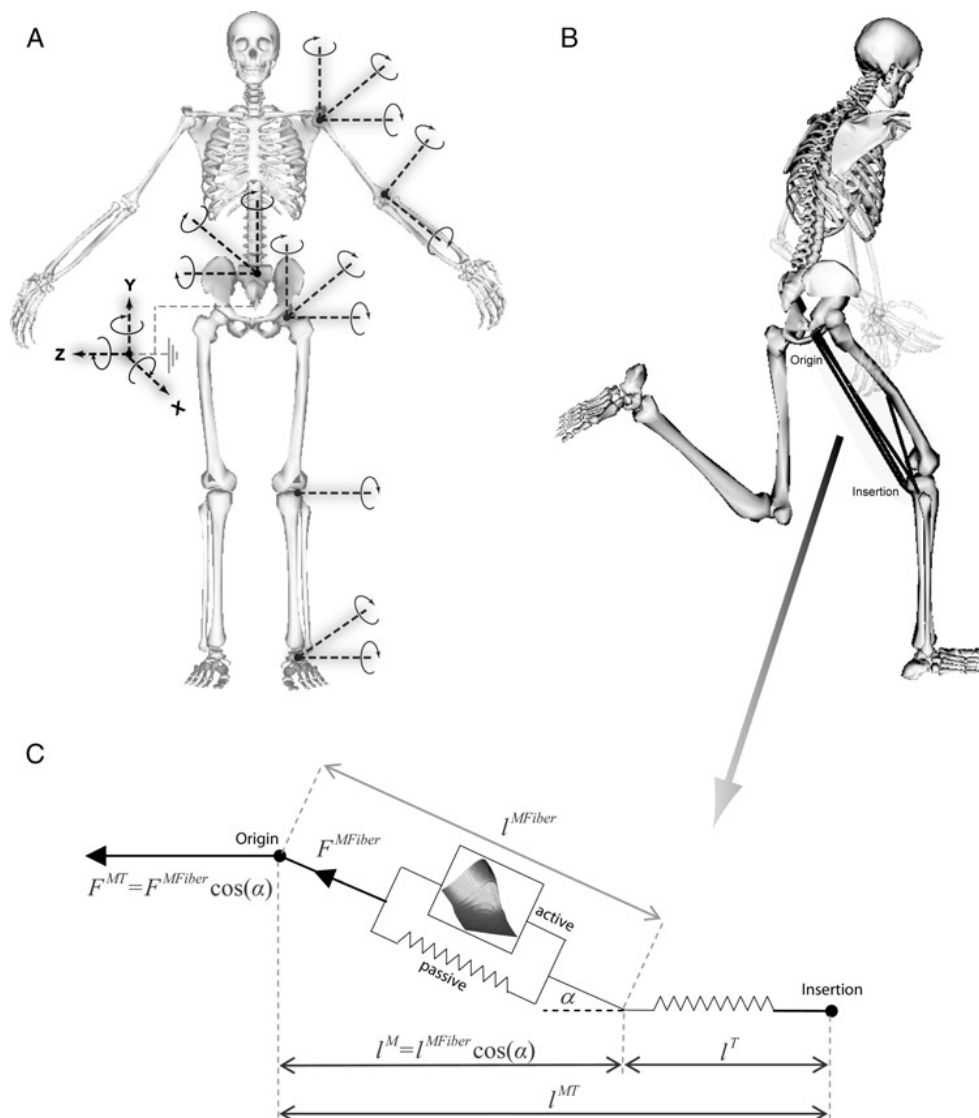


FIGURE 1—Three-dimensional musculoskeletal computer model of the body used in this study. **A**, The skeleton was represented as a multibody linkage containing 11 degrees of freedom. **B**, The lower limb joints and trunk were driven by 92 musculotendon actuators, whereas the upper limb joints were driven by 10 ideal torque actuators. For clarity, only the four hamstring muscles for the right lower limb are shown in the figure. **C**, Each musculotendon actuator was represented as a Hill-type physiological muscle in series with tendon. Musculotendon length (l^{MT}) was equal to the sum of the muscle (l^M) and tendon lengths (l^T), where l^M was defined as the projection of the muscle fiber length (l^{MFiber}) in the direction of the tendon. Muscle pennation angle is represented by the symbol α . Musculotendon force (F^{MT}) was defined as the projection of the muscle fiber force (F^{MFiber}) in the direction of the tendon.

number of active muscles computed is greater for nonlinear compared with linear criteria (30). Third, this criterion has been previously shown to predict lower limb muscle forces

that have similar time histories to experimental measurements of EMG activity during walking (2) and running (16,29).

TABLE 1. Musculotendon force–length–velocity properties for each of the individual hamstrings.

Property	SM	ST	BF ^{LH}	BF ^{SH}
Tendon slack length, l_s^T (m)	0.3440	0.2755	0.3350	0.1517
Tendon compliance, ϵ_0^T	0.033	0.033	0.033	0.033
Optimal muscle fiber length, l_0^M (m)	0.0800	0.2010	0.1000	0.1103
Maximum shortening velocity, V_{max} (m·s ⁻¹)	1.600	4.020	2.000	2.206
Maximum isometric force, F_0^M (N)	3864	1230	2688	2412
Optimal muscle fiber pennation angle, α_0 (°)	15.0	13.0	11.6	12.3

l_s^T Based on data reported by Delp et al. (11).

ϵ_0^T Recommended value reported by Zajac (46).

l_0^M Based on data reported by Wickiewicz et al. (42) and Ward et al. (41).

V_{max} Calculated as $20 \times l_0^M$.

α_0 Based on data reported by Ward et al. (41).

The hamstring muscle complex was represented by three biarticular structures (SM, ST, and BF^{LH}) and one uni-articular structure (BF^{SH}). For each individual hamstring muscle, the primary outcome measures of interest were musculotendon length, velocity, force, power, and work. These parameters were calculated as follows. Musculotendon length (l^{MT}) was equal to the sum of the muscle (l^M) and tendon lengths (l^T), where l^M was defined as the projection of the muscle fiber length (l^{MFiber}) in the direction of the tendon (Fig. 1C). Musculotendon strain was calculated as the change in l^{MT} from that assumed for the static standing calibration trial (expressed as a percentage increase or decrease). Musculotendon velocity (V^{MT}) was represented as the first derivative of length with respect to time, i.e., $V^{MT} = dl^{MT}/dt$. Musculotendon force (F^{MT}) was defined as the projection of the muscle fiber force (F^{MFiber}) in the direction of the tendon (Fig. 1C). Musculotendon power (P^{MT}) was calculated as the product of musculotendon force and velocity, i.e., $P^{MT} = F^{MT}V^{MT}$. Work was found by integrating power with respect to time; that is, by calculating the area under the power–time curve. Positive work represented power generation (concentric contraction) and negative work represented power absorption (eccentric contraction).

Data analysis. Data were analyzed for the designated lower limb of interest for each subject (i.e., the left side for four subjects and the right side for three subjects). To evaluate the similarity between the moments derived from inverse dynamics and those produced by the muscles, the RMS of the difference between the two joint moments was calculated for each subject and then averaged across all subjects. This process was repeated for all six lower limb joint moments. The primary outcome measures of interest (musculotendon length, velocity, force, and power) were normalized as a percentage of the full stride cycle (0%–100%) from ipsilateral toe-off to the following ipsilateral

toe-off for each individual hamstring muscle. Toe-off (rather than foot-strike) was used to define the start and finish of the stride cycle because this is the least critical period in terms of hamstring muscle function. Once time normalized for each subject, data were then averaged across subjects to generate mean (± 1 SD) plots for each individual hamstring muscle. Hamstring EMG activity onset and offset times across the stride cycle were visually determined using the Taeger–Kaiser energy operator–filtered signal (36). In addition to generating plots, discrete variables were extracted from the data set. Various maxima and minima points that were readily identifiable on the musculotendon length, velocity, force, and power profiles for each individual hamstring muscle were selected. The total amount of positive and negative work done during swing, stance, and over the full stride cycle were also calculated. Group mean (± 1 SD) values for each of the variables for each individual hamstring muscle were calculated.

RESULTS

The average sprinting speed for the cohort was $8.95 \pm 0.70 \text{ m}\cdot\text{s}^{-1}$ (range = $7.90\text{--}9.72 \text{ m}\cdot\text{s}^{-1}$). Overall, there was close agreement between the joint moments derived from inverse dynamics and those derived from the computed muscle forces (Fig. 2). The average RMS of the difference between the two joint moments was found to be less than $0.05 \text{ N}\cdot\text{m}\cdot\text{kg}^{-1}$, with the exception of the transverse plane hip moment (internal/external rotation) where the average RMS of the difference was $0.45 \text{ N}\cdot\text{m}\cdot\text{kg}^{-1}$. The evident discrepancy between muscle-computed and inverse dynamics-computed transverse plane hip moment was most likely attributable to errors in the experimental data (e.g., soft tissue artifact). However, this discrepancy was not considered to be of any major consequence for predicting hamstring muscle forces because (a) the amplitude of the transverse plane

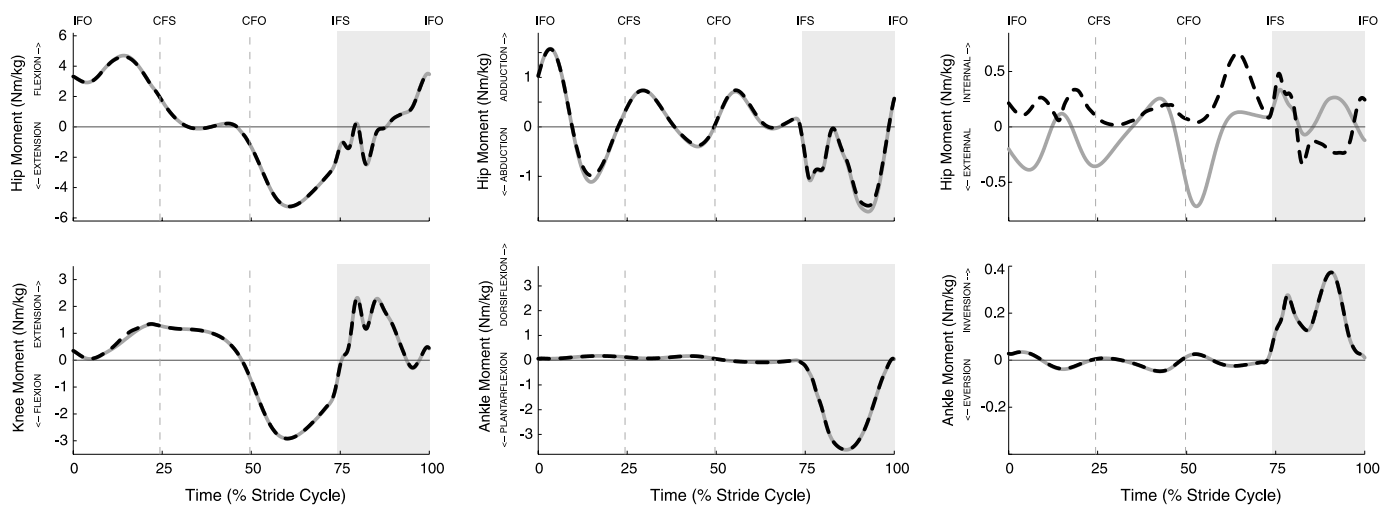


FIGURE 2—Group mean lower limb internal joint moments derived from inverse dynamics (solid gray line) and those derived from the computed muscle forces (dashed black line) across a full stride cycle. The light gray shading in each panel indicates the stance phase of the stride cycle. IFO, ipsilateral foot-off; CFS, contralateral foot-strike; CFO, contralateral foot-off; IFS, ipsilateral foot-strike.

hip moment was quite small relative to the sagittal plane hip and knee moments and (b) the biarticular hamstrings are not primary axial rotators of the hip joint. The static optimization analysis was therefore deemed successful in generating a set of muscle forces that could adequately recover the joint moments derived from inverse dynamics.

The biarticular hamstring muscles lengthened from early swing (~20% of the stride cycle) until terminal swing (~60% of the stride cycle), after which they shortened and continued to do so for the duration of stance (Fig. 3, row 1). Peak musculotendon strain for BF^{LH} during sprinting was, on average, 12.0% ± 2.6%, which exceeded the peak values of musculotendon strain for SM and ST by 2.2% and 3.3%, respectively (Table 2). Furthermore, the time of peak musculotendon strain for BF^{LH} preceded that for SM and ST by approximately 1.5% of the stride cycle.

During early swing (0%–20% of the stride cycle), the rate at which the hamstring muscles shortened increased initially and then reduced (Fig. 3, row 2). The average peak musculotendon shortening velocity at this time ranged from 0.74 ± 0.09 m·s⁻¹ for BF^{SH} to 1.04 ± 0.12 m·s⁻¹ for ST (Table 2). During the middle stages of swing (20%–60% of the stride cycle), the musculotendon lengthening velocity of the hamstrings showed a characteristic biphasic pattern (Fig. 3, row 2). The average peak musculotendon lengthening velocity at this time ranged from -0.71 ± 0.05 m·s⁻¹ for BF^{SH} to -1.04 ± 0.13 m·s⁻¹ for ST (Table 2). For BF^{LH}, the first peak in the musculotendon lengthening velocity during swing was always larger than the second, whereas the opposite was true for BF^{SH}. For SM and ST, the two peaks in the musculotendon lengthening velocity during swing were closer in magnitude, with some subjects having a larger first

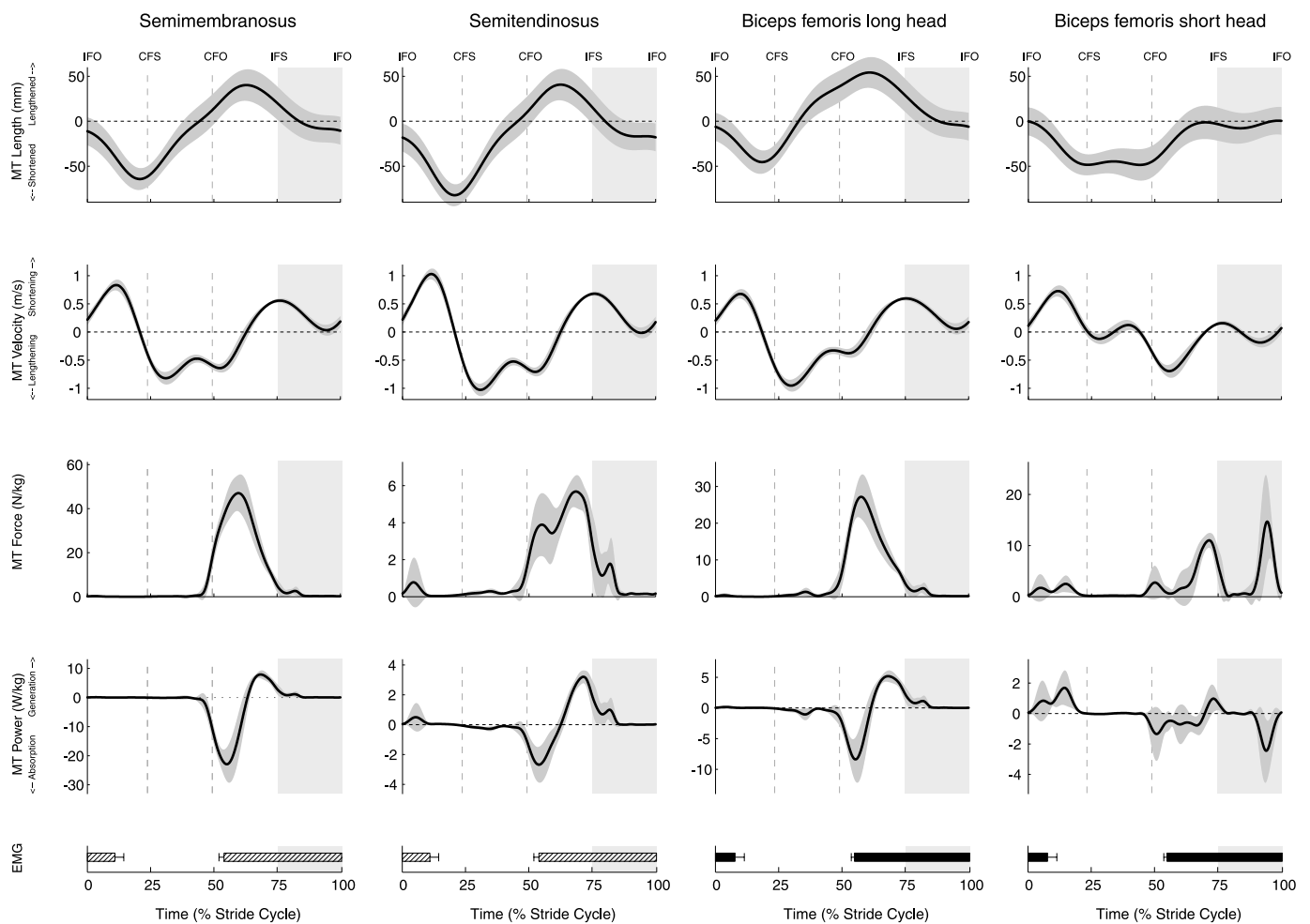


FIGURE 3—Musculotendon (MT) length (*top row*), velocity (*second row*), force (*third row*), and power (*fourth row*) for each hamstring muscle across a full stride cycle. Each panel displays the group mean (*solid black line*) ± 1 SD (*gray band*). The group mean ± 1 SD onset and offset times as a percent of the stride cycle for the medial (*horizontal bar filled with black diagonal lines*) and lateral (*solid black horizontal bar*) hamstrings EMG data are displayed in the *bottom panels*. It was assumed that the surface electrodes mounted over the medial hamstrings recorded the combined EMG activity from semimembranosus and semitendinosus, whereas the surface electrodes mounted over the lateral hamstrings recorded the combined EMG activity from biceps femoris long head and short head. Note therefore that the onset and offset times for the medial hamstrings EMG included in the columns for semimembranosus and semitendinosus represent the same data. Similarly, the onset and offset times for the lateral hamstrings EMG included in the columns for biceps femoris long head and short head represent the same data. The *light gray shading* in each panel indicates the stance phase of the stride cycle. IFO, ipsilateral foot-off; CFS, contralateral foot-strike; CFO, contralateral foot-off; IFS, ipsilateral foot-strike.

AQ1

TABLE 2. Mean \pm 1 SD values for the various discrete parameters extracted from the data set (i.e., musculotendon length, velocity, force, power, and work for each of the hamstring muscles).

	SM	ST	BF ^{LH}	BF ^{SH}
Length				
Peak lengthened state (% change from static pose)	9.84 \pm 1.15	8.73 \pm 1.31	11.98 \pm 2.63	—
Time of peak lengthened state (% stride cycle)	62.76 \pm 1.56	62.37 \pm 1.53	60.87 \pm 1.71	—
Velocity				
First peak shortening velocity (m·s ⁻¹)	0.84 \pm 0.10	1.04 \pm 0.12	0.69 \pm 0.08	0.74 \pm 0.09
Time first peak shortening velocity (% stride cycle)	11.36 \pm 0.99	11.34 \pm 1.00	9.80 \pm 1.03	11.70 \pm 1.15
Peak lengthening velocity (m·s ⁻¹)	-0.84 \pm 0.08	-1.04 \pm 0.13	-0.96 \pm 0.12	-0.71 \pm 0.05
Time peak lengthening velocity (% stride cycle)	34.20 \pm 8.17	33.97 \pm 8.31	29.80 \pm 0.70	55.80 \pm 1.39
Second peak shortening velocity (m·s ⁻¹)	0.56 \pm 0.04	0.69 \pm 0.06	0.60 \pm 0.04	0.16 \pm 0.07
Time second peak shortening velocity (% stride cycle)	75.97 \pm 1.21	75.79 \pm 1.18	75.10 \pm 1.73	76.74 \pm 1.35
Force				
Peak force during swing (N·kg ⁻¹)	46.81 \pm 6.25	5.49 \pm 0.78	26.35 \pm 5.15	10.36 \pm 1.47
Time peak force during swing (% stride cycle)	59.34 \pm 2.16	66.94 \pm 5.32	57.40 \pm 1.03	72.00 \pm 1.97
Peak force during stance (N·kg ⁻¹)	6.48 \pm 1.63	3.64 \pm 0.73	4.61 \pm 0.99	14.78 \pm 7.99
Time peak force during stance (% stride cycle)	74.47 \pm 1.31	74.47 \pm 1.31	74.47 \pm 1.31	91.31 \pm 7.60
Power				
Peak power absorption (W·kg ⁻¹)	-22.39 \pm 5.40	-2.70 \pm 1.01	-8.31 \pm 3.34	-2.60 \pm 1.90
Time peak power absorption (% stride cycle)	55.07 \pm 1.40	54.99 \pm 2.78	55.11 \pm 1.24	85.96 \pm 13.92
Peak power generation (W·kg ⁻¹)	7.66 \pm 1.14	3.13 \pm 0.46	5.00 \pm 0.84	2.05 \pm 1.04
Time peak power generation (% stride cycle)	68.07 \pm 1.13	72.11 \pm 1.99	67.66 \pm 1.16	21.21 \pm 23.06
Work				
Negative work done during swing (J·kg ⁻¹)	-1.06 \pm 0.25	-0.13 \pm 0.05	-0.34 \pm 0.12	-0.07 \pm 0.07
Positive work done during swing (J·kg ⁻¹)	0.31 \pm 0.06	0.13 \pm 0.04	0.24 \pm 0.04	0.09 \pm 0.03
Negative work done during stance (J·kg ⁻¹)	0.00 \pm 0.00	0.00 \pm 0.00	0.00 \pm 0.00	-0.06 \pm 0.05
Positive work done during stance (J·kg ⁻¹)	0.06 \pm 0.02	0.04 \pm 0.02	0.05 \pm 0.02	0.01 \pm 0.00
Total negative work done (J·kg ⁻¹)	-1.06 \pm 0.25	-0.13 \pm 0.05	-0.34 \pm 0.12	-0.13 \pm 0.10
Total positive work done (J·kg ⁻¹)	0.37 \pm 0.07	0.17 \pm 0.04	0.29 \pm 0.05	0.10 \pm 0.03

peak, whereas others displayed a larger second peak. During terminal swing (60%–75% of the stride cycle), the musculotendon shortening velocity of the hamstring muscles increased once more (Fig. 3, row 2). The average peak musculotendon shortening velocity at this time occurred just after foot-strike and ranged in magnitude from 0.16 \pm 0.07 m·s⁻¹ for BF^{SH} to 0.69 \pm 0.06 m·s⁻¹ for ST (Table 2). The musculotendon shortening velocity of the hamstrings then decreased during the first half of stance. Whereas a musculotendon lengthening velocity occurred for BF^{SH} during midstance for all subjects, such was not the case for the biarticular hamstring muscles. A musculotendon lengthening velocity during midstance was displayed by only three subjects for ST and by only two subjects for BF^{LH} and SM.

The static optimization analysis predicted that SM, ST, and BF^{LH} produced force during terminal swing and early stance, whereas BF^{SH} produced force during terminal swing and the second half of stance (Fig. 3, row 3). Overall, there was reasonable agreement between the time during the stride cycle when the hamstring muscles were predicted to develop force and the time when the hamstring muscles were found to display EMG activity (Fig. 3, row 3 vs row 5). Average peak musculotendon force ranged from 5.49 \pm 0.78 N·kg⁻¹ for ST to 46.81 \pm 6.25 N·kg⁻¹ for SM (Table 2). In comparison to stance, peak musculotendon force produced during swing was increased by 7.2-fold, 1.5-fold, and 5.7-fold for SM, ST, and BF^{LH}, respectively, whereas it was decreased by 0.7-fold for BF^{SH}.

All hamstring muscles underwent a period of power absorption followed by a period of power generation during terminal swing (Fig. 3, row 4). The average peak musculotendon power absorption during terminal swing ranged from -2.60 \pm 1.90 W·kg⁻¹ for BF^{SH} to -22.39 \pm 5.40 W·kg⁻¹ for

SM, whereas the average peak musculotendon power generation during terminal swing ranged from 1.12 \pm 0.69 W·kg⁻¹ for BF^{SH} to 7.66 \pm 1.14 W·kg⁻¹ for SM (Table 2). BF^{SH} also underwent a period of musculotendon power absorption during terminal stance (average magnitude of -2.47 \pm 2.01 W·kg⁻¹) and a period of musculotendon power generation during early swing (average magnitude of 1.90 \pm 1.06 W·kg⁻¹), which were likely a result of the optimization algorithm preferentially distributing load onto the BF^{SH} to control knee extension in late stance and then facilitate rapid knee flexion during early swing.

The biarticular hamstrings performed negative work only during terminal swing, whereas BF^{SH} performed a small amount of negative work during both terminal swing and terminal stance (Table 2). All of the hamstring muscles performed more positive work during swing than during stance. The average total amount of negative work done ranged from -0.13 \pm 0.05 J·kg⁻¹ for ST to -1.06 \pm 0.25 J·kg⁻¹ for SM, whereas the average total amount of positive work done ranged from 0.10 \pm 0.03 J·kg⁻¹ for BF^{SH} to 0.37 \pm 0.07 J·kg⁻¹ for SM. Semitendinosus was the only hamstring muscle not found to perform more negative work than positive work. In comparison to the total amount of positive work, the total amount of negative work was decreased 0.76-fold for ST and increased by 2.86-fold for SM.

DISCUSSION

The purposes of the present study were to quantify the biomechanical load (i.e., musculotendon strain, velocity, force, power, and work) experienced by the hamstrings across a full stride cycle during overground sprinting and to

compare the biomechanical load across the four hamstring muscles (i.e., SM, ST, BF^{LH}, and BF^{SH}). The main outcomes can be summarized as follows. First, the biarticular hamstrings undergo a stretch–shortening cycle during sprinting, with the lengthening phase occurring during terminal swing and shortening phase commencing just before foot-strike and continuing throughout stance. The timing of this stretch–shortening cycle corresponds with the period of hamstring EMG activity as measured in this study (Fig. 3, row 5) and in many previous studies (7,21,23,25,26,35,45). Second, the biomechanical load on the biarticular hamstring muscles was found to be greatest during terminal swing. At this time in the stride cycle, ST, SM, and BF^{LH} all reached peak musculotendon strain, produced peak musculotendon force, and performed much negative work. Third, when comparing the various hamstring muscles, the following results were found: (i) BF^{LH} had the largest peak musculotendon strain (12.0% increase in length from upright stance position), (ii) ST displayed the greatest musculotendon lengthening velocity, and (iii) SM produced the highest musculotendon force, absorbed and generated the most musculotendon power, and performed the largest amount of positive and negative work. These outcomes have implications for improving existing understanding of the pathomechanics of sprinting-related hamstring muscle strain-type injuries.

When comparing data from the present study with that from previous studies, the majority of the observed discrepancies are most likely attributable to the combined effect of three main factors. First, differences in the procedures used to record experimental data. In particular, several prior studies have measured data while sprinting on a treadmill (6,7,39), whereas data from the present study as well as those from Schache et al. (33) were measured while sprinting overground. Frishberg (14) compared treadmill and overground sprinting at 9.2 m·s⁻¹ for five male athletes and found several trunk and lower limb kinematic parameters to be different between the two conditions. Second, differ-

ences in the computational approach adopted to estimate muscle forces. Thelen et al. (39) and Chumanov et al. (6,7) used a forward dynamics simulation approach (38), whereas Schache et al. (33) and the present study used an inverse dynamics–based static optimization approach (3). All studies have applied the same general performance criterion (i.e., minimization of the sum of the square of muscle activations [3]). However, whereas most studies have not imposed additional constraints on when, in the stride cycle, muscle activations can be predicted to occur, Chumanov et al. (7) explicitly constrained the hamstring and rectus femoris muscles to be inactive for a brief period during terminal stance and early swing. Third, variability in the maximum sprinting speeds investigated may explain, to some degree, discrepancies in reported results. The average sprinting speed in the present study was 9.0 m·s⁻¹, whereas Schache et al. (33) recorded data at 7.4 m·s⁻¹ and Chumanov et al. (7) used average maximum speeds of 8.0 and 7.1 m·s⁻¹ for males and females, respectively. It is therefore possible that the larger hamstrings muscle forces in the present study compared with those in Schache et al. (33) and Chumanov et al. (7) are at least partially attributable to differences in test speeds. However, other studies (e.g., Thelen et al. [39] and Chumanov et al. [6]) involved maximum sprinting speeds that were similar in magnitude to the present study; hence, contrasting results in this instance cannot be explained on the basis of test speeds alone.

Despite the methodological differences among studies conducted to date, there is remarkable qualitative consistency in the reported findings. All studies have found the biarticular hamstrings to be subjected to large loads during the terminal swing phase of sprinting (6,7,33,39), with such loads exceeding those during stance (7,33). Furthermore, when comparing the various hamstrings, it has been found that BF^{LH} experiences the greatest musculotendon strain with respect to upright stance (6,7,34,40) and develops its peak musculotendon force slightly earlier in swing (6), whereas

TABLE 3. Quantitative data for musculotendon force and work obtained from the present study compared to previous studies.

	V_{max} (m·s ⁻¹)	SM	ST	BF ^{LH}	BF ^{SH}	NET
Peak stance MT force (N·kg ⁻¹)						
Schache et al. (33)	7.5 ± 0.1	—	—	—	—	31.9 ± 11.4
Chumanov et al. (7)	7.1 and 8.0 ^a	12.1 ± 2.4	6.2 ± 2.2	11.6 ± 1.9	—	—
Present study	9.0 ± 0.7	6.5 ± 1.6	3.6 ± 0.7	4.6 ± 1.0	14.8 ± 8.0	—
Peak swing MT force (N·kg ⁻¹)						
Thelen et al. (39)	9.3	—	—	17.6	—	—
Chumanov et al. (6)	8.2 ± 0.8 and 9.1 ± 0.6 ^b	27.9 ± 7.6	7.9 ± 1.8	21.4 ± 5.4	—	52.0 ± 13.4
Schache et al. (33)	7.5 ± 0.1	—	—	—	—	46.5 ± 4.3
Chumanov et al. (7)	7.1 and 8.0 ^a	23.9 ± 3.5	5.9 ± 1.9	13.2 ± 1.5	—	—
Present study	9.0 ± 0.7	46.8 ± 6.3	5.5 ± 0.8	26.4 ± 5.2	10.4 ± 1.5	—
Positive MT work (J·kg ⁻¹)						
Chumanov et al. (7)	7.1 and 8.0 ^a	0.5 ± 0.1	0.3 ± 0.0	0.4 ± 0.1	—	—
Present study	9.0 ± 0.7	0.4 ± 0.1	0.2 ± 0.0	0.3 ± 0.1	0.1 ± 0.0	—
Negative MT work (J·kg ⁻¹)						
Chumanov et al. (6)	8.2 ± 0.8 and 9.1 ± 0.6 ^b	1.0 ± 0.4	0.4 ± 0.2	0.8 ± 0.3	—	2.6 ± 1.0
Schache et al. (33)	7.5 ± 0.1	—	—	—	—	0.7 ± 0.1
Chumanov et al. (7)	7.1 and 8.0 ^a	0.7 ± 0.1	0.4 ± 0.1	0.5 ± 0.1	—	—
Present study	9.0 ± 0.7	1.1 ± 0.3	0.1 ± 0.1	0.3 ± 0.1	0.1 ± 0.1	—

— Data not reported.

^a Average maximum sprinting speed for females (*n* = 3) and males (*n* = 12), respectively (SD not reported).

^b Average maximum sprinting speed for females (*n* = 5) and males (*n* = 14), respectively.

V_{max} average maximum sprinting speed.

SM generates the largest peak musculotendon force and performs the greatest amount of work (6,7). These findings are all in agreement with the main outcomes from the present study. A quantitative comparison of results obtained from the various studies is given in Table 3. In some instances, data are reasonably similar; for example, the negative work done by SM during sprinting. However, for other parameters such as peak stance musculotendon force, data from the present study differ from equivalent data presented by Chumanov et al. (7) (see below).

Musculoskeletal modeling is the only practicable method for determining quantities such as muscle force, power, and work done under *in vivo* conditions (29). There is much evidence in the literature to show that computer-based models of the musculoskeletal system accurately predict biomechanical behavior. For instance, studies have compared model-derived estimates of hip- and knee-joint contact forces against simultaneously recorded *in vivo* data from instrumented (strain-gauged) joint implants for common activities of daily living, including walking (19,24) and stair climbing (19). These studies presented calculated joint contact forces that can be considered to be in good agreement with those directly measured from the instrumented joint implants. Although generating accurate estimates of joint contact forces is a necessary, but not sufficient, condition for concluding that the corresponding lower limb muscle forces are also accurate, confidence in model-derived estimates can be further increased by qualitatively comparing patterns of muscle forces with measured EMG data. In this regard, several studies have demonstrated that an inverse dynamics-based static optimization approach, as was used in the present study, is capable of producing lower limb muscle forces that have similar time histories to experimental measurements of EMG data for walking at the preferred speed (3) and running (16,29).

Unfortunately, as quantities such as muscle force, power, and work done cannot be measured *in vivo* by noninvasive means, it is not possible to directly validate estimates of hamstrings biomechanical load obtained in the present study. However, there are numerous factors that provide indirect evidence to indicate that the results from this study are reasonable. First, inverse dynamics-based joint moments in the present study are qualitatively and quantitatively consistent with equivalent data reported in the literature (1,32). Second, the estimation of large biomechanical loads on the biarticular hamstring muscles during the terminal swing phase of sprinting is in agreement with EMG studies that have reported peak activity of the medial and lateral hamstrings to occur during terminal swing (21,26,45). Third, sagittal plane moment arms for each of the hamstring muscles in the model plotted against hip- and knee-joint angle are consistent with experimental data from studies that have directly measured hamstrings moment arms using cadaveric specimens (see Figures, Supplemental Digital Contents 1 and 2, Sagittal plane moment arms at the hip and knee joint for each of the hamstring muscles in the model compared with

available experimental data from studies that have directly measured hamstrings moment arms using cadaveric specimens). Finally, the estimated distribution of musculotendon force across the various hamstring muscles is consistent with their force-generating capacity based on muscle architecture. The distribution of musculotendon force across the hamstring muscles was primarily determined by the maximum isometric force (F_0^M) attributed to each muscle in the model. A given muscle's F_0^M is proportional to its physiological cross-sectional area (PCSA), which is a measure of the number of parallel muscle fibers acting within a muscle. Muscles with a larger PCSA have a greater force-generating capacity (41,42). Studies have used cadavers to directly calculate PCSA for the various hamstring muscles (41,42). Ward et al. (41) and Wickiewicz et al. (42) reported PCSA to range from 16.9 to 18.4 cm² and 4.8 to 5.4 cm² for SM and ST, respectively. Ward et al. (41) measured a PCSA of 11.3 cm² and 5.1 cm² for BF^{LH} and BF^{SH}, respectively, whereas Wickiewicz et al. (42) measured a PCSA of 12.8 cm² for the entire biceps femoris muscle. Taken together, these data indicate that the force-generating capacity of the hamstring muscles is greatest for SM and BF^{LH} and smallest for ST and BF^{SH}. Furthermore, the force-generating capacity of SM exceeds that of BF^{LH}. The relative distribution of musculotendon force across the various hamstring muscles calculated in the present study is therefore consistent with what would be expected on the basis of reported PCSA measurements.

The present study was associated with several limitations and assumptions. First, only a single representative trial was analyzed per subject. It is acknowledged that it would have been ideal to have analyzed multiple trials for each subject. However, for a trial to be deemed successful, subjects were required to complete a full stride cycle of valid force plate contacts for the designated lower limb of interest. It typically required several attempts to obtain a representative trial. To avoid the potential confounding effect of fatigue, the study was therefore limited to a single trial per subject. Second, the outputs of the musculoskeletal model are sensitive to the values assumed for the musculotendon force-length-velocity properties. Such properties were not directly measured for each participant in the present study; rather literature-derived estimates were used (Table 1). However, every effort was made to obtain data that were considered reasonable. For example, pennation angle (α_0) for each individual hamstring muscle matched mean data reported by Ward et al. (41). Furthermore, optimal muscle fiber lengths (l_0^M) for SM, ST, and BF^{LH} were based on data reported by Wickiewicz et al. (42), whereas l_0^M for BF^{SH} was based on data reported by Ward et al. (41). Where it was not possible to source direct measurements of certain hamstrings properties, values were based on recommendations reported by others: data for tendon compliance (ϵ_0^T) were obtained from Zajac (46), whereas data for tendon slack length (l_s^T) were obtained from Delp et al. (11). It is also worth noting in this regard that the magnitudes of certain musculotendon force-length-velocity

properties are far more critical when the relative dynamics within the musculotendon unit is of key interest, i.e., quantifying the dynamics of the tendon versus muscle components. Thelen et al. (39) have previously demonstrated that incremental variations in the value assumed for tendon compliance (ϵ_0^T in Table 1) substantially influences predictions of BF^{LH} tendon stretch and work done during sprinting. Analyses in the present study were therefore restricted to the quantification of net musculotendon dynamics, which is unfortunate because it is likely that tendon function *in vivo* has an important role in fast movements such as sprinting by storing and releasing energy.

Third, estimates of hamstrings musculotendon force, power, and work done in this study are also limited to the particular method for calculating these parameters. Musculotendon forces were calculated using inverse dynamics-based static optimization. This approach is computationally efficient and has been commonly applied to estimate lower limb muscle forces during locomotion (3,9,16,24,29). However, unlike a dynamic optimization algorithm, static optimization neglects muscle activation dynamics (3). Although it has been shown that static and dynamic optimization algorithms yield similar results when applied to walking (3) and slower speeds of running (29), it is not currently known whether these different computational methods generate consistent results for faster locomotion speeds (i.e., sprinting). The performance criterion used to solve the optimization problem was the sum of the square of muscle activations (3). Although this specific criterion has been applied by previous researchers to compute lower limb muscle forces during sprinting (6,7,33,39), it is acknowledged that minimization of muscle stress during sprinting may not be the most important consideration. Furthermore, such performance criteria may be limited in their capacity to predict cocontraction among antagonistic pairs of muscles (8).

One parameter that would seem to have been somewhat underestimated in this study was peak stance musculotendon force for the biarticular hamstrings. Only BF^{SH} was predicted to be producing force in the second half of stance. As previously mentioned, the magnitude of peak stance hamstrings musculotendon force from the current study is less than that from Chumanov et al. (7). Peak stance hamstrings force ranged from $3.64 \text{ N}\cdot\text{kg}^{-1}$ for ST to $14.78 \text{ N}\cdot\text{kg}^{-1}$ for BF^{SH} in this study, whereas it ranged from $6.2 \text{ N}\cdot\text{kg}^{-1}$ for ST to $12.1 \text{ N}\cdot\text{kg}^{-1}$ for SM in the study by Chumanov et al. (7) (Table 3). Prior investigations recording lower limb muscle EMG activity during sprinting have found the medial and lateral hamstrings to be active throughout stance (7,21,23,25,26,35,45). Similarly, EMG activity measured from the medial and lateral hamstrings in this study was found to commence during terminal swing and continue throughout stance until the start of initial swing (Fig. 3, row 5). Although the relationship between EMG and muscle force for fast dynamic contractions is complicated and affected by many factors (12), such experimental data would suggest that, for the biarticular hamstrings during stance, the pre-

dicted magnitude of musculotendon force in the present study may be lower than what would be expected.

This inconsistency is most likely attributable to the computational approach used to calculate muscle forces; that is, the inability of inverse dynamics-based static optimization when combined with a minimum-stress performance criterion to adequately predict antagonistic cocontraction. Evidence for this assertion is provided by Collins (8), who evaluated the performance of a variety of optimization algorithms in calculating muscle forces during walking. Although minimization of the sum of muscle activations squared was not specifically tested, optimization algorithms that were included were all found to be particularly insensitive to the prediction of antagonistic quadriceps-hamstrings activity during stance. Predicting high levels of biarticular hamstrings activity throughout stance when there is a net hip flexor moment during the second half of stance and a net knee extensor moment for the majority of stance would not be (from a computational perspective) the most energy-efficient way to distribute the joint moments across the various lower limb muscles. Large muscle forces from the biarticular hamstrings during the first half of stance would likely require greater activations to be computed from the knee extensor muscles, so as to counter the unwanted mechanical effect of the hamstrings at the knee joint and maintain equality with the inverse dynamics-based joint moments. Hence, the hip extensor moment during the first half of stance was preferentially distributed onto the gluteus maximus muscle. In a similar manner, large muscle forces from the biarticular hamstrings during the second half of stance would likely require greater activations to be computed from the hip flexor and knee extensor muscles to maintain equality with the inverse dynamics moments.

Cocontraction of antagonistic muscles can be used to modulate the impedance and thus stability of a joint, which would seem advantageous during the stance phase of sprinting when the lower limb is subjected to a high-frequency impact force. Rather interestingly, it has been demonstrated that people who have learned to cope with compromised knee joint stability (i.e., anterior cruciate ligament deficiency) display increased stance phase hamstrings EMG activity during locomotion in comparison to a group of healthy counterparts (5). It is therefore speculated that after foot-strike during sprinting, the hamstrings are active not to counter the external moments generated largely by the GRF, but rather to provide alternative functions, such as joint stability and/or proprioception.

Because the biarticular hamstring muscles all reached peak musculotendon strain, produced peak musculotendon force, and performed much negative work during the terminal swing phase of sprinting, it would seem that the hamstrings are likely to be most vulnerable to injury at this time in the stride cycle. Unlike concentric contractions, eccentric contractions have been shown to be capable of producing muscle fiber damage (28). Furthermore, the conclusion that the hamstrings are likely to be at greater risk of injury during

terminal swing as opposed to the stance phase concurs with the findings from two recently published, yet independent, case reports that unexpectedly captured biomechanical data of a running athlete suffering a hamstring muscle strain injury (18,34). Both of these studies identified terminal swing as the period in the stride cycle when the injury stimulus most likely occurred.

Most hamstring muscle strain injuries involve the biceps femoris muscle (4). It was therefore of interest to determine whether there are biomechanical reasons for this clinical observation; hence parameters such as musculotendon strain, velocity, force, power, and work were compared for each individual hamstring muscle. Based on data from the present study as well as data from previous studies (6,7), the propensity for hamstring muscle strain-type injuries to frequently involve biceps femoris cannot be simply explained on the basis of peak force or the total amount of negative work done because both of these parameters were estimated to be greatest for SM not BF^{LH} or BF^{SH}. In accordance with Thelen et al. (40) and Chumanov et al. (6,7), the amount of musculotendon strain (lengthening with respect to upright stance) was found to distinguish BF^{LH} from SM and ST. An average peak strain of 12.0% was experienced by BF^{LH} during sprinting, which was 2.2% and 3.3% greater than that for SM and ST, respectively (Table 2). These data therefore indicate that the degree of musculotendon strain may be the more relevant parameter in understanding the apparent vulnerability of biceps femoris to injury. This conclusion is consistent with the results from an animal-based study, whereby muscle damage after an eccentric contraction was found not simply to be a function of peak muscle force but rather was

due to the magnitude of the strain experienced by the musculotendon unit during contraction (28).

In summary, the present study found the biarticular hamstrings (SM, ST, and BF^{LH}) to be lengthening, producing peak force, and performing much negative work (energy absorption) during the terminal swing phase of the stride cycle. This study also found differing biomechanical loads for each individual hamstring muscle: BF^{LH} exhibited the largest peak strain, ST displayed the greatest lengthening velocity, and SM produced the highest peak force, absorbed and generated the most power, and performed the largest amount of positive and negative work. As peak musculotendon force and strain for BF^{LH}, ST, and SM occurred around the same time during terminal swing, it is suggested that this period in the stride cycle may be when the biarticular hamstrings are at greatest injury risk. On this basis, it is recommended that hamstring injury prevention or rehabilitation programs should be preferentially biased toward strengthening exercises that primarily involve eccentric contractions performed with high loads at longer musculotendon lengths.

Financial support for this project was provided by the Physiotherapy Research Foundation Tagged Sports Physiotherapy Australia research grant (T08-THE/SPA(1)018), the Australian Research Council Discovery Projects grant DP0772838, and the Australian Research Council Linkage Projects grant LP110100262.

The authors thank Doug Rosemond for his assistance with experimental data collection.

The authors have no conflicts of interest to declare.

The results of the present study do not constitute endorsement by the American College of Sports Medicine.

REFERENCES

1. Ae M, Miyashita K, Yokoi T, Hashihara Y. Mechanical power and work done by the muscles of the lower limb during running at different speeds. In: Jonsson B, editor. *Biomechanics X-B*. Champaign (IL): Human Kinetics Publishers, Inc; 1987. p. 895–9.
2. Anderson FC, Pandy MG. Dynamic optimization of human walking. *J Biomech Eng*. 2001;123:381–90.
3. Anderson FC, Pandy MG. Static and dynamic optimization solutions for gait are practically equivalent. *J Biomech*. 2001;34:153–61.
4. Askling CM, Tengvar M, Saartok T, Thorstensson A. Acute first-time hamstring strains during high-speed running. *Am J Sports Med*. 2007;35:197–206.
5. Boerboom AL, Hof AL, Halbertsma JPK, et al. Atypical hamstrings electromyographic activity as a compensatory mechanism in anterior cruciate ligament deficiency. *Knee Surg Sports Traumatol Arthrosc*. 2001;9:211–6.
6. Chumanov ES, Heiderscheid BC, Thelen DG. The effect of speed and influence of individual muscles on hamstring mechanics during the swing phase of sprinting. *J Biomech*. 2007;40:3555–62.
7. Chumanov ES, Heiderscheid BC, Thelen DG. Hamstring musculotendon dynamics during stance and swing phases of high-speed running. *Med Sci Sports Exerc*. 2011;43(3):525–32.
8. Collins JJ. The redundant nature of locomotor optimization laws. *J Biomech*. 1995;28:251–67.
9. Crowninshield RD, Brand RA. A physiologically based criterion of muscle force prediction in locomotion. *J Biomech*. 1981;14: 793–801.
10. Delp SL, Anderson FC, Arnold AS, et al. OpenSim: open-source software to create and analyze dynamic simulations of movement. *IEEE Trans Biomed Eng*. 2007;54:1940–50.
11. Delp SL, Loan P, Hoy MG, Zajac FE, Topp EL, Rosen JM. An interactive graphics-based model of the lower extremity to study orthopaedic surgical procedures. *IEEE Trans Biomed Eng*. 1990; 37:757–67.
12. Disselhorst-Klug C, Schmitz-Rode T, Rau G. Surface electromyography and muscle force: limits in sEMG–force relationship and new approaches for applications. *Clin Biomech*. 2009;24:225–35.
13. Ekstrand J, Hagglund M, Walden M. Epidemiology of muscle injuries in professional football (soccer). *Am J Sports Med*. 2011; 39:1226–32.
14. Frishberg BA. An analysis of overground and treadmill sprinting. *Med Sci Sports Exerc*. 1983;15(6):478–85.
15. Fuller CW, Laborde F, Leather RJ, Molloy MG. International rugby board rugby world cup 2007 injury surveillance study. *Br J Sports Med*. 2008;42:452–9.
16. Glitsch U, Baumann W. The three-dimensional determination of internal loads in the lower extremity. *J Biomech*. 1997;30:1123–11.
17. Hamner SR, Seth A, Delp SL. Muscle contributions to propulsion and support during running. *J Biomech*. 2010;43:2709–16.
18. Heiderscheid BC, Hoerth DM, Chumanov ES, Swanson SC, Thelen BJ, Thelen DG. Identifying the time of occurrence of a hamstring strain injury during treadmill running: a case study. *Clin Biomech*. 2005;20:1072–8.

19. Heller MO, Bergmann G, Deuretzbacher G, et al. Musculo-skeletal loading conditions at the hip during walking and stair climbing. *J Biomech.* 2001;34:883–93.
20. Hermens HJ, Freriks B, Disselhorst-Klug C, Rau G. Development of recommendations for SEMG sensors and sensor placement procedures. *J Electromyogr Kinesiol.* 2000;10:361–71.
21. Higashihara A, Ono T, Kubota J, Okuwaki T, Fukubayashi T. Functional differences in the activity of the hamstring muscles with increasing running speed. *J Sports Sci.* 2010;28:1085–92.
22. Holzbaur KR, Murray WM, Delp SL. A model of the upper extremity for simulating musculoskeletal surgery and analyzing neuromuscular control. *Ann Biomed Eng.* 2005;33:829–40.
23. Jonhagen S, Ericson MO, Nemeth G, Eriksson E. Amplitude and timing of electromyographic activity during sprinting. *Scand J Med Sci Sports.* 1996;6:15–21.
24. Kim H-J, Fernandez JW, Akbarshahi M, Walter JP, Fregly BJ, Pandy MG. Evaluation of predicted knee joint muscle forces during gait using an instrumented knee implant. *J Orthop Res.* 2009;27:1326–11.
25. Kyröläinen H, Avela J, Komi PV. Changes in muscle activity with increasing running speed. *J Sports Sci.* 2005;23:1101–9.
26. Kyröläinen H, Komi PV, Belli A. Changes in muscle activity patterns and kinetics with increasing running speed. *J Strength Cond Res.* 1999;13:400–6.
27. Li X, Zhou P, Aruin AS. Taeger–Kaiser energy operation of surface EMG improves muscle activity onset detection. *Ann Biomed Eng.* 2007;35.
28. Lieber RL, Friden J. Muscle damage is not a function of muscle force but active muscle strain. *J Appl Physiol.* 1993;74:520–6.
29. Pandy MG, Andriacchi TP. Muscle and joint function in human locomotion. *Annu Rev Biomed Eng.* 2010;12:401–33.
30. Pedersen DR, Brand RA, Cheng C, Arora JS. Direct comparison of muscle force predictions using linear and non-linear programming. *J Biomech Eng.* 1987;109:192–9.
11. Reinschmidt C, Van Den Bogert AJ, Murphy N, Lundberg A, Nigg BM. Tibiocalcaneal motion during running, measured with external and bone markers. *Clin Biomech.* 1997;12:8–16.
32. Schache AG, Blanch PD, Dorn TW, Brown NAT, Rosemond D, Pandy MG. Effect of running speed on lower limb joint kinetics. *Med Sci Sports Exerc.* 2011;43(7):525–32.
33. Schache AG, Kim H-J, Morgan DL, Pandy MG. Hamstring muscle forces prior to and immediately following an acute sprinting-related muscle strain injury. *Gait Posture.* 2010;32:136–40.
34. Schache AG, Wrigley TV, Baker R, Pandy MG. Biomechanical response to hamstring muscle strain injury. *Gait Posture.* 2009;29:332–8.
35. Simonsen EB, Thomsen L, Klausen K. Activity of mono- and biarticular leg muscles during sprint running. *Eur J Appl Physiol Occup Physiol.* 1985;54:524–32.
36. Solnik S, Rider P, Steinweg K, Devita P, Hortobagyi T. Taeger–Kaiser energy operator signal conditioning improves EMG onset detection. *Eur J Appl Physiol.* 2010;110:489–98.
37. Stacoff A, Reinschmidt C, Stüssi E. The movement of the heel within a running shoe. *Med Sci Sports Exerc.* 1992;24(6):695–701.
38. Thelen DG, Anderson FC. Using computed muscle control to generate forward dynamic simulations of human walking from experimental data. *J Biomech.* 2006;39:1107–15.
39. Thelen DG, Chumanov ES, Best TM, Swanson SC, Heiderscheid BC. Simulation of biceps femoris musculotendon mechanics during the swing phase of sprinting. *Med Sci Sports Exerc.* 2005;37(11):1911–8.
40. Thelen DG, Chumanov ES, Hoerth DM, et al. Hamstring muscle kinematics during treadmill sprinting. *Med Sci Sports Exerc.* 2005;37(1):108–14.
41. Ward SR, Eng CM, Smallwood LH, Lieber RL. Are current measurements of lower extremity muscle architecture accurate? *Clin Orthop Rel Res.* 2009;467:1074–82.
42. Wickiewicz TL, Roy RR, Powell PL, Edgerton VR. Muscle architecture of the human lower limb. *Clin Orthop Rel Res.* 1983;179:275–83.
43. Wood GA. Biomechanical limitations to sprint running. In: Van Gheluwe B, Atha J, editors. *Current Research in Sports Biomechanics.* Basel (Switzerland): Karger; 1987. p. 58–71.
44. Yamaguchi GT, Zajac FE. A planar model of the knee joint to characterise the knee extensor mechanism. *J Biomech.* 1989;22:1–10.
45. Yu B, Queen RM, Abbey AN, Liu Y, Moorman CT, Garrett WE. Hamstring muscle kinematics and activation during overground sprinting. *J Biomech.* 2008;41:3121–6.
46. Zajac FE. Muscle and tendon: properties, models, scaling, and application to biomechanics and motor control. In: Bourne JR, editor. *CRC Critical Reviews in Biomedical Engineering.* Boca Raton (FL): CRC Press; 1989. p. 359–411.
47. Zajac FE. Muscle coordination of movement: a perspective. *J Biomech.* 1993;26:109–24.

ESTIMATES OF MUSCLE FUNCTION IN GAIT DEPEND ON HOW FOOT-GROUND CONTACT IS MODELED

Tim Dorn¹, Yi-Chung Lin¹ and Marcus Pandy¹

¹ Department of Mechanical Engineering, The University of Melbourne, Australia.
Email: t.dorn@pgrad.unimelb.edu.au

INTRODUCTION

Computational analyses of leg-muscle function in human locomotion commonly assume that foot-ground contact occurs at discrete points on the foot. Kinematic constraints acting at these contact points restrict the motion of the foot and therefore alter model calculations of muscle function. The aim of this study was to evaluate how predictions of muscle function obtained from musculoskeletal models are influenced by the model used to simulate ground contact.

METHODS

Gait experiments were performed on 14 healthy adults during walking (1.46 ± 0.11 m/s) and heel running (3.42 ± 0.13 m/s). A generic musculoskeletal model containing 54 muscles was scaled to each subject and muscle forces computed for each trial using inverse kinematics, inverse dynamics and static optimization [1]. Muscle function was determined by quantifying the contributions of all action forces (muscles, gravity and velocity) to the vertical, fore-aft and mediolateral components of the ground reaction force. These quantities were calculated for six models of foot-ground contact (Table 1) using a recently developed pseudo-inverse algorithm [2].

Table 1: Six foot-ground contact models used in the study.

	Contact Model	Contact Loc.	Kinematic Constraints		DOF
			linear [X Y Z]	rotational [X Y Z]	
Time independent weightings	BALL	CoP	[1 1 1]	[0 0 0]	3
	UNIVERSAL	CoP	[1 1 1]	[0 1 0]	2
	HINGE	CoP	[1 1 1]	[1 1 0]	1
	WELD	CoP	[1 1 1]	[1 1 1]	0
Time dependent weightings	SINGLEPOINT	CoP	[1 1 1]	f(CoP)	f(CoP)
	MULTIPOINT	5 pts	f(CoP)	N/A	f(CoP)

Single- and multiple-point contact models were evaluated. The single-point models assumed contact to occur at the measured center of pressure location. The multiple-point model assumed contact to occur at five contact points distributed around the surface of the foot (Fig. 1). Weightings between 0 and 1 were assigned to each contact point, describing their tolerance to

resist linear translations and angular rotations (Table 1). Zero represented an unconstrained degree-of-freedom, and one represented a fully constrained degree-of-freedom.

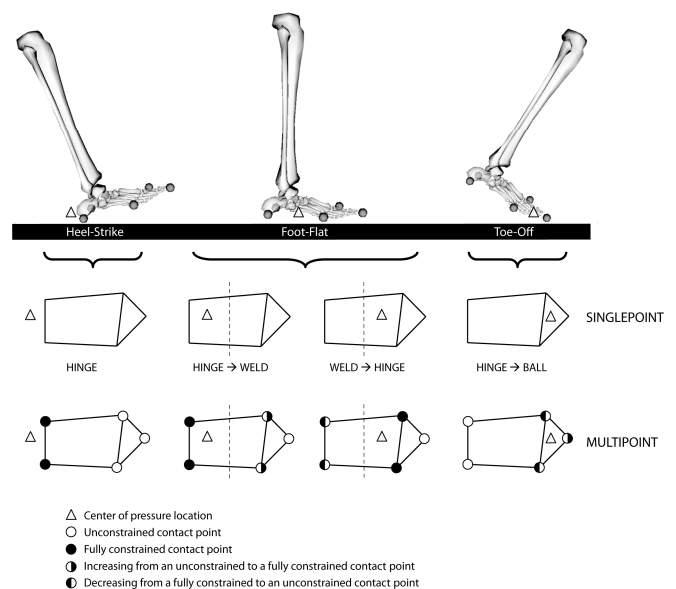


Figure 1: Diagram illustrating how time-dependent kinematic constraint weightings were applied to the foot contact points.

RESULTS AND DISCUSSION

The results showed that two factors – the number of foot-ground contact points assumed in the model and the type of kinematic constraint enforced at each point – affect model predictions of muscle coordination (Fig. 2). Specifically: i) kinematic constraints applied in the sagittal plane affect model calculations of muscle contributions to the vertical and fore-aft ground reaction forces (compare HINGE and WELD); ii) kinematic constraints applied in the frontal plane affect calculations of muscle contributions to the mediolateral ground reaction force (compare UNIVERSAL and HINGE); and iii) kinematic constraints applied in the transverse plane have little effect on the calculations of muscle function (compare BALL and UNIVERSAL).

Effects on the actions of individual muscles were also evident. For example, in the first half of stance, the primary contributor to support in

walking depended on the presence of a sagittal plane rotational kinematic constraint (about the mediolateral foot axis). Gluteus medius, gluteus maximus and vasti generated the majority of vertical ground force when this constraint was enforced, whereas soleus and gastrocnemius dominated when the constraint was removed.

Determining the most valid contact model is difficult because individual muscle contributions to the ground reaction force cannot be measured experimentally. Each contact model should at the very least satisfy the superposition principle. This principle requires the sum of all action force contributions to equal the total measured ground reaction force. Superposition error (the difference between the measured and model summed ground force) indicated that the HINGE, WELD and SINGLEPOINT models were incapable of recovering the ground force in the mediolateral direction (Fig. 3). The BALL and MULTIPOINT models generated the least superposition error, yet their relative predictions of muscle coordination were very different. This finding illustrates an important limitation of superposition: this principle can quantify the accuracy with which the various action forces sum to the total ground force, but it cannot verify the calculations of the contributions of the individual action forces themselves. Superposition is therefore necessary but not sufficient for validating model predictions of multi-articular muscle coordination [1].

CONCLUSIONS

As ground-force decomposition analyses become more widespread, careful consideration should be

given to the formulation of the model used to simulate ground contact. The results of the present study illustrate the sensitivity of calculations of muscle coordination to the chosen model of foot-ground contact. These findings have implications for analyses of leg-muscle function in gait, particularly if the results of such analyses are to guide clinical decision making.

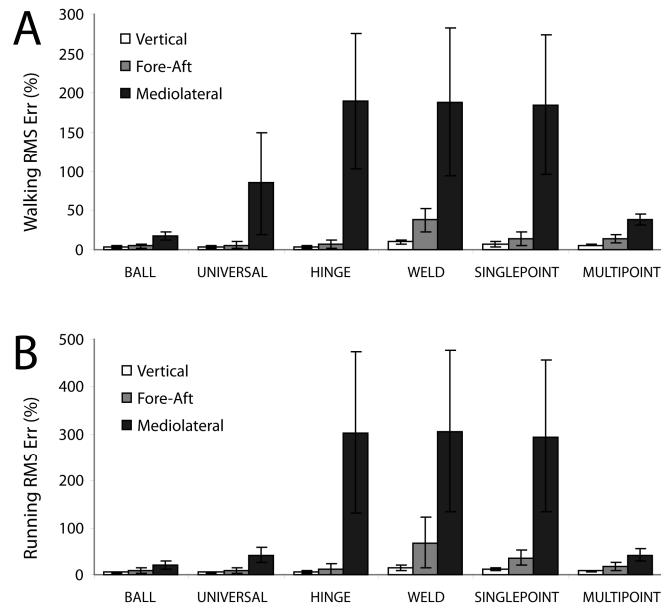


Figure 3: Superposition error for each contact model for walking (A) and running (B).

REFERENCES

1. Anderson FC., et al. *Gait & Posture* 17(2): 159-169, 2003.
2. Lin YC., et al. *Int J Num Methods in Biomed Eng.* 2010.

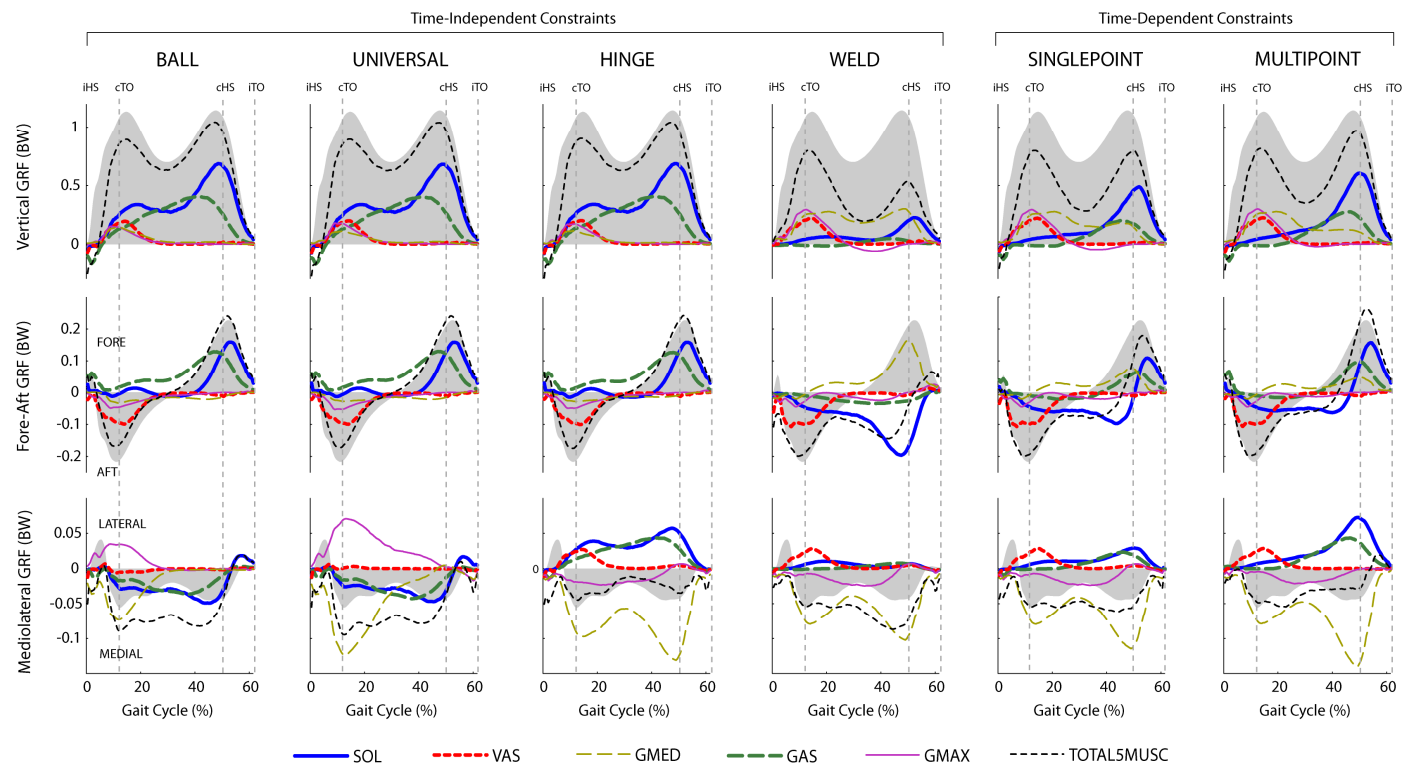


Figure 2: Contributions of major muscle groups and their summed total to the net ground reaction force for self selected walking.

BIOMECHANICAL STRATEGIES FOR INCREASING RUNNING SPEED

¹Tim Dorn, ¹Anthony Schache and ¹Marcus Pandy

¹Department of Mechanical Engineering, The University of Melbourne, Australia; email: t.dorn@pgrad.unimelb.edu.au

SUMMARY

The purpose of this study was to identify the key muscle groups responsible for increasing running speed.

INTRODUCTION

Running speed is increased by either pushing on the ground harder (thereby increasing stride length), or pushing on the ground more frequently (thereby increasing stride frequency). Previous research has shown that to achieve speeds greater than ~5m/s, runners appear to become increasingly reliant upon more frequent ground contact of similar force rather than more forceful ground contacts [1]. This may occur because faster running speeds reduce the duration of stance phase, thus limiting the time that muscles can generate and transmit force to the ground [2]. Significant increases in swing phase peak hip flexor, hip extensor and knee flexor joint moments have also been observed to occur with increasing running speed [1]. The purpose of the present study was to identify the muscle groups responsible for these speed regulating functions during the stance and swing phase of running, over the full range of typical human running speeds.

METHODS

Overground gait data were collected for nine healthy active participants, who walked and ran over a range of speeds (Table 1). Stride length, stride frequency and effective vertical impulse were calculated for each trial. Effective vertical impulse (the impulse required to elevate the body against gravity, thus determining the body's aerial time) was computed as the area between the vertical ground reaction force trajectory and the line representing one bodyweight [3].

A generic musculoskeletal model actuated by 92 muscles was scaled to the dimensions of each subject. Individual muscle forces were computed using inverse kinematics, inverse dynamics and static optimization [3]. Mechanical power for each muscle group was calculated by summing the product of musculotendon force and velocity for each line-of-action in the muscle group. Musculotendon work was calculated from the area under the power-time curve, and summed for each line-of-action in the muscle group. Concentric contractions represented energy generation (positive work) and eccentric contractions represented energy absorption (negative work) by the muscle-tendon. A pseudo-inverse ground force decomposition method was used to calculate the contributions of each muscle to the ground reaction force [4]. Five contact points were distributed over the foot, and kinematic constraints were defined according to the center of pressure location to realistically simulate foot-ground interaction.

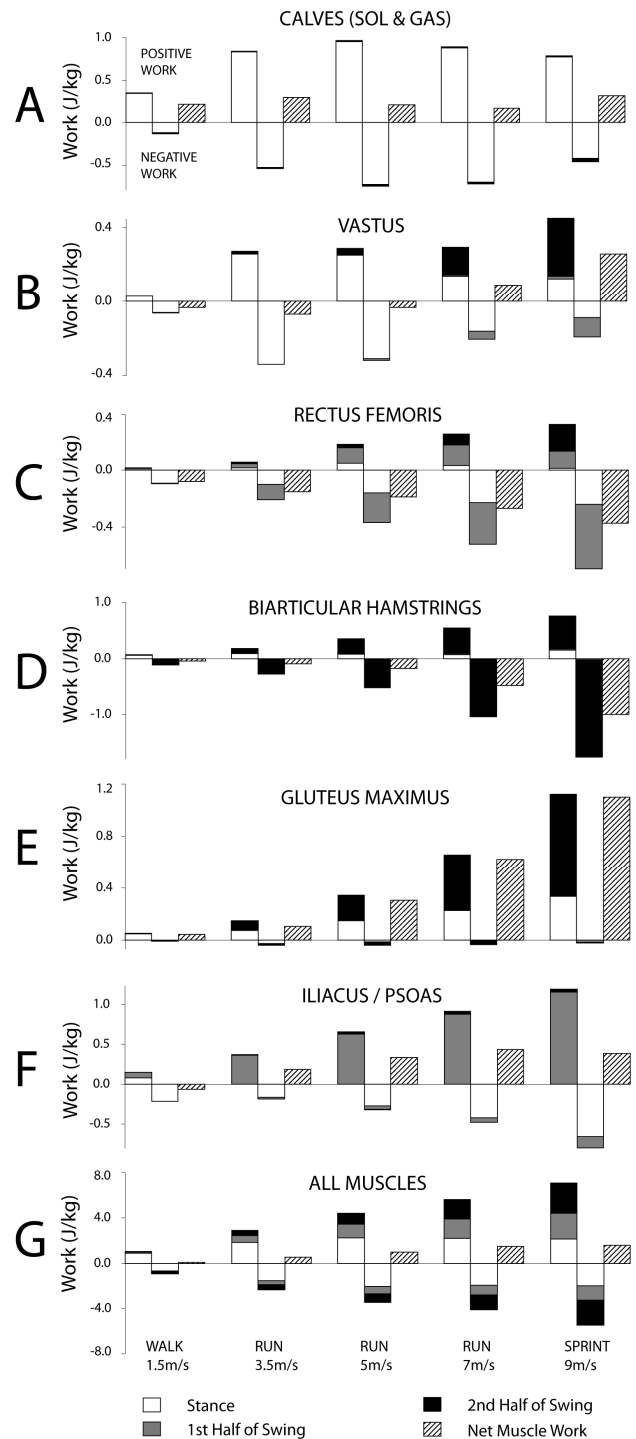


Figure 1: Work done by muscle groups at different speeds.

RESULTS AND DISCUSSION

For speeds up to 7m/s, subjects pushed on the ground harder. The total absolute work done by all lower limb muscles in stance monotonically increased from 1.566 J/kg in walking to 4.133J/kg at 7m/s running (Fig. 1G, Table 1). The peak vertical ground force also monotonically increased with speed up to 7m/s, and was primarily composed of the soleus, gastrocnemius and vasti muscles (Fig. 2). These three muscles therefore act in unison to support the body against gravity and were almost exclusively activated in stance (Fig. 1A, B). Finally, the effective vertical impulse increased from walking up to 7m/s, allowing greater relative aerial time for contralateral leg swing (Fig. 3).

Table 1: Desired and actual gait speeds recorded with their total muscular stance and swing work (positive and negative).

Desired Speed (m/s)	Actual Speed (m/s)	Muscular Stance Work (J/kg)	Muscular Swing Work (J/kg)
WALK 1.5m/s	1.50 ± 0.12 n=8	+ 0.868 - 0.698	+ 0.170 - 0.241
RUN 3.5m/s	3.49 ± 0.12 n=9	+ 1.845 - 1.545	+ 1.046 - 0.819
RUN 5m/s	5.17 ± 0.13 n=9	+ 2.270 - 2.048	+ 2.168 - 1.430
RUN 7m/s	6.96 ± 0.13 n=8	+ 2.173 - 1.960	+ 3.467 - 2.172
SPRINT 9m/s	8.97 ± 0.70 n=7	+ 2.034 - 1.885	+ 4.950 - 3.505

Increasing the running speed from 7m/s to 9m/s saw the total stance phase muscular work decrease from 4.133 J/kg to 3.919 J/kg (Fig. 1G, Table 1). Furthermore, the peak vertical ground force remained almost identical at 7m/s and 9m/s (Fig. 2). Based on these observations, stance phase mechanics are unable to explain the increase in running speed. However, despite a similar vertical ground force trajectory from 7m/s to 9m/s, a diminished effective vertical impulse was observed because of reduced ground-contact time from 145ms to 118ms, thus reducing the body's aerial time in swing. If this phenomena is indeed caused by insufficient stance phase time for muscles to generate and transmit force to the ground [2], then the only option for the body to increase speed is to increase the stride length (i.e., swing the leg more rapidly during the swing phase). Indeed, we observed significant increases in swing phase work by the hip spanning muscles between 7m/s and 9m/s ($p < 0.01$). Specifically, iliacus/psoas and gluteus maximus generated energy at the hip (Fig 1E, F),

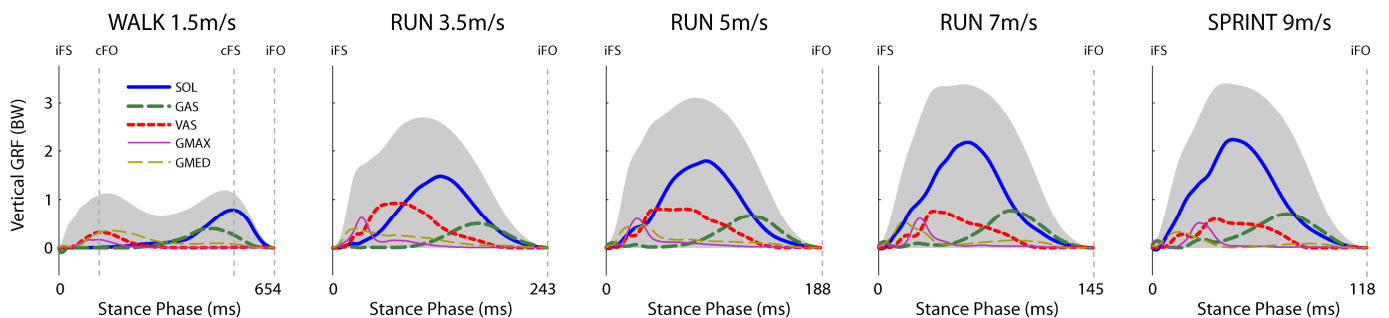


Figure 2: Contributions by five prime mover muscles to the vertical ground reaction force across different speeds of locomotion.

while rectus femoris and hamstrings absorbed energy at the hip and knee (Fig 1C, D), consistent with swing phase trends of the hip and knee joint moments [1]. The amount of work generation and absorption in these hip muscles was found to significantly increase with speed ($p < 0.01$), most likely due to the requirement of ever-increasing stride frequencies in the event of ever-decreasing aerial times.

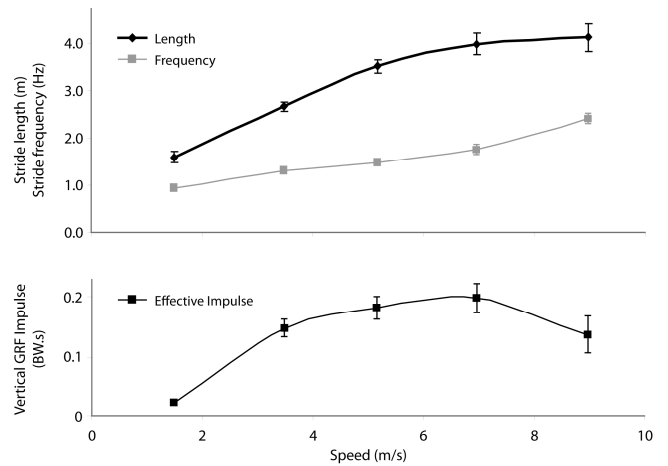


Figure 3: Stride length, stride frequency and effective vertical ground force impulse as a function of locomotion speed.

CONCLUSIONS

Running speed is brought about by a combination of stance and swing phase mechanics. Up to a running speed of 7m/s, soleus, gastrocnemius and vasti are responsible for pushing on the ground harder to increase speed by virtue of a greater stride length. Beyond 7m/s, the ability of these muscles to produce more forceful impacts appears to be compromised, requiring the iliacus/psoas, gluteus maximus, rectus femoris and hamstrings, to work harder in the swing phase to more rapidly reposition the limbs. The result is an increase in running speed by virtue of a greater stride frequency.

REFERENCES

- Schache AG, et al. *Med Sci Sports Exerc.* **In press**, 2011.
- Weyand PG, et al. *J Appl Physiol.* **89**:1991-99, 2010.
- Weyand PG, et al. *J Appl Physiol.* **108**:950-61, 2000.
- Delp SL, et al. *IEEE Trans. Biomed Eng.* **54**:1940-50, 2007.
- Lin YC, et al. *Int J Num Methods Biomed Eng.* 2010.

MUSCLE COORDINATION OF HUMAN SPRINTING

¹Tim Dorn, ¹Anthony Schache and ¹Marcus Pandy

¹Department of Mechanical Engineering, The University of Melbourne, Australia; email: t.dorn@pgrad.unimelb.edu.au

SUMMARY

The aim of this study was to investigate the functional roles of the lower-limb muscles during overground human sprinting.

INTRODUCTION

Sprinting demands great muscular strength and flexibility. Precisely timed muscular contractions are essential for rapidly swinging the limbs in preparation for foot-strike [1], and for minimizing horizontal retarding ground forces, maximizing vertical support ground forces and maintaining balance during stance [2]. Previous research in sprinting biomechanics has been typically based on two sources of data: i) basic kinematic and kinetic variables (e.g., ground reaction force, stride length and stride frequency) [2]; and ii) model computed joint variables (e.g., moments, powers and work) [3]. Such approaches, however, are limited in their ability to identify the muscle groups responsible for accelerating the limbs and whole body center-of-mass. Assessing the functional roles of the lower-limb muscles during sprinting is further complicated by the presence of dynamic coupling, (i.e., any muscle force will simultaneously induce accelerations in all the joints, even those not spanned by the muscle). The purpose of this study was to understand the functional roles that muscles play in overground sprinting by identifying and quantifying their individual contributions to the ground reaction force, joint moments and joint accelerations.

METHODS

Gait data were collected for seven healthy active participants (mass: 73.1 ± 8.6 kg, age 27 ± 8 yrs), each of whom ran on level ground at $\sim 90\%$ of his/her maximum speed. A generic 3D musculoskeletal model actuated by 92 lower-limb muscles and 10 arm torques was scaled to the dimensions of each subject. Musculotendon forces were solved using inverse kinematics and static optimization [4]. Musculotendon power was calculated from the product of musculotendon force and velocity. Musculotendon work was calculated from the area under the power-time curve. A pseudo-inverse induced acceleration analysis was performed to calculate the individual muscle contributions to the ground reaction force and joint accelerations [4]. Five contact points were distributed over the foot, and kinematic constraints were defined according to the center of pressure location to realistically simulate foot-ground interaction.

RESULTS AND DISCUSSION

The group mean sprinting speed was 8.97 ± 0.70 m/s, with an average stance and swing phase duration of 118 ms and 346 ms, respectively. With such a short ground contact time, the

soleus, gastrocnemius and vasti were rapidly activated to generate significant knee extension (2.1 Nm/kg) and ankle plantarflexion (3.4 Nm/kg) moments (Fig 1, Table 1). These muscles also dominated the makeup of the ground reaction force in vertical support and fore-aft progression (Fig. 2). Soleus provided the majority of vertical support (2 BW). Although vasti also contributed significantly to support (0.6 BW), it did so whilst generating considerable retarding horizontal forces throughout stance, a characteristic not desired in maximal effort sprinting [2]. The arm torques contributed to $<1\%$ of the ground force in all directions, suggesting that arm-swing dynamics do not provide speed enhancing benefits to the sprinter, but instead contribute to balancing the angular momentum of the lower-limb segments so as to stabilize the body during each stride [5].

During swing, rapid limb positioning yielded i) a peak hip flexion moment of 4.27 Nm/kg, generated by the iliacus/psoas and rectus femoris; ii) a peak hip extension moment of 5.57 Nm/kg, generated mostly by the hamstrings and gluteus maximus; iii) a peak knee flexion moment of 2.96 Nm/kg, generated by the hamstrings; and iv) a peak knee extension moment of 2.92 Nm/kg generated by the vasti and rectus femoris (Fig. 1, Table 1).

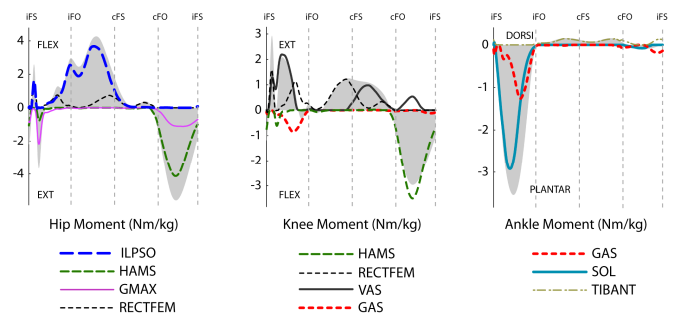


Figure 1: Individual muscle contributions to the sagittal plane joint moment of the hip, knee and ankle. Results are shown over a full gait cycle. iFS, iFO, cFS and cFO represent ipsilateral foot-strike, ipsilateral foot-off, contralateral foot-strike and contralateral foot-off respectively.

The ipsilateral (stance leg) muscles contributed 97% of the total ground force during the sprint cycle. In accelerating the lower-limb joints, however, both ipsilateral and contralateral leg muscles contributed significantly to the acceleration of the ipsilateral joint (Fig. 3). Their contributions were generally out of phase, such that the summation of ipsilateral and contralateral muscle contributions equated to the observed net

joint acceleration. For the hip, large extension accelerations produced by the ipsilateral hamstrings and gluteus maximus in terminal swing were opposed by flexion accelerations produced by the contralateral iliacus/psoas. For the knee, large flexion accelerations produced by the ipsilateral iliacus/psoas in initial swing were opposed by extension accelerations produced by the contralateral hamstrings and gluteus maximus. For the ankle, large dorsiflexion accelerations produced by the ipsilateral iliacus/psoas in initial swing were opposed by plantarflexion accelerations produced by the contralateral hamstrings and gluteus maximus. The dominating effects by these three muscles are reflected in the calculations of mechanical work done (Table 1). Perhaps most significantly, the hamstrings absorbed an average of 1.76 J/kg of energy during terminal swing, which may explain its apparent vulnerability to strain-type injury [3].

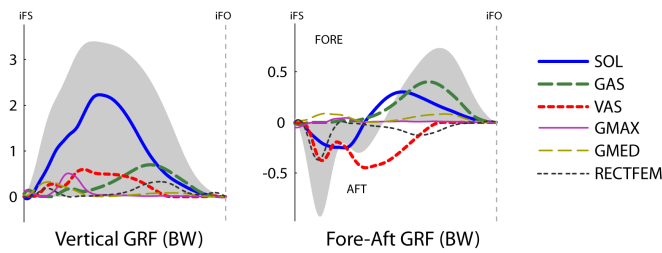


Figure 2: Individual ipsilateral muscle contributions to the vertical and fore-aft ground reaction force.

Finally, the present study offers additional insight into joint preparation for ground contact during sprinting. Small preactivation of the gastrocnemius prior to foot-strike (Fig. 1) generated rapid ankle plantarflexion acceleration, which, together with the hamstrings and co-contracting tibialis anterior, controlled the position of the ankle prior to foot-strike (Fig. 3). These findings are consistent with EMG studies [1], although the effects of preactivation on ankle joint motion have not previously been demonstrated.

CONCLUSIONS

Sprinting is a mechanically complex movement actuated by the powerful and precisely timed contractions of

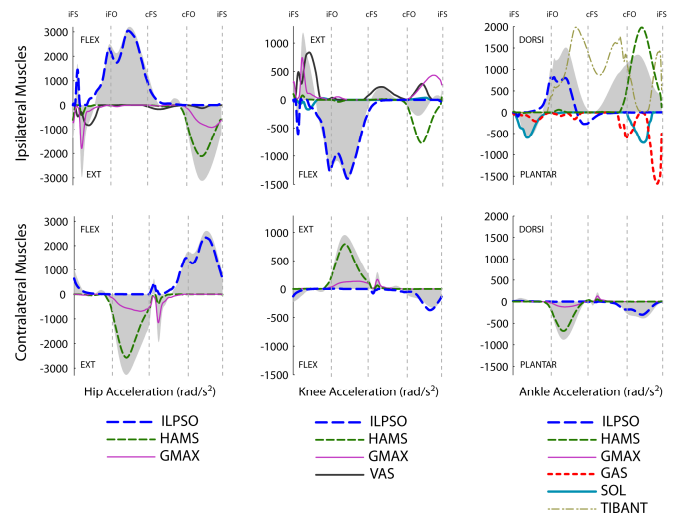


Figure 3: Muscle contributions to the joint acceleration of the sagittal hip, knee and ankle. The sum of the shaded regions of each column equate to the total acceleration of the joint.

the major lower-limb muscles. The ipsilateral leg muscles generate almost all the ground reaction force associated with vertical support and forward progression, the majority of which is contributed by the soleus, gastrocnemius and vasti. During swing, the ipsilateral and contralateral leg muscles simultaneously induce opposing joint accelerations about the hip, knee and ankle such that their summation yielded the net accelerations associated with sprinting. Although some of our findings may appear to be counter-intuitive, they reflect the concept of dynamic coupling that is inherent in all mechanical linkage systems.

REFERENCES

1. Mero A, et al. *Med Sci Sports Exerc.* **19**:266-274, 1987.
2. Hunter JP, et al. *J Applied Biomech.* **21**:31-43, 2005.
3. Schache AG, et al. *Med Sci Sports Exerc.* **In press**, 2011.
4. Lin YC, et al. *Int J Num Methods Biomed Eng*, 2010.
5. Hinrichs RN. *Int J of Sport Biomech.* **3**:242-263, 1987.

Table 1: Peak force and work done by individual muscles during overground sprinting over one stride cycle. Positive work indicates energy generation (concentric contraction); negative work indicates energy absorption (eccentric contraction).

MUSCLE	PEAK FORCE (BW)		POSITIVE WORK (J/kg)		NEGATIVE WORK (J/kg)	
	Stance	Swing	Stance	Swing	Stance	Swing
ILPSO	5.88 ± 0.34	8.73 ± 1.14	0.00 ± 0.00	1.19 ± 0.17	-0.66 ± 0.13	-0.14 ± 0.02
HAMS	1.35 ± 0.41	8.86 ± 1.06	0.15 ± 0.04	0.61 ± 0.12	0.00 ± 0.00	-1.76 ± 0.22
GMAX	2.85 ± 0.81	2.10 ± 0.74	0.34 ± 0.08	0.78 ± 0.11	0.00 ± 0.00	-0.03 ± 0.00
RECTFEM	2.42 ± 0.64	2.79 ± 0.41	0.01 ± 0.00	0.31 ± 0.13	-0.25 ± 0.07	-0.46 ± 0.07
VAS	4.81 ± 0.72	2.06 ± 0.43	0.13 ± 0.02	0.33 ± 0.11	-0.09 ± 0.00	-0.11 ± 0.01
GAS	2.82 ± 0.22	0.39 ± 0.06	0.32 ± 0.03	0.01 ± 0.00	-0.03 ± 0.00	-0.04 ± 0.00
SOL	7.32 ± 0.52	0.17 ± 0.04	0.45 ± 0.03	0.01 ± 0.00	-0.39 ± 0.03	0.00 ± 0.00

WHICH MUSCLES POWER THE HUMAN RUNNING STRIDE?

Tim W. Dorn, Yi-Chung Lin, Anthony G. Schache, Marcus G. Pandy

Department of Mechanical Engineering, The University of Melbourne, Victoria 3010, Australia

INTRODUCTION

Running is a physically demanding activity that requires explosive delivery of muscle power to the ground during stance, and precise, yet rapid limb coordination during swing. In particular, as running speed increases, greater metabolic energy in the form of muscle mechanical work is required to power the motion of: i) the center-of-mass (i.e., external power); and ii) the individual limb segments (i.e., internal power) [1,2]. The purpose of this study was to quantify the contributions that individual muscles make to the external and internal power of the body across a range of running speeds so as to identify the key muscle groups in coordinating a full running stride.

METHODS

Overground marker kinematics and ground force data were collected for nine healthy active participants, who ran at four different speeds: 3.5 m/s, 5.2 m/s, 7.0 m/s and 9.0 m/s. OpenSim [3] was then used to perform the following computational analyses. First, a generic musculoskeletal model actuated by 92 lower-limb musculotendon structures and 10 upper-limb torques was scaled to the dimensions of each subject. Individual muscle forces were then computed for each running speed of each subject using inverse kinematics, inverse dynamics and static optimization (Fig. 1). A pseudo-inverse induced acceleration analysis was developed in OpenSim to calculate the contributions of each muscle force to the net ground reaction force and joint accelerations of the body [4]. Five contact points located on the sole of the model's foot were used to simulate the interaction between the foot and the ground. During periods of ground contact, the measured center-of-pressure was used to control the stiffness of each contact point relative to the ground according to rules governing the heel-strike, foot-flat and toe-off phases of stance [4]. In this way, the ground contact model was naturally adapted to the contact patterns

exhibited by both rearfoot- and forefoot-strike runners. The external power contribution of each muscle was computed as the product of the muscle's contribution to the ground reaction force and the center-of-mass velocity. The internal power contribution of each muscle was computed by performing a segment power analysis [5] to quantify the transfer of mechanical power between the muscles and segments of the body. By generating power to a segment, a muscle tends to accelerate the segment in the direction of its current motion; the opposite applies for power absorption. Mechanical work was computed as the area under the respective power-time curves.

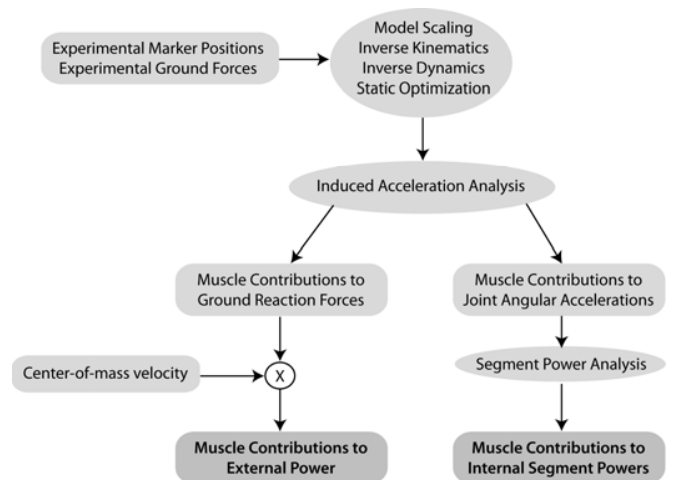


Fig 1: Computational pipeline to compute the internal and external power produced by individual muscles

RESULTS

Four muscles, all from the ipsilateral (stance) leg, contributed to the stance phase external power produced at all running speeds: SOL, GAS, VAS and RF (Fig. 2). SOL, VAS and RF absorbed external power thus decelerating the body horizontally during the first half of stance, whereas SOL and GAS generated external power thus accelerating the body forwards during the second half of stance (Fig. 2A). In the vertical direction, the ankle plantarflexors, SOL and GAS generated roughly 75% of the ground reaction force and external power to support and propel the body upwards, with the knee extensors VAS and RF contributing the remaining 25% (Fig. 2B).

ILPSO and RF generated muscle work to the heaviest body segment, the trunk, while GMAX and HAMS absorbed muscle work from the trunk, over the running stride cycle (Fig. 3). Almost all muscle work generated by the ipsilateral SOL and GAS was directed to powering the same (ipsilateral) leg – although interestingly, a significant proportion of work generated by the ipsilateral GMAX and HAMS was directed to the opposite (contralateral) leg. These quantities remained generally consistent in proportion but increased in magnitude as running speed increased, with the exception of the ankle plantarflexors, SOL and GAS.

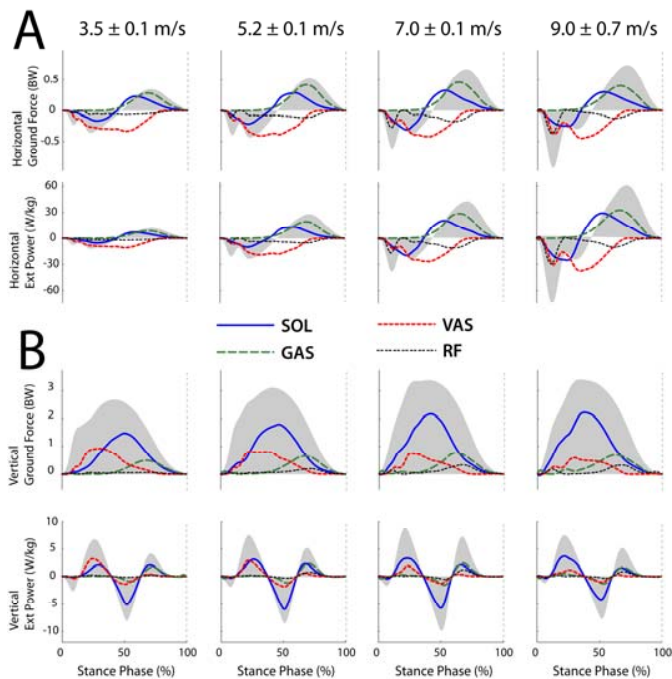


Fig 2: Muscle contributions to the ground reaction force and external power in the A) horizontal; and B) vertical direction

DISCUSSION

All major muscle groups are important in powering the running stride cycle, however muscle functionality can be divided into two groups: the stance phase and swing phase muscle groups.

In the stance phase, SOL, GAS, VAS and RF provide the external power required to move the center-of-mass. In particular, eccentric contractions by SOL, VAS and RF in the first half of stance absorb energy and decelerate the body horizontally whereas concentric contractions by SOL and GAS in the second half of stance generate energy to propel the body forwards. Muscle power particularly from SOL and GAS help to overcome gravity and accelerate the center-of-

mass upwards to achieve long aerial times and large stride lengths, both of which are particularly important for running at high speeds.

In the swing phase, the hip-spanning muscles, ILPSO, GMAX, HAMS and RF synergistically coordinate the lower-limbs into motion – presumably to rapidly power the leg forwards before decelerating it in preparation for foot strike. Unlike the stance phase where the external power and ground reaction force is made up by the stance leg muscles, the swing phase is powered by the hip-spanning muscles of both legs. For example, approximately 30% of the positive work generated by GMAX and HAMS, and 30% of the negative work absorbed by the ILPSO and RF, is being transmitted to and from the contralateral leg, respectively (Fig. 3). This coupled coordination strategy is brought about by the phenomenon of dynamic coupling – where any muscle, irrespective of its attachment site, has the ability to transmit force and power to every segment in the body [5].

In summary, the motion of the center-of-mass during running is powered primarily by the more distal limb-muscles, SOL, GAS, VAS and RF of the stance leg, whereas the lower-limb segments are powered primarily by the more proximal limb-muscles, ILPSO, GMAX, HAMS and RF of both legs. These proximal limb-muscles coordinate the running stride cycle by virtue of dynamic coupling and power redistribution.

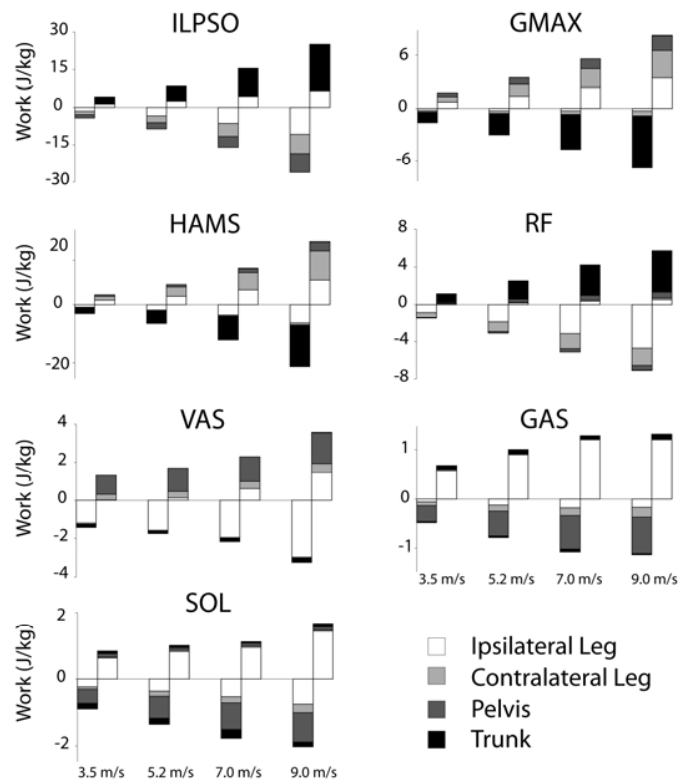


Fig 3: Muscle work (ipsilateral-leg) delivered (+) and absorbed (-) to the major body segments of the skeleton during a running stride

REFERENCES

1. Willems PA, et al. *J Exp Biol.* **198**:379-93, 1995.
2. Arampatzis A, et al. *J Biomech.* **33**:457-63, 2000.
3. Delp SL, et al. *IEEE Trans. Biomed Eng.* **54**:1940-50, 2007.
4. Lin YC, et al. *Int J Num Methods Biomed Eng.* **27**:436-49, 2011.
5. Fregly BJ, et al. *J Biomech.* **29**:81-90, 1996

References

- Abbott, B. C. and Wilkie, D. R. (1953). The relation between velocity of shortening and the tension-length curve of skeletal muscle. *J Physiol*, 120(1-2):214–223.
- Ae, M., Miyashita, K., Yokoi, T., and Hashihara, Y. (1987). Mechanical power and work done by the muscles of the lower limb during running at different speeds. In Jonsson, B., editor, *Biomechanics X-B*, volume 6B, pages 895–899. Human Kinetics Publishers, Inc., Champaign, Illinois.
- Akbarshahi, M., Schache, A. G., Fernandez, J. W., Baker, R., Banks, S., and Pandy, M. G. (2010). Non-invasive assessment of soft-tissue artifact and its effect on knee joint kinematics during functional activity. *J Biomech*, 43(7):1292–301.
- An, K. N., Takahashi, K., Harrigan, T. P., and Chao, E. Y. (1984). Determination of muscle orientations and moment arms. *J Biomech Eng*, 106(3):280–2.
- Anderson, F. C. and Pandy, M. G. (1999). A dynamic optimization solution for vertical jumping in three dimensions. *Comput Methods Biomech Biomed Engin*, 2(3):201–231.
- Anderson, F. C. and Pandy, M. G. (2001a). Dynamic optimization of human walking. *J Biomech Eng*, 123(5):381–90.
- Anderson, F. C. and Pandy, M. G. (2001b). Static and dynamic optimization solutions for gait are practically equivalent. *J Biomech*, 34(2):153–61.
- Anderson, F. C. and Pandy, M. G. (2003). Individual muscle contributions to support in normal walking. *Gait & Posture*, 17(2):159–69.
- Arampatzis, A., Bruggemann, G. P., and Metzler, V. (1999). The effect of

REFERENCES

- speed on leg stiffness and joint kinetics in human running. *J Biomech*, 32(12):1349–53.
- Arampatzis, A., Knicker, A., Metzler, V., and Bruggemann, G. P. (2000). Mechanical power in running: a comparison of different approaches. *J Biomech*, 33(4):457–63.
- Arnold, A. S., Anderson, F. C., Pandy, M. G., and Delp, S. L. (2005). Muscular contributions to hip and knee extension during the single limb stance phase of normal gait: a framework for investigating the causes of crouch gait. *J Biomech*, 38(11):2181–9.
- Arnold, A. S., Salinas, S., Asakawa, D. J., and Delp, S. L. (2000). Accuracy of muscle moment arms estimated from mri-based musculoskeletal models of the lower extremity. *Comput Aided Surg*, 5(2):108–19.
- Arnold, A. S., Thelen, D. G., Schwartz, M. H., Anderson, F. C., and Delp, S. L. (2007). Muscular coordination of knee motion during the terminal-swing phase of normal gait. *J Biomech*, 40(15):3314–24.
- Azevedo, L. B., Lambert, M. I., Vaughan, C. L., O’Connor, C. M., and Schwelling, M. P. (2009). Biomechanical variables associated with achilles tendinopathy in runners. *Br J Sports Med*, 43(4):288–92.
- Azizi, E., Brainerd, E. L., and Roberts, T. J. (2008). Variable gearing in pennate muscles. *Proc Natl Acad Sci U S A*, 105(5):1745–50.
- Bahler, A. S., Fales, J. T., and Zierler, K. L. (1968). The dynamic properties of mammalian skeletal muscle. *J Gen Physiol*, 51(3):369–84.
- Bazett-Jones, D. M., Cobb, S. C., Joshi, M. N., Cashin, S. E., and Earl, J. E. (2011). Normalizing hip muscle strength: establishing body-size-independent measurements. *Arch Phys Med Rehabil*, 92(1):76–82.
- Belli, A., Kyrolainen, H., and Komi, P. V. (2002). Moment and power of lower limb joints in running. *Int J Sports Med*, 23(2):136–41.
- Besier, T. F., Fredericson, M., Gold, G. E., Beaupre, G. S., and Delp, S. L. (2009). Knee muscle forces during walking and running in patellofemoral pain patients and pain-free controls. *J Biomech*, 42(7):898–905.
- Bezodis, I. N., Kerwin, D. G., and Salo, A. I. (2008). Lower-limb mechanics during the support phase of maximum-velocity sprint running. *Med Sci Sports Exerc*, 40(4):707–15.
- Biewener, A. A., Farley, C. T., Roberts, T. J., and Temaner, M. (2004).

- Muscle mechanical advantage of human walking and running: implications for energy cost. *J Appl Physiol*, 97(6):2266–74.
- Boerboom, A., Hof, A., Halbertsma, J., Raaij, J., Schenk, W., Diercks, R., and Horn, J. (2001). Atypical hamstrings electromyographic activity as a compensatory mechanism in anterior cruciate ligament deficiency. *Knee Surgery, Sports Traumatology, Arthroscopy*, 9(4):211–216.
- Brand, R. A., Crowninshield, R. D., Wittstock, C. E., Pedersen, D. R., Clark, C. R., and van Krieken, F. M. (1982). A model of lower extremity muscular anatomy. *J Biomech Eng*, 104(4):304–10.
- Brown, L. M., Gonzalez-Serratos, H., and Huxley, A. F. (1984). Sarcomere and filament lengths in passive muscle fibres with wavy myofibrils. *J Muscle Res Cell Motil*, 5(3):293–314.
- Buchanan, T. S., Lloyd, D. G., Manal, K., and Besier, T. F. (2004). Neuromusculoskeletal modeling: estimation of muscle forces and joint moments and movements from measurements of neural command. *J Appl Biomech*, 20(4):367–95.
- Buchanan, T. S., Lloyd, D. G., Manal, K., and Besier, T. F. (2005). Estimation of muscle forces and joint moments using a forward-inverse dynamics model. *Med Sci Sports Exerc*, 37(11):1911–6.
- Buchanan, T. S., Moniz, M. J., Dewald, J. P., and Zev Rymer, W. (1993). Estimation of muscle forces about the wrist joint during isometric tasks using an emg coefficient method. *J Biomech*, 26(4-5):547–60.
- Buczek, F. L. and Cavanagh, P. R. (1990). Stance phase knee and ankle kinematics and kinetics during level and downhill running. *Med Sci Sports Exerc*, 22(5):669–77.
- Buford, W. L., J., Ivey, F. M., J., Malone, J. D., Patterson, R. M., Peare, G. L., Nguyen, D. K., and Stewart, A. A. (1997). Muscle balance at the knee—moment arms for the normal knee and the acl-minus knee. *IEEE Trans Rehabil Eng*, 5(4):367–79.
- Byrnes, W. C., McCullage, P., Dickinson, A., and Noble, J. (1993). Incidence and severity of injury following aerobic training programs emphasising running, racewalking, or step aerobics. *Med Sci Sports Exerc*, 25(5):25–81.
- Cappozzo, A., Catani, F., Leardini, A., Benedetti, M. G., and Croce, U. D. (1996). Position and orientation in space of bones during movement: experimental artefacts. *Clin Biomech*, 11(2):90–100.

REFERENCES

- Cavagna, G. A. (2009). The two asymmetries of the bouncing step. *Eur J Appl Physiol*, 107(6):739–42.
- Cavagna, G. A., Franzetti, P., Heglund, N. C., and Willems, P. (1988). The determinants of the step frequency in running, trotting and hopping in man and other vertebrates. *J Physiol*, 399:81–92.
- Cavagna, G. A. and Kaneko, M. (1977). Mechanical work and efficiency in level walking and running. *J Physiol*, 268(2):467–81.
- Cavagna, G. A., Komarek, L., and Mazzoleni, S. (1971). The mechanics of sprint running. *J Physiol*, 217(3):709–21.
- Cavagna, G. A., Legramandi, M. A., and Peyre-Tartaruga, L. A. (2008). Old men running: mechanical work and elastic bounce. *Proc Biol Sci*, 275(1633):411–8.
- Cavagna, G. A., Willems, P. A., Franzetti, P., and Detrembleur, C. (1991). The two power limits conditioning step frequency in human running. *J Physiol*, 437:95–108.
- Challis, J. H. (1995). A procedure for determining rigid body transformation parameters. *J Biomech*, 28(6):733–7.
- Chapman, A. E. and Caldwell, G. E. (1983a). Factors determining changes in lower limb energy during swing in treadmill running. *J Biomech*, 16(1):69–77.
- Chapman, A. E. and Caldwell, G. E. (1983b). Kinetic limitations of maximal sprinting speed. *J Biomech*, 16(1):79–83.
- Cheung, J. T. and Zhang, M. (2005). A 3-dimensional finite element model of the human foot and ankle for insole design. *Arch Phys Med Rehabil*, 86(2):353–8.
- Chumanov, E. S., Heiderscheit, B. C., and Thelen, D. G. (2007). The effect of speed and influence of individual muscles on hamstring mechanics during the swing phase of sprinting. *J Biomech*, 40(16):3555–62.
- Chumanov, E. S., Heiderscheit, B. C., and Thelen, D. G. (2011). Hamstring musculotendon dynamics during stance and swing phases of high-speed running. *Med Sci Sports Exerc*, 43(3):525–532.
- Close, R. I. (1972). Dynamic properties of mammalian skeletal muscles. *Physiol Rev*, 52(1):129–97.

- Collins, J. J. (1995). The redundant nature of locomotor optimization laws. *J Biomech*, 28(3):251–67.
- Corn, R. J. and Knudson, D. (2003). Effect of elastic-cord towing on the kinematics of the acceleration phase of sprinting. *J Strength Cond Res*, 17(1):72–5.
- Correa, T. A., Baker, R., Graham, H. K., and Pandy, M. G. (2011). Accuracy of generic musculoskeletal models in predicting the functional roles of muscles in human gait. *J Biomech*, 44(11):2096–105.
- Correa, T. A. and Pandy, M. G. (2011). A mass-length scaling law for modeling muscle strength in the lower limb. *J Biomech*, In press.
- Crowninshield, R. D. (1978). Use of optimization techniques to predict muscle forces. *Journal of Biomechanical Engineering*, 100(2):88–92.
- Crowninshield, R. D. and Brand, R. A. (1981). A physiologically based criterion of muscle force prediction in locomotion. *J Biomech*, 14(11):793–801.
- Davies, C. T. (1980). Effects of wind assistance and resistance on the forward motion of a runner. *J Appl Physiol*, 48(4):702–9.
- De Groote, F., Van Campen, A., Jonkers, I., and De Schutter, J. (2010). Sensitivity of dynamic simulations of gait and dynamometer experiments to hill muscle model parameters of knee flexors and extensors. *J Biomech*, 43(10):1876–83.
- Delecluse, C. (1997). Influence of strength training on sprint running performance. current findings and implications for training. *Sports Med*, 24(3):147–56.
- Delecluse, C., Van Coppenolle, H., Willems, E., Van Leemputte, M., Diels, R., and Goris, M. (1995). Influence of high-resistance and high-velocity training on sprint performance. *Med Sci Sports Exerc*, 27(8):1203–9.
- Delp, S. L., Anderson, F. C., Arnold, A. S., Loan, P., Habib, A., John, C. T., Guendelman, E., and Thelen, D. G. (2007). Opensim: open-source software to create and analyze dynamic simulations of movement. *IEEE Trans Biomed Eng*, 54(11):1940–50.
- Delp, S. L., Hess, W. E., Hungerford, D. S., and Jones, L. C. (1999). Variation of rotation moment arms with hip flexion. *J Biomech*, 32(5):493–501.
- Delp, S. L. and Loan, J. P. (1995). A graphics-based software system to

REFERENCES

- develop and analyze models of musculoskeletal structures. *Comput Biol Med*, 25(1):21–34.
- Delp, S. L., Loan, J. P., Hoy, M. G., Zajac, F. E., Topp, E. L., and Rosen, J. M. (1990). An interactive graphics-based model of the lower extremity to study orthopaedic surgical procedures. *IEEE Trans Biomed Eng*, 37(8):757–67.
- Derrick, T. R., Hamill, J., and Caldwell, G. E. (1998). Energy absorption of impacts during running at various stride lengths. *Med Sci Sports Exerc*, 30(1):128–35.
- Devita, P., Helseth, J., and Hortobagyi, T. (2007). Muscles do more positive than negative work in human locomotion. *J Exp Biol*, 210(Pt 19):3361–73.
- Devita, P., Janshen, L., Rider, P., Solnik, S., and Hortobagyi, T. (2008). Muscle work is biased toward energy generation over dissipation in non-level running. *J Biomech*, 41(16):3354–9.
- Devita, P. and Skelly, W. A. (1990). Intrasubject variability of lower extremity joint moments of force during the stance phase of running. *Human Movement Science*, 9(2):99–115.
- Di Prampero, P. E., Capelli, C., Pagliaro, P., Antonutto, G., Girardis, M., Zamparo, P., and Soule, R. G. (1993). Energetics of best performances in middle-distance running. *J Appl Physiol*, 74(5):2318–24.
- Dietz, V., Schmidtbleicher, D., and Noth, J. (1979). Neuronal mechanisms of human locomotion. *J Neurophysiol*, 42(5):1212–22.
- Dillman, C. J. (1975). Kinematic analyses of running. *Exerc Sport Sci Rev*, 3:193–218.
- Disselhorst-Klug, C., Schmitz-Rode, T., and Rau, G. (2009). Surface electromyography and muscle force: limits in semg-force relationship and new approaches for applications. *Clin Biomech*, 24(3):225–235.
- Donelan, J. M., Kram, R., and Kuo, A. D. (2002). Simultaneous positive and negative external mechanical work in human walking. *J Biomech*, 35(1):117–24.
- Edman, K. A. and Reggiani, C. (1987). The sarcomere length-tension relation determined in short segments of intact muscle fibres of the frog. *J Physiol*, 385:709–32.
- Elftman, H. (1940). The work done by muscles in running. *Am J Physiol*, 129(3):672–684.

- Elliott, B. C. and Blanksby, B. A. (1976). A cinematographic analysis of overground and treadmill running by males and females. *Med Sci Sports*, 8(2):84–7.
- Erdemir, A., McLean, S., Herzog, W., and van den Bogert, A. J. (2007). Model-based estimation of muscle forces exerted during movements. *Clin Biomech*, 22(2):131–54.
- Ferris, D. P., Louie, M., and Farley, C. T. (1998). Running in the real world: adjusting leg stiffness for different surfaces. *Proc Biol Sci*, 265(1400):989–94.
- Flynn, T. W. and Soutas-Little, R. W. (1995). Patellofemoral joint compressive forces in forward and backward running. *J Orthop Sports Phys Ther*, 21(5):277–82.
- Folland, J. P., Mc Cauley, T. M., and Williams, A. G. (2008). Allometric scaling of strength measurements to body size. *Eur J Appl Physiol*, 102(6):739–45.
- Forwood, M. R., Neal, R. J., and Wilson, B. D. (1985). Scaling segmental moments of inertia for individual subjects. *J Biomech*, 18(10):755–61.
- Frederick, E. C. (1986). Factors affecting peak vertical ground reaction forces in running. *Journal of applied biomechanics*, 2:41–49.
- Fregly, B. J. and Zajac, F. E. (1996). A state-space analysis of mechanical energy generation, absorption, and transfer during pedaling. *J Biomech*, 29(1):81–90.
- Friederich, J. A. and Brand, R. A. (1990). Muscle fiber architecture in the human lower limb. *J Biomech*, 23(1):91–5.
- Frishberg, B. A. (1983). An analysis of overground and treadmill sprinting. *Med Sci Sports Exerc*, 15(6):478–85.
- Fukashiro, S., Itoh, M., Ichinose, Y., Kawakami, Y., and Fukunaga, T. (1995). Ultrasonography gives directly but noninvasively elastic characteristic of human tendon in vivo. *Eur J Appl Physiol Occup Physiol*, 71(6):555–7.
- Fukunaga, T., Roy, R. R., Shellock, F. G., Hodgson, J. A., and Edgerton, V. R. (1996). Specific tension of human plantar flexors and dorsiflexors. *J Appl Physiol*, 80(1):158–65.
- Garner, B. A. and Pandy, M. G. (2000). The obstacle-set method for

REFERENCES

- representing muscle paths in musculoskeletal models. *Comput Methods Biomech Biomed Engin*, 3(1):1–30.
- Gazendam, M. G. and Hof, A. L. (2007). Averaged emg profiles in jogging and running at different speeds. *Gait & Posture*, 25(4):604–14.
- Glitsch, U. and Baumann, W. (1997). The three-dimensional determination of internal loads in the lower extremity. *J Biomech*, 30(11-12):1123–31.
- Goldberg, S. and Kepple, T. M. (2009). Muscle-induced accelerations at maximum activation to assess individual muscle capacity during movement. *J Biomech*, 42(7):952–955.
- Gordon, A. M., Huxley, A. F., and Julian, F. J. (1966). The variation in isometric tension with sarcomere length in vertebrate muscle fibres. *J Physiol*, 184(1):170–92.
- Hamner, S. R., Seth, A., and Delp, S. L. (2010). Muscle contributions to propulsion and support during running. *J Biomech*, 43(14):2709–2716.
- Hart, J. M., Ko, J.-W. K., Konold, T., and Pietrosimione, B. (2010). Sagittal plane knee joint moments following anterior cruciate ligament injury and reconstruction: A systematic review. *Clin Biomech*, 25(4):277–283.
- Heintz, S. and Gutierrez-Farewik, E. M. (2007). Static optimization of muscle forces during gait in comparison to emg-to-force processing approach. *Gait & Posture*, 26(2):279–88.
- Heise, G. D. and Martin, P. E. (2001). Are variations in running economy in humans associated with ground reaction force characteristics? *Eur J Appl Physiol*, 84(5):438–42.
- Hennessy, L. and Kilty, J. (2001). Relationship of the stretch-shortening cycle to sprint performance in trained female athletes. *J Strength Cond Res*, 15(3):326–31.
- Hermens, H. J., Freriks, B., Disselhorst-Klug, C., and Rau, G. (2000). Development of recommendations for semg sensors and sensor placement procedures. *J Electromyogr Kinesiol*, 10(5):361–74.
- Higashihara, A., Ono, T., Kubota, J., Okuwaki, T., and Fukubayashi, T. (2010). Functional differences in the activity of the hamstring muscles with increasing running speed. *Journal of Sports Sciences*, 28(10):1085–1092.
- Hill, A. V. (1938). The heat shortening and the dynamic constants of muscle. *Proc. R. Soc. Lond.*, 126(B):136–195.

- Hinrichs, R. N. (1987). Upper extremity function in running. ii: Angular momentum considerations. *International Journal of Sport Biomechanics*, 3(3):242–263.
- Hoang, P. D., Herbert, R. D., Todd, G., Gorman, R. B., and Gandevia, S. C. (2007). Passive mechanical properties of human gastrocnemius muscle tendon units, muscle fascicles and tendons in vivo. *J Exp Biol*, 210(Pt 23):4159–68.
- Hortobagyi, T., Solnik, S., Gruber, A., Rider, P., Steinweg, K., Helseth, J., and DeVita, P. (2009). Interaction between age and gait velocity in the amplitude and timing of antagonist muscle coactivation. *Gait & Posture*, 29(4):558–64.
- Hreljac, A. (2004). Impact and overuse injuries in runners. *Med Sci Sports Exerc*, 36(5):845–9.
- Hreljac, A. (2005). Etiology, prevention, and early intervention of overuse injuries in runners: a biomechanical perspective. *Phys Med Rehabil Clin N Am*, 16(3):651–67, vi.
- Hreljac, A., Marshall, R. N., and Hume, P. A. (2000). Evaluation of lower extremity overuse injury potential in runners. *Med Sci Sports Exerc*, 32(9):1635–41.
- Hunter, B. V., Thelen, D. G., and Dhaher, Y. Y. (2009). A three-dimensional biomechanical evaluation of quadriceps and hamstrings function using electrical stimulation. *IEEE Trans Neural Syst Rehabil Eng*, 17(2):167–75.
- Hunter, J. P., Marshall, R. N., and McNair, P. (2005). Relationships between ground reaction force impulse and kinematics of sprint-running acceleration. *J Appl Biomech*, 21(1):31–43.
- Hunter, J. P., Marshall, R. N., and McNair, P. J. (2004). Interaction of step length and step rate during sprint running. *Med Sci Sports Exerc*, 36(2):261–71.
- Hurd, W. J. and Snyder-Mackler, L. (2007). Knee instability after acute acl rupture affects movement patterns during the mid-stance phase of gait. *J Orthop Res*, 25(10):1369–77.
- Huxley, H. (1995). The working stroke of myosin crossbridges. *Biophys J*, 68(4 Suppl):55S–56S; discussion 57S–58S.
- Huxley, H. E. (2008). Memories of early work on muscle contraction and

REFERENCES

- regulation in the 1950's and 1960's. *Biochem Biophys Res Commun*, 369(1):34–42.
- Ishikawa, M. and Komi, P. V. (2007). The role of the stretch reflex in the gastrocnemius muscle during human locomotion at various speeds. *J Appl Physiol*, 103(3):1030–6.
- Ishikawa, M., Pakaslahti, J., and Komi, P. V. (2007). Medial gastrocnemius muscle behavior during human running and walking. *Gait & Posture*, 25(3):380–4.
- Jacobs, R., Bobbert, M. F., and van Ingen Schenau, G. J. (1993). Function of mono- and biarticular muscles in running. *Med Sci Sports Exerc*, 25(10):1163–73.
- Johnson, M. D. and Buckley, J. G. (2001). Muscle power patterns in the mid-acceleration phase of sprinting. *J Sports Sci*, 19(4):263–72.
- Jonhagen, S., Ericson, M. O., Nemeth, G., and Eriksson, E. (1996). Amplitude and timing of electromyographic activity during sprinting. *Scand J Med Sci Sports*, 6:15–21.
- Jonkers, I., Spaepen, A., Papaioannou, G., and Stewart, C. (2002). An emg-based, muscle driven forward simulation of single support phase of gait. *J Biomech*, 35(5):609–19.
- Joumaa, V. and Herzog, W. (2010). Force depression in single myofibrils. *J Appl Physiol*, 108(2):356–62.
- Joyce, G. C. and Rack, P. M. (1969). Isotonic lengthening and shortening movements of cat soleus muscle. *J Physiol*, 204(2):475–91.
- Kadaba, M. P., Ramakrishnan, H. K., and Wootten, M. E. (1990). Measurement of lower extremity kinematics during level walking. *J Orthop Res*, 8(3):383–92.
- Kaneko, M. (1990). Mechanics and energetics in running with special reference to efficiency. *J Biomech*, 23 Suppl 1:57–63.
- Katz, B. (1939). The relationship between force and speed in muscular contraction. *J. Physiol. (London)*, 96(45).
- Kawakami, Y., Abe, T., Kuno, S. Y., and Fukunaga, T. (1995). Training-induced changes in muscle architecture and specific tension. *Eur J Appl Physiol Occup Physiol*, 72(1-2):37–43.

- Kawamori, N. and Haff, G. G. (2004). The optimal training load for the development of muscular power. *J Strength Cond Res*, 18(3):675–84.
- Keller, T. S., Weisberger, A. M., Ray, J. L., Hasan, S. S., Shiavi, R. G., and Spengler, D. M. (1996). Relationship between vertical ground reaction force and speed during walking, slow jogging, and running. *Clin Biomech*, 11(5):253–259.
- Kepple, T. M., Siegel, K. L., and Stanhope, S. (1997a). The use of two foot-floor models to examine the role of the ankle plantarflexors in the forward acceleration of normal gait. *Gait & Posture*, 5(2):172–173.
- Kepple, T. M., Siegel, K. L., and Stanhope, S. J. (1997b). Relative contributions of the lower extremity joint moments to forward progression and support during gait. *Gait & Posture*, 6(1):1–8.
- Kibler, W. B., Goldberg, C., and Chandler, T. J. (1991). Functional biomechanical deficits in running athletes with plantar fasciitis. *Am J Sports Med*, 19(1):66–71.
- Kim, H. J., Fernandez, J. W., Akbarshahi, M., Walter, J. P., Fregly, B. J., and Pandy, M. G. (2009). Evaluation of predicted knee-joint muscle forces during gait using an instrumented knee implant. *J Orthop Res*, 27(10):1326–31.
- Kivi, D. M., Maraj, B. K., and Gervais, P. (2002). A kinematic analysis of high-speed treadmill sprinting over a range of velocities. *Med Sci Sports Exerc*, 34(4):662–6.
- Klein Horsman, M. D., Koopman, H. F., van der Helm, F. C., Prose, L. P., and Veeger, H. E. (2007). Morphological muscle and joint parameters for musculoskeletal modelling of the lower extremity. *Clin Biomech*, 22(2):239–47.
- Komi, P. V. (1984). Physiological and biomechanical correlates of muscle function: effects of muscle structure and stretch-shortening cycle on force and speed. *Exerc Sport Sci Rev*, 12:81–121.
- Komi, P. V. (2000). Stretch-shortening cycle: a powerful model to study normal and fatigued muscle. *J Biomech*, 33(10):1197–206.
- Komi, P. V., Belli, A., Huttunen, V., Bonnefoy, R., Geysant, A., and Lacour, J. R. (1996). Optic fibre as a transducer of tendomuscular forces. *Eur J Appl Physiol Occup Physiol*, 72(3):278–80.
- Komi, P. V., Salonen, M., Jarvinen, M., and Kokko, O. (1987). In

REFERENCES

- vivo registration of achilles tendon forces in man. i. methodological development. *Int J Sports Med*, 8 Suppl 1:3–8.
- Kubo, K., Kanehisa, H., Takeshita, D., Kawakami, Y., Fukashiro, S., and Fukunaga, T. (2000). In vivo dynamics of human medial gastrocnemius muscle-tendon complex during stretch-shortening cycle exercise. *Acta Physiol Scand*, 170(2):127–35.
- Kuitunen, S., Komi, P. V., and Kyrolainen, H. (2002). Knee and ankle joint stiffness in sprint running. *Med Sci Sports Exerc*, 34(1):166–73.
- Kunz, H. and Kaufmann, D. A. (1981). Biomechanical analysis of sprinting: decathletes versus champions. *Br J Sports Med*, 15(3):177–81.
- Kuo, A. D. (1998). A least-squares estimation approach to improving the precision of inverse dynamics computations. *J Biomech Eng*, 120(1):148–59.
- Kuo, P. L., Li, P. C., and Li, M. L. (2001). Elastic properties of tendon measured by two different approaches. *Ultrasound Med Biol*, 27(9):1275–84.
- Kyrolainen, H., Avela, J., and Komi, P. V. (2005). Changes in muscle activity with increasing running speed. *J Sports Sci*, 23(10):1101–9.
- Kyrolainen, H., Komi, P. V., and Belli, A. (1999). Changes in muscle activity patterns and kinetics with increasing running speed. *Journal of Strength and Conditioning Research*, 13(4):400–406.
- Lee, E. J. and Herzog, W. (2008). Residual force enhancement exceeds the isometric force at optimal sarcomere length for optimized stretch conditions. *J Appl Physiol*, 105(2):457–62.
- Lee, S. S. and Piazza, S. J. (2009). Built for speed: musculoskeletal structure and sprinting ability. *J Exp Biol*, 212(Pt 22):3700–7.
- Li, X., Zhou, P., and Aruin, A. S. (2007). Teager-kaiser energy operation of surface emg improves muscle activity onset detection. *Ann Biomed Eng*, 35(9):1532–8.
- Lichtwark, G. A., Bougoulias, K., and Wilson, A. M. (2007). Muscle fascicle and series elastic element length changes along the length of the human gastrocnemius during walking and running. *J Biomech*, 40(1):157–64.
- Lichtwark, G. A. and Wilson, A. M. (2005). In vivo mechanical properties of the human achilles tendon during one-legged hopping. *J Exp Biol*, 208(Pt 24):4715–25.

- Lieber, R. L. and Friden, J. (1993). Muscle damage is not a function of muscle force but active muscle strain. *J Appl Physiol*, 74(2):520–526.
- Lieberman, D. E., Venkadesan, M., Werbel, W. A., Daoud, A. I., D’Andrea, S., Davis, I. S., Mang’eni, R. O., and Pitsiladis, Y. (2010). Foot strike patterns and collision forces in habitually barefoot versus shod runners. *Nature*, 463(7280):531–5.
- Lin, Y. C., Dorn, T. W., Schache, A. G., and Pandy, M. G. (2011a). Comparison of different methods for estimating muscle forces in human movement. *Journal of Engineering in Medicine*, In press.
- Lin, Y. C., Kim, H. J., and Pandy, M. G. (2011b). A computationally efficient method for assessing muscle function during human locomotion. *International Journal for Numerical Methods in Biomedical Engineering*, 27:436–49.
- Liu, M. Q., Anderson, F. C., Pandy, M. G., and Delp, S. L. (2006). Muscles that support the body also modulate forward progression during walking. *J Biomech*, 39(14):2623–30.
- Liu, M. Q., Anderson, F. C., Schwartz, M. H., and Delp, S. L. (2008). Muscle contributions to support and progression over a range of walking speeds. *J Biomech*, 41(15):3243–52.
- Lloyd, D. G. and Besier, T. F. (2003). An emg-driven musculoskeletal model to estimate muscle forces and knee joint moments in vivo. *J Biomech*, 36(6):765–76.
- Lu, T. W. and O’Connor, J. J. (1999). Bone position estimation from skin marker co-ordinates using global optimisation with joint constraints. *J Biomech*, 32(2):129–34.
- Luhtanen, P. and Komi, P. V. (1978). *Mechanical factors influencing the running speed. In: Biomechanics VI (Asmussen, E., Jrgensen, K., eds.)*. University Park Press, Baltimore.
- Macera, C. A., Pate, R. R., Powell, K. E., Jackson, K. L., Kendrick, J. S., and Craven, T. E. (1989). Predicting lower-extremity injuries among habitual runners. *Arch Intern Med*, 149(11):2565–8.
- Macera, C. A., Pate, R. R., Woods, J., Davis, D. R., and Jackson, K. L. (1991). Posttrace morbidity among runners. *Am J Prev Med*, 7(4):194–8.
- Maganaris, C. N., Baltzopoulos, V., Ball, D., and Sargeant, A. J. (2001). In

REFERENCES

- vivo specific tension of human skeletal muscle. *J Appl Physiol*, 90(3):865–72.
- Magnusson, S. P., Narici, M. V., Maganaris, C. N., and Kjaer, M. (2008). Human tendon behaviour and adaptation, in vivo. *J Physiol*, 586(1):71–81.
- Manal, K., Gonzalez, R. V., Lloyd, D. G., and Buchanan, T. S. (2002). A real-time emg-driven virtual arm. *Comput Biol Med*, 32(1):25–36.
- Mann, R. and Herman, J. (1985). Kinematic analysis of olympic sprint performance: men’s 200 meters. *International Journal of Sport Biomechanics*, 1:151–162.
- Mann, R. A. and Hagy, J. (1980). Biomechanics of walking, running, and sprinting. *Am J Sports Med*, 8(5):345–50.
- Mann, R. A., Moran, G. T., and Dougherty, S. E. (1986). Comparative electromyography of the lower extremity in jogging, running, and sprinting. *American Journal of Sports Medicine*, 14(6):501–510.
- Mann, R. V. (1981). A kinetic analysis of sprinting. *Med Sci Sports Exerc*, 13(5):325–8.
- Margaria, R., Cerretelli, P., Aghemo, P., and Sassi, G. (1963). Energy cost of running. *J Appl Physiol*, 18:367–70.
- McClay, I. and Manal, K. (1999). Three-dimensional kinetic analysis of running: significance of secondary planes of motion. *Med Sci Sports Exerc*, 31(11):1629–1637.
- McCrorry, J. L., Martin, D. F., Lowery, R. B., Cannon, D. W., Curl, W. W., Read, H. M., J., Hunter, D. M., Craven, T., and Messier, S. P. (1999). Etiologic factors associated with achilles tendinitis in runners. *Med Sci Sports Exerc*, 31(10):1374–81.
- McGowan, C. P., Neptune, R. R., and Herzog, W. (2010). A phenomenological model and validation of shortening-induced force depression during muscle contractions. *J Biomech*, 43(3):449–54.
- McIntosh, A. S., Beatty, K. T., Dwan, L. N., and Vickers, D. R. (2006). Gait dynamics on an inclined walkway. *J Biomech*, 39(13):2491–502.
- Mendiguchia, J., Alentorn-Geli, E., and Brughelli, M. (2011). Hamstring strain injuries: are we heading in the right direction? *Br J Sports Med*, In press.

- Mercer, J. A., Bezodis, N. E., Russell, M., Purdy, A., and DeLion, D. (2005). Kinetic consequences of constraining running behavior. *Journal of Sports Science and Medicine*, 4(2):144–152.
- Mercer, J. A., Vance, J., Hreljac, A., and Hamill, J. (2002). Relationship between shock attenuation and stride length during running at different velocities. *European Journal Of Applied Physiology*, 87(4-5):403–408.
- Mero, A. (1988). Force-time characteristics and running velocity of male sprinters during the acceleration phase of sprinting. *Research Quarterly for Exercise and Sport*, 59(2):94.
- Mero, A. and Komi, P. V. (1987). Electromyographic activity in sprinting at speeds ranging from sub-maximal to supra-maximal. *Med Sci Sports Exerc*, 19(3):266–74.
- Mero, A., Komi, P. V., and Gregor, R. J. (1992). Biomechanics of sprint running. a review. *Sports Med*, 13(6):376–92.
- Morse, C. I., Thom, J. M., Reeves, N. D., Birch, K. M., and Narici, M. V. (2005). In vivo physiological cross-sectional area and specific force are reduced in the gastrocnemius of elderly men. *J Appl Physiol*, 99(3):1050–5.
- Morse, C. I., Tolfrey, K., Thom, J. M., Vassilopoulos, V., Maganaris, C. N., and Narici, M. V. (2008). Gastrocnemius muscle specific force in boys and men. *J Appl Physiol*, 104(2):469–74.
- Muramatsu, T., Muraoka, T., Takeshita, D., Kawakami, Y., Hirano, Y., and Fukunaga, T. (2001). Mechanical properties of tendon and aponeurosis of human gastrocnemius muscle in vivo. *J Appl Physiol*, 90(5):1671–8.
- Muraoka, T., Muramatsu, T., Fukunaga, T., and Kanehisa, H. (2005). Elastic properties of human achilles tendon are correlated to muscle strength. *J Appl Physiol*, 99(2):665–9.
- Myer, G. D., Ford, K. R., Brent, J. L., Divine, J. G., and Hewett, T. E. (2007). Predictors of sprint start speed: the effects of resistive ground-based vs. inclined treadmill training. *J Strength Cond Res*, 21(3):831–6.
- Nagano, A., Gerritsen, K. G., and Fukashiro, S. (2000). A sensitivity analysis of the calculation of mechanical output through inverse dynamics: a computer simulation study. *J Biomech*, 33(10):1313–8.
- Nelson, R. C., Dillman, C. J., Lagasse, P., and Bickett, P. (1972).

REFERENCES

- Biomechanics of overground versus treadmill running. *Med Sci Sports*, 4(4):233–40.
- Neptune, R. R. and Kautz, S. A. (2001). Muscle activation and deactivation dynamics: the governing properties in fast cyclical human movement performance? *Exerc Sport Sci Rev*, 29(2):76–80.
- Neptune, R. R. and McGowan, C. P. (2011). Muscle contributions to whole-body sagittal plane angular momentum during walking. *J Biomech*, 44(1):6–12.
- Neptune, R. R., Wright, I. C., and Van Den Bogert, A. J. (2000). A method for numerical simulation of single limb ground contact events: Application to heel-toe running. *Comput Methods Biomech Biomed Engin*, 3(4):321–334.
- Neptune, R. R., Zajac, F. E., and Kautz, S. A. (2004). Muscle force redistributes segmental power for body progression during walking. *Gait Posture*, 19(2):194–205.
- Nett, T. (1964). Foot plant in running. *Track Technique*, 15:462–463.
- Nigg, B. M. (1985). Biomechanics, load analysis and sports injuries in the lower extremities. *Sports Med*, 2(5):367–79.
- Nigg, B. M. (2001). The role of impact forces and foot pronation: a new paradigm. *Clin J Sport Med*, 11(1):2–9.
- Nigg, B. M. and Bobbert, M. (1990). On the potential of various approaches in load analysis to reduce the frequency of sports injuries. *J Biomech*, 23 Suppl 1:3–12.
- Nigg, B. M., De Boer, R. W., and Fisher, V. (1995). A kinematic comparison of overground and treadmill running. *Med Sci Sports Exerc*, 27(1):98–105.
- Nigg, B. M. and Herzog, W. (2007). *Biomechanics of the musculo-skeletal system*. John Wiley & Sons, Chichester, England, 3rd ed edition.
- Novacheck, T. F. (1995). Walking, running, and sprinting: a three-dimensional analysis of kinematics and kinetics. *Instr Course Lect*, 44:497–506.
- Novacheck, T. F. (1998). The biomechanics of running. *Gait Posture*, 7(1):77–95.
- O’Brien, T. D., Reeves, N. D., Baltzopoulos, V., Jones, D. A., and Maganaris,

-
- C. N. (2010). In vivo measurements of muscle specific tension in adults and children. *Exp Physiol*, 95(1):202–10.
- Ozcaldiran, B. and Durmaz, B. (2008). Isokinetic muscle strength for ankle extensors and flexors: a comparison between elite sprint runners and swimmers. *J Sports Med Phys Fitness*, 48(3):300–4.
- Page, S. G. and Huxley, H. E. (1963). Filament lengths in striated muscle. *J Cell Biol*, 19:369–90.
- Pandy, M. G. (2001). Computer modeling and simulation of human movement. *Annu Rev Biomed Eng*, 3:245–73.
- Pandy, M. G. and Anderson, F. C. (2000). Dynamic simulation of human movement using large-scale models of the body. *Phonetica*, 57(2-4):219–28.
- Pandy, M. G. and Andriacchi, T. P. (2010). Muscle and joint function in human locomotion. *Annu Rev Biomed Eng*, 12:401–33.
- Pandy, M. G., Lin, Y. C., and Kim, H. J. (2010). Muscle coordination of mediolateral balance in normal walking. *J Biomech*, 43(11):2055–64.
- Raikova, R. T. and Prilutsky, B. I. (2001). Sensitivity of predicted muscle forces to parameters of the optimization-based human leg model revealed by analytical and numerical analyses. *J Biomech*, 34(10):1243–55.
- Rassier, D. E. and Herzog, W. (2005). Force enhancement and relaxation rates after stretch of activated muscle fibres. *Proc Biol Sci*, 272(1562):475–80.
- Reinbolt, J. A., Haftka, R. T., Chmielewski, T. L., and Fregly, B. J. (2007). Are patient-specific joint and inertial parameters necessary for accurate inverse dynamics analyses of gait? *IEEE Trans Biomed Eng*, 54(5):782–93.
- Reinbolt, J. A., Schutte, J. F., Fregly, B. J., Koh, B. I., Haftka, R. T., George, A. D., and Mitchell, K. H. (2005). Determination of patient-specific multi-joint kinematic models through two-level optimization. *J Biomech*, 38(3):621–6.
- Remy, C. D. and Thelen, D. G. (2009). Optimal estimation of dynamically consistent kinematics and kinetics for forward dynamic simulation of gait. *J Biomech Eng*, 131(3):031005.
- Riemer, R. and Hsiao-Weckler, E. T. (2008). Improving joint torque calculations: optimization-based inverse dynamics to reduce the effect of motion errors. *J Biomech*, 41(7):1503–9.

REFERENCES

- Riley, P. O., Dicharry, J., Franz, J., Croce, U. D., Wilder, R. P., and Kerrigan, D. C. (2008). A kinematics and kinetic comparison of overground and treadmill running. *Med Sci Sports Exerc*, 40(6):1093–100.
- Roberts, T. J., Marsh, R. L., Weyand, P. G., and Taylor, C. R. (1997). Muscular force in running turkeys: the economy of minimizing work. *Science*, 275(5303):1113–5.
- Rudolph, K. S., Axe, M. J., Buchanan, T. S., Scholz, J. P., and Snyder-Mackler, L. (2001). Dynamic stability in the anterior cruciate ligament deficient knee. *Knee Surg Sports Traumatol Arthrosc*, 9(2):62–71.
- Salo, A. I., Bezodis, I. N., Batterham, A. M., and Kerwin, D. G. (2011). Elite sprinting: Are athletes individually step frequency or step length reliant? *Med Sci Sports Exerc*, 43(6):1055–62.
- Sasaki, K. and Neptune, R. R. (2006). Differences in muscle function during walking and running at the same speed. *J Biomech*, 39(11):2005–13.
- Sasaki, K., Neptune, R. R., Burnfield, J. M., and Mulroy, S. J. (2008). Muscle compensatory mechanisms during able-bodied toe walking. *Gait Posture*, 27(3):440–6.
- Satterthwaite, P., Norton, R., Larmer, P., and Robinson, E. (1999). Risk factors for injuries and other health problems sustained in a marathon. *Br J Sports Med*, 33(1):22–6.
- Sawicki, G. S., Lewis, C. L., and Ferris, D. P. (2009). It pays to have a spring in your step. *Exerc Sport Sci Rev*, 37(3):130–8.
- Schache, A. G., Baker, R., and Lamoreux, L. W. (2008). Influence of thigh cluster configuration on the estimation of hip axial rotation. *Gait Posture*, 27(1):60–9.
- Schache, A. G., Blanch, P. D., Dorn, T. W., Brown, N. A., Rosemond, D., and Pandy, M. G. (2011a). Effect of running speed on lower-limb joint kinetics. *Med Sci Sports Exerc*, 43(7):1260–1271.
- Schache, A. G., Dorn, T. W., Blanch, P. D., Brown, N. A., and Pandy, M. G. (2011b). Mechanics of the human hamstring muscles during sprinting. *Med Sci Sports Exerc*, In press.
- Schache, A. G., Kim, H. J., Morgan, D. L., and Pandy, M. G. (2010). Hamstring muscle forces prior to and immediately following an acute sprinting-related muscle strain injury. *Gait Posture*.

-
- Seth, A. and Delp, S. L. (2009). Estimates of muscle function depend on constraints that characterize ground contact. *XII International Symposium on Computer Simulation in Biomechanics, Cape Town, South Africa*.
- Seth, A. and Pandy, M. G. (2007). A neuromusculoskeletal tracking method for estimating individual muscle forces in human movement. *J Biomech*, 40(2):356–66.
- Seth, A., Sherman, M., Eastman, P., and Delp, S. (2010). Minimal formulation of joint motion for biomechanisms. *Nonlinear Dyn*, 62(1):291–303.
- Simonsen, E. B., Thomsen, L., and Klausen, K. (1985). Activity of mono- and biarticular leg muscles during sprint running. *Eur J Appl Physiol Occup Physiol*, 54(5):524–32.
- Simpson, K. J. and Bates, B. T. (1990). The effects of running speed on lower extremity joint moments generated during the support phase. *International Journal of Sport Biomechanics*, 6:309–324.
- Solnik, S., DeVita, P., Rider, P., Long, B., and Hortobagyi, T. (2008). Teager-kaiser operator improves the accuracy of emg onset detection independent of signal-to-noise ratio. *Acta Bioeng Biomech*, 10(2):65–8.
- Solnik, S., Rider, P., Steinweg, K., DeVita, P., and Hortobagyi, T. (2010). Teager-kaiser energy operator signal conditioning improves emg onset detection. *Eur J Appl Physiol*, 110(3):489–98.
- Stefanyshyn, D. J., Stergiou, P., Lun, V. M., Meeuwisse, W. H., and Worobets, J. T. (2006). Knee angular impulse as a predictor of patellofemoral pain in runners. *American Journal of Sports Medicine*, 34(11):1844–1851.
- Swanson, S. C. and Caldwell, G. E. (2000). An integrated biomechanical analysis of high speed incline and level treadmill running. *Med Sci Sports Exerc*, 32(6):1146–55.
- Talbot, J. A. and Morgan, D. L. (1998). The effects of stretch parameters on eccentric exercise-induced damage to toad skeletal muscle. *Journal of Muscle Research and Cell Motility*, 19:237–245.
- Thelen, D. G. (2003). Adjustment of muscle mechanics model parameters to simulate dynamic contractions in older adults. *J Biomech Eng*, 125(1):70–7.
- Thelen, D. G. and Anderson, F. C. (2006). Using computed muscle control to

REFERENCES

- generate forward dynamic simulations of human walking from experimental data. *J Biomech*, 39(6):1107–15.
- Thelen, D. G., Anderson, F. C., and Delp, S. L. (2003). Generating dynamic simulations of movement using computed muscle control. *J Biomech*, 36(3):321–8.
- Thelen, D. G., Chumanov, E. S., Best, T. M., Swanson, S. C., and Heiderscheit, B. C. (2005). Simulation of biceps femoris musculotendon mechanics during the swing phase of sprinting. *Med Sci Sports Exerc*, 37(11):1931–8.
- Thelen, D. G., Chumanov, E. S., Sherry, M. A., and Heiderscheit, B. C. (2006). Neuromusculoskeletal models provide insights into the mechanisms and rehabilitation of hamstring strains. *Exerc Sport Sci Rev*, 34(3):135–41.
- Thordarson, D. B. (1997). Running biomechanics. *Clin Sports Med*, 16(2):239–47.
- van der Walt, W. H. and Wyndham, C. H. (1973). An equation for prediction of energy expenditure of walking and running. *J Appl Physiol*, 34(5):559–63.
- van Gent, R. N., Siem, D., van Middelkoop, M., van Os, A. G., Bierma-Zeinstra, S. M., and Koes, B. W. (2007). Incidence and determinants of lower extremity running injuries in long distance runners: a systematic review. *Br J Sports Med*, 41(8):469–80; discussion 480.
- van Ingen Schenau, G. J., de Koning, J. J., and de Groot, G. (1994). Optimisation of sprinting performance in running, cycling and speed skating. *Sports Med*, 17(4):259–75.
- van Mechelen, W. (1992). Running injuries: A review of the epidemiological literature. *Sports Medicine*, 14(5):320–335.
- Vardaxis, V. and Hoshizaki, T. B. (1989). Power patterns of the leg during the recovery phase of the sprinting stride for advanced and intermediate sprinters. *International Journal of Sport Biomechanics*, 5:332–349.
- Volkov, N. I. and Lapin, V. I. (1979). Analysis of the velocity curve in sprint running. *Med Sci Sports*, 11(4):332–7.
- Wakeling, J. M., Blake, O. M., Wong, I., Rana, M., and Lee, S. S. M. (2011). Movement mechanics as a determinate of muscle structure, recruitment and coordination. *Philosophical Transactions of the Royal Society B-Biological Sciences*, 366(1570):1554–1564.

- Walter, S. D., Hart, L. E., McIntosh, J. M., and Sutton, J. R. (1989). The ontario cohort study of running-related injuries. *Arch Intern Med*, 149(11):2561–4.
- Ward, S. R., Eng, C. M., Smallwood, L. H., and Lieber, R. L. (2009). Are current measurements of lower extremity muscle architecture accurate? *Clin Orthop Relat Res*, 467(4):1074–82.
- Ward-Smith, A. J. (1985). A mathematical theory of running, based on the first law of thermodynamics, and its application to the performance of world-class athletes. *J Biomech*, 18(5):337–49.
- Webb, P., Saris, W. H., Schoffelen, P. F., Van Ingen Schenau, G. J., and Ten Hoor, F. (1988). The work of walking: a calorimetric study. *Med Sci Sports Exerc*, 20(4):331–7.
- Wen, D. Y., Puffer, J. C., and Schmalzried, T. P. (1998). Injuries in runners: a prospective study of alignment. *Clin J Sport Med*, 8(3):187–94.
- Weyand, P. G., Bundle, M. W., McGowan, C. P., Grabowski, A., Brown, M. B., Kram, R., and Herr, H. (2009). The fastest runner on artificial legs: different limbs, similar function? *J Appl Physiol*, 107(3):903–11.
- Weyand, P. G., Sandell, R. F., Prime, D. N., and Bundle, M. W. (2010). The biological limits to running speed are imposed from the ground up. *J Appl Physiol*, 108(4):950–61.
- Weyand, P. G., Sternlight, D. B., Bellizzi, M. J., and Wright, S. (2000). Faster top running speeds are achieved with greater ground forces not more rapid leg movements. *J Appl Physiol*, 89(5):1991–9.
- Willems, P. A., Cavagna, G. A., and Heglund, N. C. (1995). External, internal and total work in human locomotion. *J Exp Biol*, 198(Pt 2):379–93.
- Williams, K. R. and Cavanagh, P. R. (1983). A model for the calculation of mechanical power during distance running. *J Biomech*, 16(2):115–28.
- Williams, K. R. and Cavanagh, P. R. (1987). Relationship between distance running mechanics, running economy, and performance. *J Appl Physiol*, 63(3):1236–45.
- Wilson, G. J., Newton, R. U., Murphy, A. J., and Humphries, B. J. (1993). The optimal training load for the development of dynamic athletic performance. *Med Sci Sports Exerc*, 25(11):1279–86.

REFERENCES

- Winter, D. A. (1983). Moments of force and mechanical power in jogging. *J Biomech*, 16(1):91–7.
- Winter, D. A. (2009). *Biomechanics and motor control of human movement*. John Wiley & Sons, Inc., New York, 4th edition edition.
- Winter, D. A. and Bishop, P. J. (1992). Lower extremity injury. biomechanical factors associated with chronic injury to the lower extremity. *Sports Med*, 14(3):149–56.
- Wojtyra, M. (2003). Multibody simulation model of human walking. *Mechanics based design of structures and machines*, 31(3):357–379.
- Woledge, R. C., Curtin, N. A., and Homsher, E. (1985). Energetic aspects of muscle contraction. *Monogr Physiol Soc*, 41:1–357.
- Wood, G. (1987). Biomechanical limitations to sprint running. *Medicine and sport science*, 25:58–71.
- Xiao, M. and Higginson, J. (2010). Sensitivity of estimated muscle force in forward simulation of normal walking. *J Appl Biomech*, 26(2):142–9.
- Xiao, M. and Higginson, J. S. (2008). Muscle function may depend on model selection in forward simulation of normal walking. *J Biomech*, 41(15):3236–3242.
- Yokozawa, T., Fujii, N., and Ae, M. (2007). Muscle activities of the lower limb during level and uphill running. *J Biomech*, 40(15):3467–75.
- Yu, B., Queen, R. M., Abbey, A. N., Liu, Y., Moorman, C. T., and Garrett, W. E. (2008). Hamstring muscle kinematics and activation during overground sprinting. *J Biomech*, 41(15):3121–6.
- Zajac, F. E. (1989). Muscle and tendon: properties, models, scaling, and application to biomechanics and motor control. *Crit Rev Biomed Eng*, 17(4):359–411.
- Zajac, F. E. and Gordon, M. E. (1989). Determining muscle’s force and action in multi-articular movement. *Exerc Sport Sci Rev*, 17:187–230.
- Zajac, F. E., Neptune, R. R., and Kautz, S. A. (2002). Biomechanics and muscle coordination of human walking. part i: introduction to concepts, power transfer, dynamics and simulations. *Gait Posture*, 16(3):215–32.